Title
Hydrologic dynamics of the Greenland Ice Sheet from remote sensing and field measurements

Author
Chu, Vena

Publication Date
2015

Peer reviewed|Thesis/dissertation

UNIVERSITY OF CALIFORNIA

Los Angeles

Hydrologic dynamics of the Greenland Ice Sheet from remote sensing and field measurements

A dissertation submitted in partial satisfaction of the

requirements for the degree Doctor of Philosophy

in Geography

by

Vena Chu

2015

ABSTRACT OF THE DISSERTATION

Hydrologic dynamics of the Greenland Ice Sheet

from remote sensing and field measurements

by

Vena Chu

Doctor of Philosophy in Geography

University of California, Los Angeles, 2015

Professor Laurence Smith, Chair

The current need for forecasting Greenland Ice Sheet contributions to global sea level rise is complicated by the lack of understanding of ice sheet hydrology. The proportion of meltwater contributing to sea level rise, as well as the pathways transporting meltwater on, through, and out of the ice sheet, are not well understood. Remote sensing of hydrologic dynamics in combination with small-scale fieldwork allows examination of broad spatial and temporal trends in the Greenland hydrologic system responding to a changing climate. This dissertation reviews the current state of knowledge on Greenland Ice Sheet hydrology, and examines three components of the Greenland hydrologic system: (1) fjord sediment plumes as an indicator of meltwater output, (2) supraglacial streamflow as an indicator of meltwater input to the ice sheet, and (3) moulin distribution and formation as a mechanism diverting meltwater from the surface of the ice sheet to the bed.

Buoyant sediment plumes that develop in fjords downstream of outlet glaciers are controlled by numerous factors, including meltwater runoff. MODIS retrievals of sediment

plume concentration show a strong regional and seasonal response to meltwater production on the ice sheet surface, despite limitations in fjords with rapidly calving glaciers, providing a tool for tracking meltwater release to the ocean.

Summertime field observations and high-resolution satellite imagery reveal extensive supraglacial river networks across the southwestern ablation zone transporting large volumes of meltwater to moulins, yet these features remain poorly mapped and their discharges unquantified. A GIS modeling framework is developed to spatially adapt Manning's equation for use with high-resolution WorldView-2 imagery to map supraglacial river discharge.

Moulins represent connections between surface meltwater on the Greenland ice sheet and subglacial drainage networks, where increased meltwater can enhance ice sliding dynamics. A new high-resolution moulin dataset in western Greenland created from WorldView-1/2 imagery in the 2012 record melt year is used to assess moulin distribution and formation. Moulin locations show a significantly different distribution compared to geospatial variables in the entire study area, with moulins forming in areas of thinner ice, higher velocity and extensional strain rate, as well as lower surface elevation and slope, and higher bed elevation and slope.

The dissertation of Vena Chu is approved.

Gregory S. Okin

Yongwei Sheng

Steven A. Margulis

Laurence Smith, Committee Chair

University of California, Los Angeles

2015

This dissertation is dedicated to my mom and my brother.

TABLE OF CONTENTS

CHAPTER 3:
Adaptation of the Manning Equation for Remote Estimation of Supraglacial River Discharge Using GIS Modelling and WorldView-2 Satellite Imagery

LIST OF FIGURES

Figure

LIST OF TABLES

Table

ACKOWLEDGMENTS

Funding for this research was provided by the National Aeronautics and Space Administration (NASA) through the Cryospheric Sciences Program (Grants #NNGO5GN89G, # NNX11AQ38G, and #NNX14AH93G), by the NASA Graduate Student Researchers Program Fellowship (#NNX09AM25H), by the Society of Women Geographers National Fellowship, and by the UCLA Dissertation Year Fellowship. I thank my advisor, Larry Smith, for many years of unwavering support, and for the time and energy spent teaching me how to do field work, how to write a paper, how to mentor students, how to give a talk, and how to interview. I thank my committee members Greg Okin, Yongwei Sheng, and Steve Margulis for their guidance, encouragement, and career advice.

Each chapter of this dissertation has either been published, is in revision, or will be submitted for publication in a peer-reviewed journal. Chapter 1 was published in 2014 in *Progress in Physical Geography*. Chapter 2 was published in 2012 in *The Cryosphere* with co-authors Larry Smith, Åsa Rennermalm, Rick Forster, and Jason Box. Chapter 3 is in revision in *GIScience & Remote Sensing* with co-authors Larry Smith, Kang Yang, Carl Legleiter, Colin Gleason, and Åsa Rennermalm. Chapter 4 will be submitted for publication with co-authors Larry Smith, Colin Gleason, Kang Yang, and Lincoln Pitcher.

For providing logistical support for field work in Greenland, I thank CH2MHILL Polar Services (CPS) and Kangerlussuaq International Science Support (KISS). I thank Paul Morin, Claire Porter, and Carl Reim from the Polar Geospatial Center at the University of Minnesota for providing WorldView imagery for Chapters 3 and 4. I thank Åsa Rennermalm for supporting and mentoring me through many field seasons in Greenland. I thank Lincoln Pitcher and Colin Gleason for their friendship and teamwork, and for making fieldwork infinitely more fun.

For their camaraderie and support in graduate school, I would like to thank Scott Stephenson, Jida Wang, Kate Willis, Tom Narins, Evan Lyons, Andrew Fricker, Mia Bennett, Matt Mersel, Corey Rovzar, Tamlin Pavelsky, Will Hobbs, Stephanie Pau, Lorna Apper, Christine Zuhlsdorf, Guoqiong Song, Kang Yang, Pablo Fuentenebro, and Jenny Goldstein. For their friendship and encouragement over the years, I also thank Christina Bahng, Sean Baxter, Sherita Solis, Daisy Tsao, Nicole Copuz, Grant Wang, and Jonathan Dochterman. Finally, I give my heartfelt thanks to my family: my cousins, my grandparents, my brother, and most of all my mother.

VITA

EDUCATION

C.Phil, Geography, University of California, Los Angeles 2014

Committee: Laurence Smith (chair), Greg Okin, Yongwei Sheng, Steve Margulis
Dissertation title: Hydrologic dynamics of the Greenland ice sheet from remote sensing and field measurements

M.A., Geography, University of California, Los Angeles 2009

Committee: Laurence Smith (chair), Greg Okin, Yongwei Sheng
Thesis title: Estuary sediment plume response to surface melting and supraglacial lake drainages on the Greenland Ice Sheet

B.A., University of California, Los Angeles 2006

Majors: Geography and Economics, with college honors
Minor: Accounting

EMPLOYMENT HISTORY

Graduate Student Researcher, Department of Geography, UCLA	2009-2014
Teaching Assistant, Department of Geography, UCLA	2008-2013
Staff Accountant, RBZ LLP, Los Angeles, CA	2006-2007

AWARDS AND HONORS

2015	American Geophysical Union Outstanding Student Paper Award
2014-2015	UCLA Dissertation Year Fellowship
2013-2014	Society of Women Geographers National Fellowship
2012	UCLA Department of Geography Graduate Research Publication Award
2010	UCLA Graduate Summer Research Mentorship Award
2010	UCLA Department of Geography Graduate Research Publication Award
2009-2012	NASA Graduate Student Researchers Program
2009	Association of American Geographers R.S. Tarr Student Illustrated Paper Award
2007-2010	UCLA Department of Geography Chancellor's Prize

PUBLICATIONS

Chu, V.W. (2014). Greenland ice sheet hydrology: a review. *Progress in Physical Geography*, 38(1): 19-54.

Chu, V.W., Smith, L.C., Rennermalm, A.K., Forster, R.R., Box, J.E., and Reeh, N. (2009). Sediment plume response to surface melting and supraglacial lake drainages on the Greenland ice sheet. *Journal of Glaciology*, 55(104): 1072-1082.

Chu, V.W., Smith, L.C., Rennermalm, A.K., Forster, R.R., and Box, J.E. (2012). Hydrologic controls on coastal suspended sediment plumes around the Greenland Ice Sheet. *The Cryosphere*, 6(1): 1-19.

Chu, V.W., Smith, L.C., Yang, K., Leglieter, C.J., Gleason, C.J., and Rennermalm, A.K. (in revision). Adaptation of Manning's equation for remote estimation of supraglacial river discharge using GIS modeling and WorldView-2 satellite imagery. *GIScience & Remote Sensing*.

Gleason, C.J., Smith, L.C., Finnegan, D.C., LeWinter, A.L., Pitcher, L.H., and **Chu, V.W.** (in press). Semi-automated classification of time-lapse RGB imagery for a remote Greenlandic river. *Hydrology and Earth System Sciences*.

Rennermalm, A.K., Moustafa, S.E., Mioduszewski J., **Chu, V.W.**, Forster, R.R., Hagedorn, B., Harper, J.T., Mote, T.L., Robinson, D.A., Shuman, C.A., Smith, L.C., and Tedesco, M. (2013). Understanding Greenland ice sheet hydrology using an integrated multi-scale approach. *Environmental Research Letters*, 8(1): 1–14.

Rennermalm, A.K., Smith, L.C., Stroeve, J.C., and **Chu, V.W.** (2009). Does sea ice influence Greenland ice sheet surface-melt? Environmental Research Letters, 4, 024011.

Rennermalm, A.K., Smith, L.C., **Chu, V.W.**, Forster, R.R., Box, J.E., and B. Hagedorn. Proglacial river stage, discharge, and temperature datasets from the Akuliarusiarsuup Kuua River northern tributary, Southwest Greenland, 2008–2011 (2012). *Earth System Science Data*, 4: 1-12.

Rennermalm, A.K., Smith, L.C., **Chu, V.W.**, Box, J.E., Forster, R.R., van den Broeke, M., van As, D., and S. E. Moustafa (2013). Evidence of meltwater retention within the Greenland ice sheet. *The Cryosphere*, 7(5): 1433–1445.

Smith, L.C., **Chu, V.W.**, Yang, K., Gleason, C.J., Pitcher, L.H., Rennermalm, A.K., Legleiter, C.J., Behar, A.E., Overstreet, B.T., Moustafa, S.E., Tedesco, M., Forster, R.R., LeWinter, A.L., Finnegan, D.C., Sheng, Y., and J. Balog (2015). Efficient meltwater drainage through supraglacial streams and rivers on the southwest Greenland ice sheet. *Proceedings of the National Academy of Sciences*, 112(4):1001-1006.

SELECTED CONFERENCE PRESENTATIONS AND SEMINARS

Chu, V.W., Smith, L.C., Yang, K., Legleiter, C.J., Gleason, C.J., and A.K. Rennermalm (2015). Supraglacial streamflow into moulins on the Greenland ice sheet. *Association of American Geographers Annual Meeting*, Chicago, IL, 21-25 April, 2015.

Chu, V.W., Smith, L.C., Yang, K., Legleiter, C.J., Gleason, C.J., Rennermalm, A.K., Pitcher, L.H., and R.R. Forster (2014). Remote estimation of Greenland Ice Sheet supraglacial river discharge using GIS modeling and WorldView-2 satellite imagery. *American Geophysical Union Fall Meeting*, San Francisco, CA, 15-19 December, 2014.

Chu, V.W. (2014) Greenland Ice Sheet supraglacial rivers. *Lamont-Doherty Earth Observatory Division of Marine Geology and Geophysics*, Palisades, NY, 8 September, 2014.

Chu, V.W. (2014) Greenland Ice Sheet hydrology. *Joint Science Education Project (JSEP)*, Kangerlussuaq, Greenland, 8 July, 2014.

Chu, V.W. (2014) Greenland Ice Sheet supraglacial rivers. *Society of Women Geographers Triennial Meeting*, Pittsburgh, PA, 23-26 May, 2014.

Chu, V.W., Smith, L.C., Yang, K., Rennermalm, A.K., Forster, R.R., Gleason, C.J., Legleiter, C.J., Behar, A.E., Tedesco, M., Overstreet, B.T., Pitcher, L.H., and S.E. Moustafa (2014). Remote sensing of supraglacial river discharge on the Greenland Ice Sheet. *Program for Arctic Regional Climate Assessment (PARCA) Meeting*, Greenbelt, MD, 28-29 January, 2014.

Chu, V.W. (2011) Hydrologic controls of sediment plume behavior around the Greenland Ice Sheet. *UCLA Department of Atmospheric & Oceanic Sciences Coastal Seminar*, Los Angeles, CA, 11 May, 2011.

Chu, V.W., L.C. Smith, A.K. Rennermalm, R.R. Forster, J.E. Box, and N. Reeh (2008). Response of sediment plumes to Greenland ice sheet surface melt. American Geophysical Union Fall Meeting, San Francisco, CA, 15-19 December, 2008.

Chapter 1

Greenland Ice Sheet Hydrology: A Review

1.1 Abstract

Understanding the Greenland ice sheet (GrIS) hydrology is essential for evaluating response of ice dynamics to a warming climate and future contributions to global sea level rise. Recently observed increases in temperature and melt extent over the GrIS have prompted numerous remote sensing, modeling, and field studies gauging the response of the ice sheet and outlet glaciers to increasing meltwater input, providing a quickly growing body of literature describing seasonal and annual development of the GrIS hydrologic system. This system is characterized by supraglacial streams and lakes that drain through moulins, providing an influx of meltwater into englacial and subglacial environments that increases basal sliding speeds of outlet glaciers in the short-term. However, englacial and subglacial drainage systems may adjust to efficiently drain increased meltwater without significant changes to ice dynamics over seasonal and annual scales. Both proglacial rivers originating from land-terminating glaciers and subglacial conduits under marine-terminating glaciers represent direct meltwater outputs in the form of fjord sediment plumes, visible in remotely sensed imagery. This review provides the current state of knowledge on GrIS surface water hydrology, following ice sheet surface meltwater production and transport via supra-, en-, sub-, and proglacial processes to final meltwater export to the ocean. With continued efforts targeting both process-level and systems analysis of the hydrologic system, the larger picture of how future changes in Greenland hydrology will affect ice sheet glacier dynamics and ultimately global sea level rise can be advanced.

1.2 Introduction

The Greenland ice sheet (GrIS) has been experiencing increasing surface melt (Fettweis et al., 2011; Bhattacharya et al., 2009; Box, 2013) and accelerated freshwater runoff to the ocean (Dyurgerov et al., 2010), contributing to global sea level rise (Rignot et al., 2011; Shepherd and Wingham, 2007; Bamber and Riva, 2010; Shepherd et al., 2012) and influencing estuarine and ocean circulation (Fichefet, 2003; J. Bamber et al., 2012; Straneo et al., 2010; Marsh et al., 2010). While understanding of recent meltwater contributions to the ocean has become clearer due to an increase in available data from satellite remote sensing, projecting plausible future scenarios remains highly uncertain because of a lack of understanding of the processes that control sea level rise, particularly an unstable ice sheet (Nicholls and Cazenave, 2010; Milne et al., 2009). Paleoclimatic reconstructions have shown contribution of meltwater amounting to sea levels that are meters above modern sea level in response to modest warming, with peak rates possibly exceeding 1 m/century, cautioning that the rate of future melting and sea level rise may be much higher than currently thought (Overpeck et al., 2006). However, studies have also shown that glaciological conditions required for such a large increase in sea level are unlikely (Pfeffer, 2011; Pfeffer et al., 2008), and estimate that Greenland's contribution to sea level rise by the end of this century will be ~22 cm (Bindschadler et al., 2013), with a possible rate of ~0.7-0.8 mm/yr (Fettweis et al., 2008). A large unknown in such projections is the role of meltwater: how it contributes to dynamic changes in outlet glaciers and what fraction of meltwater produced on the surface of the GrIS becomes runoff into the ocean (Rennermalm et al., 2013).

Ice sheet surface melting has been observed through automatic weather stations (AWS) on the ice surface and through remote sensing, employing radar and thermal data to detect surface and/or near-surface presence of meltwater or surface temperatures above the melting point. Melt records from the satellite era have shown positive trends in melt extent since 1972 (Abdalati and Steffen, 2001; Mote, 2007; Mernild et al., 2011a), and a pronounced trend in winter surface temperatures (Hall et al., 2008; Van As, 2011; Box, 2013; Hanna et al., 2012). Models combined with AWS data have shown an overall dominant warming since 1840, with a cooling period from 1932 – 1992, and a very significant warming trend since 1994 attributed to intensifying anthropogenic warming and decreasing sulfate cooling from volcanic eruptions (Box, 2013). Additionally, this recent warming trend in 1995/95 began with a step-like increase of both melt extent and temperature coinciding with a sign reversal in the North Atlantic Oscillation (NAO) index (Bhattacharya et al., 2009). The increase in melt extent has been dominated by strong warming in the western GrIS rather than the eastern portion (Abdalati and Steffen, 2001; Steffen and Box, 2001; Hanna et al., 2012), with the northwestern sector showing the highest annual trend in surface temperature (Hall et al., 2013; Van As, 2011). Over the period 1982-2011, observations at Summit, Greenland suggest a warming rate six times the global average (McGrath et al., 2013). Satellite data have shown a string of record-setting years in the recent decade, from the melt anomalies of 2002, 2007, and 2010 (Mote, 2007; Tedesco et al., 2008; Steffen et al., 2004; Mernild et al., 2011a), to the most recent extreme 2012 melt event that covered 98% of the GrIS surface (Nghiem et al., 2012; Hall et al., 2013; Bennartz et al., 2013; Tedesco et al., 2013).

Mass of the GrIS is gained from snowfall and lost by melt and iceberg calving. Surface mass balance (SMB) refers to mass exchanges at the surface of the ice sheet, where accumulation occurs through snowfall as well as refreezing of meltwater, and ablation of the surface consists of melt as well as sublimation. Mass balance measurements quantify these processes and are directly linked to the meteorological parameters that govern accumulation and ablation. While SMB varies spatially, a broad upper region of mass surplus is the accumulation zone, and a broad lower region of mass deficit is the ablation zone, with the boundary between the two zones defined as the equilibrium line altitude (ELA, Figure 1-1). Together, SMB and ice discharge through calving represent total mass balance, which has become increasingly negative, driven by two main components increasing dramatically in the first decade of the 21st century: ice discharge and melt (van den Broeke et al., 2009; Allison et al., 2009). While interannual variability in mass balance is mostly accounted for by variation in accumulation through precipitation, anomalies in ice discharge and meltwater runoff significantly exceed decadal variability of precipitation. These anomalies led to a general trend of mass loss (Sasgen et al., 2012; van den Broeke et al., 2009), yet consensus on exactly how much mass has been lost has not been reached, due to different accounting methodologies and varying time spans (Cazenave, 2006; Vernon et al., 2013; Shepherd et al., 2012).

New satellite measurements have allowed a more robust understanding of Greenland SMB and ice discharge. In particular, gravimetry measurements from the Gravity Recovery and Climate Experiment (GRACE) provide observations of mass loss independent of other remote sensing estimates and models (Velicogna and Wahr, 2005; Wouters et al., 2008; Cazenave et al., 2009; Chen et al., 2006; Velicogna, 2009; Harig and Simons, 2012), and have shown agreement with other assessments (van den Broeke et al., 2009; Rignot et al., 2011; Shepherd et al., 2012). From 2002 – 2011, the GrIS experienced an average -240±18 Gt/yr of ice mass loss as measured by GRACE, similar to the -240±18 Gt/yr from modeled SMB and remotely sensed ice discharge (Sasgen et al., 2012). Increasing accumulation in the ice sheet interior and southeast (Box et al., 2006; Burgess et al., 2010; Miège et al., 2013) has mostly been exceeded by losses in the marginal ablation zone (Luthcke et al., 2006; Ettema et al., 2009; Zwally et al., 2011). Further showing that mass loss is dominated by different components regionally, two regions with high rates of mass loss show very different proportions: the southeast is dominated by ice discharge and the southwest by melting and runoff (van den Broeke et al. 2011; Sasgen et al. 2012). Each remotely sensed or modeled mass loss component contains large uncertainties, and therefore it is important to partition mass loss into an ice dynamics component and meltwater runoff component, particularly for regional analyses.

Dynamic changes to outlet glacier velocity, calving rate, and ice thickness are a main contributor to increasing GrIS mass losses. Losses are exponentially higher at the margin (van de Wal et al., 2008) with rapid thinning of both outlet glaciers and the ice sheet itself (Krabill, 2004; Thomas et al., 2009; Pritchard et al., 2009). Outlet glaciers are categorized into land-terminating glaciers and marine-terminating glaciers, most of which lie in deep channels with beds below sea level and end either as a floating glacier tongue or by joining an ice shelf (Cuffey and Paterson, 2010). Marine-terminating outlet glaciers have shown increases in total ice discharge (Rignot, 2004; Howat et al., 2007) and velocity (Rignot and Kanagaratnam, 2006; Moon et al., 2012), with velocity speedups recently extending to the northwest (Khan et al., 2010). Ocean interactions with marine-terminating glaciers include destabilized calving fronts (Nick et al., 2010; Thomas, 2004) and enhanced ice-bottom melting from warm ocean waters (D. M. Holland et al., 2008; Rignot and Steffen, 2008). These dynamic changes to outlet glaciers and the GrIS margin are the primary concern for modeling reasonable projections of future mass losses. Possible feedbacks from increasing meltwater input could further accelerate mass loss, but meltwater transport processes are much less studied than changes in outlet glacier velocity, ice discharge, and thickness.

Meltwater runoff possibly accounts for more than half of GrIS mass loss (van den Broeke et al., 2009; Sasgen et al., 2012), yet the complex pathways transporting meltwater from the ice sheet surface to the ice edge and the ocean are still not well understood. Runoff is important for ice sheet mass loss as direct input to sea level rise, but also in its interaction with englacial and subglacial channels, affecting ice dynamics (Bartholomew et al., 2012).

Remote sensing provides robust measures of meltwater production on the ice surface, showing increasing melt extent and intensity over the last decade (Bhattacharya et al., 2009; Mote, 2007; Fettweis et al., 2011; Mernild et al., 2011a; Tedesco et al., 2011), but models are still required to account for complete surface energy balance and to fully explain the process of meltwater becoming runoff. Model variation in accounting for meltwater retention and refreezing in firn complicates estimates of true runoff from the ice sheet (Pfeffer and Meier, 1991; Bøggild et al., 2005; Reijmer et al., 2012). Models have shown increased runoff from regional drainage basins as well as for the entire ice sheet over the last half a century (Dyurgerov et al., 2010; Box et al., 2006; Ettema et al., 2009; Box, 2013; Mernild et al., 2008; Mernild et al., 2010a; Mernild et al., 2010b), yet significant increases in runoff have mostly been offset by increased precipitation in mass balance estimates (Hanna et al., 2008; Hanna, 2005). However, projections of 21st century mass balance show that runoff increases may exceed increased precipitation (Tedesco and Fettweis, 2012). A key and unknown process scientists seek to understand is how increased meltwater input into the englacial and subglacial drainage systems affects ice dynamics.

Changes in meltwater input to the englacial and subglacial environments are widely shown to be related to ice dynamics, and questions remain about how changing meltwater input volumes affect englacial and subglacial network organization. Short-term speedups of both the land-terminating portions of the ice sheet (Zwally et al., 2002; Palmer et al., 2011; Bartholomew et al., 2010) and fast moving marine-terminating outlet glaciers (Joughin et al., 2008a; Shepherd et al., 2009; Andersen et al., 2011) have been observed following increased meltwater production as well as from rapid drainage of supraglacial lakes (e.g., Das et al., 2008). These observations prompted the hypothesis that increased ice sheet surface meltwater enters the subglacial environment, increasing glacier flow through basal lubrication of the ice-bedrock interface (e.g., Zwally et al. 2002). Basal sliding is tied to englacial and subglacial drainage organization. Less developed subglacial networks are inefficient at draining large volumes of meltwater and can be overwhelmed to cause short-term increases in ice motion (Colgan et al., 2011a). However, examination of drainage network development throughout the melt season shows greater drainage efficiency as subglacial conduits develop with increasing meltwater input, causing instead decreased basal sliding, as inferred from observations of velocities responding to seasonal melting (Sundal et al., 2011; Schoof, 2010). With discrete meltwater pulses shown to increase short-term basal sliding yet seasonal increases in meltwater production shown to decrease basal sliding, the question of how ice dynamics will respond to future warming scenarios is tied to englacial and subglacial drainage organization and development.

Meltwater produced on the ice surface is transported from its origin in a variety of ways. Meltwater can move through supraglacial stream networks and lakes and potentially connect to englacial and subglacial pathways through moulins and crevasses that drain supraglacial water features. Alternatively, meltwater that is not routed from the surface can be retained through refreezing or become stored interannually in supraglacial lakes and water-filled fractures (Figure 1-1). Supraglacial lakes have gained widespread scientific interest with their propensity to drain rapidly into the ice sheet and trigger short-term velocity changes and sustained uplift (Das et al., 2008; Doyle et al., 2013). To this end, numerous studies have mapped the occurrence and seasonal evolution of supraglacial lakes and have modeled lake depth and volume (Selmes et al., 2011; Tedesco and Steiner, 2011; Banwell et al., 2012; Tedesco et al., 2012; Box and Ski, 2007; Chu et al., 2009; Georgiou et al., 2009; Hoffman et al., 2011; Johansson and Brown, 2012; Krawczynski et al., 2009; Lampkin, 2011; Leeson et al., 2012; Liang et al., 2012; Lüthje et al., 2006; McMillan et al., 2007; Sneed and Hamilton, 2007; Sundal et al., 2009; Fitzpatrick et al., 2013). Supraglacial streams are a dominant feature of the GrIS ablation zone and can deliver a constant supply of water to moulins during the melt season, thereby playing an important role in contributing water to the englacial and subglacial environments. Despite the importance of supraglacial streams in understanding ice sheet hydrology, they remain poorly studied due to the inadequate spatial resolutions of available satellite imagery and logistical difficulty in obtaining spatially varied in situ measurements of stream properties. Crucial to addressing the proportion of meltwater moving off the ice sheet is a review of the progress made in understanding the process of meltwater generation, retention, and export.

This paper summarizes the current understanding of the GrIS surface water hydrologic system, with an emphasis on recent findings and highlighting remaining gaps in knowledge. Supraglacial hydrology in particular is given the most thorough treatment as it is the area of research with the most to gain from new satellite data. There are a number of thorough reviews of glacial hydrology for various types of glaciers and for various components therein, including alpine glaciers (Fountain and Walder, 1998; Hooke, 1989; Hybbard and Nienow, 1997), polythermal glaciers (Irvine-Fynn et al., 2011a), water-filled englacial channels known as Röthlisberger channels (Walder, 2010), jökulhlaups (Björnsson, 2010; Roberts, 2005), glacier storage (Jansson et al., 2003), calving (van der Veen, 2002), subglacial water in ice sheets (Bell, 2008), and melt-induced influences on dynamics of the GrIS (Mair, 2012). None of these reviews focus uniquely on GrIS hydrology as a system, and the emphasis on the linkages between supraglacial and proglacial environments presented here, essentially a "snow-to-sea" approach, is particularly novel. A recent article argues for the importance of studying various components of the GrIS hydrology as a multi-scaled system (Rennermalm et al., 2013), and this review assesses the current state of knowledge of GrIS hydrology in a similar fashion with the following structure: (1) ice sheet surface meltwater production, (2) supraglacial storage and drainage, (3) englacial and subglacial networks and conduits, (4) ice dynamics, (5) proglacial environments, and (6) ocean interactions with meltwater runoff and outlet glaciers.

1.3 Ice sheet surface meltwater production

Melting of snow and ice, driven by the net flux of energy from the atmosphere to the ice sheet surface, primarily accounts for ablation of the GrIS. The ablation zone is where the ice sheet surface loses mass by the end of the year and generates meltwater runoff. Surface melt that occurs in the accumulation zone can infiltrate through snow and firn to either refreeze or possibly become runoff. Firn is snow that has survived for at least a year, an intermediate step between newly fallen unsaturated snow and glacier ice. The accumulation zone can be categorized into three typical glacier facies with varying hydrologic processes: 1) the dry snow zone where no melting occurs in the interior; 2) the percolation zone, where surface meltwater percolates into snow and firn before refreezing; and 3) the wet snow zone, where all the snow deposited since the previous summer has warmed to 0°C by the end of the melt season. In the lower wet snow zone, meltwater can pool into slush regions beneath the slush limit, the highest point from which mass escapes he glacier as flowing water (Figure 1-1; Cuffey and Paterson, 2010). Size and distribution of different facies are governed by elevation, seasonal progression, and annual variations in accumulation and melt extent.

Surface meltwater production is given by the energy balance at the ice sheet surface:

$$\begin{aligned} M &= SW_{\downarrow} + SW_{\uparrow} + LW_{\downarrow} + LW_{\uparrow} + SHF + LHF + G_S \\ &= SW_{\text{net}} + LW_{\text{net}} + SHF + LHF + G_S \qquad (1\text{-}1) \\ &= R_{\text{net}} + SHF + LHF + G_S \end{aligned}$$

where M is melt energy ($M = 0$ if surface temperature is less than 273.15 K), $SW_{\downarrow}$ and $SW_{\uparrow}$ are downward and upward shortwave radiation, $LW_{\downarrow}$ and $LW_{\uparrow}$ are downward and upward shortwave radiation, SHF is sensible heat flux, LHF is latent heat flux, G_S is subsurface conductive heat flux, and R_{net} is net radiation (van den Broeke et al., 2008). Albedo, the ratio of the upward to downward shortwave radiation, is an important modifier of the energy budget that varies widely temporally and spatially over the glacier surface, ranging from 0.1 for dirty ice to more than 0.9 for fresh snow (Cuffey and Paterson, 2010). Different surface mass balance models account for a in different ways, such as using an aging curve approach for the decreasing albedo of fresh snow (Hock, 2005), or formulating albedo as a linear function of both snow density and cloudiness (Ettema et al., 2010; Greuell and Konzelmann, 1994). The sensible heat and latent heat components are together called the turbulent fluxes, driven by temperature and moisture gradients as well as turbulence in the lower atmosphere. Ablation is primarily driven by net radiation, which is possibly greater than turbulent fluxes by a factor of three (Konzelmann and Braithwaite, 1995), except near the ice margin where turbulent sensible heat flux from the tundra becomes more important (van den Broeke et al., 2008). Though incoming solar energy dominates surface meltwater production in the ablation zone (van den Broeke et al., 2008), interannual variability in melt can be regionally partitioned within the ablation zone. A study on surface energy balance in southwestern Greenland for 2009 and 2010 (a record melt year) found that melt excess over between the two years in the upper ablation zone is due to both high temperatures and low albedo while melting in the lower ablation zone near the ice margin is accounted for by temperatures alone (van As et al., 2012). This suggests that expansion of bare ice area and associated albedo changes farther in the GrIS interior can play large role in meltwater production.

Melting of the snowpack increases snow grain size, in turn decreasing surface albedo, and further enhancing melting in a feedback mechanism, which has been demonstrated over 97% of the GrIS and can account for more than half of the overall increase in melting (Tedesco et al., 2011; Box et al., 2012). Decreased surface albedo, resulting from both the temperature-albedo feedback and the presence of dust, can enhance melting rates and increase runoff. As snow melts, the ice surface is exposed, and this darker ice surface has a lower albedo that increases the amount of solar energy absorbed, thereby further decreasing albedo through increased meltwater production. This feedback between meltwater accumulation and decreased albedo corresponds to a darkening of the GrIS surface in the late summer (Greuell, 2000). GrIS surface darkening is also strikingly visible as dark wavy bands seen in the western ablation zone (Figure 1-2; Wientjes et al., 2011) and also in the northeast (Bøggild et al. 2010). These bands are caused by seasonal melting of old ice revealing a surface layer of dust previously deposited higher on the ice sheet, with the pattern typical for the outcropping of stratified layers. Deposition of wind-blown dust can also contribute to this debris layer, but is a much smaller source (Wientjes et al., 2011).

The aggregation of dust particles can form clusters of sediment that enhance ice melt because of lowered albedo and create water-filled cryoconite holes (MacDonell and Fitzsimons, 2008). Studies in other polar regions find that the presence of cryoconite holes represent the transition between a melting ice cover common on temperate and polythermal glaciers and the frozen surface of the interior, with these features contributing to runoff as they grow and lose their isolation, joining in supraglacial stream networks (Fountain et al., 2004; Irvine-Fynn et al., 2011b). Microorganisms flourish in cryoconite holes as the interaction between the sediment and water creates a nutrient source, and as the organic matter has a high light absorbency, it further decreases albedo (Wientjes et al., 2011). These impurities significantly affect the albedo of the GrIS surface, with uniform dust layers showing albedos of ~0.3 and large cryoconite holes showing albedos of ~0.1 (Bøggild et al. 2010). The potential for dust and biotic factors to enhance melting via reduction in albedo is still an important unknown and will greatly affect modeled estimates of meltwater production (Stibal et al., 2012).

Complex firn processes of melting and refreezing govern the proportion of surface meltwater production that becomes meltwater runoff. As the melting season progresses, metamorphic processes transform firn into ice, thereby closing void spaces and turning permeable firn into a layer impermeable to water flow. Competing processes of pore refreezing from vertical flow and superimposed ice formation from refreezing of horizontal water flow both contribute to water storage (Bøggild et al. 2005; Humphrey et al. 2012). The percolation zone is a region of high interest for studying initiation of runoff, and is where much of the increased surface melt is occurring. While perennially covered by snow and firn, surface meltwater can penetrate depths of 10 m or more of cold firn and can persist for many months to either refreeze or migrate down glacier to become runoff (Humphrey et al., 2012). Generally, water at higher elevations percolating into underlying subfreezing firn will refreeze, releasing latent heat and raising the temperature of the firn to the point where meltwater can start to percolate and drain freely. Below the ELA, firn that becomes superimposed ice is thus melted twice before running off. If this is not accounted for in modeling the energy expenditure on the surface, models will show much more water leaving the system than actually is actually observed (Cuffey and Paterson, 2010).

Another aspect of meltwater retention is firn densification, which reduces firn volume but increases its density, and increases with time and depth. This process is mainly controlled by meltwater refreezing that intensifies with both increasing mean annual temperature and accumulation rate (Braithwaite and Laternser 1994; Hörhold et al. 2011). Field studies have found considerable meltwater infiltration contributing to densification in the percolation zone (Brown et al., 2012), and modeling shows highest possible retention in the lower percolation zone and the wet snow zone near the ELA (Fausto et al., 2009). Translating short-term elevation changes into mass changes can be misleading without accounting for densification

(Reeh, 2008), and future predictions of sea level rise can overestimate levels by 5 cm over 150 years without incorporating refreezing process (Pfeffer and Meier, 1991).

While meltwater percolation and refreezing can release heat to warm the surrounding snow and firn at the beginning of the melt season, meltwater may also cause a sustained warming on ice temperatures when it does not completely refreeze during the winter, in a process known as cryo-hydrologic warming (Phillips et al., 2010). This provides a mechanism for rapid thermal response of the GrIS to climate warming. Phillips et al. (2013) included this mechanism in their model of ice velocity and showed that increased velocities in the southern Greenland inland wet snow zone over 2001-2007 matched observations better than with no cryo-hydrologic warming built in. This ice speedup is due to an increase in the extent of basal sliding permitted by temperate bed conditions (Phillips et al., 2013), which adds another mechanism by which a warming climate may affect ice dynamics.

1.4 Supraglacial storage and drainage

Surface meltwater generated at the beginning of the melt season percolates through snow and firn to refreeze at depth. This process of percolation and refreezing increases the rate of transformation from the surrounding snow and firn to ice, and gradually forms a saturated firn layer. Low relief areas accumulating meltwater when thin firn saturates to the surface forms slush zones and supraglacial lakes. This water storage may feed arborescent stream networks as channels incise and connect, representing a change from a system dominated by water percolation to a system dominated by channelized stream flow, punctuated by ponding lakes and drainage into the ice sheet through fractures and moulins (Figure 1-1). Satellite images show the western ablation zone littered with supraglacial melt ponds and dense networks of streams developing throughout the melt season (Figure 1-3). While the role of supraglacial lakes and streams as temporary storage for meltwater is important for diurnal and seasonal hydrologic cycles, sudden drainage of lakes and streamflow through cracks and moulins play an important role in rapidly transporting meltwater into the GrIS. Understanding the spatial distribution and seasonal progression of these hydrologic features is an ongoing process of mapping and modeling with increasingly finer resolutions and greater spatial coverage, allowing for a broader understanding of ice sheet-wide reactions to increased melting.

1.4.1 Supraglacial lakes

Meltwater can pond in depressions over impermeable ice or dense firn to establish supraglacial lakes that appear over multiple years in the same locations and can inject large amounts of meltwater into the ice sheet through fast drainage events. Supraglacial lakes tend to reform in the same locations over the lower ablation zone from year to year, with seasonal progression showing lake formation at progressively higher elevations as well as increasing lake drainage frequency in lower elevations. Numerous studies have mapped the occurrence and seasonal evolution of lakes in various regions, with the high temporal resolution of MODIS playing a pivotal role in examining lake dynamics (Fitzpatrick et al., 2013; Selmes et al., 2011; Box and Ski, 2007; Liang et al., 2012; Sundal et al., 2009; Leeson et al., 2012; Chu et al., 2009). These studies have shown that lake location and area are driven by time of season, elevation, and topography (Lüthje et al., 2006): numerous small lakes cluster in low elevations near the margin (but above crevasse fields), large lakes less clustered that form in the same locations over multiple years at higher elevations (~1000 – 1200 m) and are less clustered, and sparse underdeveloped lakes form above ~1200 m (Lampkin, 2011; Liang et al., 2012). Since lake area is more controlled by topography than melt rate, lake development will likely accelerate in a warmer climate because of melting at higher elevations where surface slopes are small (Lüthje et al., 2006). Tracking seasonal and annual lake development and drainage, especially in the context of a warming climate, is crucial for assessing lake importance for storage and transport of meltwater into the ice sheet.

Interest in supraglacial lakes has been particularly high since 2006, with numerous studies on the distribution and drainage of lakes showing their importance in delivering large quantities of meltwater to the englacial and subglacial systems, causing short-term velocity changes and sustained uplift (Das et al., 2008; Hoffman et al., 2011; Box and Ski, 2007; Bartholomew et al., 2011a; Doyle et al., 2013). Das et al. (2008) provided the first known observation of a meltwater pathway through thick, cold ice, showing that a lake emptying with a drainage rate of 8700 m^3/s resulted in uplift and ice velocity increases within 24 hours. Additionally, Doyle et al. (2013) showed that horizontal ice motion during rapid lake drainage is dominated by ice tectonic deformation related to the opening and closing of multiple fractures. In a study tracking lake area in three regions (southwest, north, and northeast), Sundal et al. (2009) found a high correlation between annual peak total lake area and modeled annual runoff. However, Selmes et al. (2011) also tracked rapidly draining lakes for the entire GrIS and showed an inverse relationship between the occurrence of rapid drainages and regional mass loss, indicating that dynamic mass losses in the southeast and northwest have little to do with rapid lake drainages (Figure 1-4). For example, the southeast has relatively few, small lakes, yet exhibits significant mass loss, possibly explained by steep slopes (Selmes et al., 2011; Sundal et al., 2009). These studies have advanced our knowledge of supraglacial lakes as a mechanism for rapid response to surface meltwater changes that increase short-term ice velocities through decreased basal friction, discussed further in section 5.

Assessing the potential storage or influx of meltwater into the ice sheet through rapid drainage requires modeling lake depth and volume. Algorithms range from physically-based retrievals of lake bathymetry (Tedesco and Steiner, 2011; Sneed and Hamilton, 2007;

Georgiou et al., 2009; McMillan et al., 2007) to empirical models relating remotely sensed reflectance to depth (Box and Ski, 2007; Fitzpatrick et al., 2013). Lake bottom melting rates are also controlled by albedo, and because a positive feedback from increased water depth reduces lake surface albedo and increases shortwave radiation absorption. The ablation beneath lakes is estimated to be ~100-116% greater than the nearby bare ice from in situ measurements (Tedesco et al., 2012) and ~110-170% from models (Lüthje et al., 2006). Typical assumptions of a homogenous ice substrate and therefore uniform bottom albedo within a lake and for all lakes (Sneed and Hamilton, 2007) have been shown to be very limiting due to the presence of dark cryoconite (Tedesco and Steiner, 2011), and is a caveat of many reflectance-depth parameterizations (Box and Ski, 2007).

To understand how much water is necessary to initiate the process of lake drainage, studies have found that lake diameters between 0.25 and 0.8 km (Krawczynski et al., 2009) and lake volumes of at least 31.5 x 10^6 m^3 (Box and Ski, 2007) contain sufficient water to hydrofracture through ice. However, this does not indicate that there exists a critical lake volume threshold to initiate rapid drainage, and Fitzpatrick et al. (2013) found that lake size does not influence its drainage mechanism.

1.4.2 Supraglacial streams

The understanding of supraglacial streams presented in this section primarily originates from studies of glaciers, as limited research has occurred on streams of the GrIS. Supraglacial streams form when meltwater incises surface channels once thermal erosion exceeds surface ablation. From early season ponding of water in lakes and slush, meltwater in areas of higher slope drains down-glacier through the snowpack, forming rills that combine into channels and progressing towards more efficient transport in an arborescent network as more ice is exposed and channels are enlarged (Cuffey and Paterson, 2010). Contributions to stream runoff include flows from saturated slush and channel erosion, precipitation, surface melting, and spillover from water-filled moulins, crevasses, and supraglacial lakes (Marston, 1983). Factors distinguishing supraglacial streams from terrestrial streams are the lack of available sediment, rapid form adjustment, and thermal and frictional melting of a channel that add to its discharge (Knighton, 1981). Particularly unique is the fact that discharge rapidly increases downstream due to both inflow from tributaries and melting of the channel, but is also shows highly variable because of complex drainage patterns and seepage from streams not deeply incised (Knighton, 1981).

The dependence on ice and snow melt allows stream discharge to show a very pronounced diurnal cycle compared to terrestrial streams, with a rapid decline in streamflow at low sun angles (Knighton, 1985; Knighton, 1972; Ferguson, 1973). High discharge in the beginning of the melting season can prompt meanders to develop as well as modify existing channels (Ferguson, 1973), but if channels survive for more than a year, discharge may not be as important in channel morphology (Hambrey, 1977). Streams are either annual, forming each year, or perennial, re-forming in the same channels over multiple years (McGrath et al., 2011). Perennial streams are typically large and incised streams that are covered in snow bridges at the beginning of the melt season with a main trunk width of ~1 – 30 m (Yang and Smith, 2013; Knighton, 1981). While supraglacial streams are unique in carrying little or no sediment load on surfaces without debris (the glacier margin is an exception), streams do carry an ice load that could influence flow behavior, but very little research has been conducted on its effects (Knighton, 1985).

Stream formation is initiated when down-cutting by surface channels exceeds surface ablation rates. Channel incision is driven mostly by thermal erosion, but 25 – 50% is forced by shortwave radiation and sensible heat flux, with stream temperatures as low as 0.005 – 0.01°C able to incise channels at rates of 3.8 – 5.8 cm/day (Marston, 1983). The main parameters that drive channel incision rates are temperature loss to the ice, meltwater discharge, and channel slope (Jarosch and Gudmundsson, 2012). A theoretical treatment of channel incision rate for water-filled channels with round cross-sections is shown in Isenko et al. (2005) as:

$$\frac{dr}{dt} = \frac{B}{q\rho_i}\frac{Q}{\pi r^2}\Delta T \tag{1-2}$$

where *dr* is the thickness of melted ice, *B* equals $2.64\text{x}10^3$ J/m^3/K for turbulent flow at 0°C, *q* is the latent heat of melting ($3.35\text{x}10^5$ J/kg, ρ_i is the ice density, *Q* is discharge, *r* is the channel radius (of the round cross-section), and *T* is temperature. This formulation focuses on changes in incision rate due to changes in temperature. Another estimate of incision rate of supraglacial channels is presented in Fountain and Walder (1998):

$$\frac{dr}{dt} = \frac{1}{2}\left(\frac{\pi}{2\eta}\right)^{\frac{3}{8}}\left(\frac{g\rho_w}{q\rho_i}\right)S^{\frac{19}{16}}Q^{\frac{5}{8}} \tag{1-3}$$

where η is Manning's roughness (0.01 s/m$^{1/3}$ for ice), ρ_w is the water density, *S* is slope. This treatment does not take into account ice deformation and vertical ice motion, but calculations using typical glacier values for η and *S* show that incision rates are proportional to $Q^{0.6}$ (Fountain and Walder, 1998).

Hydraulic geometry is an empirical theory linking changes in width (*w*), depth (*d*), and velocity (*v*) both downstream and at cross-sections to discharge (*Q*) (e.g., Kostrzewski and Zwolinski, 1995; Leopold and Maddock, 1953):

$$w = aQ^b, d = cQ^f, v = kQ^m \tag{1-4}$$

where $a \times c \times k = 1$ and $b + f + m = 1$ at cross-sections. While Equation 1-4 also applies to downstream discharge variations, the coefficients and exponents will be different for points in a downstream direction from those for a given cross-section (Leopold and Maddock, 1953). For supraglacial streams, velocity has been shown to have the highest rate of change with discharge, driven by both steep slopes and relatively low resistance from smooth stream beds (Knighton, 1981; Brykala, 1999; Marston, 1983). Hydraulic geometry exponents represent sensitivity of parameters to changes in discharge, and also show higher rates of change for depth than for width, indicating that channel beds are more easily eroded than channel banks (Marston, 1983).

The majority of studies conducting extensive supraglacial field measurements over time outside the GrIS focus on meandering tendency and channel incision, comparing them to alluvial streams (Hambrey, 1977). Despite differences from alluvial streams, particularly the ability to rapidly adjust stream form and the lack of sediment load, Knighton (1972) found a general similarity between the form of meanders developed in alluvial valleys and on ice, indicating the larger importance of hydrodynamics in meander formation. This is echoed by Parker (1975), showing that while hydrodynamic considerations alone cannot produce meandering in alluvial rivers without sediment transport, meandering in supraglacial streams can occur as long as flow is supercritical. Straight channels are restricted to areas with strong structural control from cracks and crevasses or very steep glacier slopes (Marston 1983). Channel roughness in supraglacial streams, indicated by Manning's n, is generally lower compared to terrestrial streams, but the wide range of values (0.14 – 0.39; Kostrzewski and Zwolinski, 1995; Marston, 1983) calls into question the characterization of supraglacial streams as homogeneous and smooth, specifically with a Manning's n value of 0.01 typically used for modeling supraglacial stream flow (Irvine-Fynn et al., 2011a).

Understanding stream processes on the GrIS has not been a priority in remote sensing or field studies until very recently. While there are numerous field studies of supraglacial streams on Arctic glaciers (Dozier, 1976; Knighton, 1972; Marston, 1983) or in the laboratory (Isenko et al., 2005), very few exist for the GrIS. McGrath et al. (2011) provide a detailed study of one moulin-drained stream catchment in the Sermeq Avannarleq region of western Greenland, with a main stream of 1-4 m in width, 1-6 m in depth, and incision rate of 3.3±0.47 cm/day over the 15 day study period in August 2009. In modeling the mass budget of the basin, moulin drainage was found to comprise 52% of the total water output (McGrath et al., 2011). Small-scale field studies like this are crucial for understanding meltwater transport processes and fluxes. Mappings of supraglacial streams have not been attempted until recently due to the limitations in satellite spatial resolutions. Recent availability of high-resolution commercial satellite imagery, such as WorldView-2 (~2 m multispectral resolution), over the western GrIS allows mapping streams networks with widths varying between a meter to tens of meters (Yang and Smith, 2013). As more data become available, providing wider spatial and higher temporal coverage, automated methods to delineate streams will be required (Yang and Smith, 2012) due to the time intensity of manually delineating dense stream networks, which has only been done for small study areas (Colgan, et al., 2011b; McGrath et al., 2011).

1.4.3 Crevasses and moulins

Crevasses and moulins connect the supraglacial and englacial environments, providing pathways for surface water to drain into the ice sheet when intersecting streams and lakes. Crevasses are fractures formed from tension, and their patterns are controlled by the directions of the principal stresses, opening in the direction of maximum tension which is typically perpendicular to a glacier's longitudinal stress field (Cuffey and Paterson, 2010; Colgan et al., 2011b; van der Veen, 1998). Ice movement then can rotate and bend crevasses depending on velocity gradients. For example, Colgan et al. (2011b) found that crevasse fields near Jakobshavn Isbrae have rotated 45% between 1985 and 2009, possibly due to an acceleration of the glacier that has increased southbound flow at the expense of westbound flow in the area. The study also found a 13% increase in crevasse extent, proposing that the changes in extent and orientation are due to overall thinning and steepening of the western ablation area.

Crevasse fields are abundant in the lower ablation zone and allow for a spatially distributed drainage of meltwater into englacial channels, with drainage rates highly correlated with areal extent (Lampkin et al., 2013). McGrath et al. (2011) found that crevasse drainage accounted for 48% of total meltwater output from a moulin-drained basin at a rate of (1.40±1.13) x 10^4 m^3 d^{-1}, and showed that crevasses dampened the diurnal cycle of meltwater input. This translates to a slower and steadier discharge over the short-term compared to rapid meltwater injection from moulins, which has consequences for ice dynamics (McGrath et al., 2011). Since most observations of ice uplift and increased velocity are in response to discrete meltwater from either rapid lake drainage through moulins or short-term melt pulses (Bartholomew et al., 2012; Zwally et al., 2002; Das et al., 2008), crevasse-dominated drainage may not result in a similar response. Slower drainage into the englacial and subglacial environments may allow for efficient adjustment of meltwater input, rather than basal sliding from overwhelmed subglacial conduits.

In contrast to the spatially distributed, slower meltwater drainage through crevasse fields, moulins provide rapid, near-vertical drainage of larger upstream areas of surface meltwater into englacial and subglacial systems (McGrath et al., 2011). A crevasse that opens across a supraglacial stream can propagate down to intersect englacial channels, and when the water-filled crevasse closes as it is advected into an area of compression, the energy in the meltwater can keep a pathway open and enlarge it into a moulin; in other words, crevasses precondition the ice for moulin formation (Holmlund, 1988). Moulins are also created from episodic supraglacial lake drainages, with fractures beneath lakes possibly breaching the full ice thickness (Das et al., 2008), but are less common (Phillips et al., 2011). In fact, a strong correlation between modeled moulin locations and elevated along-flow tension (which produces crevasse fields) rather than supraglacial lake location shows that moulins are more commonly formed through stream intersection with crevasses rather than forming underneath lakes (Catania et al., 2008). New crevasses can intersect supraglacial streams upstream of existing moulins to form new moulins, and this can occur near-annually, leaving a string of moulins with increasing ages going down-glacier (Holmlund, 1988; McGrath et al., 2011). While modeled crevasse drainage shows dampened diurnal variations, slower transfer times (representing sustained meltwater input), and low meltwater drainage per crevasse, moulins allow for rapid pulses of meltwater draining a large, well-developed catchment (McGrath et al., 2011; Colgan et al., 2011b). This elevates the importance of moulins as an immediate and relatively un-dampened transfer of water into the ice sheet with a potential to overwhelm the subglacial hydrologic system to cause uplift and increase basal sliding.

Repeat aerial photography and high-resolution satellite imagery are useful in conjunction with digital elevation models (DEM) for tracking crevasse and moulin distributions. Mapped crevasses between 1985 and 2009 in the western ablation zone showed high positional stability as well as little overlap between crevasse fields and areas with supraglacial lakes and streams (Colgan et al., 2011b). Moulin distribution in the same area was modeled using slope, elevation, and aspect, and validated with locations from the field and from high-resolution imagery, showing that moulins occurred with interannual locational stability, between 300 m a.s.l. and 800 m a.s.l. elevation and a density of ~12/km^2 (Phillips et al., 2011). Using ice-penetrating radar to monitor moulin properties, Catania and Neumann (2010) found that moulins persist for multiple years (average ~11 years) and drain the volumetric equivalent of multiple lakes per year, possibly contributing to an established network of englacial channels.

1.5 Englacial and subglacial drainage

Englacial conduits fed by meltwater from crevasses and moulins connect the supraglacial environment to the subglacial network. Similar to the research on supraglacial streams, much of the theory presented here are from studies of other Arctic and temperate glaciers. Supraglacial stream incision and subsequent roof closure by ice deformation has been proposed as a possible mechanism for englacial conduit formation, called cut and closure (Gulley et al., 2009a). Fountain and Walder (1998) describe this process, whereby surface channels melt down into the ice very quickly as they steepen, then they will reach a point where the steam is so deeply incised that the overlying ice can close above the channel, forming a tunnel. This tunnel, which still has a water source, can continue to deepen and steepen until hitting the bed of an over-deepened basin, which is a topographical depression in the bedrock where a lake would likely form if there was no ice above it. At this point, the channel slope will decrease because the frictional energy of the water can only deepen up-glacier of the bedrock. Finally, a stable channel is established when channel wall melt rates balance ice deformation closure rates.

The theory behind channelized englacial flow was developed by Röthlisberger (1972) and Shreve (1972), establishing that englacial conduits are sustained when meltwater enlargement overcomes the tendency for closure from the inward creep of ice. Their papers also discussed whether englacial networks are fast drainage systems composed of large tunnels or a slow drainage system with a distributed network of linked cavities (Figure 1-5; Fountain and Walder, 1998; Hooke, 1989). The term Röthlisberger-channel (R-channel) flow has come to represent the physical model of conduit flow through large channels (Röthlisberger, 1972), with conservation of energy describing the balance between a source (frictional dissipation of energy in flowing water) and two sinks (energy absorbed by water and energy that melts ice walls), and conservation of momentum described as the relationship between discharge, channel size, and hydraulic gradient (Walder, 2010).

Shreve (1972) concluded that the englacial system is an arborescent network of fast flow (consistent with R-channels), likening them to supraglacial channel networks (Irvine-Fynn et al., 2011a; Walder, 2010). Additionally, dye-tracing experiments have shown that there is a rapid transition from distributed to channelized drainage in parts of the drainage system closed by ice deformation in winter (Cowton et al., 2013). However, field studies have shown that these theoretical models of conduit flow may not conform to reality. Boreholes drilled in Storglaciaren, Sweden predominantely intersect hydraulically connected englacial fracture-like features that are smaller, and with slower water velocities, than traditional conduits, suggesting that englacial water is transported through an interconnected network of fractures rather than large conduits (Fountain et al., 2005). Further field studies are needed to modify theoretical models of englacial drainage.

Englacial conduits can only exist if the tendency for closure, from the inward creep of ice, is balanced by channel enlargement from the energy dissipated by moving meltwater (Fountain and Walder, 1998). While crevasse and moulin propagation can occur without being water-filled as long as the tensile stresses are higher than the ice-overburden stresses, the presence of water allows for more efficient propagation through hydrofracturing. The rate of hydrofracture propagation, u, is controlled by inflow, where a large amount of discharge is needed to maintain water pressure to continue the fracture process (Alley et al., 2005):

$$u = \frac{QM}{-4\sigma_{\tau}' d_f \vartheta} \tag{1-5}$$

Equation 1-5 describes deepening velocity, u, where Q is discharge, $M = 5\text{x}10^{9}$ Pa, d_f is fracture depth, $\vartheta = 8\text{x}10^{-3}$Pa/s, and σ_{τ}' is longitudinal crack-forming deviatoric stress. Colgan et al. (2011b) apply a crevasse propagation model from van der Veen (1998) and find that ice thinning and steeper surface slopes both enhance crevasse propagation. Furthermore, numerous modeling studies show that water in crevasses significantly increases propagation englacially (van der Veen, 1998; Benn et al., 2009). Moulins are maintained by meltwater flowing through them, where frictional dissipation converts potential energy to heat; crevasses otherwise could not propagate to greater depths without being sustained by meltwater. An approximation of fracture penetration depth from van der Veen (2007) shows that it is mainly dominated by the meltwater flux into the fracture/crevasse:

$$d_f \approx (\frac{p_w}{p_i})^{2/3} Qt \tag{1-6}$$

where p_w is water pressure, p_i is ice-overburden pressure, and t is time, and refreezing is not included. Surveys of englacial conduits in various glacial environments show that conduits can only penetrate through thick ice to the bed when intersected by supraglacial water features (Gulley et al., 2009b). Since water flux is more important for propagation than tensile stress, supraglacial lakes and streams become important sources and links for increasing fracture depths to the bed.

High-volume water flow from supraglacial lake drainages and streamflow into moulins can increase pressures and sustain englacial conduits. Lake drainages may be able to drive hydrofractures through thick, cold ice (~980 km thickness, Das et al. 2008), but large volumes of water are needed for meltwater to penetrate to the bed (Krawczynski et al., 2009). Krawczynski et al. (2009) modeled the water volume and crack geometry necessary to drive cracks through 1 – 1.5 km of subfreezing ice, and found that lakes larger than ~0.25 km in diameter are sufficient for hydrofracturing. As a large majority of lakes along the western margin of Greenland larger than this threshold, therefore there is great potential for rapid transport of water to the bed (Selmes et al., 2011). Dissipation of frictional energy from flowing meltwater converts potential energy to heat such that crevasses and moulins can be maintained and propagated to greater depths. Without continued meltwater input, refreezing and plugging off water at the base of moulins and englacial channels reduce probability of further downward water propagation (Boon and Sharp, 2003).

Subglacial drainage organization is largely inferred from observations of ice velocity changes in response to seasonal melt input, indicating a seasonal switch from linked cavities to channel-dominated subglacial drainage (Schoof, 2010; Sundal et al., 2011; Bartholomew, et al., 2011b; Chandler et al., 2013). Indeed, subglacial drainage systems take on two stable organizations: one of slow flow through linked cavities and another of fast flow through large channels (Kamb, 1987; Bell, 2008). Larger channels will tend to grow at the expense of smaller ones, and linked cavities will coalesce into a less complicated network with fewer, larger conduits (Figure 1-5a; Hock and Hooke, 1993). However, a sustained water source is needed in order for water pressure to overcome ice-overburden pressure, similar to englacial channels. Measurements of subglacial drainage are highly limited, with only a handful of borehole studies assessing distribution and monitoring networks at a process level. Borehole measurements have shown basal water pressure to be 95% of the ice-overburden pressure, and small changes in basal water pressure can account for almost 40% of a glacier speedup (Sugiyama et al., 2011). Field studies also show that basal crevasses can extend many tens of meters above the bed, enabling them to possibly modulate basal water pressure (Harper et al., 2010).

In contrast to channel development in the englacial environment, channels in the subglacial environment are affected by a debris layer on the bedrock, providing obstacles to flow, and friction between sediment and bedrock. Channels can incise into the bedrock with permeable bed sediments, but hydraulic conductivity is low because of melting under pressure (Fountain and Walder, 1998). Subglacial erosion, measured from sediment fluxes derived from meltwater exiting outlet glaciers, also provides an indicator of surface meltwater contact with the bed. Measurements of subglacial erosion are limited for the GrIS, and previous estimates of ~0.01 mm/yr from east Greenland (Andrews et al., 1994) are low compared to ~0.1-10 mm/yr from temperature glaciers (Hallet et al., 1996). However, recent estimates of subglacial erosion rates in west Greenland were found to be 1.6-2.7 mm/yr, a significant increase over previous estimates and suggesting that where surface meltwaters are able to access the bed, the rate of erosion by ice sheets is comparable to rapid erosion observed at temperate alpine glaciers (Cowton et al., 2012). Efficiency of both englacial and subglacial drainage networks are important unknowns affecting the response of ice dynamics to increased meltwater drainage.

1.6 Ice dynamics

Dynamic changes refer to increased ice sheet and outlet glacier velocities that can increase calving, retreat, and thinning, which in turn can increase melting as the ice moves to lower elevations with higher temperatures. A main mechanism for GrIS surface meltwater to influence ice dynamics is when meltwater penetrates to the bed and causes basal sliding and short-term ice velocity speedups. This is one of the greatest concerns for future scenarios of climate change and understanding the GrIS's contributions to sea level rise, because the possibly non-linear relationship between increased melting and dynamic changes is not given proper treatment in current ice dynamics models (Meehl et al., 2007). The greatest difficulty in assessing current hypotheses of outlet glacier response to increased meltwater input is the lack of field data for training models. While the availability of satellite data allowing for estimates of outlet glacier and ice sheet velocities (e.g., Joughin et al. 2010; Moon et al. 2012), questions still remain about the processes driving these velocity changes.

1.6.1 Outlet glacier velocity changes and peripheral thinning

Changes in outlet glacier velocities and calving rates are a main contributor to the increasing ice mass losses. Outlet glaciers have shown increases in total ice discharge (Rignot, 2004; Howat et al., 2007) as well as velocity (Rignot and Kanagaratnam, 2006), with velocity speedups recently extending to the northwest (Khan et al., 2010). These dynamic changes to outlet glaciers and the ice sheet margin are the primary concern for modeling reasonable projections of future mass losses because of their unstable nature and possible feedbacks from increasing meltwater input.

Dynamic thinning of both fast moving outlet glaciers and the general ice sheet periphery is tied directly and indirectly into mass loss. Thinning brings the ice surface to lower elevations with higher temperatures, contributing to a feedback of enhanced melting. Losses are exponentially higher at the margin (van den Broeke et al., 2008) due to rapid thinning of near-coastal outlet glaciers (Krabill, 2004; Sole et al., 2011; Pritchard et al., 2009; Thomas et al., 2009; Csatho et al., 2008). Tracking the ice-front position of Jakobshavn Isbrae to before the satellite era shows intermittent thinning (Thomas, 2004) and periods of ice front retreat. Dynamics of marine-terminating glaciers are highly sensitive to glacier width and bed topography, with wider glaciers grounded over deeper basal depressions tending to be closer to floatation and less sensitive to retreat from thinning (Enderlin et al., 2013). For outlet glaciers with extensive floating tongues, ocean interactions may be more important in driving dynamic changes (See section 7.2).

Velocity changes have shown complex spatial patterns over the last decade, with distinct variations between land-terminating glaciers and marine-terminating glaciers. Sole et al. (2008) found that land-terminating glacial outlets have thinning rates comparable to ablation rates, but marine-terminating glacial outlets experience much higher rates of thinning. Similar results in Pritchard et al. (2009) showed that fast-flowing areas thin more rapidly than slow-flowing areas, particularly in the two areas experiencing highest mass losses: the northwest and southeast. This suggests that thinning of land-terminating glaciers is primarily driven by temperatures, while marine-terminating glaciers are more susceptible to dynamic thinning from changes at the calving front (Sole et al., 2008). Modeling studies, even combined with remote sensing observations, are limited by coarse resolutions and broad scale, making them inadequate for resolving complex behaviors of individual glacier outlets. For example, the scale of most outlet glaciers is small (<5 km width) compared to most model resolutions, and means that models cannot accurately represent location topography, fjord water circulation, terminus sea ice, or local climatic variations (Moon et al., 2012).

1.6.2 Response of ice dynamics to inputs of supraglacial meltwater

Increased meltwater inputs to the ice sheet through surface melting and supraglacial lake drainages have been linked to rapid changes in ice dynamics. Both fast moving outlet glaciers (Joughin et al., 1996; Andersen et al., 2010; Joughin et al., 2008a) and the slower moving ice sheet (Zwally et al., 2002; Joughin et al., 2008b; van de Wal et al., 2008; Palmer et al., 2011; Bartholomew et al., 2012; Shepherd et al., 2009) have shown short-term seasonal speedups in response to enhanced melting or discrete meltwater pulses from lake drainages. Under future warming scenarios, models suggest enhanced sensitivity of ice sheet movement in response to high melting, retreat, and thinning (Parizek and Alley, 2004).

However, other recent studies have alternately hypothesized that basal sliding will not simply increase with more meltwater input despite sensitivity to discrete meltwater pulses. Schoof (2010) modeled subglacial conduit formation and closure in response to meltwater flow and found that water input variability, not just mean input, was the primary driver of short-term glacier velocity increases. This suggests that discrete and rapid meltwater input changes are necessary to trigger a dynamic response, such as those inputs derived from large supraglacial lake drainages or a particularly enhanced diurnal melt cycle (Schoof, 2010; Selmes et al., 2011). Sundal et al. (2011) echoed this argument and found peak velocities positively correlated to melting, yet also found that glaciers slow down after a velocity threshold of 1.4 cm/day is exceeded and that overall speedups over the second half of the summer are 62% slower in warmer years. This slowing effect is not expected if basal lubrication is the primary mechanism by which meltwater interacts with ice dynamics, but instead fits the model of subglacial drainage becoming more efficient, switching from linked cavity to channel drainage systems and reducing melt-induced speedups (Sundal et al., 2011). This hypothesis of decreased basal sliding and efficient subglacial drainage with more meltwater input support observations of decreasing mean annual velocities (Colgan et al., 2011b; van de Wal et al., 2008), even with melt-induced acceleration from discrete meltwater pulses. Furthermore, observations of discrete melt inputs from supraglacial lake drainages show speedups lasting for ~1 day, if detected at all, suggesting that even with perturbation of the subglacial environment the system can drain large volumes of water relatively efficiently (Hoffman et al., 2011). Observations also show that longitudinal coupling is not observed at distances greater than 10 km (Bartholomew et al., 2010), with outlet glacier sensitivity to variations in meltwater input decreasing exponentially with distance from the calving front (Andersen et al., 2011).

The seasonal progression of GrIS dynamic changes in response to meltwater variability illustrates both cases of inefficient and efficient drainage. Basal sliding through meltwater lubrication can be thought of as a special case linking ice sheet dynamic changes to englacial and subglacial drainage organization, where conduits are not as developed and inefficient at draining large volumes of meltwater. This concept of the englacial and subglacial system is representative of the beginning of the melt season, where the first wave of high meltwater input rates can overwhelm the subglacial water pressure and cause a rapid response in glacier uplift and movement. Velocities increase when subglacial water storage increases enough to pressurize conduits and cause basal sliding (Bartholomaus et al., 2008). The seasonal progression of meltwater influx aids in the evolution of efficient channelized englacial and subglacial environments. Sustained meltwater inputs enlarge conduits and connect networks to a point where meltwater is efficiently drained through the system without overwhelming it. At this point, sudden large increases in meltwater input can be diffused more easily into higher subglacial discharge and offset with further conduit enlargement, but could still cause speedup by overwhelming the subglacial capacity if meltwater input is very large. Meltwater inputs decrease as the melt season draws to a close, and in conjunction with the now efficient subglacial system, resulting in lower basal water pressures and a gradual slowdown (Bartholomew et al., 2010; Lüthi, 2010; Schoof, 2010). Therefore, while discrete meltwater pulses can cause short-term changes in ice velocity and uplift, future warming scenarios mainly focus on longer summer melting seasons and warmer temperatures which may not affect ice dynamics as much if the englacial and subglacial systems can efficiently evacuate that meltwater from the GrIS to rivers and/or fjords of the proglacial zone.

1.7 Proglacial environments

The GrIS proglacial hydrologic environment consists of rivers and lakes draining the ice margin as well as non-glacially influenced river and lakes formed from snowmelt and precipitation (Figure 1-1). Of the 434 proglacial meltwater outlets from land-terminating portions of the ice sheet, 75% exit through rivers into fjords and 25% end in lakes (Lewis and Smith, 2009). Some proglacial lakes function as reservoirs dammed by the ice sheet edge, and occasionally drain catastrophically in events referred to as jökulhlaups (Roberts, 2005). The hundreds of coastal fjords around Greenland also include ~400 possible meltwater outlets from marine-terminating glaciers (Lewis and Smith, 2009). Because these outlets are typically subglacial, their number cannot be determined with certainty. Both land-terminating and marine-terminating glacier environments reveal meltwater export through buoyant plumes of sediment in fjords, discussed in section 7.1. The southwest margin contains the largest proglacial region, a ~1,000 km long section rich in braided rivers formed from high sediment loads. Suspended sediment load changes signify meltwater export from the ice sheet, with meltwater gathering fine sediments from glacier erosion as well as from fluvial and aeolian erosion. Terrestrial river time series of discharge are particularly useful for calibrating and validating surface mass balance models (Mernild et al., 2011b; van As et al., 2012), providing information about seasonal development of the supra- and subglacial drainage systems (Palmer et al., 2011; Bhatia et al., 2011; Bartholomew, et al., 2011b), and potentially capturing jökulhlaups (Russell et al. 2011).

1.7.1 Jökulhlaups

Jökulhlaups are sudden releases of meltwater originating from water impounded by or stored within a glacier that result in significant increases in discharge lasting minutes to several weeks (Roberts, 2005; Cuffey and Paterson, 2010). These floods occur because of the positive feedback between melt and the ability of drainage paths to convey water. Discharge increases melt through frictional heating and this increased melting enlarges channels and further increases discharge until a significant depletion of volume or pressure of the source water occurs (Cuffey and Paterson, 2010). There are generally two main processes that drive ice-dammed and subglacial lake drainage. Drainage may begin by expanding already existing conduits in a slow process where the water pressure remains lower than ice-overburden pressure at the dam, or it may be initiated by increasingly high lake levels that can bring the ice dam into flotation and open up a gap for water flow (Björnsson, 2010; Roberts, 2005).

An ice-dammed lake near Kangerlussuaq in southwest Greenland has experienced successive drainage events from 2007-2012, following 20 years of stability (Russell et al., 2011). A catastrophic drainage in August of 2007 (Mernild, 2008) reinstated a regime of fairly consistent late summer drainage up to the latest even in August of 2012 (Figure 1-6). The proximity to Kangerlussuaq and its logistical support base allows a unique opportunity for detailed field studies of controls on jökulhlaup magnitude and frequency. Detailed assessments of local processes suggest that onset of this new cycle of ice-dammed lake drainages is caused by ice-margin changes in advance/retreat as well as ice thickness and a hydrologic response to lowered mass balance (Russell et al., 2011; Russell, 2009). While peak jökulhlaup discharge in this system is primarily controlled by lake volume (Roberts, 2005; Tweed and Russell, 1999), Russell et al. (2011) study finds that peak discharge is much higher than predicted in models because of an unusually short englacial/subglacial pathway. Furthermore, a feedback of glacier advance after the lake drainage produces lower discharge with each successive drainage (Russell et al., 2011). This is illustrated with the second drainage in 2008 occurring when the lake was not full, indicating different trigger mechanisms or a weakened ice dam (Mernild and Hasholt, 2009). Though jökulhlaups are most often studied in the field, Larsen et al. (2013) showed that potential jökulhlaup lakes in Greenland can be identified through remote sensing of lake surface area and analysis of temporal anomalies in surface area.

1.7.2 River discharge

Monitoring discharge from streams and rivers draining the GrIS allows for not only assessing actual meltwater losses but also for inferring englacial/subglacial drainage network organization. Proglacial runoff measurements integrate a variety of drivers, such as surface melt rate and transport and meltwater transport through englacial and subglacial drainage networks. However, such observations are very rare (Mernild and Hasholt, 2009; Rennermalm et al., 2012a; Rasch et al., 2011; Mernild et al., 2010a) due to the logistical difficulties in such remote areas, and often rely on modeling efforts for understanding meltwater output (Bøggild et al. 2002; Mernild et al. 2011a; Mernild et al. 2010b). Particularly for questions about melt-enhanced basal lubrication, monitoring outflows in comparison to both inflows and velocity changes is needed. River discharge coupled with simultaneous observations of tracers can be used to establish travel time and infer subglacial drainage efficiency (Chandler et al., 2013). Covington et al. (2012) focused on the effects of englacial conduit system organization on proglacial river discharge, finding that changes in storage in englacial/subglacial networks on short time scales are much smaller than their ability to transmit water and thus do not have a significant effect on discharge.

These field studies are crucial for modeling the water budget of both proglacial and ice sheet catchments to assess seasonal water storage and release. Over multiple years, contrasts in indicators of ablation can infer differences in storage (Jansson et al., 2003). In particular, Rennermalm et al. (2012b) compared three years of proglacial discharge measurements at three different sites draining a single ice sheet catchment near Kangerlussuaq to modeled ice sheet surface meltwater production, and found that the water budget could not be closed. Instead, their study suggests that 12% - 53% of ice sheet surface runoff is retained within the glacier each melt year. Furthermore, another study found evidence of meltwater escape during the cold season, indicating that the hydrologic network may remain open and active beyond the melt season (Rennermalm et al., 2012b), which has been suggested in other studies outside of Greenland (Hagen et al., 2003; Wadham et al., 2000).

1.8 Ocean interactions

The ocean plays a large part in in influencing mass loss for marine-terminating outlet glaciers through interactions with floating tongues via ocean warming and circulation (Joughin et al., 2012). High sea-surface temperatures, low sea ice concentrations, and reduced ice mélange formation at the calving front have triggered multi-year retreats of large glaciers (Howat et al., 2010). Calving icebergs and sediment-rich subglacial discharge contribute to a stratification of cold, fresh meltwater overlying warm, salty subtropical water, which in turn affects fjord circulation that can transport heat to outlet glaciers (Straneo et al., 2011). For marine-terminating outlet glaciers, meltwater runoff can govern total ice discharge through increased calving susceptibility and submarine melting from forced marine convection (Box and Colgan, 2013). Land-terminating segments of the GrIS interact with the ocean through glacial meltwater outflows mixing in fjord waters. This meltwater is visible from space as buoyant sediment plumes, which is a useful indicator of ice sheet surface meltwater loss to the ocean.

1.8.1 Direct meltwater input into fjords

While ice sheet surface hydrology can be assessed using river discharge, the scarcity of such data requires other indicators of meltwater runoff to be explored, such as buoyant sediment plumes in fjords of outlet glaciers and rivers draining the ice sheet. Suspended sediment from glacial erosion is transported from the basal environment in meltwater runoff, with concentrations affected by glaciological variables such as glacier size, sliding speed, ice flux, and meltwater production (Hallet et al., 1996; Hasholt et al., 2006). Sediment-rich meltwater entering fjords from both marine-terminating outlet glaciers land-terminating glaciers (via rivers) can become buoyant on the water surface, creating a clear sediment plume visible in satellite imagery through its contrasting spectral signature from clear marine water (Figure 1-7). These sediment plumes represent a linkage between meltwater produced on the ice sheet surface and meltwater released to the ocean (Chu et al., 2009; McGrath et al., 2010; Tedstone and Arnold, 2012). Plume development is controlled by a complex combination of factors both on land and after entering the fjord, but is still predominantly driven by the kinetic energy of river discharge in the upper fjord environment where rivers first enter the coastal zone (Syvitski et al., 1985). The presence of sediment plumes in outlet glacier fjords signals freshwater release from the ice sheet to the ocean, with plumes showing lower salinity and higher suspended sediment concentration (SSC) (Chu et al., 2009). In particular, the study by Chu et al. (2009) in Kangerlussuaq Fjord in southwest Greenland was the first attempt to use sediment plumes as an indicator of meltwater output, and introduced remote sensing of plumes as a viable tool for assessing meltwater release in comparison to surface meltwater production as a primary driver.

High spatial covariance between ice sheet surface melting and fjord plume SSC indicate that regions with high melt produce more sediment (Figure 1-8; Chu et al., 2012). However, outlet glacier environments also provide insight into the physical mechanisms by which sediment is dispersed from glacier outlets to fjords. Buoyant plumes are most readily detected downstream of rivers draining land-terminating glaciers, owing to high SSC and minimal obstruction by calving ice (Figure 1-1a). Although sediment plumes can also be detected and traced to ice sheet meltwater release from marine terminating glaciers, they are restricted to fjords with minimal iceberg calving and sea ice influence (Chu et al., 2012; Tedstone and Arnold, 2012). Furthermore, for sediment-rich meltwater to form a buoyant plume at an outlet of a marine-terminating glacier, the meltwater released subglacially hundreds of meters beneath the fjord surface jet must become buoyant, which is typically the case if SSC does not exceed ~40,000 mg/L (Mulder and Syvitski, 1995; Mugford and Dowdeswell, 2011). Regardless of environment, as buoyant plumes move farther down fjord, sediment dispersal and settling rates are further influenced by tides (Castaing and Allen, 1981; Dowdeswell and Cromack, 1991; Bowers et al., 1998; Halverson and Pawlowicz, 2008), wind (Stumpf et al., 1993; Whitney, 2005), and sea ice (Hasholt, 1996). Even with potential iceberg obstruction of satellite remote sensing of fjord surface sediment, the ability to detect and monitor plumes from space represents one of the few ways to observe hydrologic release of meltwater from the Greenland ice sheet over large spatial scales. Sediment plumes remain an opportunity for detecting meltwater output, and future studies should explore meltwater routing to assess lag times, fjord circulation dynamics, and the proportion of subglacial discharge jets becoming buoyant plumes.

1.8.2 Ocean warming effect on tidewater glaciers

While basal lubrication from enhanced meltwater input is the dominant mechanism for increased velocities on land-terminating glaciers and some marine-terminating glaciers, calving effects and the interactions with the ocean may be more of a driving force for marine-terminating outlet glaciers with an extensive floating tongue. Floating tongues and ice shelves provide a buttressing back-stress transmitted to the upstream ice flow from drag exerted by lateral walls, slower-flowing ice, and basal resistance on grounded spots (Cuffey and Paterson, 2010). Floating tongue break-up can reduce the buttressing effect and propagate force perturbations up-glacier that are sustained by thinning (Thomas, 2004; Howat et al., 2005).

The fjord of Jakobshavn Isbrae has been shown to exert great control over the outlet glacier's calving and velocity. Calving and ice discharge on the outlet glacier has experienced rapid increases, particularly from a change in flow dynamics around 1998 after half a century of terminus stability (van der Veen et al., 2011; Sohn et al., 1998) with velocity increases of 30% during that time (Thomas, 2004). The loss of a substantial portion of the floating tongue can decrease the buttressing effect and trigger these anomalous speed increases due to a reduced amount of back-force (Thomas et al., 2003; Thomas, 2004; Joughin et al., 2004), with similar observations in Helheim Glacier (Howat et al., 2005) and smaller southeastern glaciers (Howat et al., 2008). Collapse of the floating tongue and over 10 km of retreat over 1997-2001 have been observed (Csatho et al., 2008), suggesting that the lower parts of the glacier respond to local surface summer melting as well as breakup of sea ice and icebergs (Sohn et al., 1998). However, decreased back-stress from floating tongue loss is not the only control on calving rates, and van der Veen et al. (2011) hypothesized that weakening ice or change in bed properties could have caused velocity shifts in Jakobshavn Isbrae. Another large calving event in 2010 that caused 25% of the floating tongue of Petermann Glacier in northwest Greenland to break off illustrates similar circumstances, but there was no corresponding glacier speedup, suggesting that for some of these glaciers, melt-enhanced basal lubrication may still be a prominent driver of dynamic changes (Nick et al., 2012).

The most direct indicator of ocean influence is the thinning and glacier acceleration associated with ocean temperature and circulation. Thinning occurs both at the surface from warm air temperatures as well as along the bottom of their submerged faces from warm ocean waters (Motyka et al., 2011; Holland et al., 2008). Ocean warming and inflow of subtropical waters is shown to be related to periods of glacier retreat (Walsh et al., 2012; Christoffersen et al., 2011; Straneo et al., 2010). Walsh et al. (2012) measured thinning, retreat, and velocity of central eastern Greenland marine-terminating glaciers, finding a synchronicity in changes and a distinct difference between glacier retreat north and south of 69° N latitude, which corresponds to the northern limit of transported subtropical waters. The greater velocities and rates of thinning for glaciers south of 69°N interacting with warmer ocean waters indicate that coastal heat transport is a primary driver of marine-terminating glacier changes (Walsh et al., 2012; Straneo et al., 2010).

Bottom melting is a very significant mechanism for mass loss, both from direct melting and from deep incisions forming bottom channels in the ice, affecting grounding-line stability of the floating tongue (Rignot and Steffen, 2008). Submarine melting rates have been measured to be two orders of magnitude larger than surface melt rates, but comparable to rates of iceberg discharge (Rignot et al., 2010). This large control that sea-surface temperature and ocean circulation have on dynamic changes in outlet glaciers suggests that in future warming scenarios with warmer oceans, glacier thinning and retreat may become enhanced. Furthermore, decreasing sea ice extent, which can increase ocean heating, is a possible driver for enhanced GrIS melting through onshore advection of the warmer air (Rennermalm et al., 2009).

1.9 Conclusion

The most pressing limitation in predicting GrIS contributions to sea level rise is the uncertainty arising from the effect of increased meltwater input into englacial and subglacial environments and subsequent response of ice velocities. The understanding of GrIS hydrology presented here is mainly inferred from alpine and Arctic glaciers, with the assumption that the processes will scale up to the ice sheet. Numerous studies refer to rapid uplift and increased glacier velocities from changes in meltwater input as an analogue of GrIS outlet glacier dynamic response to increasing meltwater (Bartholomew et al., 2010; Colgan et al., 2011a; Sundal et al., 2011). While peak ice flow velocities are higher in high-melt years than in low-melt years, annual velocities may be unrelated to annual surface melt due to englacial and subglacial drainage organization development throughout the melt season, which increases efficiency of meltwater transport and dispersal. Both processes, melt-induced acceleration through basal lubrication and velocity slow-down with evolution of englacial and subglacial efficiency, occur simultaneously over a melting season. It is an open question as to whether one process will dominate over the other in the future, and whether increased melting can change these mechanisms.

Reliance on surface observations and theoretical models makes it difficult to study englacial and subglacial environments. While englacial and subglacial conduit network development most likely varies spatially, inferences from surface meltwater production and ice movement are not sophisticated enough to establish the exact nature of englacial and subglacial hydrology. Temporal and spatial development of these internal networks remains poorly understood and yet is a key factor in determining annual glacier velocity cycles. This linkage between surface melting and ice dynamics is the most compelling knowledge gap in the pursuit of understanding future GrIS contributions to sea level rise, yet all components of the GrIS hydrologic system influence this mechanism and require a better understanding.

A string of extreme melt events between 2007 and 2012 brings to the forefront questions of how albedo changes will affect melting, and how this increased meltwater translates into either increased water retention through refreezing and storage or increased runoff. The positive feedback between increasing melt and decreasing albedo can be enhanced by earlier melt onset exposing bare ice prematurely, meltwater pooling into supraglacial lakes, and the presence of dust on the ice surface. This dust is typically exposed through the melting of outcropping ice, but an important unknown is the contribution from enhanced dry or wet deposition of wind-blown dust to albedo feedbacks.

With surface meltwater able to penetrate cold firn before refreezing or migrating down glacier, partitioning meltwater into runoff becomes a key problem. While there is a general understanding that refreezing occurs at higher elevations and runoff forms at lower elevations, the processes of meltwater percolation, refreezing, and firn densification are not well parameterized. Furthermore, meltwater retention and movement at depth show that runoff initiation is controlled by at least the upper 10 m of the firn layer rather than just surface conditions (Humphrey et al., 2012), limiting the capability of near surface remote sensing to identify runoff initiation. Better models of firn densification and meltwater retention are needed to aid remotely sensed studies of runoff formation, though this will require more *in situ* process studies of these phenonema. Models lacking accurate treatments of these processes may lead to an overestimation of sea level rise.

As knowledge of hydrologic processes becomes more integrated with ice dynamics, the importance of supraglacial meltwater transport and drainage through streams, lakes, moulins, and crevasses has become heightened. In particular, the question of the importance of supraglacial lakes compared to moulins and crevasses in delivering water to the englacial and subglacial environments needs to be quantified and understood. While fast supraglacial lake drainages can provide meltwater directly to the bed to locally influence ice dynamics, they cannot account for spatially extensive dynamic changes in mass loss and glacier velocity. Field investigations have been limited to the western GrIS and may not be representative for the entire GrIS. Therefore, models need to incorporate the spatial diversity that drives hydrologic and ice dynamic responses regionally. Studies are only beginning to address the spatial and temporal influx of meltwater into the ice sheet through moulins and crevasses aided by the increasing availability of high-resolution satellite imagery.

In contrast to the strong body of research focusing on supraglacial lakes, there is very little unique work about GrIS supraglacial streams, moulins, and crevasses, and knowledge about their morphology is primarily inferred from research on glaciers. This lack of attention is mostly owing to inadequate spatial resolutions of commonly available satellite imagery for capturing their small size and logistical difficulties in field work. However, the overemphasis on supraglacial lake drainages as a key factor in rapidly injecting large volumes of meltwater to the bed has been detrimental to understanding how meltwater leaves the GrIS surface. The few studies of GrIS supraglacial hydrologic features show that moulins provide rapid drainage of large upstream areas into englacial and subglacial systems, while crevasses provide a slower, more spatially distributed drainage. In contrast to the intermittent meltwater supply from lake drainages into moulins, supraglacial streams provide a steady supply of large volumes of meltwater into moulins during the melt season, leaving them one of the most important and unstudied features for understanding hydrologic inputs to the ice sheet and to the ocean. Advancing techniques in mapping supraglacial stream networks will aid in assessing stream morphology, channel efficiency, and meltwater flux. The lack of understanding of the proportion of meltwater produced at the surface that moves into channelized streams and rivers to drain into the ice sheet through fractures and moulins hinders more accurate assessments of future ice sheet response to warmer temperatures.

Proglacial environments provide a great opportunity for assessing true meltwater flux into the ocean through river discharge. Monitoring proglacial river discharge in Greenland is one of the few ways to quantify meltwater flux from land-terminating outlet glaciers, and the handful of existing river discharge datasets have provided evidence for meltwater retention, jökulhlaups, and subglacial drainage organization. However, these observations are rare because of logistic challenges and inaccessibility of most proglacial rivers. Moving forward requires development of remote sensing techniques for quantifying discharge, with studies in other areas showing that remotely measuring width in braided rivers can be used to retrieve discharge, given knowledge of hydraulic geometry relationships and parameters (e.g., Ashmore and Sauks, 2006; Smith et al., 1996).

Buoyant sediment plumes remain a viable yet largely unexplored tool for assessing meltwater export at large spatial scales due to their presence around the ice sheet in fjords draining both land- and marine-terminating glaciers. Visible in remote sensing imagery, their seasonal presence broadly correlates with surface melting around the GrIS, with higher melt regions producing plumes with higher sediment concentrations that persist longer in the fjords. The main limitation in linking plumes to surface melt lies in the different controls of sediment output from different outlet glacier types. Fast-flowing marine-terminating glacier outlets are more challenging for plume observations due to calved icebergs obstructing detection and the dependence on subglacial discharge rising hundreds of meters to form buoyant plumes. While remote sensing of proglacial river discharge and fjord sediment plumes is still in its infancy, advancements in assessing these two components comprising meltwater runoff would greatly improve understanding of the GrIS's future contributions to sea level rise.

Increasingly available remote sensing technologies and interest in GrIS hydrologic components have increased understanding of ice sheet response to future warming scenarios. Transformative studies have come out of data from satellites launched during the 2000s, with GRACE providing independent estimates of mass loss and MODIS offering high-temporal resolution for tracking supraglacial lake dynamics, for example. Remote sensing is the most reasonable technique for merging small-scale *in situ* observations with coarser-scale models because of greater spatio-temporal coverage from satellite imagery. However, difficulties lie in obtaining spatially extensive *in situ* observations and particularly in integrating small-scale field studies with coarse large-scale model outputs. Site-specific field studies on the GrIS are rare in comparison to measurements from small Arctic or alpine glaciers due to the logistical difficulties in working on the ice sheet (and even proglacially), even with a number of field research sites offering science support. Despite these limitations, an intense interest shown by the scientific community to understand GrIS vulnerabilities in future warming scenarios, particularly with hydrologic implications, provides great opportunities for overcoming these challenges.

1.10 Figures

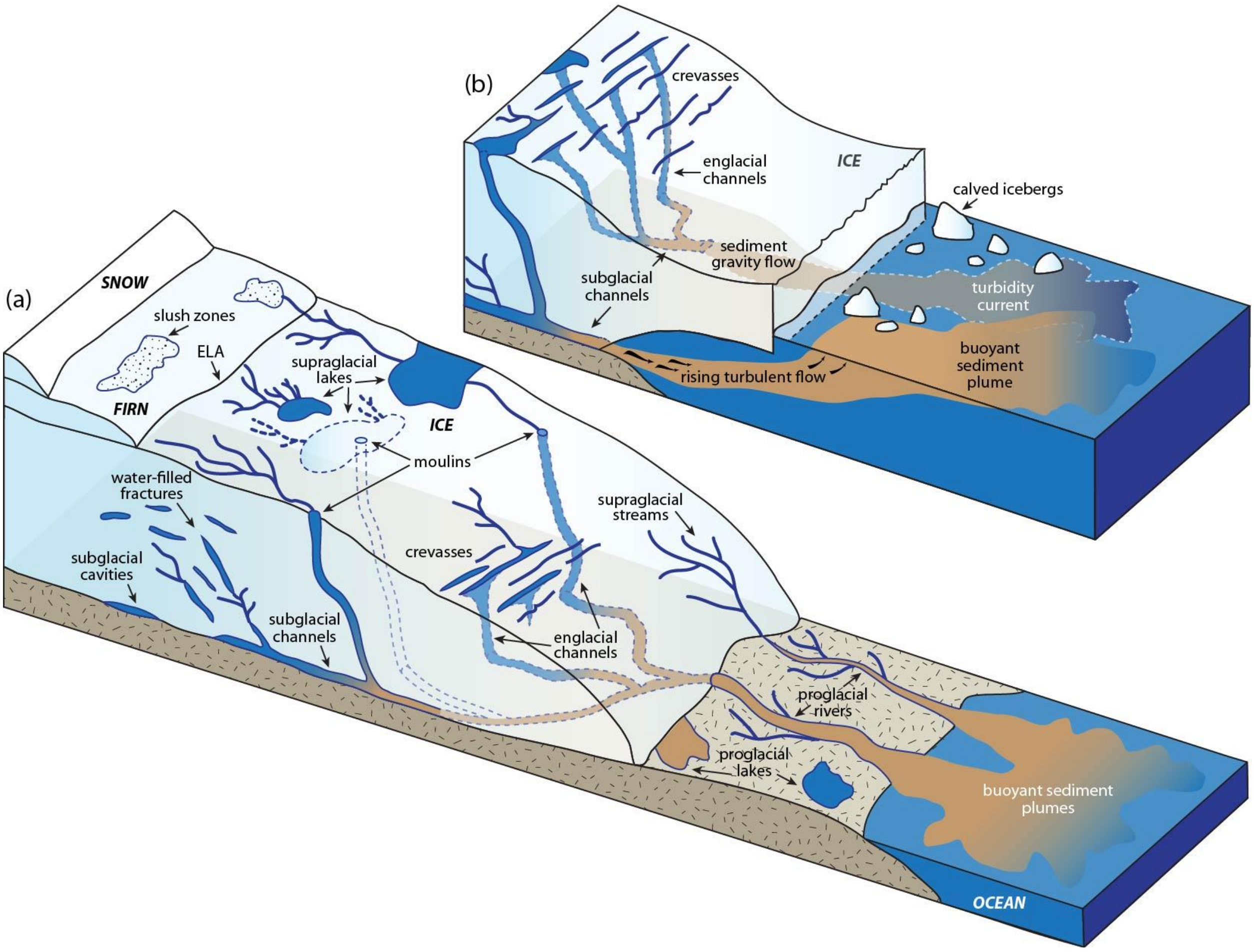

Figure 1-1. Elements of the Greenland ice sheet hydrologic system. (a) In the accumulation zone above the equilibrium line altitude (ELA), water percolating through the snow/firn can pool into slush zones and channelize into supraglacial streams. In the ablation zone beneath the ELA, meltwater pools in supraglacial lakes and flows through streams into crevasses and moulins, entering englacial and subglacial conduits emerging into proglacial rivers and lakes. As meltwater moves through the system, erosional debris increases sediment concentration making glacial-melt lakes and rivers sediment-rich (and leaving precipitation and snowmelt lakes clear of sediment). Finally, meltwater entering the ocean produces a buoyant sediment plume in the fjord. (b) Differences for marine-terminating glaciers lie in meltwater outlet mechanisms. Sediment-rich subglacial discharge released tens to hundreds of meters below the water surface either rises to form a buoyant plume or forms a turbidity current beneath the surface. Modified from Cuffey and Paterson (2010).

Figure 1-2. Distinct albedo zones on the ice surface, with cleaner high-albedo bare ice on the left contrasting low-albedo bare ice with outcropping dust on the right (photo by author, 19 July 2012).

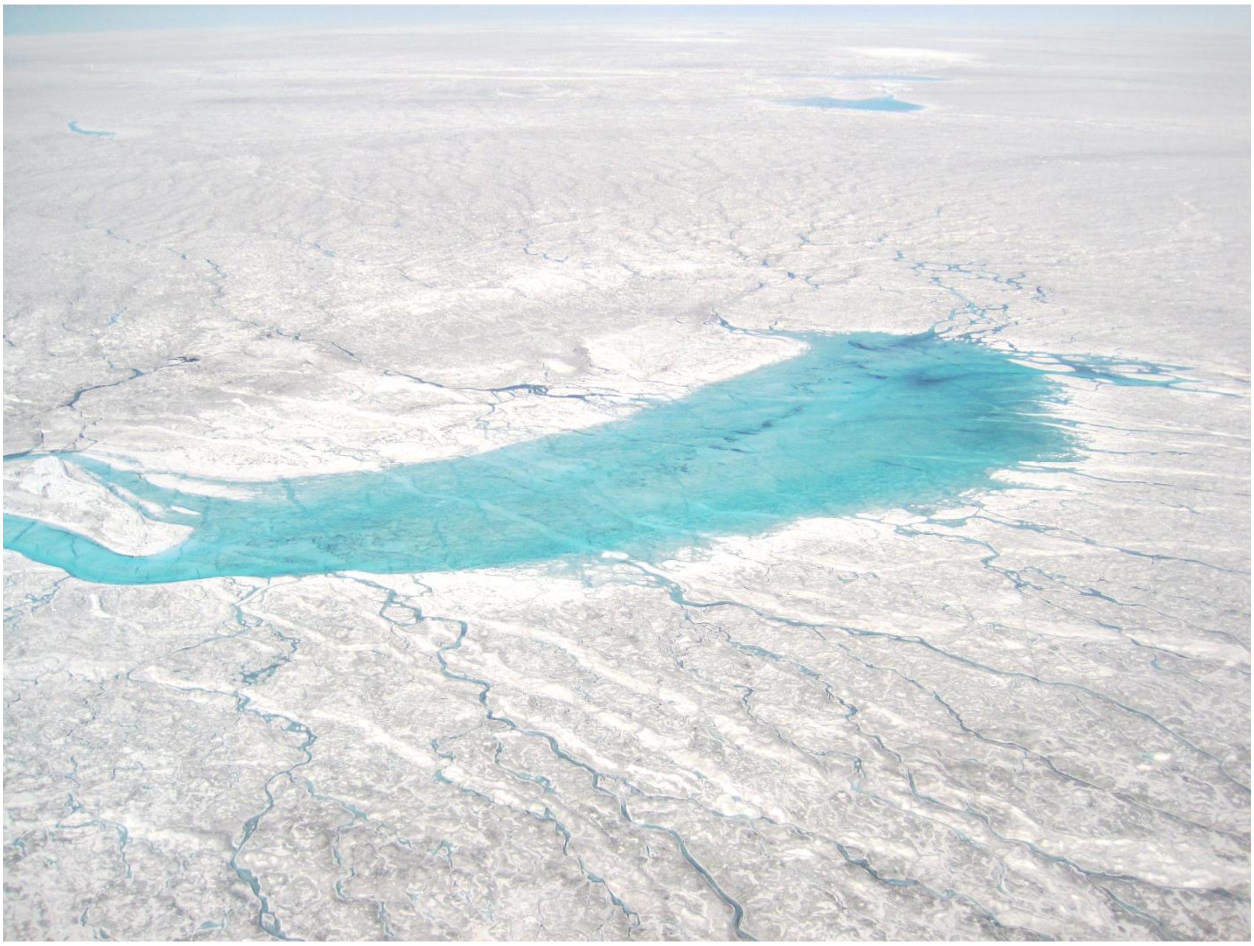

Figure 1-3. The supraglacial hydrologic network in the southwest GrIS ablation zone showing supraglacial streams flowing into a lake, with a large output stream to the left of the image (photo by author, 19 July 2012).

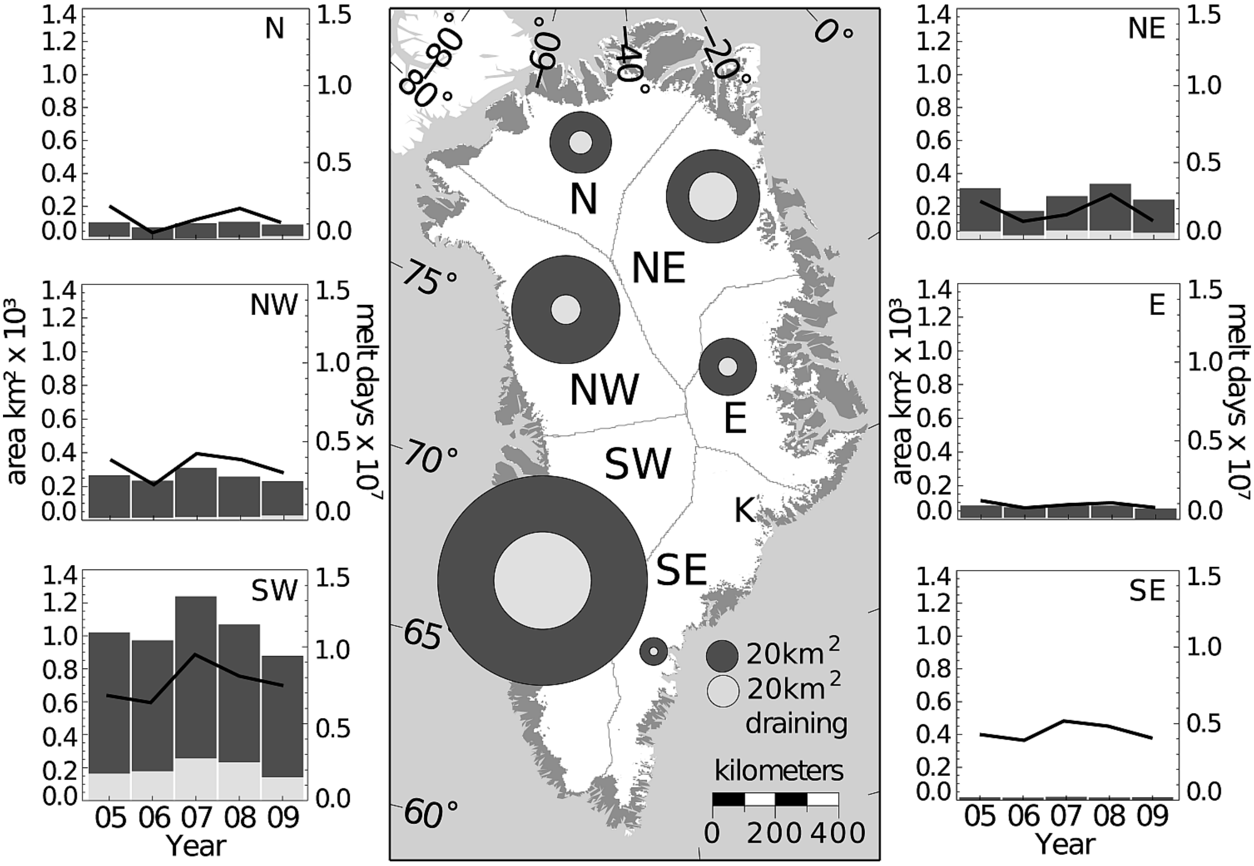

Figure 1-4. Distribution of lakes and rapid drainage events over 2005-2009 from MODIS satellite imagery. The total area of lakes (dark gray) and total area of lakes that drained suddenly (light gray) are mapped for six regions of the GrIS (circles show mean area). Bar plots show interannual variation with melt intensity superimposed.
Source: From Selmes et al. (2011). Permission obtained from source author.

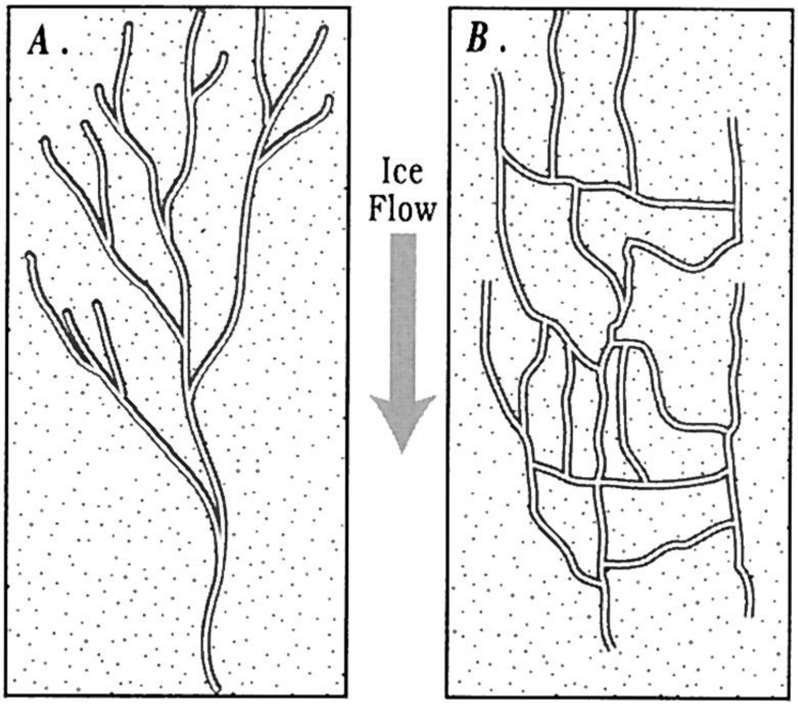

Figure 1-5. (a) Idealized plan view of a fast arborescent drainage system, and (b) a slow non-arborescent drainage system with linked cavities. *Source:* From Fountain and Walder (1998). Permission obtained from source author.

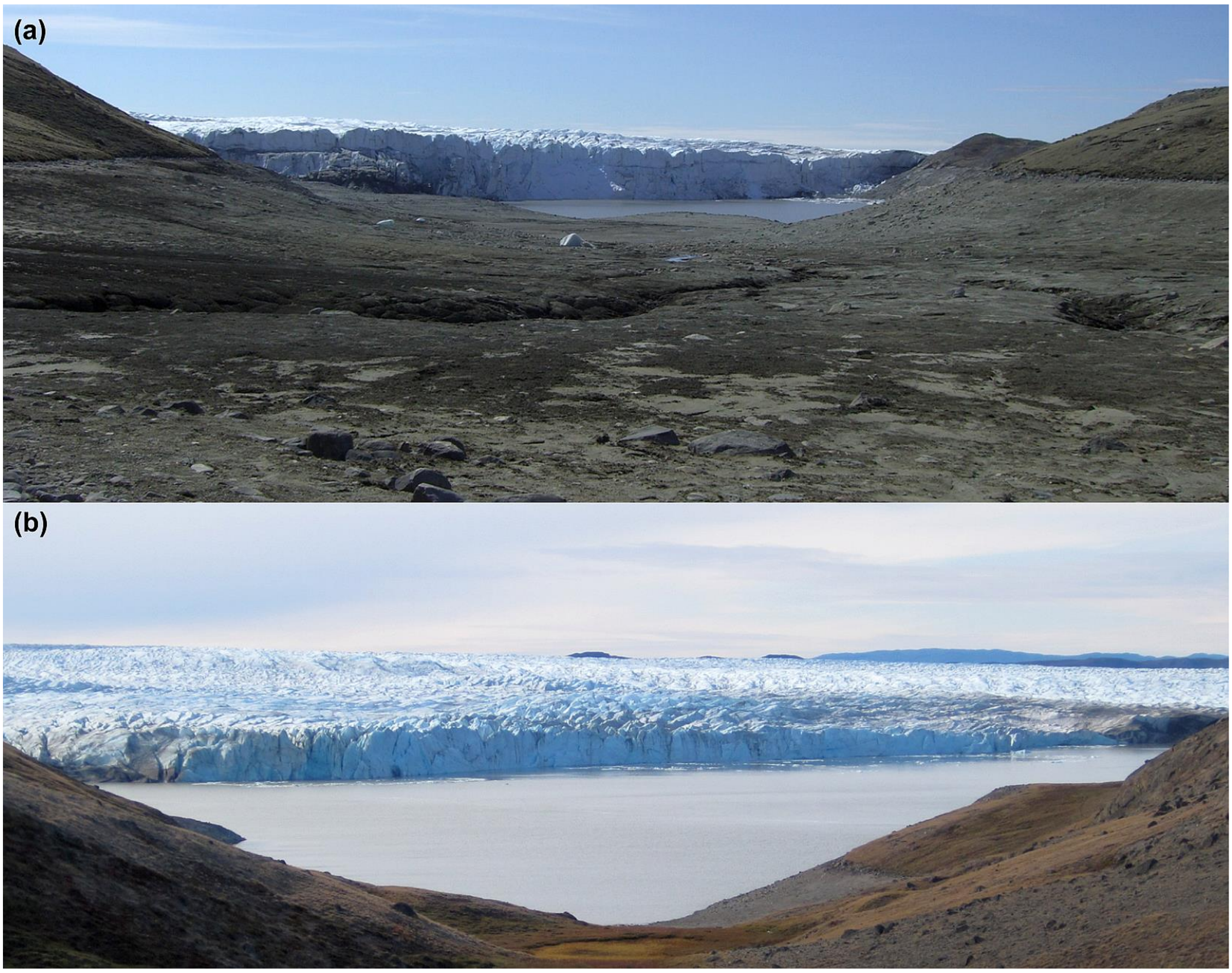

Figure 1-6. The ice-dammed lake near Russell Glacier in southwest Greenland has recently experienced numerous jokulhlaups when high lake levels breach the ice dam. (a) The lake as seen in June 2008 from the perspective of the dry lake bed, almost a year after a jokulhlaup occurred on 31 August 2007 and before the jokulhlaup on 31 August 2008, with current water levels seen in comparison to the high-water shoreline. (b) The lake as seen in August 2010 with a larger lake volume (photos by author).

Figure 1-7. Buoyant sediment plume, entering the fjord from the left, representing an outburst of sediment-rich freshwater from the ice sheet (photo by author, 3 June 2008).

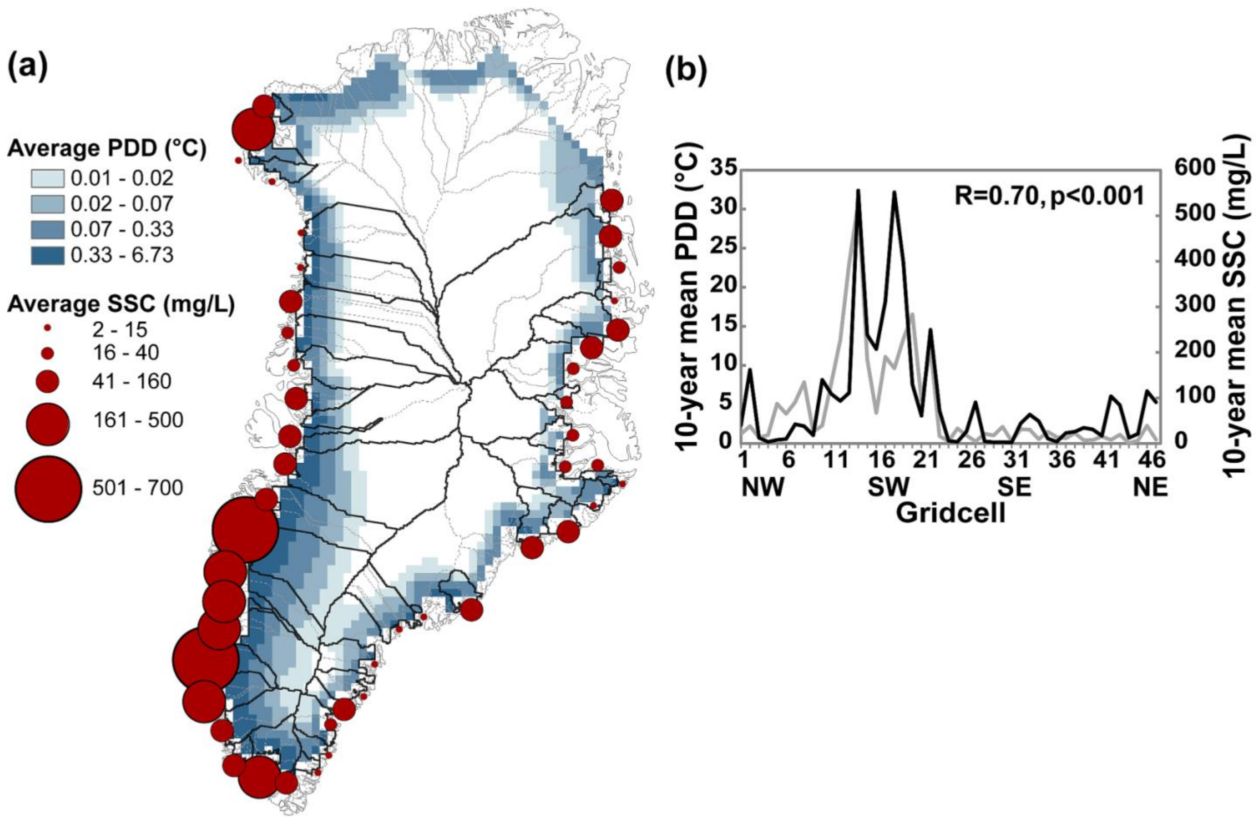

Figure 1-8. (a) Map of 10-year mean ice sheet meltwater production for 2000-2009 (PDD) and fjord plume suspended sediment concentration (SSC, circles) for drainage basins with available data. (b) Spatial variation of 10-year mean PDD (grey line) and SSC (black line), starting in the northwest and going counterclockwise towards the northeast. Modified from Chu et al. (2012).

1.11 References

Abdalati, W., & Steffen, K. (2001). Greenland ice sheet melt extent: 1979-1999. *Journal of Geophysical Research*, *106*(D24), 983–988. doi:10.1029/2001JD900181

Alley, R. B., Dupont, T. K., Parizek, B. R., & Anandakrishnan, S. (2005). Access of surface meltwater to beds of sub-freezing glaciers: preliminary insights. *Annals of Glaciology*, *40*, 8–14. doi:10.3189/172756405781813483

Allison, I., Alley, R. B., Fricker, H. A., Thomas, R. H., & Warner, R. C. (2009). Ice sheet mass balance and sea level. *Antarctic Science*, *21*(05), 413. doi:10.1017/S0954102009990137

Andersen, M. L., Larsen, T. B., Nettles, M., Elósegui, P., Van As, D., Hamilton, G. S., Stearns, L. A., Davis, J. L., Ahlstrøm, A. P., De Juan, J., Ekström, G., Stenseng, L., Khan, S. A., Forsberg, R., & Dahl-Jensen, D. (2010). Spatial and temporal melt variability at Helheim Glacier, East Greenland, and its effect on ice dynamics. *Journal of Geophysical Research*, *115*(F4), 1–18. doi:10.1029/2010JF001760

Andresen, C. S., Straneo, F., Ribergaard, M. H., Bjørk, A. A., Andersen, T. J., Kuijpers, A., Nørgaard-Pedersen, N., Kjær, K. H., Schjøth, F., Weckström, K., & Ahlstrøm, A. P. (2011). Rapid response of Helheim Glacier in Greenland to climate variability over the past century. *Nature Geoscience*, *5*(1), 37–41. doi:10.1038/ngeo1349

Bamber, J. L., & Riva, R. (2010). The sea level fingerprint of recent ice mass fluxes. *The Cryosphere*, *4*(4), 621–627. doi:10.5194/tc-4-621-2010

Banwell, A. F., Arnold, N. S., Willis, I. C., Tedesco, M., & Ahlstrøm, A. P. (2012). Modeling supraglacial water routing and lake filling on the Greenland Ice Sheet. *Journal of Geophysical Research*, *117*(F4), 1–11. doi:10.1029/2012JF002393

Bartholomaus, T. C., Anderson, R. S., & Anderson, S. P. (2008). Response of glacier basal motion to transient water storage. *Nature Geoscience, 1*(1), 33–37. doi:10.1038/ngeo.2007.52

Bartholomew, I. D., Nienow, P., Mair, D., Hubbard, A. L., King, M. A., & Sole, A. (2010). Seasonal evolution of subglacial drainage and acceleration in a Greenland outlet glacier. *Nature Geoscience, 3*(6), 408–411. doi:10.1038/ngeo863

Bartholomew, I. D., Nienow, P., Sole, A., Mair, D., Cowton, T., & King, M. A. (2012). Short-term variability in Greenland Ice Sheet motion forced by time-varying meltwater drainage: Implications for the relationship between subglacial drainage system behavior and ice velocity. *Journal of Geophysical Research, 117*(F3), 1–17. doi:10.1029/2011JF002220

Bartholomew, I. D., Nienow, P., Sole, A., Mair, D., Cowton, T., King, M. A., & Palmer, S. (2011a). Seasonal variations in Greenland Ice Sheet motion: Inland extent and behaviour at higher elevations. *Earth and Planetary Science Letters*, *307*(3-4), 271–278. doi:10.1016/j.epsl.2011.04.014

Bartholomew, I. D., Nienow, P., Sole, A., Mair, D., Cowton, T., Palmer, S., & Wadham, J. L. (2011b). Supraglacial forcing of subglacial drainage in the ablation zone of the Greenland ice sheet. *Geophysical Research Letters*, *38*(8), 1–5. doi:10.1029/2011GL047063

Bell, R. E. (2008). The role of subglacial water in ice-sheet mass balance. *Nature Geoscience*, *1*, 297–304. doi:10.1038/ngeo186

Benn, D. I., Gulley, J. D., Luckman, A., Adamek, A., & Glowacki, P. S. (2009). Englacial drainage systems formed by hydrologically driven crevasse propagation. *Journal of Glaciology*, *55*(191), 513–523. doi:10.3189/002214309788816669

Bhatia, M. P., Das, S. B., Kujawinski, E. B., Henderson, P. B., Burke, A., & Charette, M. A. (2011). Seasonal evolution of water contributions to discharge from a Greenland outlet glacier: insight from a new isotope-mixing model. *Journal of Glaciology*, *57*(205), 929–941. doi:10.3189/002214311798043861

Bhattacharya, I., Jezek, K. C., Wang, L., & Liu, H. (2009). Surface melt area variability of the Greenland ice sheet: 1979–2008. *Geophysical Research Letters*, *36*(20), 1–6. doi:10.1029/2009GL039798

Björnsson, H. (2010). Understanding jökulhlaups: from tale to theory. *Journal of Glaciology*, *56*(200), 1002–1010. doi:10.3189/002214311796406086

Bøggild, C. E., Brandt, R. E., Brown, K. J., & Warren, S. G. (2010). The ablation zone in northeast Greenland: ice types, albedos and impurities. *Journal of Glaciology*, *56*(195), 101–113. doi:10.3189/002214310791190776

Bøggild, C. E., Forsberg, R., & Reeh, N. (2005). Meltwater retention in a transect across the Greenland ice sheet. *Annals of Glaciology*, *40*, 169–173. doi:10.3189/172756405781813546

Bøggild, C. E., Knudby, C. J., Knudsen, M. B., & Starzer, W. (1999). Snowmelt and runoff modelling of an Arctic hydrological basin in west Greenland. *Hydrological Processes*, *13*(12), 1989–2002. doi:10.1002/(SICI)1099-1085(199909)13:12/13<1989::AID-HYP848>3.0.CO;2-Y

Boon, S., & Sharp, M. J. (2003). The role of hydrologically-driven ice fracture in drainage system evolution on an Arctic glacier. *Geophysical Research Letters*, *30*(18), 3–6. doi:10.1029/2003GL018034

Bowers, D. G., Boudjelas, S., & Harker, G. E. L. (1998). The distribution of fine suspended sediments in the surface waters of the Irish Sea and its relation to tidal stirring. *International Journal of Remote Sensing*, *19*(14), 2789–2805. doi:10.1080/014311698214514

Box, J. E. (2002). Survey of Greenland instrumental temperature records: 1873-2001. *International Journal of Climatology*, *22*(15), 1829–1847. doi:10.1002/joc.852

Box, J. E., Bromwich, D. H., Veenhuis, B. A., Bai, L.-S., Stroeve, J. C., Rogers, J. C., Steffen, K., Haran, T., & Wang, S.-H. (2006). Greenland Ice Sheet surface mass balance variability (1988 – 2004) from calibrated Polar MM5 output. *Journal of Climate*, *19,* 2783–2800. doi:10.1175/JCLI3738.1

Box, J. E., Fettweis, X., Stroeve, J. C., Tedesco, M., Hall, D. K., & Steffen, K. (2012). Greenland ice sheet albedo feedback: thermodynamics and atmospheric drivers. *The Cryosphere*, *6*(4), 821–839. doi:10.5194/tc-6-821-2012

Box, J. E., & Ski, K. (2007). Remote sounding of Greenland supraglacial melt lakes: implications for subglacial hydraulics. *Journal of Glaciology*, *53*(181), 257–265. doi:10.3189/172756507782202883

Box, J. E., Yang, L., Bromwich, D. H., & Bai, L.-S. (2009). Greenland Ice Sheet Surface Air Temperature Variability: 1840–2007. *Journal of Climate*, *22*(14), 4029–4049. doi:10.1175/2009JCLI2816.1

Braithwaite, R. J., & Laternser, M. (1994). Variations of near-surface firn density in the lower accumulation area of the Greenland ice sheet, Pikitsoq, West Greenland. *Journal of Glaciology*, *40*(136), 6–9.

Brown, J., Bradford, J. H., Harper, J. T., Pfeffer, W. T., Humphrey, N. F., & Mosley-Thompson, E. (2012). Georadar-derived estimates of firn density in the percolation zone, western Greenland ice sheet. *Journal of Geophysical Research*, *117*(F1), 1–14. doi:10.1029/2011JF002089

Brykala, D. (1999). Hydraulic geometry of a supraglacial stream on the Waldemar Glacier (Spitsbergen) in the summer. *Polish Polar Studies*, *26*, 51–64.

Burgess, E. W., Forster, R. R., Box, J. E., Mosley-Thompson, E., Bromwich, D. H., Bales, R. C., & Smith, L. C. (2010). A spatially calibrated model of annual accumulation rate on the Greenland Ice Sheet (1958–2007). *Journal of Geophysical Research*, *115*(F2), 1–14. doi:10.1029/2009JF001293

Castaing, P., & Allen, G. P. (1981). Mechanisms controlling seaward escape of suspended sediment from the Gironde: a macrotidal estuary in France. *Marine Geology*, *40*, 101–118.

Catania, G. A., & Neumann, T. A. (2010). Persistent englacial drainage features in the Greenland Ice Sheet. *Geophysical Research Letters*, *37*(2), 1–5. doi:10.1029/2009GL041108

Catania, G. A., Neumann, T. A., & Price, S. F. (2008). Characterizing englacial drainage in the ablation zone of the Greenland ice sheet. *Journal of Glaciology*, *54*(187), 567–578. doi:10.3189/002214308786570854

Cazenave, A. (2006). How fast are the ice sheets melting? *Science*, *314*(5803), 1250–2. doi:10.1126/science.1133325

Cazenave, A., Dominh, K., Guinehut, S., Berthier, E., Llovel, W., Ramillien, G., Ablain, M., & Larnicol, G. (2009). Sea level budget over 2003–2008: A reevaluation from GRACE space gravimetry, satellite altimetry and Argo. *Global and Planetary Change*, *65*(1-2), 83–88. doi:10.1016/j.gloplacha.2008.10.004

Chen, J. L., Wilson, C. R., & Tapley, B. D. (2006). Satellite gravity measurements confirm accelerated melting of Greenland ice sheet. *Science*, *313*(5795), 1958–60. doi:10.1126/science.1129007

Christoffersen, P., Mugford, R. I., Heywood, K. J., Joughin, I., Dowdeswell, J. A., Syvitski, J. P. M., Luckman, A., & Benham, T. J. (2011). Warming of waters in an East Greenland fjord prior to glacier retreat: mechanisms and connection to large-scale atmospheric conditions. *The Cryosphere, 5*(3), 701–714. doi:10.5194/tc-5-701-2011

Chu, V. W., Smith, L. C., Rennermalm, A. K., Forster, R. R., & Box, J. E. (2012). Hydrologic controls on coastal suspended sediment plumes around the Greenland Ice Sheet. *The Cryosphere*, *6*(1), 1–19. doi:10.5194/tc-6-1-2012

Chu, V. W., Smith, L. C., Rennermalm, A. K., Forster, R. R., Box, J. E., & Reeh, N. (2009). Sediment plume response to surface melting and supraglacial lake drainages on the Greenland ice sheet. *Journal of Glaciology*, *55*(194), 1072–1082. doi:10.3189/002214309790794904

Colgan, W., Rajaram, H., Anderson, R. S., Steffen, K., Phillips, T., Joughin, I., Zwally, H. J., & Abdalati, W. (2011a). The annual glaciohydrology cycle in the ablation zone of the Greenland ice sheet: Part 1. Hydrology model. *Journal of Glaciology*, *57*(204), 697–709. doi:10.3189/002214311797409668

Colgan, W., Steffen, K., McLamb, W. S., Abdalati, W., Rajaram, H., Motyka, R. J., Phillips, T., & Anderson, R. S. (2011b). An increase in crevasse extent, West Greenland: Hydrologic implications. *Geophysical Research Letters*, *38*(18), 1–7. doi:10.1029/2011GL048491

Covington, M. D., Banwell, A. F., Gulley, J. D., Saar, M. O., Willis, I., & Wicks, C. M. (2012). Quantifying the effects of glacier conduit geometry and recharge on proglacial hydrograph form. *Journal of Hydrology*, *414-415*, 59–71. doi:10.1016/j.jhydrol.2011.10.027

Cowton, T., Nienow, P., Bartholomew, I. D., Sole, A., & Mair, D. (2012). Rapid erosion beneath the Greenland ice sheet. *Geology*, *40*(4), 343–346. doi:10.1130/G32687.1

Csatho, B., Schenk, T., van der Veen, C. J., & Krabill, W. B. (2008). Intermittent thinning of Jakobshavn Isbræ, West Greenland, since the Little Ice Age. *Journal of Glaciology*, *54*(184), 131–144. doi:10.3189/002214308784409035

Cuffey, K. M., & Paterson, W. S. B. (2010). *The Physics of Glaciers* (Fourth Edi., p. 704). Academic Press.

Das, S. B., Joughin, I., Behn, M. D., Howat, I. M., King, M. A., Lizarralde, D., & Bhatia, M. P. (2008). Fracture propagation to the base of the Greenland Ice Sheet during supraglacial lake drainage. *Science*, *320*(5877), 778–81. doi:10.1126/science.1153360

Dowdeswell, J. A., & Cromack, M. (1991). Behavior of a glacier-derived suspended sediment plume in a small inlet. *Journal of Geology*, *99*, 111–123.

Dozier, J. (1976). An examination of the variance minimization tendencies of a supraglacial stream. *Journal of Hydrology*, *31*, 359–380.

Dyurgerov, M. B., Bring, A., & Destouni, G. (2010). Integrated assessment of changes in freshwater inflow to the Arctic Ocean. *Journal of Geophysical Research*, *115*(D12), 1–9. doi:10.1029/2009JD013060

Ettema, J., van den Broeke, M. R., Van Meijgaard, E., van de Berg, W. J., Bamber, J. L., Box, J. E., & Bales, R. C. (2009). Higher surface mass balance of the Greenland ice sheet revealed by high-resolution climate modeling. *Geophysical Research Letters*, *36*(12), 1–5. doi:10.1029/2009GL038110

Fausto, R. S., Mernild, S. H., Hasholt, B., Ahlstrøm, A. P., & Knudsen, N. T. (2012). Modeling suspended sediment concentration and transport, Mittivakkat Glacier, Southeast Greenland. *Arctic, Antarctic, and Alpine Research*, *44*(3), 306–318. doi:10.1657/1938-4246-44.3.306

Ferguson, R. I. (1973). Sinuosity of Supraglacial Streams. *Geological Society of America Bulletin*, (1). doi:10.1130/0016-7606(1973)84<251

Fettweis, X., Hanna, E., & Gall, H. (2008). Estimation of the Greenland ice sheet surface mass balance for the 20th and 21st centuries. *The Cryosphere*, *2*, 117–129. doi:10.5194/tc-2-117-2008

Fettweis, X., Tedesco, M., van den Broeke, M. R., & Ettema, J. (2011). Melting trends over the Greenland ice sheet (1958–2009) from spaceborne microwave data and regional climate models. *The Cryosphere*, *5*(2), 359–375. doi:10.5194/tc-5-359-2011

Fountain, A. G., Schlichting, R. B., Jansson, P., & Jacobel, R. W. (2005). Observations of englacial water passages: a fracture-dominated system. *Annals of Glaciology*, *40*(1), 25–30. doi:10.3189/172756405781813762

Fountain, A. G., Tranter, M., Nylen, T. H., Lewis, K. J., & Mueller, D. R. (2004). Evolution of cryoconite holes and their contribution to meltwater runoff from glaciers in the McMurdo Dry Valleys, Antarctica. *Journal of Glaciology*, *50*(168), 35–45. doi:10.3189/172756504781830312

Fountain, A. G., & Walder, J. S. (1998). Water flow through temperate glaciers. *Reviews of Geophysics*, *36*(3), 299–328. doi:10.1029/97RG03579

Frauenfeld, O. W., Knappenberger, P. C., & Michaels, P. J. (2011). A reconstruction of annual Greenland ice melt extent, 1784–2009. *Journal of Geophysical Research*, *116*(D8), 1–7. doi:10.1029/2010JD014918

Georgiou, S., Shepherd, A., McMillan, M., & Nienow, P. (2009). Seasonal evolution of supraglacial lake volume from ASTER imagery. *Journal of Glaciology*, *50*(52), 95–100. doi:10.3189/172756409789624328

Greuell, W. (2000). Melt-water accumulation on the surface of the Greenland Ice Sheet: Effect on albedo and mass balance. *Geografiska Annaler*, *82*(4), 489–498.

Gulley, J. D., Benn, D. I., Muller, D., & Luckman, A. (2009). A cut-and-closure origin for englacial conduits in uncrevassed regions of polythermal glaciers. *Journal of Glaciology*, *55*(189), 66–80.

Gulley, J. D., Benn, D. I., Screaton, E., & Martin, J. B. (2009). Mechanisms of englacial conduit formation and their implications for subglacial recharge. *Quaternary Science Reviews*, *28*(19-20), 1984–1999. doi:10.1016/j.quascirev.2009.04.002

Hagen, J. O., Kohler, J., Melvold, K., & Winther, J. (2003). Glaciers in Svalbard: mass balance, runoff and freshwater flux. *Polar Research*, *22*(2), 145–159. doi:10.1111/j.1751-8369.2003.tb00104.x

Hall, D. K., Williams, R. S., Luthcke, S. B., & DiGirolamo, N. E. (2008). Greenland ice sheet surface temperature, melt and mass loss: 2000 – 06. *Journal of Glaciology*, *54*(184), 81–93. doi:10.3189/002214308784409170

Halverson, M. J., & Pawlowicz, R. (2008). Estuarine forcing of a river plume by river flow and tides. *Journal of Geophysical Research*, *113*(C9), 1–15. doi:10.1029/2008JC004844

Hambrey, M. J. (1977). Supraglacial drainage and irs relationship to structure, with particular reference to Charles Rabors Bre, Okstindan, Norway. *Norsk Geografisk Tidsskrift*, *31*(2), 69–77.

Hanna, E. (2005). Runoff and mass balance of the Greenland ice sheet: 1958–2003. *Journal of Geophysical Research*, *110*(D13), 1–16. doi:10.1029/2004JD005641

Hanna, E., & Cappelen, J. (2003). Recent cooling in coastal southern Greenland and relation with the North Atlantic Oscillation. *Geophysical Research Letters*, *30*(3), 30–32. doi:10.1029/2002GL015797

Hanna, E., Huybrechts, P., Steffen, K., Cappelen, J., Huff, R., Shuman, C. A., Irvine-Fynn, T. D. L., Wise, S., & Griffiths, M. (2008). Increased runoff from melt from the Greenland Ice Sheet: A response to global warming. *Journal of Climate*, *21*(2), 331–341. doi:10.1175/2007JCLI1964.1

Harper, J. T., Bradford, J. H., Humphrey, N. F., & Meierbachtol, T. W. (2010). Vertical extension of the subglacial drainage system into basal crevasses. *Nature*, *467*(7315), 579–82. doi:10.1038/nature09398

Hasholt, B. (1996). Sediment transport in Greenland. *Response*, (236), 105–114.

Hock, R. (2005). Glacier melt: a review of processes and their modelling. *Progress in Physical Geography*, *29*(3), 362–391. doi:10.1191/0309133305pp453ra

Hock, R., & Hooke, R. L. (1993). Evolution of the internal drainage system in the lower part of the ablation area of Storglaciären, Sweden. *Geological Society of America Bulletin*, *105*(4), 537–546. doi:10.1130/0016-7606(1993)105<0537

Hoffman, M. J., Catania, G. A., Neumann, T. A., Andrews, L. C., & Rumrill, J. A. (2011). Links between acceleration, melting, and supraglacial lake drainage of the western Greenland Ice Sheet. *Journal of Geophysical Research*, *116*(F4), 1–16. doi:10.1029/2010JF001934

Holland, D. M., Thomas, R. H., De Young, B., Ribergaard, M. H., & Lyberth, B. (2008). Acceleration of Jakobshavn Isbræ triggered by warm subsurface ocean waters. *Nature Geoscience*, *1*(10), 659–664. doi:10.1038/ngeo316

Holmlund, P. (1988). Internal geometry and evolution of moulins, Storglaciären, Sweden. *Journal of Glaciology*, *34*(117), 242–248.

Hooke, R. L. (1989). Englacial and subglacial hydrology: A qualitative review. *Arctic and Alpine Research*, *21*(3), 221–233.

Hörhold, M. W., Kipfstuhl, S., Wilhelms, F., Freitag, J., & Frenzel, A. (2011). The densification of layered polar firn. *Journal of Geophysical Research*, *116*(F1), 1–15. doi:10.1029/2009JF001630

Howat, I. M., Joughin, I., & Scambos, T. A. (2007). Rapid changes in ice discharge from Greenland outlet glaciers. *Science*, *315*(5818), 1559–61. doi:10.1126/science.1138478

Humphrey, N. F., Harper, J. T., & Pfeffer, W. T. (2012). Thermal tracking of meltwater retention in Greenland's accumulation area. *Journal of Geophysical Research*, *117*(F1), 1–11. doi:10.1029/2011JF002083

Hybbard, B., & Nienow, P. (1997). Alpine subglacial hydrology. *Quaternary Science Reviews*, *16*(9), 939–955. doi:10.1016/S0277-3791(97)00031-0

Irvine-Fynn, T. D. L., Bridge, J. W., & Hodson, A. J. (2011). In situ quantification of supraglacial cryoconite morphodynamics using time-lapse imaging: an example from Svalbard. *Journal of Glaciology*, *57*(204), 651–657. doi:10.3189/002214311797409695

Irvine-Fynn, T. D. L., Hodson, A. J., Moorman, B. J., Vatne, G., & Hubbard, A. L. (2011). Polythermal glacier hydrology: a review. *Reviews of Geophysics*, *49*(RG4002), 1–37. doi:10.1029/2010RG000350

Isenko, E., Naruse, R., & Mavlyudov, B. (2005). Water temperature in englacial and supraglacial channels: Change along the flow and contribution to ice melting on the channel wall. *Cold Regions Science and Technology*, *42*(1), 53–62. doi:10.1016/j.coldregions.2004.12.003

Jansson, P., Hock, R., & Schneider, T. (2003). The concept of glacier storage: a review. *Journal of Hydrology*, *282*(1-4), 116–129. doi:10.1016/S0022-1694(03)00258-0

Jarosch, A. H., & Gudmundsson, M. T. (2012). A numerical model for meltwater channel evolution in glaciers. *The Cryosphere*, *6*(2), 493–503. doi:10.5194/tc-6-493-2012

Johansson, A. M., & Brown, I. A. (2012). Observations of supra-glacial lakes in west Greenland using winter wide swath Synthetic Aperture Radar. *Remote Sensing Letters*, *3*(6), 531–539. doi:10.1080/01431161.2011.637527

Joughin, I., Abdalati, W., & Fahnestock, M. (2004). Large fluctuations in speed on Greenland's Jakobshavn Isbrae glacier. *Nature* 432(7017), 608-610.

Joughin I., Alley, R. B., and Holland, D. M. (2012). Ice-sheet response to oceanic forcing. *Science* 338(6111), 1172-1176.

Joughin, I., Das, S. B., King, M. A., Smith, B. E., Howat, I. M., & Moon, T. (2008b). Seasonal speedup along the western flank of the Greenland Ice Sheet. *Science*, *320*(5877), 781–3. doi:10.1126/science.1153288

Joughin, I., Howat, I. M., Fahnestock, M., Smith, B. E., Krabill, W. B., Alley, R. B., Stern, H., and Truffer, M. (2008a). Continued evolution of Jakobshavn Isbræ following its rapid speedup. *Journal of Geophysical Research*, 113(F4), 1–14. doi:10.1029/2008JF001023

Joughin, I., Smith, B. E., Howat, I. M., Scambos, T. A., & Moon, T. (2010). Greenland flow variability from ice-sheet-wide velocity mapping. *Journal of Glaciology*, *56*(197), 415–430. doi:10.3189/002214310792447734

Joughin, I., Tulaczyk, S., Fahnestock, M., & Kwok, R. (1996). A mini-surge on the Ryder Glacier, Greenland, observed by satellite radar interferometry. *Science*, *274*(5285), 228–230.

Kamb, B. (1987). Glacier surge mechanism based on linked cavity configuration of the basal water conduit system. *Journal of Geophysical Research*, *92*(B9), 9083. doi:10.1029/JB092iB09p09083

Khan, S. A., Wahr, J., Bevis, M., Velicogna, I., & Kendrick, E. (2010). Spread of ice mass loss into northwest Greenland observed by GRACE and GPS. *Geophysical Research Letters*, *37*(6), 1–5. doi:10.1029/2010GL042460

Knighton, A. D. (1972). Meandering habit of supraglacial streams. *Geological Society of America Bulletin*, *83*(1), 201–204. doi:10.1130/0016-7606(1972)83

Knighton, A. D. (1981). Channel Form and Flow Characteristics of Supraglacial Streams, Austre Okstindbreen, Norway. *Arctic and Alpine Research*, *13*(3), 295–306.

Knighton, A. D. (1985). Channel form Adjustment in Supraglacial Streams, Austre Okstindbreen, Norway. *Arctic and Alpine Research*, *17*(4), 451–466.

Knudsen, N. T., Yde, J. C., & Gasser, G. (2003). Suspended sediment transport in glacial meltwater during the initial quiescent phase after a major surge event at Kuannersuit Glacier, Greenland. *Geografisk Tidsskrift - Danish Journal of Geography*, *107*(1), 1–8.

Konzelmann, T., & Braithwaite, R. J. (1995). Variations of ablation, albedo and energy balance at the margin of the Greenland ice sheet, Kronprins Christian Land, eastern north Greenland. *Journal of Glaciology*, *41*(137), 174–182.

Kostrzewski, A., & Zwolinski, Z. (1995). Hydraulic geometry of a supraglacial stream, Ragnarbreen, Spitsbergen. *Quaestiones Geographicae*, (4), 165–176.

Krabill, W. B. (2004). Greenland Ice Sheet: Increased coastal thinning. *Geophysical Research Letters*, *31*(24), 2–5. doi:10.1029/2004GL021533

Krawczynski, M. J., Behn, M. D., Das, S. B., & Joughin, I. (2009). Constraints on the lake volume required for hydro-fracture through ice sheets. *Geophysical Research Letters*, *36*(10), 1–5. doi:10.1029/2008GL036765

Lampkin, D. J. (2011). Supraglacial lake spatial structure in western Greenland during the 2007 ablation season. *Journal of Geophysical Research*, *116*(F4), 1–13. doi:10.1029/2010JF001725

Larsen, M., Tøttrup, C., Mätzler, E., Naamansen, B., Petersen, D., & Thorsøe, K. (2013). A satellite perspective on jökulhlaups in Greenland. *Hydrology Research*, *44*(1), 68–77. doi:10.2166/nh.2012.195

Leeson, A. A., Shepherd, A., Palmer, S., Sundal, A. V., & Fettweis, X. (2012). Simulating the growth of supraglacial lakes at the western margin of the Greenland ice sheet. *The Cryosphere*, *6*(5), 1077–1086. doi:10.5194/tc-6-1077-2012

Leopold, L. B., & Maddock, T. J. (1953). The hydraulic geometry of stream channels and some physiographic implications. *Geological Survey Professional Paper*, *252*, 1–57.

Lewis, S. M., & Smith, L. C. (2009). Hydrologic drainage of the Greenland Ice Sheet. *Hydrological Processes*, *23*(May 2009), 2004–2011. doi:10.1002/hyp

Liang, Y.-L., Colgan, W., Lv, Q., Steffen, K., Abdalati, W., Stroeve, J. C., Gallaher, D., & Bayou, N. (2012). A decadal investigation of supraglacial lakes in West Greenland using a fully automatic detection and tracking algorithm. *Remote Sensing of Environment*, *123*, 127–138. doi:10.1016/j.rse.2012.03.020

Luthcke, S. B., Zwally, H. J., Abdalati, W., Rowlands, D. D., Ray, R. D., Nerem, R. S., Lemoine, F. G., McCarthy, J. J., & Chinn, D. S. (2006). Recent Greenland ice mass loss by drainage system from satellite gravity observations. *Science*, *314*(5803), 1286–9. doi:10.1126/science.1130776

Lüthi, M. P. (2010). Greenland's glacial basics. *Nature*, *468*, 9–10. doi:10.1038/468776a

Lüthje, M., Pedersen, L. T., Reeh, N., & Greuell, W. (2006). Modelling the evolution of supraglacial lakes on the West Greenland ice-sheet margin. *Journal of Glaciology*, *52*(179), 608–618. doi:10.3189/172756506781828386

MacDonell, S., & Fitzsimons, S. (2008). The formation and hydrological significance of cryoconite holes. *Progress in Physical Geography*, *32*(6), 595–610. doi:10.1177/0309133308101382

Mair, D. (2012). Glaciology: Research update I. *Progress in Physical Geography*, *36*(6), 813–832. doi:10.1177/0309133312460265

Marston, R. A. (1983). Supraglacial stream dynamics on the Juneau icefield. *Annals of the Association of American Geographers*, *73*(4), 597–608.

McGrath, D., Colgan, W., Steffen, K., Lauffenburger, P., & Balog, J. (2011). Assessing the summer water budget of a moulin basin in the Sermeq Avannarleq ablation region, Greenland ice sheet. *Journal of Glaciology*, *57*(205), 954–964. doi:10.3189/002214311798043735

McGrath, D., Steffen, K., Overeem, I., Mernild, S. H., Hasholt, B., & van den Broeke, M. R. (2010). Sediment plumes as a proxy for local ice-sheet runoff in Kangerlussuaq Fjord, West Greenland. *Journal of Glaciology*, *56*(199), 813–821. doi:10.3189/002214310794457227

McMillan, M., Nienow, P., Shepherd, A., Benham, T. J., & Sole, A. (2007). Seasonal evolution of supra-glacial lakes on the Greenland Ice Sheet. *Earth and Planetary Science Letters*, *262*(3-4), 484–492. doi:10.1016/j.epsl.2007.08.002

Meehl, G. A., Stocker, T. F., Collins, W. D., Friedlingstein, P., Gaye, A. T., Gregory, J. M., Kitoh, A., Knutti, R., Murphy, J. M., Noda, A., Raper, S. C. B., Watterson, I. G., Weaver, A. J., & Zhao, Z. C. (2007). Global Climate Projections. In S. Solomon, Q. D., M. Manning, Z. Chen, M. Marquis, K. B. Averyt, … H. L. Miller (Eds.), *Climate Change 2007: The Physical Science Basis* (pp. 747–845). Cambridge, United Kingdom and New York, NY, USA: Cambridge University Press.

Mernild, S. H. (2008). Jökulhlaup Observed at Greenland Ice Sheet. *EOS, Transactions*, *89*(35), 1–2. doi:10.1029/2003RG000147.

Mernild, S. H., & Hasholt, B. (2009). Observed runoff, jökulhlaups and suspended sediment load from the Greenland ice sheet at Kangerlussuaq, West Greenland, 2007 and 2008. *Journal of Glaciology*, *55*(193), 855–858.

Mernild, S. H., Howat, I. M., Ahn, Y., Liston, G. E., Steffen, K., Jakobsen, B. H., Hasholt, B., Fog, B., & Van As, D. (2010a). Freshwater flux to Sermilik Fjord, SE Greenland. *The Cryosphere*, *4*(4), 453–465. doi:10.5194/tc-4-453-2010

Mernild, S. H., Liston, G. E., & Hasholt, B. (2008). East Greenland freshwater runoff to the Greenland-Iceland-Norwegian Seas 1999 – 2004 and 2071 – 2100. *Hydrological Processes*, *22*, 4571–4586. doi:10.1002/hyp

Mernild, S. H., Liston, G. E., Hiemstra, C. A., Christensen, J. H., Stendel, M., & Hasholt, B. (2011b). Surface Mass Balance and Runoff Modeling Using HIRHAM4 RCM at Kangerlussuaq (Søndre Strømfjord), West Greenland, 1950–2080. *Journal of Climate*, *24*(3), 609–623. doi:10.1175/2010JCLI3560.1

Mernild, S. H., Liston, G. E., Steffen, K., & Chylek, P. (2010b). Meltwater flux and runoff modeling in the ablation area of Jakobshavn Isbræ, West Greenland. *Journal of Glaciology*, *56*(195), 20–32. doi:10.3189/002214310791190794

Mernild, S. H., Mote, T. L., & Liston, G. E. (2011a). Greenland ice sheet surface melt extent and trends: 1960 – 2010. *Journal of Glaciology*, *57*(204), 621–628. doi:10.3189/002214311797409712

Milne, G. A., Gehrels, W. R., Hughes, C. W., & Tamisiea, M. E. (2009). Identifying the causes of sea-level change. *Nature Geoscience*, *2*(7), 471–478. doi:10.1038/ngeo544

Moon, T., Joughin, I., Smith, B. E., & Howat, I. M. (2012). 21st-century evolution of Greenland outlet glacier velocities. *Science*, *336*(6081), 576–8. doi:10.1126/science.1219985

Mote, T. L. (2007). Greenland surface melt trends 1973–2007: Evidence of a large increase in 2007. *Geophysical Research Letters*, *34*(22), 1–5. doi:10.1029/2007GL031976

Motyka, R. J., Truffer, M., Fahnestock, M., Mortensen, J., Rysgaard, S., & Howat, I. M. (2011). Submarine melting of the 1985 Jakobshavn Isbræ floating tongue and the triggering of the current retreat. *Journal of Geophysical Research*, *116*(F1), 1–17. doi:10.1029/2009JF001632

Mugford, R. I., & Dowdeswell, J. A. (2011). Modeling glacial meltwater plume dynamics and sedimentation in high-latitude fjords. *Journal of Geophysical Research*, *116*(F1), 1–20. doi:10.1029/2010JF001735

Mulder, T., & Syvitski, J. P. M. (1995). Turbidity currents generated at river mouths during exceptional discharges to the world oceans. *Journal of Geology*, *103*, 285–299.

Nghiem, S. V., Hall, D. K., Mote, T. L., Tedesco, M., Albert, M. R., Keegan, K., Shuman, C. A., DiGirolamo, N. E., & Neumann, G. (2012). The extreme melt across the Greenland ice sheet in 2012. *Geophysical Research Letters*, *39*(20), 6–11. doi:10.1029/2012GL053611

Nicholls, R. J., & Cazenave, A. (2010). Sea-level rise and its impact on coastal zones. *Science*, *328*(5985), 1517–20. doi:10.1126/science.1185782

Nick, F. M., Luckman, A., Vieli, A., van der Veen, C. J., Van As, D., van de Wal, R. S. W., Pattyn, F., Hubbard, A. L., & Floricioiu, D. (2012). The response of Petermann Glacier, Greenland, to large calving events, and its future stability in the context of atmospheric and oceanic warming. *Journal of Glaciology*, *58*(208), 229–239. doi:10.3189/2012JoG11J242

Nick, F. M., van der Veen, C. J., Vieli, A., & Benn, D. I. (2010). A physically based calving model applied to marine outlet glaciers and implications for the glacier dynamics. *Journal of Glaciology*, *56*(199), 781–794. doi:10.3189/002214310794457344

Oswald, G. K. A., & Gogineni, S. P. (2012). Mapping basal melt under the Northern Greenland Ice Sheet. *IEEE Transactions on Geoscience and Remote Sensing*, *50*(2), 585–592. doi:10.1109/TGRS.2011.2162072

Overpeck, J. T., Otto-Bliesner, B. L., Miller, G. H., Muhs, D. R., Alley, R. B., & Kiehl, J. T. (2006). Paleoclimatic evidence for future ice-sheet instability and rapid sea-level rise. *Science*, *311*(5768), 1747–50. doi:10.1126/science.1115159

Palmer, S., Shepherd, A., Nienow, P., & Joughin, I. (2011). Seasonal speedup of the Greenland Ice Sheet linked to routing of surface water. *Earth and Planetary Science Letters*, *302*(3-4), 423–428. doi:10.1016/j.epsl.2010.12.037

Parizek, B. R., & Alley, R. B. (2004). Implications of increased Greenland surface melt under global-warming scenarios: ice-sheet simulations. *Quaternary Science Reviews*, *23*(9-10), 1013–1027. doi:10.1016/j.quascirev.2003.12.024

Parker, G. (1975). Meandering of supraglacial melt streams. *Water Resources Research*, *11*(4), 551–552. doi:10.1029/WR011i004p00551

Pfeffer, W. T. (2011). Land ice and sea level rise: A thirty-year perspective. *Oceanography*, *24*(2), 94–111. doi:10.5670/oceanog.2011.30

Pfeffer, W. T., Harper, J. T., & O'Neel, S. (2008). Kinematic constraints on glacier contributions to 21st-century sea-level rise. *Science*, *321*(5894), 1340–1343. doi:10.1126/science.1159099

Pfeffer, W. T., & Meier, M. F. (1991). Retention of Greenland runoff by refreezing: implications for projected future sea level change. *Journal of Geophysical Research*, *96*(C12), 22,117–22,124. doi:10.1029/91JC02502

Phillips, T., Leyk, S., Rajaram, H., Colgan, W., Abdalati, W., McGrath, D., & Steffen, K. (2011). Modeling moulin distribution on Sermeq Avannarleq glacier using ASTER and WorldView imagery and fuzzy set theory. *Remote Sensing of Environment*, *115*(9), 2292–2301. doi:10.1016/j.rse.2011.04.029

Pritchard, H. D., Arthern, R. J., Vaughan, D. G., & Edwards, L. A. (2009). Extensive dynamic thinning on the margins of the Greenland and Antarctic ice sheets. *Nature*, *461*(7266), 971–5. doi:10.1038/nature08471

Rasch, M., Elberling, B., Jakobsen, B. H., & Hasholt, B. (2011). High-resolution measurements of water discharge, sediment, and solute transport in the river Zackenbergelven, Northeast Greenland. *Arctic and Alpine Research*, *32*(3), 336–345.

Reeh, N. (2008). A nonsteady-state firn-densification model for the percolation zone of a glacier. *Journal of Geophysical Research*, *113*(F3), 1–13. doi:10.1029/2007JF000746

Rennermalm, A. K., Moustafa, S. E., Mioduszewski, J., Chu, V. W., Fortner, S. K., Hagedorn, B., Harper, J. T., Mote, T. L., Robinson, D. A., Shuman, C. A., Smith, L. C., & Tedesco, M. (2013). Understanding Greenland ice sheet hydrology using an integrated multi-scale approach. *Environmental Research Letters*, *8*(1), 1–14. doi:10.1088/1748-9326/8/1/015017

Rennermalm, A. K., Smith, L. C., Chu, V. W., Box, J. E., Fortner, S. K., & van den Broeke, M. R. (2012b). Evidence of meltwater retention within the Greenland ice sheet. *The Cryosphere Discussions*, *6*(4), 3369–3396. doi:10.5194/tcd-6-3369-2012

Rennermalm, A. K., Smith, L. C., Chu, V. W., Fortner, S. K., Box, J. E., & Hagedorn, B. (2012a). Proglacial river stage, discharge, and temperature datasets from the Akuliarusiarsuup Kuua River northern tributary, Southwest Greenland, 2008–2011. *Earth System Science Data*, *4*(1), 1–12. doi:10.5194/essd-4-1-2012

Rennermalm, A. K., Smith, L. C., Stroeve, J. C., & Chu, V. W. (2009). Does sea ice influence Greenland ice sheet surface-melt? *Environmental Research Letters*, *4*(2), 024011. doi:10.1088/1748-9326/4/2/024011

Rignot, E. (2004). Rapid ice discharge from southeast Greenland glaciers. *Geophysical Research Letters*, *31*(10), 2–5. doi:10.1029/2004GL019474

Rignot, E., & Kanagaratnam, P. (2006). Changes in the velocity structure of the Greenland Ice Sheet. *Science*, *311*(5763), 986–90. doi:10.1126/science.1121381

Rignot, E., & Steffen, K. (2008). Channelized bottom melting and stability of floating ice shelves. *Geophysical Research Letters*, *35*(2), 2–6. doi:10.1029/2007GL031765

Rignot, E., Velicogna, I., van den Broeke, M. R., Monaghan, A., & Lenaerts, J. T. M. (2011). Acceleration of the contribution of the Greenland and Antarctic ice sheets to sea level rise. *Geophysical Research Letters*, *38*(5), 1–5. doi:10.1029/2011GL046583

Roberts, M. J. (2005). Jökulhlaups: A reassessment of floodwater flow through glaciers. *Reviews of Geophysics*, *43*(RG1002), 1–21. doi:10.1029/2003RG000147.

Röthlisberger, H. (1972). Water pressure in intra- and subglacial channels. *Journal of Glaciology*, *11*(62), 177–203.

Russell, A. J. (2009). Jökulhlaup (ice-dammed lake outburst flood) impact within a valley-confined sandur subject to backwater conditions, Kangerlussuaq, West Greenland. *Sedimentary Geology*, *215*(1-4), 33–49. doi:10.1016/j.sedgeo.2008.06.011

Russell, A. J., Carrivick, J. L., Ingeman-nielsen, T., Yde, J. C., Williams, M., & Jo, A. (2011). A new cycle of jökulhlaups at Russell Glacier, Kangerlussuaq, West Greenland. *Journal of Glaciology*, *57*(202), 238–246. doi:10.3189/002214311796405997

Sasgen, I., van den Broeke, M. R., Bamber, J. L., Rignot, E., Sørensen, L. S., Wouters, B., Martinec, Z., Velicogna, I., & Simonsen, S. B. (2012). Timing and origin of recent regional ice-mass loss in Greenland. *Earth and Planetary Science Letters, 333-334,* 293–303. doi:10.1016/j.epsl.2012.03.033

Schneider, T., Bronge, C., Geografiska, S., Series, A., & Geography, P. (2008). Suspended sediment transport in the Storglaciaren drainage basin. *Geografiska Annaler*, *78*(2/3), 155–161.

Schoof, C. (2010). Ice-sheet acceleration driven by melt supply variability. *Nature*, *468*(7325), 803–6. doi:10.1038/nature09618

Selmes, N., Murray, T., & James, T. D. (2011). Fast draining lakes on the Greenland Ice Sheet. *Geophysical Research Letters*, *38*(15), 1–5. doi:10.1029/2011GL047872

Shepherd, A., Hubbard, A. L., Nienow, P., King, M. A., McMillan, M., & Joughin, I. (2009). Greenland ice sheet motion coupled with daily melting in late summer. *Geophysical Research Letters*, *36*(1), 2–5. doi:10.1029/2008GL035758

Shepherd, A., & Wingham, D. J. (2007). Recent sea-level contributions of the Antarctic and Greenland ice sheets. *Science*, *315*(5818), 1529–32. doi:10.1126/science.1136776

Shreve, R. L. (1972). Movement of water in glaciers. *Journal of Glaciology*, *11*(62), 205–213.

Sneed, W. A., & Hamilton, G. S. (2007). Evolution of melt pond volume on the surface of the Greenland Ice Sheet. *Geophysical Research Letters*, *34*(3), 5–8. doi:10.1029/2006GL028697

Sohn, H.-G., Jezek, K. C., & van der Veen, C. J. (1998). Jakobshavn glacier, West Greenland: 30 years of spaceborne observations. *Geophysical Research Letters*, *25*(14), 2699–2702. doi:10.1029/98GL01973

Sole, A., Mair, D. W. F., Nienow, P. W., Bartholomew, I. D., King, M. A., Burke, M. J., & Joughin, I. (2011). Seasonal speedup of a Greenland marine-terminating outlet glacier forced by surface melt–induced changes in subglacial hydrology. *Journal of Geophysical Research*, *116*(F3), 1–11. doi:10.1029/2010JF001948

Sole, A., Payne, T., Bamber, J. L., Nienow, P., & Krabill, W. B. (2008). Testing hypotheses of the cause of peripheral thinning of the Greenland Ice Sheet: is land-terminating ice thinning at anomalously high rates? *The Cryosphere*, *2*(4), 673–710. doi:10.5194/tcd-2-673-2008

Sørensen, L. S., Simonsen, S. B., Nielsen, K., Lucas-Picher, P., Spada, G., Adalgeirsdottir, G., Forsberg, R., & Hvidberg, C. S. (2011). Mass balance of the Greenland ice sheet (2003–2008) from ICESat data – the impact of interpolation, sampling and firn density. *The Cryosphere*, *5*(1), 173–186. doi:10.5194/tc-5-173-2011

Steffen, K., & Box, J. E. (2001). Surface climatology of the Greenland ice sheet: Greenland Climate Network 1995-1999. *Journal of Geophysical Research*, *106*(D24), 33,951–33,964. doi:10.1029/2001JD900161

Steffen, K., Nghiem, S. V., Huff, R., & Neumann, G. (2004). The melt anomaly of 2002 on the Greenland Ice Sheet from active and passive microwave satellite observations. *Geophysical Research Letters*, *31*(20), 1–5. doi:10.1029/2004GL020444

Straneo, F., Curry, R. G., Sutherland, D. A., Hamilton, G. S., Cenedese, C., Våge, K., & Stearns, L. A. (2011). Impact of fjord dynamics and glacial runoff on the circulation near Helheim Glacier. *Nature Geoscience*, *4*(5), 322–327. doi:10.1038/ngeo1109

Straneo, F., Hamilton, G. S., Sutherland, D. A., Stearns, L. A., Davidson, F., Hammill, M. O., Stenson, G. B., & Rosing-Asvid, A. (2010). Rapid circulation of warm subtropical waters in a major glacial fjord in East Greenland. *Nature Geoscience*, *3*(3), 182–186. doi:10.1038/ngeo764

Stumpf, R. P., Gelfenbaum, G., & Pennock, J. R. (1993). Wind and tidal forcing of a buoyant plume, Mobile Bay, Alabama. *Continental Shelf Research*, *13*(11), 1281–1301. doi:10.1016/0278-4343(93)90053-Z

Sugiyama, S., Skvarca, P., Naito, N., Enomoto, H., Tsutaki, S., Tone, K., Marinsek, S., & Aniya, M. (2011). Ice speed of a calving glacier modulated by small fluctuations in basal water pressure. *Nature Geoscience*, *4*(9), 597–600. doi:10.1038/ngeo1218

Sundal, A. V., Shepherd, A., Nienow, P., Hanna, E., Palmer, S., & Huybrechts, P. (2009). Evolution of supra-glacial lakes across the Greenland Ice Sheet. *Remote Sensing of Environment*, *113*(10), 2164–2171. doi:10.1016/j.rse.2009.05.018

Sundal, A. V., Shepherd, A., Nienow, P., Hanna, E., Palmer, S., & Huybrechts, P. (2011). Melt-induced speed-up of Greenland ice sheet offset by efficient subglacial drainage. *Nature*, *469*(7331), 521–4. doi:10.1038/nature09740

Syvitski, J. P. M., Asprey, K. W., Clattenburg, D. A., & Hodge, G. D. (1985). The prodelta environment of a fjord: suspended particle dynamics. *Sedimentology*, *32*, 83–107. doi:10.1111/j.1365-3091.1985.tb00494.x

Tedesco, M., & Fettweis, X. (2012). 21st century projections of surface mass balance changes for major drainage systems of the Greenland ice sheet. *Environmental Research Letters, 7*(4), 045405. doi:10.1088/1748-9326/7/4/045405

Tedesco, M., Fettweis, X., van den Broeke, M. R., van de Wal, R. S. W., Smeets, C. J. P. P., van de Berg, W. J., Serreze, M. C., & Box, J. E. (2011). The role of albedo and accumulation in the 2010 melting record in Greenland. *Environmental Research Letters*, *6*(1), 014005. doi:10.1088/1748-9326/6/1/014005

Tedesco, M., Lüthje, M., Steffen, K., Steiner, N., Fettweis, X., Willis, I., Bayou, N., & Banwell, A. F. (2012). Measurement and modeling of ablation of the bottom of supraglacial lakes in western Greenland. *Geophysical Research Letters, 39*(2), 1–5. doi:10.1029/2011GL049882

Tedesco, M., Serreze, M. C., & Fettweis, X. (2008). Diagnosing the extreme surface melt event over southwestern Greenland in 2007. *The Cryosphere, 2*, 159–166. doi:10.5194/tc-2-159-2008

Tedesco, M., & Steiner, N. (2011). In-situ multispectral and bathymetric measurements over a supraglacial lake in western Greenland using a remotely controlled watercraft. *The Cryosphere, 5*(2), 445–452. doi:10.5194/tc-5-445-2011

Tedstone, A. J., & Arnold, N. S. (2012). Automated remote sensing of sediment plumes for identification of runoff from the Greenland ice sheet. *Journal of Glaciology, 58*(210), 699–712. doi:10.3189/2012JoG11J204

Thomas, R. H. (2004). Force-perturbation analysis of recent thinning and acceleration of Jakobshavn Isbræ, Greenland. *Journal of Glaciology*, *50*(168), 57–66. doi:10.3189/172756504781830321

Thomas, R. H., Abdalati, W., Frederick, E., Krabill, W. B., Manizade, S., & Steffen, K. (2003). Investigation of surface melting and dynamic thinning on Jakobshavn Isbræ, Greenland. *Journal of Glaciology*, *49*(165), 231–239. doi:10.3189/172756503781830764

Thomas, R. H., Frederick, E., Krabill, W. B., Manizade, S., & Martin, C. (2009). Recent changes on Greenland outlet glaciers. *Journal of Glaciology*, *55*(189), 147–162. doi:10.3189/002214309788608958

Tweed, F. S., & Russell, A. J. (1999). Controls on the formation and sudden drainage of glacier-impounded lakes: implications for jökulhlaup characteristics. *Progress in Physical Geography*, *23*(1), 79–110. doi:10.1177/030913339902300104

van As, D., Hubbard, A. L., Hasholt, B., Mikkelsen, A. B., van den Broeke, M. R., & Fausto, R. S. (2012). Large surface meltwater discharge from the Kangerlussuaq sector of the Greenland ice sheet during the record-warm year 2010 explained by detailed energy balance observations. *The Cryosphere*, *6*(1), 199–209. doi:10.5194/tc-6-199-2012

van de Wal, R. S. W., Boot, W., van den Broeke, M. R., Smeets, C. J. P. P., Reijmer, C. H., Donker, J. J. A., & Oerlemans, J. (2008). Large and rapid melt-induced velocity changes in the ablation zone of the Greenland Ice Sheet. *Science*, *321*(5885), 111–3. doi:10.1126/science.1158540

van den Broeke, M. R., Bamber, J. L., Ettema, J., Rignot, E., Schrama, E. J. O., van de Berg, W. J., Van Meijgaard, E., Velicogna, I., & Wouters, B. (2009). Partitioning recent Greenland mass loss. *Science*, *326*(5955), 984–6. doi:10.1126/science.1178176

van den Broeke, M. R., Bamber, J. L., Lenaerts, J. T. M., & Rignot, E. (2011). Ice sheets and sea level: thinking outside the box. *Surveys in Geophysics*, *32*(4-5), 495–505. doi:10.1007/s10712-011-9137-z

van den Broeke, M. R., Smeets, P., Ettema, J., van der Veen, C. J., van de Wal, R. S. W., & Oerlemans, J. (2008). Partitioning of melt energy and meltwater fluxes in the ablation zone of the west Greenland ice sheet. *The Cryosphere*, *2*, 178–189. doi:10.5194/tc-2-179-2008

van der Veen, C. J. (1998). Fracture mechanics approach to penetration of surface crevasses on glaciers. *Cold Regions Science and Technology*, *27*(1), 31–47. doi:10.1016/S0165-232X(97)00022-0

van der Veen, C. J. (2002). Calving glaciers. *Progress in Physical Geography*, *26*(1), 96–122. doi:10.1191/0309133302pp327ra

van der Veen, C. J. (2007). Fracture propagation as means of rapidly transferring surface meltwater to the base of glaciers. *Geophysical Research Letters*, *34*(1), 1–5. doi:10.1029/2006GL028385

van der Veen, C. J., Plummer, J. C., & Stearns, L. A. (2011). Controls on the recent speed-up of Jakobshavn Isbræ, West Greenland. *Journal of Glaciology*, *57*(204), 770–782.

Velicogna, I. (2009). Increasing rates of ice mass loss from the Greenland and Antarctic ice sheets revealed by GRACE. *Geophysical Research Letters*, *36*(19), 5–8. doi:10.1029/2009GL040222

Velicogna, I., & Wahr, J. (2005). Greenland mass balance from GRACE. *Geophysical Research Letters*, *32*(18), 10–13. doi:10.1029/2005GL023955

Wadham, J. L., Tranter, M., & Dowdeswell, J. A. (2000). Hydrochemistry of meltwaters draining a polythermal-based , high-Arctic glacier, south Svalbars: II. Winter and early Spring. *Hydrological Processes*, *14*, 1767–1786. doi:10.1002/1099-1085(200007)14:10<1767::AID-HYP103>3.0.CO;2-Q

Walder, J. S. (2010). Röthlisberger channel theory: its origins and consequences. *Journal of Glaciology*, *56*(200), 1079–1086. doi:10.3189/002214311796406031

Walsh, K. M., Howat, I. M., Ahn, Y., & Enderlin, E. M. (2012). Changes in the marine-terminating glaciers of central east Greenland, 2000–2010. *The Cryosphere*, *6*(1), 211–220. doi:10.5194/tc-6-211-2012

Whitney, M. M. (2005). Wind influence on a coastal buoyant outflow. *Journal of Geophysical Research*, *110*(C3), 1–15. doi:10.1029/2003JC002261

Wientjes, I. G. M., van de Wal, R. S. W., Reichart, G. J., Sluijs, A., & Oerlemans, J. (2011). Dust from the dark region in the western ablation zone of the Greenland ice sheet. *The Cryosphere*, *5*(3), 589–601. doi:10.5194/tc-5-589-2011

Willis, I. C., Richards, K. S., & Sharp, M. J. (1996). Links between proglacial stream suspended sediment dynamics, glacier hydrology and glacier motion at Midtdalsbreen, Norway. *Hydrological Processes*, *10*, 629–648. doi:10.1002/(SICI)1099-1085(199604)10:4<629::AID-HYP396>3.0.CO;2-6

Wouters, B., Chambers, D., & Schrama, E. J. O. (2008). GRACE observes small-scale mass loss in Greenland. *Geophysical Research Letters*, *35*(20), 0–4. doi:10.1029/2008GL034816

Yang, K., & Smith, L. C. (2013). Supraglacial streams on the Greenland Ice Sheet delineated from combined spectral – shape information in high-resolution satellite imagery. *IEEE Geoscience and Remote Sensing Letters*, *10*(4), 801–805.

Zwally, H. J., Abdalati, W., Herring, T., Larson, K., Saba, J. L., & Steffen, K. (2002). Surface melt-induced acceleration of Greenland ice-sheet flow. *Science, 297*(5579), 218–22. doi:10.1126/science.1072708

Zwally, H. J., Li, J., Brenner, A. C., Beckley, M. A., Cornejo, H. G., Dimarzio, J., Giovinetto, M. B., Neumann, T. A., Robbins, J., Saba, J. L., Yi, D., & Wang, W. (2011). Greenland ice sheet mass balance: distribution of increased mass loss with climate warming; 2003 – 07 versus 1992 – 2002. *Journal of Glaciology, 57*(201), 88–102. doi:10.3189/002214311795306682

Chapter 2

Hydrologic Controls on Coastal Suspended Sediment Plumes around the Greenland Ice Sheet

2.1 Abstract

Rising sea levels and increased surface melting of the Greenland ice sheet have heightened the need for direct observations of meltwater release from the ice edge to ocean. Buoyant sediment plumes that develop in fjords downstream of outlet glaciers are controlled by numerous factors, including meltwater runoff. Here, Moderate Resolution Imaging Spectroradiometer (MODIS) satellite imagery is used to average surface suspended sediment concentration (SSC) in fjords around ~80% of Greenland from 2000-2009. Spatial and temporal patterns in SSC are compared with positive-degree-days (PDD), a proxy for surface melting, from the Polar MM5 regional climate model. Over this decade significant geographic covariance occurred between ice sheet PDD and fjord SSC, with outlet type (land- vs. marine-terminating glaciers) also important. In general, high SSC is associated with high PDD and/or a high proportion of land-terminating glaciers. Unlike previous site-specific studies of the Watson River plume at Kangerlussuaq, temporal covariance is low, suggesting that plume dimensions best capture interannual runoff dynamics whereas SSC allows assessment of meltwater signals across much broader fjord environments around the ice sheet. Remote sensing of both plume characteristics thus offers a viable approach for observing spatial and temporal patterns of meltwater release from the Greenland ice sheet to the global ocean.

2.2 Introduction

The Greenland ice sheet is undergoing increasing melt intensity and extent (Mote, 2007; Bhattacharya et al., 2009) in response to warming air temperatures (Tedesco et al., 2008; Hanna et al., 2008; Box et al., 2009). Ice mass loss has accelerated in the last decade (Rignot et al., 2008; Chen et al., 2006), with increasing accumulation in the ice sheet interior (Box et al., 2006; Burgess et al., 2010) exceeded by losses in the marginal ablation zone (Ettema et al., 2009; Luthcke et al., 2006). Losses are exponentially higher at the margin (van den Broeke et al., 2008) with rapid thinning of near-coastal outlet glaciers (Krabill et al., 2004; Pritchard et al., 2009). Marine-terminating outlet glaciers have also shown increases in total ice discharge (Howat et al., 2007; Rignot et al., 2004) and velocity (Rignot and Kanagaratnam, 2006; Joughin et al., 2010), with accelerated ice loss recently extending to the northwest (Khan et al., 2010). By the end of this century, Greenland's contribution to global sea level rise may total ~17 - 54 cm (Pfeffer et al., 2008), and perhaps reach an annual rate ~0.7 - 0.8 mm/yr (Fettweis et al., 2008).

While ice discharge is the primary form of mass loss for most marine-terminating outlet glaciers (Mernild et al., 2010a), meltwater runoff possibly contributes more than half the total mass loss for the ice sheet as a whole (van den Broeke et al., 2009). Mass-loss estimates using GRACE gravity data also require knowledge of meltwater runoff, but must currently use modeled estimates rather than direct observations (Velicogna, 2009). Increased meltwater production has been linked to ice velocity increases in fast moving outlet glaciers (Shepherd et al., 2009; Joughin et al., 1996; Andersen et al., 2010), as well as seasonal speedups of the broader, slower moving ice sheet (van de Wal et al., 2008; Palmer et al., 2011; Joughin et al., 2008). Meltwater can be transported to the bed through moulins and possibly well-developed englacial drainage networks (Catania and Neumann, 2010).

Drainages of supraglacial lakes can also establish links between the surface and the bed, decreasing basal friction and increasing short-term ice velocities (Das et al., 2008; Schoof, 2010; Box and Ski, 2007). Dynamic changes on land-terminating ice have been attributed to bedrock lubrication from increased meltwater (Zwally et al., 2002; Sundal et al., 2009; Bartholomew et al., 2010), and while marine-terminating glaciers additionally experience destabilized calving fronts (Thomas et al., 2003; Amundson et al., 2008) and enhanced ice-bottom melting from warm ocean waters (Yin et al., 2011; Holland et al., 2008; Straneo et al., 2010), surface melt is a primary link to increased basal sliding through changes in subglacial conduits (Sole et al., 2011; Colgan et al., 2011).

A prime obstacle to quantifying and incorporating runoff processes into models of ice sheet dynamics is a scarcity of direct observations of meltwater exiting the ice sheet, both in rivers draining the ice sheet and from beneath marine-terminating glaciers (Rignot and Steffen, 2008). Therefore, the amount of meltwater that truly reaches the ocean (rather than refreezing or being retained by the ice sheet) is presently unknown. Meltwater production on the ice sheet surface can be modeled from climate data (Ettema et al., 2009; Fettweis, 2007;Box et al., 2006), or observed using remote sensing (Abdalati and Steffen, 1997; Smith et al., 2003; Hall et al., 2008; Tedesco, 2007). However, its release from the ice sheet edge to the ocean remains largely unstudied. Existing research consists of a handful of modeling efforts (Lewis and Smith, 2009; Mernild et al., 2010b; Boggild et al., 1999; Mernild et al., 2011) and site-specific field studies (Mernild and Hasholt, 2009; McGrath et al., 2010; Stott and Grove, 2001; Rasch et al., 2000; Chu et al., 2009).

Buoyant sediment plumes that develop in fjords downstream of outlet glaciers and rivers offer a link between ice sheet hydrology and the ocean that can plausibly be observed using satellite remote sensing (McGrath et al., 2010; Chu et al., 2009). Sediment is produced by abrasion as ice moves over underlying bedrock and is subsequently transported by meltwater, with sediment output affected by glaciological variables such as glacier size, sliding speed, ice flux, and meltwater production, as well as erosional susceptibility of the bedrock (Hallet et al., 1996). Plumes are formed when sediment-rich freshwater runoff from the ice sheet enters the fjord – either directly, for marine-terminating glaciers, or via rivers, for land-terminating glaciers – and floats over denser saline marine water. As meltwater enters the fjord, a buoyant plume typically develops provided sediment concentrations do not exceed ~40,000 mg/L (Mulder and Syvitski, 1995). These features are readily observed in satellite imagery, allowing remote estimation of water-quality characteristics including suspended sediment concentration (SSC) (e.g., Doxaran et al., 2002; Miller and McKee, 2004; Hu et al., 2004; Curran and Novo, 1988). The area and length of buoyant plumes have also been measured as a proxy for hydrologic outflows from the land surface to ocean (e.g., Chu et al., 2009; McGrath et al., 2010; Halverson and Pawlowicz, 2008; Lihan et al., 2008; Thomas and Weatherbee, 2006).

In the upper fjord environment where rivers first enter the coastal zone, plume spreading and mixing are driven predominantly by the kinetic energy of river discharge (Syvitski et al., 1985), but plume characteristics are still controlled by a complex combination of factors both on land and after entering the fjord. Sediment-rich meltwater from land-terminating outlet glaciers may encounter lakes, outwash plains, or braided river valleys, all of which can act as traps or sources for sediment (Hasholt, 1996; Busskamp and Hasholt, 1996); these land-terminating fjords tend to be dominated by surface meltwater (Dowdeswell and Cromack, 1991). While sediment transport in rivers from land-terminating glaciers have been commonly studied through a relationship between river discharge and suspended sediment concentration (SSC) or total sediment load, some hysteresis has been found, where limitations in sediment supply result in decreased SSC despite increased meltwater runoff (Schneider and Bronge, 1996; Willis et al., 1996; Hammer and Smith, 1983). For marine-terminating outlet glaciers, sediment export to the ocean is dominated by the distinctly different mechanisms of iceberg rafting and/or en- and sub-glacially transported meltwater runoff (Andrews et al., 1994). In both environments, as plumes move farther downstream, sediment distribution and settling rates are further influenced by tides (Halverson and Pawlowicz, 2008; Bowers et al., 1998; Castaing and Allen, 1981), wind (Stumpf et al., 1993; Whitney and Garvine, 2005), and sea ice (Hasholt, 1996).

Here, buoyant sediment plumes that develop in upper fjord environments immediately downstream (~15 - 20 km, with a maximum of 50 km) of outlet glaciers and rivers that drain the Greenland ice sheet are mapped and analyzed using optical satellite imagery, to identify the distribution and temporal characteristics of sediment and meltwater release to coastal waters. Of particular interest is how well observed spatial and temporal variations in SSC respond to meltwater production on the ice sheet, and to what extent outlet glacier environments complicate this relationship, given that sediment supply hysteresis may also play a factor. SSC is used instead of plume area or length (McGrath et al., 2010; Chu et al., 2009) in order to expand the method beyond a river mouth. Optical images from the Moderate Resolution Imaging Spectroradiometer (MODIS) satellite are used from 2000-2009 to sample buoyant plume SSC in ~230 fjords with data aggregation producing near-daily temporal resolution with 100 km x 100 km gridcells. These observations are then compared with a proxy for ice sheet surface melting (Polar MM5 modeled positive degree-days, PDD), routed through potential drainage basins derived from ice surface and bedrock topography (Lewis and Smith, 2009), as well as outlet glacier types. The end result is a synoptic, ten-year analysis of spatiotemporal plume behavior around Greenland and a first assessment of some important controls on their distribution and development.

2.3 Data and methods

To explore controls on sediment plume development, we considered (1) daily ice sheet surface melt using modeled PDD, routed into the fjords following potential drainage basins; (2) near-daily fjord SSC from calibrated MODIS satellite imagery aggregated into 100 km coastal gridcells; and (3) outlet glacier environments.

2.3.1 Ice sheet surface melt

A key driver of sediment plume behavior explored here is ice sheet hydrology as represented by production of meltwater on the ice sheet surface. The fifth generation Polar Mesoscale Model (PMM5) provides a gridded 24 km resolution output of 3-hourly temperatures across the ice sheet surface from 2000-2009 (Box et al., 2006). Data were provided in a polar stereographic projection and a mask was applied to extract temperature data over the ice sheet. From these data, time series of daily positive degree-days were extracted by averaging the three-hourly temperatures greater than 0°C for each day. PDD is a traditional measure of melt intensity based on relating the cumulative depth of ice and snow melt to the sum of positive air temperatures over a specified time interval, usually a day. It is widely used because of its simplicity in temperature-based melt-index models (Ohmura, 2001; Hock, 2003), which are viable alternatives to more sophisticated energy balance models (Bougamont et al., 2007). Here, PDDs are used untransformed as a broad-scale, simple proxy for meltwater production. While not a true approximation for meltwater runoff, PDDs have been used in previous studies to represent melt intensity (Smith et al., 2003) and have been compared to ice sheet hydrologic processes such as supraglacial lake drainage and river discharge (Mernild and Hasholt, 2009; Georgiou et al., 2009)

As a proxy for meltwater volume produced within each hydrologic drainage basin, the aforementioned PDD data were totaled over topographically determined basins and assumed to drain only to corresponding ice sheet outlet glaciers and rivers at the ice sheet edge.

The drainage basins, each unique to a 100 km coastal gridcell (for fjord sediment detection) were defined using a previously derived vector dataset of ice sheet drainage basins based on potentiometric flow networks (Lewis and Smith, 2009), modeled from a combination of bedrock topography and surface topography by assuming hydrostatic pressure conditions and no conduits flows within the ice sheet. Basins were aggregated as necessary to correspond to each 100 km coastal gridcell, with final drainage basin area, B, and ice edge length, I, defined as the total horizontal length of the ice sheet edge bounded within each drainage basin. Melt area, A_{PDD}, was calculated for each drainage basin by totaling the number of 24 km pixels with a daily PDD greater than 0°C. The fraction of drainage basin experiencing active melting, F_{PDD}, was defined as melt area divided by drainage basin size ($F_{PDD} = \frac{A_{PDD}}{B}$). Melt penetration distance, $D_{PDD} = \frac{A_{PDD}}{I}$, represented the average inland distance from the ice edge that experienced surface melting.

2.3.2 Remote sensing of sediment plumes

Methodology for MODIS remote sensing of sediment plumes is shown in the Figure 2-1 flowchart. SSC was estimated by (1) classifying 10 years of available daily MODIS imagery into ice-free 'open water' (ranging from clear water to sediment-rich water) areas in the fjords, (2) aggregating the 500 m data into 100 km gridcells to retain a high frequency temporal sampling, and (3) transform MODIS reflectance into SSC using an empirical relationship developed from field water samples to transform reflectance into SSC.

2.3.2.1 MODIS 500 m satellite imagery and quality

The MODIS instrument on NASA's Terra satellite acquired daily coverage over Greenland from 2000-2010 with seven bands in the visible and infrared spectra at 500 m spatial resolution and two bands at 250 m resolution. Time series of MODIS Level 2 500 m surface reflectance product (MOD09) (Vermote et al., 2002), atmospherically corrected for gases, aerosols, and thin cirrus clouds, was used for the melt season (May 1st–September 30th) each year. These Level 2 data are aggregated into a daily product and available as tiles in a sinusoidal grid projection. Seven MODIS tiles were needed to cover all of Greenland (Figure 2-2). MODIS data are freely available and were downloaded from the NASA Warehouse Inventory Search Tool (https://wist.echo.nasa.gov/api/). Note that while MODIS data were available for 2010, PMM5 PDD data were only available until 2009. Therefore, MODIS data were processed and displayed for 2010 but not included in 10-year averages for comparison with PDD.

Only high-quality "clear-sky" MODIS pixels were used from each daily MODIS image. High-quality clear-sky pixels were defined as having: (1) a near-nadir view with adequate solar illumination (i.e., satellite overpass between 1300 and 1700 UTC), (2) minimal cloud cover ("clear" cloud state from the MODIS internal cloud state quality flag), and (3) minimal atmospheric interference ("corrected product produced at ideal quality all bands" from the MODIS Land Assessment quality flags). These quality parameters were determined using MODIS 500 m (solar zenith data) and 1 km resolution (cloud state and atmospheric data) Quality Assurance (QA) datasets that provided quality flags for each band.

2.3.2.2 *Classification and validation of 'open water'*

'Open water' pixels were defined as high quality MODIS pixels ranging from clear water to sediment-rich water, free of both clouds and ice, and distinguished using reflectance thresholds. MODIS band 1 (620 – 670 nm), band 2 (841 – 876 nm), band 3 (459 – 479 nm), band 4 (545 – 565 nm), and band 6 (1628–1652 nm) were used with thresholds in a simplified classification scheme to mask out land, ice (including land-fast ice, sea ice, and calving icebergs), and clouds. Particular difficulty in distinguishing sediment-rich water from melting ice was due to similar spectral responses in the seven available MODIS bands, so thresholds were chosen conservatively to err on the side of missing sediment-rich water rather than over-sampling open water. Land and river pixels were identified primarily by a lower reflectance in band 2 than band 1. To distinguish clouds and ice, both of which show high reflectance in the visible bands, band 6 was used. Clouds were identified with band 6 reflectance >> band 1 reflectance. Remaining pixels with lower band 6 values were classified into ice (hereafter this class will include brash ice, patchy sea ice, icebergs, and melting states of the above) and open water. Ice was distinguished with band 2 reflectance greater than 0.5*band 1 reflectance. Finally, open water (*OW*) was then produced as a range of clear water to sediment-rich water free of clouds and ice.

The 'open water' pixel classification was verified manually using 10 ASTER Level 2 15 m surface reflectance (AST 07) images and 27 Landsat TM/ETM+ 30 m images (Figure 2-2). Scenes for both sensors were limited to those during the summer melt season where plumes could be expected as well as in areas representing contrasting outlet glacier types and different spatial locations along the coast of Greenland. Melting ice, again including brash ice, patchy sea ice, and icebergs from calving glaciers, proved difficult to discern in the MODIS data due to its similarity with sediment-rich water, caused by low resolution spatially and spectrally with just seven available bands at 500 m resolution. This distinction of open water, which includes sediment-rich water, was crucial due to this class being used to extract SSC. The various ice states were more discrete in ASTER and Landsat, allowing the higher resolution images to act as validation classifications, testing whether the restrictive MODIS thresholds used for extracting open water were adequate. Accuracy was determined by performing a supervised classification on the higher resolution images and comparing them to the MODIS classification, with the class of quality-flagged pixels from MODIS masked out due to lack of comparable class in the higher resolution imagery. As shown in the results, a high overall accuracy and particularly a high user accuracy for the open water class showed the classification to be conservative estimate of open water and adequate for estimation of SSC.

Data density and sediment persistence were calculated for each 500 m MODIS pixel from the classified open water data to characterize the frequency of data recovery and high sediment concentration. Data density, DD_{500m}, was defined as the percentage of non-ice, non-cloud open water days over the entire period, and ranges from 0 (no open water) to 100% (open water detected every day), $DD_{500m} = \frac{OW}{total\ available\ data} x100\%$. While open water is the primary classification used in further analysis, a sediment persistence metric, F_{SSC}, was used to distinguish high SSC from low SSC to understand the temporal aspects of highly concentrated sediment lingering in the fjords. The threshold of band 1 > 0.12 developed in Chu et al. (2009) was used for identifying the highest sediment concentrations, designated the "plume" as opposed to the "brackish plume" in the sediment-rich Kangerlussuaq Fjord, so the same threshold used all around Greenland should identify only the highest SSCs and provide a conservative estimate of persistence. Sediment persistence was defined as the fraction of high-SSC days (OW_{SSC}) out of OW ($F_{SSC} = \frac{OW_{SSC}}{OW}$).

2.3.2.3 MODIS spatial sampling and aggregation

Fjord spatial sampling using 2,800 regions of interest (ROIs) covering 7,500 km^2 over 230 fjords were manually delineated to enable MODIS sampling of all fjords directly draining the ice sheet via land-terminating and marine-terminating glaciers (Figure 2-3). This restriction of analysis to fjords immediately draining the ice sheet reduced sampling of plumes triggered by melting snow packs, coastal erosion, and other sedimentary processes not necessarily triggered by ice sheet meltwater runoff. ROIs were typically digitized within ~15 - 20 km and not more than 50 km of river mouths and outlet glacier termini, rather than further down-fjord or in the open ocean.

To reduce the loss of open water data from clouds and obtain more precise temporal sampling, the 500 m native-resolution MODIS data, restricted to fjord ROIs, were aggregated into 100 km x 100 km coastal gridcells to yield the final dataset for all further analyses (Figure 2-3). First, a 100 km fishnet was overlaid onto the seven mosaicked MODIS tiles to summarize the SSC data within the ROIs. MODIS tiles were reprojected from the original sinusoidal projection to match the PMM5 model output polar sinusoidal projection. For each 100 km gridcell, R_{peak} was determined from the population of data within the ROIs. R_{peak}, was defined as the median of the top 20 *OW* MODIS band 1 reflectance values (based on empirical model described in Section 2.2.4) to avoid biases from ROI placement or number of ROIs per 100 km gridcell. Furthermore, to help mitigate the effects of data loss from cloud and ice interference, a 7-day moving interval was applied over the raw data in conjunction with the spatial resampling, effectively allowing the resulting daily value to derive from a sample population anywhere within the ROIs in each 100 km gridcell, and anywhere from three days before to three days after the day of interest. While this assumes that a sample from a partially cloudy 100 km gridcell is equivalent to a cloud-free box, R_{peak}

represents the average plume state within a week, allowing a week for the best pixels to be sampled.

2.3.2.4 Calibration/validation of SSC

The final data product of daily R_{peak} aggregated into 100 km coastal gridcells was transformed into SSC using an empirical relationship between remotely sensed reflectance and *in situ* measurements of SSC.

Field samples of SSC were necessary to understand plume characteristics, how SSC relates to the presence of freshwater, and how varying levels of sediment affect the spectral reflectance of the water. *In situ* water quality data were collected 3 June 2008 in Kangerlussuaq Fjord, southwest Greenland, with surface measurements of SSC, salinity, spectral reflectance, optical depth, and temperature collected every 1 km along a 22 km transect as described in Chu et al. (2009). Additional surface water samples from Eqip Sermia, a marine-terminating fjord in western Greenland, were collected July 4, 2007 and points were selected if they overlapped with digitized ROIs near the coast where buoyant sediment plumes were found, yielding four locations around 69.79°N, 50.53°W (Figure 2-2, Table 2-1). These sites provided laboratory measurements of SSC but did not include *in situ* spectral reflectance. These additional measurements supplemented the more extensive Kangerlussuaq Fjord dataset by providing *in situ* SSCs from an environment dominated by marine-terminating glaciers. An empirical model relating SSC to MODIS reflectance (Figure 2-4) was constructed using all available field samples and simultaneous MODIS band 1 (620 – 670 nm) reflectance as per Chu et al. (2009), yielding a new revised model of:

$$R(\text{band 1}) = 3.02\ln(SSC) + 1.12 \qquad R^2 = 0.86,\ p<0.001$$

with R(band 1) as the reflectance (%) for MODIS band 1 (620 – 670 nm) and SSC measured in mg/L. The model shows reflectance very sensitive to lower SSCs but saturation at high SSCs beyond 100 mg/L.

A new data density measurement, DD_{100km}, was calculated from the aggregated data, and a threshold of $DD_{100km} > 45\%$ was applied to produce the final gridcells used for further analysis.

2.3.3 Outlet glacier environment

Outlet glacier environments provide insight into the physical mechanisms by which sediment is dispersed from glacier outlets to fjords. While sediment transport in rivers (e.g., Hasholt, 1996; Knudsen et al., 2007; Rasch et al., 2000; Hasholt and Mernild, 2008; Russell, 2007) and sediment deposition in fjords (e.g., Syvitski et al., 1996; Reeh et al., 1999; Mugford and Dowdeswell, 2010) have previously been studied in Greenland, the active sediment plumes themselves are less studied (Chu et al., 2009; Lund-Hansen et al., 2010; McGrath et al., 2010). Though glacial erosion is responsible for some of the largest sediment yields to the ocean (Hallet et al., 1996; Gurnell et al., 1996), this paper focuses specifically on the fine glacial sediments transported by meltwater which remain in suspension in coastal waters, rather than total sediment flux and/or deposition processes.

The effect of outlet glacier environments on sediment concentrations was determined by characterizing outlet glacier type (marine- or land-terminating). Lewis and Smith (2009) provide georeferenced locations of all confirmed glacier meltwater outlets (i.e., land-terminating glaciers ending in rivers or lakes or marine-terminating glaciers with the presence of a sediment plume) and all unconfirmed glacier meltwater outlets (i.e., marine-terminating glaciers with no visible plume). These outlet types were further generalized into marine-terminating and land-terminating glacier outlets, and only those that led into a corresponding 100km coastal gridcell fjord area were counted and summarized within the gridcell. Marine-terminating outlets ranged from those with visible plumes and minimal iceberg activity to those heavily calving icebergs forming a "sikussak" complex of fused icebergs and sea ice attached to the glacier terminus (Syvitski, 1996). The ASTER/Landsat remote sensing validation process also proved useful for identifying gridcells dominated by fjords with heavily calving marine-terminating glaciers and no visible plume. Land-terminating outlets release meltwater at the ice sheet margin through proglacial lakes or rivers, and only those that eventually transport meltwater to the fjord through rivers or floodplains were included here. The number of land-terminating outlets (N_L) and number of marine-terminating outlets (N_M) for each drainage basin were determined using the outlets in Lewis and Smith (2009). The counts were normalized by the total number of outlets to compute fractions of land-terminating glaciers ($F_L = \frac{N_L}{N_L+N_M}$) and marine-terminating glaciers ($F_M = \frac{N_M}{N_L+N_M}$).

2.4 Results

MODIS-derived estimates of coastal fjord SSC ranging from ~0.7 to 1,925 mg/L were retrieved all around the ice sheet except in northern Greenland where persistent sea ice precludes detection of open water (Figure 2-5, Table 2-2). PMM5-derived PDD totals for ice sheet hydrologic basins draining to 100 km coastal gridcells, range from 0 to 165°C per day. Highest intensity is found along the ice sheet edge, decreasing exponentially farther inland with increasing elevations (Figure 2-5, Table 2-2). Table 2-2 displays 10-year mean values for each parameter and each coastal gridcell/drainage basin pair. Basin mean melt area (A_{PDD}) ranges from 32 – 16,277 km^2, with mean melt penetration distance (D_{PDD}) ranging from 0.3 – 112 km inland. Drainage basin size (*B*) ranges from 553 – 142,175 km^2 with ice edge lengths (*I*) varying between 35 and 344 km. Adequate MODIS data density is found for 47 out of 83 coastal 100 km gridcells. The raw, native-resolution 500 m data show that on average a Greenland coastal ROI pixel experiences at most 26% of all days between June 1st and September 30th classified as open water (on average 14%), that is, a water pixel without cloud or ice interference, from a total of 1531 days over the ten years (DD_{500m}). On average the coastal gridcells contain 5 marine-terminating glacier outlets (*M*) and 4 land-terminating glacier outlets (*L*). Spatially and temporally aggregated 100 km gridcells for SSC show an improved data density, with a minimum threshold of DD_{100km} > 45% yielding the 47 gridcells for further analysis and a mean DD_{100km} of 75%. 10-year mean sediment persistence (F_{SSC}) averages 0.11 for the entire ice sheet, meaning gridcells show high-SSC values for one-tenth of the open water days detected on average.

The extraction of SSC through open water classification and extrapolation from an empirical model provides a broad measurement of sediment concentration around the ice sheet. The classification validation shows an overall accuracy of 79%, and specifically for the open water class, reveals a producer accuracy of 66% and a user accuracy of 82%. In other words, while only 66% of open water pixels (including sediment-rich water) have been correctly identified as open water, 82% of the pixels called open water are truly open water. This conservative estimate of open water areas was deemed adequate for estimation of SSC. The limited 25 field samples required SSC extrapolation beyond those known values in the model relating MODIS reflectance to SSC, resulting in 5.6% of extracted SSC values greater than the maximum field SSC. Comparative measurements of sediment concentration around Greenland only exist for either rivers, which show expected higher values (Hasholt, 1996), or for Kangerlussuaq Fjord, which shows a lower range of 1.5 – 367.7 mg/L for inorganic suspended particulate matter (Lund-Hansen et al., 2010). Given these limitations, analysis of SSC will rely on broad averages over temporal and spatial scales.

2.4.1 Regional characteristics: mean SSC, mean PDD, data availability, and outlet glacier environment

The aforementioned characteristics of Greenland as a whole mask strong regional differences around the edge of the ice sheet. In Table 2-2, the 100 km coastal gridcells are further aggregated into six regions: Northwest Region, West Region, Southwest Region, Southeast Region, East Region, and Northeast Region (Figure 2-3). Note that results are presented with standard deviations (*s*) for 10-year means to show variability within samples, and 10-year median SSC is also presented as another summary measure given the extrapolation of higher SSCs beyond field measurements.

The Northwest Region (Figure 2-3) consists of four coastal gridcells (numbered 1-4) and exhibits a moderately low 10-year average SSC (55 ± 63 mg/L, Table 2-2), except for one uniquely high SSC gridcell (Gridcell 2), and a moderately low average PDD (1.3 ± 0.5 °C). Gridcell 2, off the coast west of Humboldt Glacier, has a mean SSC of 162 ± 4 mg/L, above average not only for the region but for the entire ice sheet as well and a high number of land-terminating glaciers (N_L=10). In contrast, Gridcell 4 directly to the south captures a high number of marine-terminating glaciers (N_M=14) with a large swath of glaciers near to the coast, generating one of the lowest mean SSC values (4 mg/L). This region has a high DD_{100km} (86%) and a high F_{SSC} (0.11), meaning high concentrations of sediment are detected for one-tenth of the melt season, with many protected fjords and a relatively high average N_L.

The West Region (Figure 2-3) has eight coastal gridcells (numbered 5-12), including several large marine-terminating glaciers including Jakobshavn Isbrae (Gridcell 12), Store

Glacier (Gridcell 11), and Rink Glacier (Gridcell 9). The West Region has a mean SSC of 57 ± 47 mg/L (Table 2-2) similar to the Northwest Region, but a higher mean PDD (5.9 ± 3.8 °C). This region contains high velocity marine-terminating glaciers, with ones farther south characterized by floating tongues or are near-floating (Thomas et al., 2009). This region has the largest average B (49,131 km^2) and contains Jakobshavn basin, the largest at a size of 99,210 km^2. A moderate DD_{100km} (77%) and a moderately low F_{SSC} (0.07) reflect the mix of outlet and fjord types, with a low average N_L (2) and a moderate average N_M (5), but the highest fraction of marine-terminating glaciers (F_M =0.77).

The Southwest Region (Figure 2-3) is made up of eleven coastal gridcells (numbered 13-23) and has the highest average values in most parameters: highest mean SSC (262 ± 168 mg/L, Table 2-2), highest mean PDD (12.5 ± 8.2 °C), highest average A_{melt} (6,002 km^2), highest average F_{SSC} (0.21), highest average N_L as well as F_L (0.81), and the highest DD_{100km} (89%). In particular, Gridcell 14, which encompasses Russell Glacier and the downstream Kangerlussuaq Fjord, shows the highest mean SSC (555 ± 422 mg/L) and by far the highest mean PDD (30.8 ± 34.3 °C). This region's gently sloping coast and warmer climate contributing to to the geomorphological uniqueness of this region. The extensive coastal land area affords every gridcell higher F_L than F_M and many large braided rivers to disperse the sediment into long, protected fjords. Going farther south in the region with less land area shows decreased mean SSC, decreased mean PDD, and decreased SSC_P.

The Southeast Region (Figure 2-3) has eleven coastal gridcells (numbered 24-34), encompassing the same latitude range as the Southwest Region, and shows a marked difference from the Southwest with very low averages of SSC (27 ± 29 mg/L, Table 2-2), PDD (1.1 ± 0.7 °C), and F_{SSC} (0.06). A moderate average DD_{100km} (73%) despite loss of *OW* from icebergs reflects the removal of those gridcells that did not meet the data density threshold, particularly those encompassing the heavily calving Kangerdlugssuaq and Helheim Glaciers. Persistent sikussaks at the ends of these glaciers extend several kilometers and prevent any detection of *OW*. These glaciers also have very large drainage basins, so their removal is also indicated by the fairly small average *B* (9,142 km^2). In contrast with the southwest, the southeast has the highest average N_M (11, also highest F_M=0.90) and lowest average N_L (1, also lowest F_L=0.1). Most glaciers are near to the coast with steeper slopes and fairly low melting.

The East Region (Figure 2-3) consists of six coastal gridcells (numbered 35-40) around the Scoresby Sund area and shows the lowest mean SSC (22 ± 11 mg/L, Table 2-2) and one of the lowest mean PDDs (0.9 ± 0.4 °C). Average F_{SSC} is also lowest of all regions (0.05), and two gridcells (Gridcells 35 and 36) do not show any sediment persistence, indicating that only very low concentrations of sediment exist in those areas. Average DD_{100km} is one of the lowest (61%), and outlets are fairly abundant in both marine-terminating and land-terminating types draining into protected fjords. The presence of a large land area as well as some islands allows for smaller glaciers and snowpatches not connected to the ice sheet to produce sediment, so ROIs were placed to avoid those areas as much as possible.

The Northeast Region (Figure 2-3) has seven coastal gridcells (numbered 41-47). This region has the lowest average DD_{100km} (58%), and the northernmost Gridcell 47 has the lowest individual gridcell DD_{100km} (48%). The low DD_{100km} of open water pixels free of ice is problematic in the northeast as well as in the northern areas; open water detection is prevented by the persistence of sea ice and/or iceberg calving. This region has the lowest mean PDD (0.8 ± 0.7 °C), but an intermediate mean SSC (63 ± 41 mg/L). Both land-terminating and marine-terminating outlets are fairly low in number, with slightly more N_L (4) compared N_M (3).

2.4.2 Hydrologic controls on fjord SSC: spatial, interannual, seasonal, and high frequency

2.4.2.1 Spatial variability

A high spatial correlation between 2000-2009 PDD and SSC confirms that more ice sheet melting leads to more suspended sediment being mobilized by meltwater. Figure 2-5b shows a strong correlation ($R=0.70$, $p<0.001$) between the 10-year mean PDD and 10-year mean SSC moving counterclockwise around the ice sheet from the northwest to the northeast. Mean PDD and SSC for individual gridcells illustrate results from the grouped regions. The Northwest and West Regions show a slightly decoupled intensity between PDD and SSC, with Gridcell 2 in the Northwest experiencing a low average PDD but high average SSC, and Gridcells 5-8 in the West revealing higher average PDDs with lower average SSCs. The Southwest Region is distinct in high values of both, with a few gridcells (Gridcells 16-19) associated with high plume SSC's despite low ice sheet PDD. A distinct drop in both PDD and SSC denotes the movement from the western half of Greenland to the eastern half, which is characterized by overall lower average PDD and SSC intensities and less distinct jumps in both datasets. Furthermore, PDD is a significant driver of SSC in high PDD areas but not in low PDD areas. Splitting the data in half with 24 high PDD gridcells and 23 low PDD gridcells, the high PDD portion show that PDD is strongly correlated with SSC ($R=0.61$, $p=0.002$), while the low PDD data are not correlated ($R=-0.16$, $p=0.47$).

2.4.2.2 Interannual variability

Interannual variations between ice sheet PDD and plume SSC correlate for the West and Northeast regions, but lack significant correlations for the other regions (Northwest, East, Southwest, and Southeast) and for Greenland as a whole (Figure 2-6). Nine gridcells that do show strong relationships are concentrated in the northern parts of Greenland; and for the most part the southern regions show slight anti-correlation interannually (Figure 2-7d, Table 2-2). Gridcell 13 in the Southwest Region containing solely Kangerlussuaq Fjord where a strong positive interannual correlation was previously found between ice sheet melt area and sediment plume area (Chu et al., 2009) also displays this slight anti-correlation, similar to most gridcells in the Southwest Region. This region highly influences the overall interannual relationship averaged Greenland owing to high values of both PDD and SSC.

2.4.2.3 Seasonal variability

Average seasonal climatologies of ice sheet PDD and downstream fjord SSC indicate coinciding seasonal cycles, with sediment plume onset coincident or commencing after surface melt onset (Figure 2-8). Seasonal climatologies of PDD and SSC are produced by averaging across the same day-of-year (d.o.y.) over 2000-2009, given at least two observations. While ice sheet melting inherently shows autocorrelation due to the inherently seasonal nature of solar radiation, autocorrelation is present also in fjord sediment concentration due to its reliance on meltwater transport, and therefore seasonal cross-correlations between the two datasets are naturally high. Correlations here will be used simply as a metric to show relative coherence between seasonal cycles, given the inherent autocorrelation. Cross-correlation is highest for the West and Southwest Regions ($R=0.81$, $p<0.001$, $R=0.86$, $p<0.001$, respectively, Figure 2-7e, Figure 2-8), especially Gridcell 14 in the Southwest (R=0.92, p<0.001, Table 2-2). Differences between regions include PDD and SSC intensity and seasonal length of both datasets, with the Southwest Region (in particular Gridcells 17-19) exhibiting highest SSCs and highest PDDs, and longer periods of activity and persistent sediment suspension towards the end of the melt season. Plume decline occurs during PDD decline for all regions, but the Southwest indicates high-SSCs persisting during the decline in melt in contrast to Chu et al. (2009), that found apparent sediment exhaustion with sediment plume areas decreasing prior to declines in melt area. Plume onset generally follows melt onset broadly in the western regions (Northwest, West, and Southwest), but the eastern regions (Southeast, East, and Northeast) show delayed plume onset as well as early melt onset. The Southeast Region is unique in that SSC is detected throughout the beginning of the melt season at low levels (~1.62 – 2.76 mg/L) indicating no arrival of sediment-rich meltwaters until June. The East Region has very low SSC (~0.83 – 0.97 mg/L) through the melt onset period, but much data are lost to the presence of sea ice until the end of May; the Northeast Region farther north shows even greater data loss with persistent sea ice until June.

2.4.2.4 High frequency variability

High frequency time series from 2000-2009 of ice sheet PDD and plume SSC show high short term variability (Figure 2-9). SSC values from 2010 are also shown (recall PMM5 PDD data were not available after 2009). The eastern regions (Southeast, East, and Northeast), all with much fewer PDDs, show a more variable melt season onset than the western regions. Overall, near-daily data generated by spatial and temporal aggregation do not correlate well and the temporal relationship between PDD and SSC matches better in average seasonal climatologies.

2.4.2.5 *Marine-terminating vs. land-terminating glacier outlets*

Plume characteristics vary with outlet glacier environment, here categorized into two broad types: land-terminating and marine-terminating. The spatial density of land-terminating outlet glaciers (N_L) shows a low positive correlation with averaged 2000-2009 SSC around the ice sheet (R=0.32, p=0.03), while the number of marine-terminating outlet glaciers (N_M) shows a negative correlation (R=-0.42, p=0.003) (Figure 2-7a). Normalizing the number of land-terminating and marine-terminating outlets by total number of outlets for each gridcell shows that the F_L is more strongly correlated with SSC than N_L (R=0.58, p<0.001). Outlet types for the most part cluster in regions, with the Southwest showing highest F_L (0.81) and the Southeast showing highest F_M (0.91) These overall trends reverse in northern regions, with relatively high F_L (0.59) in the Northeast and high F_M (0.60) in the Northwest. The geology of the ice-free area, one of the factors controlling the erosional susceptibility of the underlying bedrock, shows mostly latitudinal variation dominated by Archaean and early Proterozoic crystalline basement rocks (Geological Survey of Denmark and Greenland (GEUS), 2003). While geologic composition is only one of many factors in the production of sediment, softer rock types might be more easily eroded to produce more sediment, yet areas with highest SSCs are made up of hard gneisses that are likely to erode more slowly, possibly excluding geology as a controlling factor in fjord SSC.

2.4.3 Other factors

F_{SSC}, a measure of how long high SSC plumes persist, is highest in the southwest with highs also in the northwest and northeast (Figure 2-7b). The Southwest Region, again containing Gridcell 13 and the Kangerlussuaq Fjord, shows that protected fjords and many land-terminating outlets in the southwest allow sediment to persist longer toward the end of the season.

DD_{100km} has a positive spatial correlation (R=0.42, p=0.003) with SSC, highlighting areas in the southeast that often lose data due to iceberg calving yet still show low mean SSC (Figure 2-7c). While DD_{100km} is a measure of open water data retrieval, here it also mostly represents the predominance of icebergs and sea ice obscuring suspended sediment detection. This relationship represents another environmental factor affecting SSC detection and intensity; data density reflects both the outlet glacier environment and the climatic regime of the region.

2.5 Discussion

MODIS-derived plume suspended sediment concentration (SSC) successfully maps average plume distribution, which is controlled by both ice sheet hydrology and outlet glacier type, around ~80% of the Greenland coastline. Spatial variations in 10-year average positive degree days (PDDs), a proxy for meltwater generation on the ice sheet surface, is the most significant driver of spatial variations in 10-year mean SSC. While SSC data generated from 100 km gridcells greatly simplifies processes of sediment transport and dispersal, their correlation with ice sheet PDD indicates that higher ice sheet melting is linked to higher SSC in surrounding coastal waters. Likewise, ice sheet PDD only represents surface meltwater production and cannot be a proxy for runoff without the inclusion of refreezing, but this broad-scale association reveals plume SSC as a viable signal of meltwater release. Furthermore, the corresponding seasonal development of PDD and SSC track each other rather well, with broadly coincident timings of melt onset and plume detection (Figure 2-8). However, the Southeast, East Regions show delayed plume onset, lagging melt onset by ~3 –

4 weeks (a lag is also seen in the Northeast Region, but is due to delayed open water detection from sea ice, which may be obstructing a plume beneath the ice), whereas the western regions (Northwest, West, and Southwest) do not. In the Southeast and East Regions, despite delayed plume onset, plume growth coincides with the rising limb of PDD, but not in the Northeast. The Southwest Region reveals highly correlated seasonal climatologies of SSC and PDD (as averaged across each day-of-year over 2000 – 2009, Figure 2-8), but also a unique lingering of high SSC persisting ~1 month during the waning of the melt season. This is notably different from the results of Chu et al. (2009), which suggest sediment exhaustion in Kangerlussuaq Fjord. This difference may be due to use of aggregated data, but is more likely due the use of SSC rather than plume area. For example, in an elongate, protected fjord environment such as Kangerlussuaq Fjord, sediment may remain suspended but plume area may contract, possibly owing to circulation. This suggests that while ice sheet meltwater runoff is a dominant control of regional plume SSC development, fjord geometry in addition to outlet glacier types are also a factor.

Buoyant plumes are most readily detected downstream of rivers draining land-terminating glaciers, owing to high SSC (~200 – 550 mg/L range on average) and minimal obstruction by calving ice. Marine-terminating glaciers, in contrast, produce lower SSC (~2 – 100 mg/L range on average) and are often obstructed by icebergs and/or sea ice. Greenland's proglacial rivers, like other proglacial systems, are characterized by extremely high suspended sediment loads (e.g., 5 – 22,000 mg/L, Hasholt, 1996). Therefore, the spatial distribution of 10-year mean SSC reveals highest concentrations (~200 – 500 mg/L) in the Southwest Region, where F_L (fraction of land-terminating glacier outlets) is highest. This differs from other studies that project highest total sediment export in areas with major calving glaciers such as the northeast and southeast (Hasholt, 1996). One reason for this contrast is that the present study identifies freshwater signals represented by fine sediments suspended in ocean surface waters, rather than total depth-integrated sediment export as measured in terrestrial rivers. Also, while other studies present SSC from rivers draining the ice sheet, here SSC is measured from fjord plumes, showing lower average values due to plume spreading and mixing with marine waters. Plume SSC may also be lower than river SSC if meltwater encounters lakes and floodplains with some sediment settling out before reaching the fjord, and may therefore be considered a conservative estimate in land-terminating outlet environments. Thus, the MODIS-derived SSCs presented here are useful for detecting fine sediments associated with freshwater release, but not total sediment export, are sensitive to outlet glacier type, and are lower than corresponding SSC values from terrestrial samples of meltwater runoff from the ice sheet.

While Chu et al. (2009) found a strong interannual relationship between ice sheet surface melt extent and plume area, the present study finds no corresponding coherence between ice sheet PDD and plume SSC. Indeed, Gridcell 13, representing the Kangerlussuaq Fjord studied by Chu et al. (2009) and McGrath et al. (2010), lacks any significant correlation ($R= -0.29$, $p=0.42$) between the two variables on an interannual scale (Figure 2-6b). This contrast stems solely from the use of SSCs rather than plume area, as the two melt datasets are highly correlated ($R=0.96$, $p<0.001$). One reason for this may be the extrapolation of SSCs using a non-linear empirical model, which also does not encompass the full range of sediment-rich water reflectances. Uncertainty in the model is difficult to quantify given that the limited number of field samples were only from two sites in the southwest, and therefore analysis of SSC has been dependent on averaged values at various scales for each gridcell. Future studies should provide more field samples from a wider array of plume states, particularly at the high-SSC range, to further refine the model. However, while plume dimensions are good indices of ice sheet hydrologic variations, their use is limited to unique environments like Kangerlussuaq Fjord, that develop large plumes at river mouths with consistent absence of calf and/or sea ice. The present approach, using SSC instead of plume dimensions, allows study of plumes in other coastal environments including marine-terminating outlet glaciers where calving ice confounds clear measurement of plume area or length.

Marine-terminating glacier outlets, particularly heavily calving ones (e.g., Helheim, Kangerdlugssuaq, Jakobshavn), provide complications to quantifying buoyant sediment plumes. While sediment from marine-terminating glacier bottom melting should rise to fjord surface waters owing to high buoyancy of the meltwater plume (Powell and Molnia, 1989), sediment plumes originating subglacially at depths up to 600 m below the fjord water surface can experience sedimentation as the plume rises to the surface when sediment fall velocities exceed the entrainment velocity of the plume (Mugford and Dowdeswell, 2011). Furthermore, the presence of a layer of freshwater at the fjord surface may prevent the plume from surfacing due to a loss in buoyancy upon mixing. In addition to meltwater, icebergs are the other major contributor of sediment to fjords (Andrews et al., 1994). Similar to subglacial meltwater inputs, sediment from icebergs melt out at depths of ~100 – 400 m, with a turbulent plume rising to the surface and sedimentation also occurring. Sediment originating from icebergs, while contributing to total sediment export, complicates the retrieval of plumes in this study because those sediments do not originate from terrestrial runoff sources. However, icebergs release sediment slowly as they melt, transporting sediment large distances downstream of the glacier front (Syvitski et al., 1996;Azetsu-Scott and Syvitski, 1999; Hasholt et al., 2006). Therefore, in fjords with moderate iceberg interference, any detection of a surface sediment plume (limited by fjord spatial sampling ~15 – 20 km from the glacier front) likely reflects input of ice sheet meltwater runoff rather than sediment from icebergs. Though heavily calving glaciers are very important to mass loss and sediment export, the sikussaks of dense icebergs circulating within the upper fjord environment prevent plume detection and are removed with a data density restriction. Similarly, while the northern part of Greenland is of interest due to extensive bottom melting (rather than iceberg calving as the primary ablation mechanism, Reeh et al., 1999), data scarcity from persistent sea ice precludes adequate SSC recovery from MODIS reflectance products. Therefore, higher spatial resolution sensors are required to study plume characteristics in areas of pervasive iceberg and sea ice cover.

At high temporal frequencies (near-daily, Figure 2-9) ice sheet PDD and plume SSC are generally uncoupled, suggesting that complex processes of meltwater routing and sediment transport are not captured in a simple relationship between broad-scale representations of ice sheet meltwater production and buoyant sediment 96lumes. Furthermore, spatio-temporal aggregation is not effective for resolving the well-known temporal resolution limitations of MODIS in narrow fjord environments (Chu et al., 2009; McGrath et al., 2009). This lack of correlation at near-daily time scales is perhaps unsurprising with the very large 100 km aggregations required to produce near-daily time series. Also, other physical factors besides terrestrial runoff influence plume dynamics in the short term, including tides and wind (e.g., Dowdeswell and Cromack, 1991; Halverson and Pawlowicz, 2008; Whitney and Garvine, 2005). Detecting short-term (days to ~ 1week) variations in terrestrial runoff from sediment plumes remains challenging from a satellite remote sensing approach.

While this broad-scale view of sediment plumes around the ice sheet presents them as signals of meltwater release to the coast, sources of uncertainty limit these datasets for quantifying true runoff flux and studying ice sheet hydrology on a process-scale. As a proxy for meltwater runoff from the ice sheet, PDD does not take into account meltwater routing or storage in the glacier and in proglacial systems, which will affect both timing and intensity of meltwater release. Future studies need to incorporate runoff models tuned by *in situ* discharge observations such as Mernild and Hasholt (2009) and Rennermalm et al. (2012). As discussed above, using SSC to represent plume characteristics has its limitations due to the site-specific calibration of MODIS reflectances, the lack of validation for the empirical model, and the spatial aggregation used to overcome the poor temporal sampling. This scale of analysis obscures many physical processes, from ice sheet meltwater routing, to sediment transport, to mixing of fjord water masses. A more in-depth understanding of the various states, processes, and relationships between ice sheet hydrology and sediment dispersal from outlet glaciers is required for remote sensing of plumes to become a useful tool in assessing total meltwater flux to the ocean.

2.6 Conclusion

This study provides a first synoptic assessment of remotely-sensed buoyant coastal sediment plumes around Greenland, and links them to ice sheet runoff from land- and marine-terminating outlet glaciers. Meltwater production on the ice sheet surface, as approximated by PDD, is the most significant driver of spatial variations in suspended sediment concentrations of coastal ocean waters. On average, land-terminating outlet glaciers produce higher plume SSCs than marine-terminating outlet glaciers, although MODIS retrievals from the latter are often obstructed by icebergs. Despite known complexities in plume formation and development processes, remotely sensed sediment plumes appear to supply viable evidence of meltwater release. As such, their detection and monitoring from space represents one of the few ways to observe hydrologic release of meltwater from the Greenland ice sheet to the global ocean over broad spatial and temporal scales.

2.7 Figures

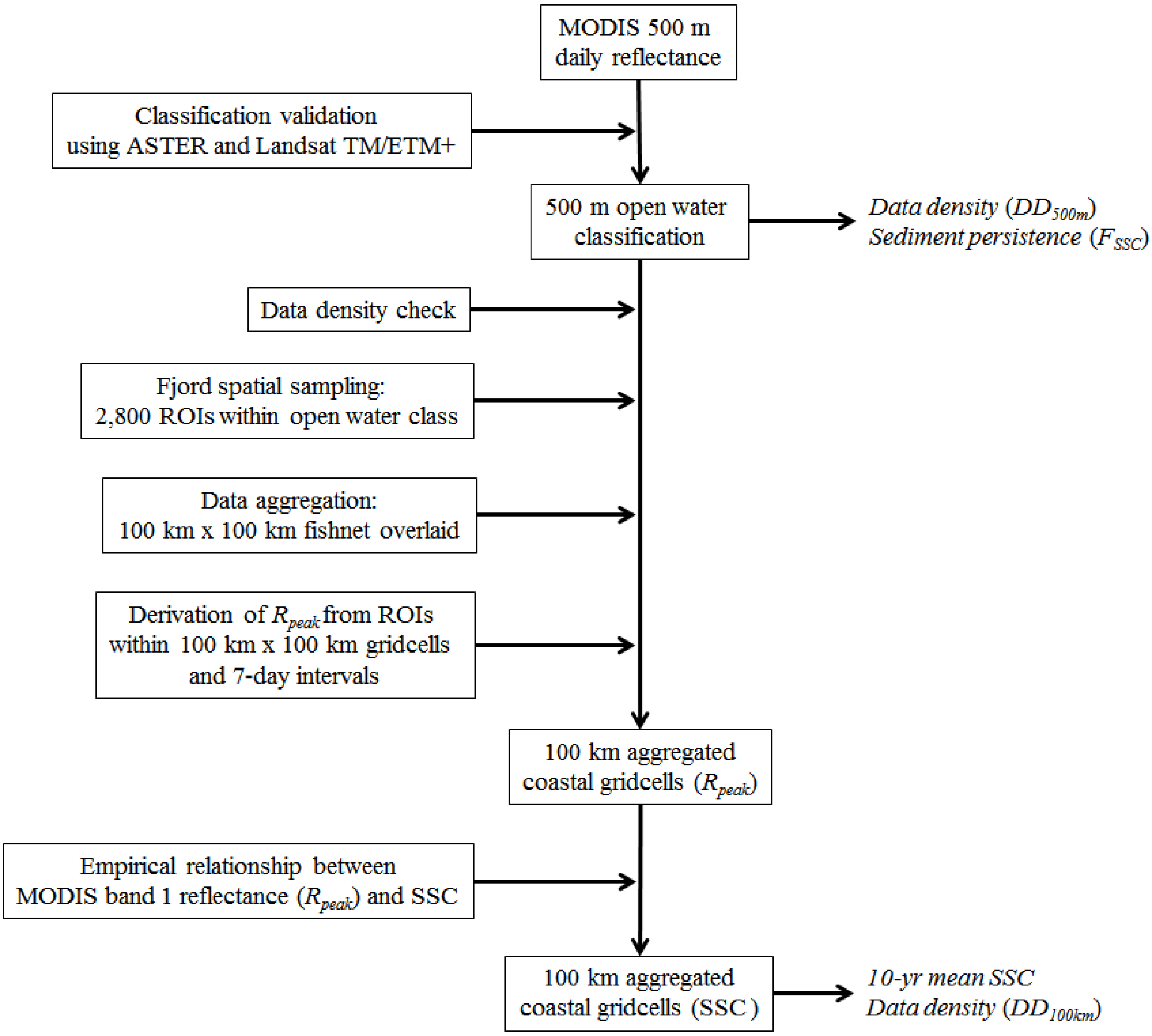

Figure 2-1. Methodology flowchart of MODIS remote sensing of sediment plumes. Daily 500 m MODIS reflectance data were classified to identify open water pixels ranging from clear water to sediment-rich water, spatially validated using higher-resolution ASTER and Landsat TM/ETM+. Resulting 500 m open water classification produced measures of sediment persistence and data density. To increase temporal sampling, data were aggregated into 100 km coastal gridcells, whose value was represented by R_{peak} within the gridcell and a 7-day interval. R_{peak} was derived from fjord ROIs that met a data density threshold. SSC was extracted for each 100 km coastal gridcell using an empirical model relating MODIS band 1 reflectance (R_{peak}) and SSC. New measures of sediment persistence and data density along with average SSC were calculated from these data.

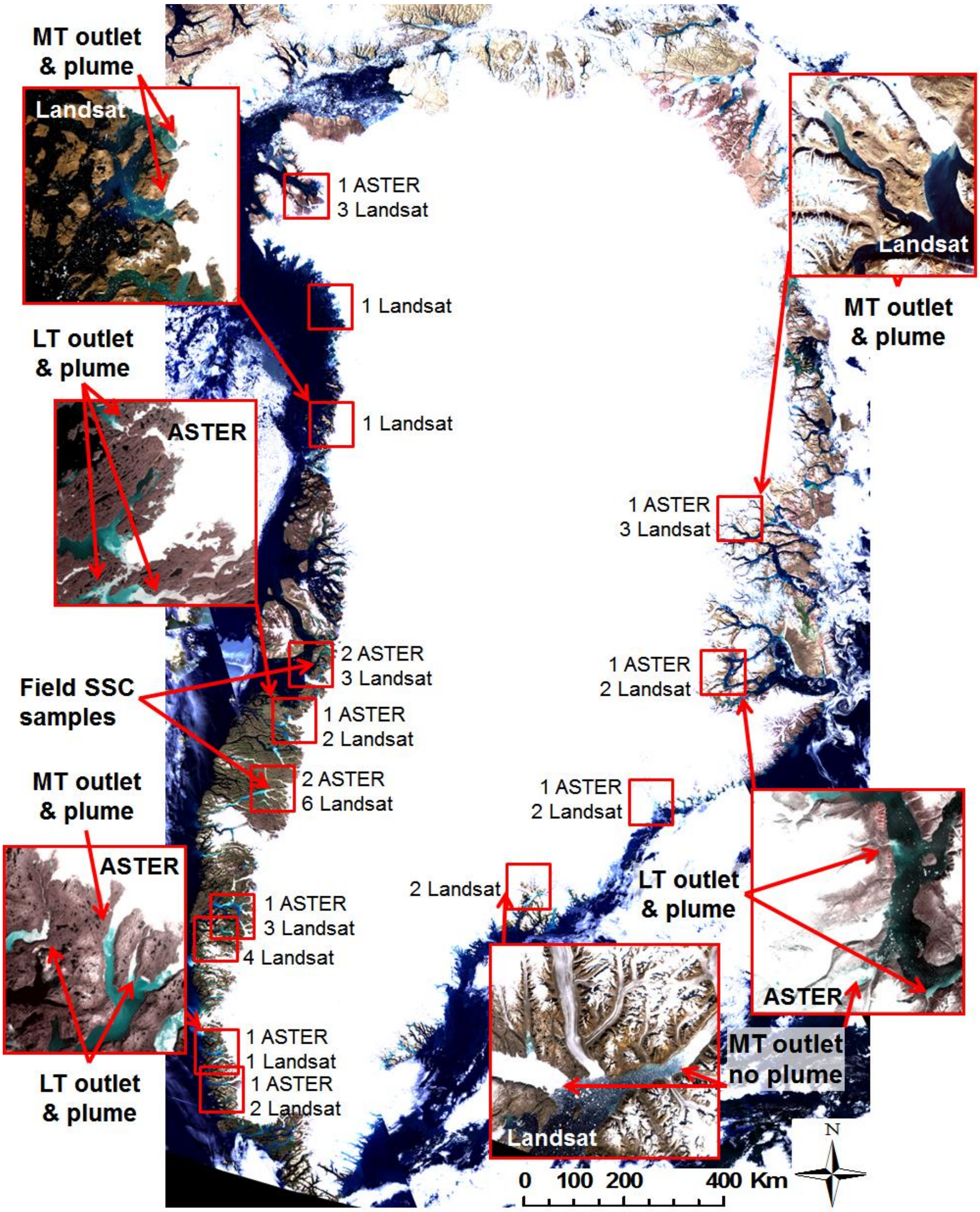

Figure 2-2. MODIS mosaic of Greenland (RGB=bands 1, 4, 3) with Landsat TM/ETM+ (RGB=bands 3, 2, 1) and ASTER (RGB=bands 2, 1, 1) image locations used for classification validation. Remote sensing analysis included all fjords directly draining the ice sheet through land-terminating glaciers (and downstream rivers) or from marine-terminating glaciers where plumes may form. Landsat and ASTER images show examples of different outlets and resulting plumes, including: (1) fjords fed by land-terminating glaciers (LT outlet & plume), with large sediment plumes forming after transport through a river floodplain, (2) fjords with marine-terminating glaciers (MT outlet & plume), few icebergs and a visible plume, and (3) fjords with marine-terminating glaciers heavily calving ice and no visible plume (MT outlet no plume).

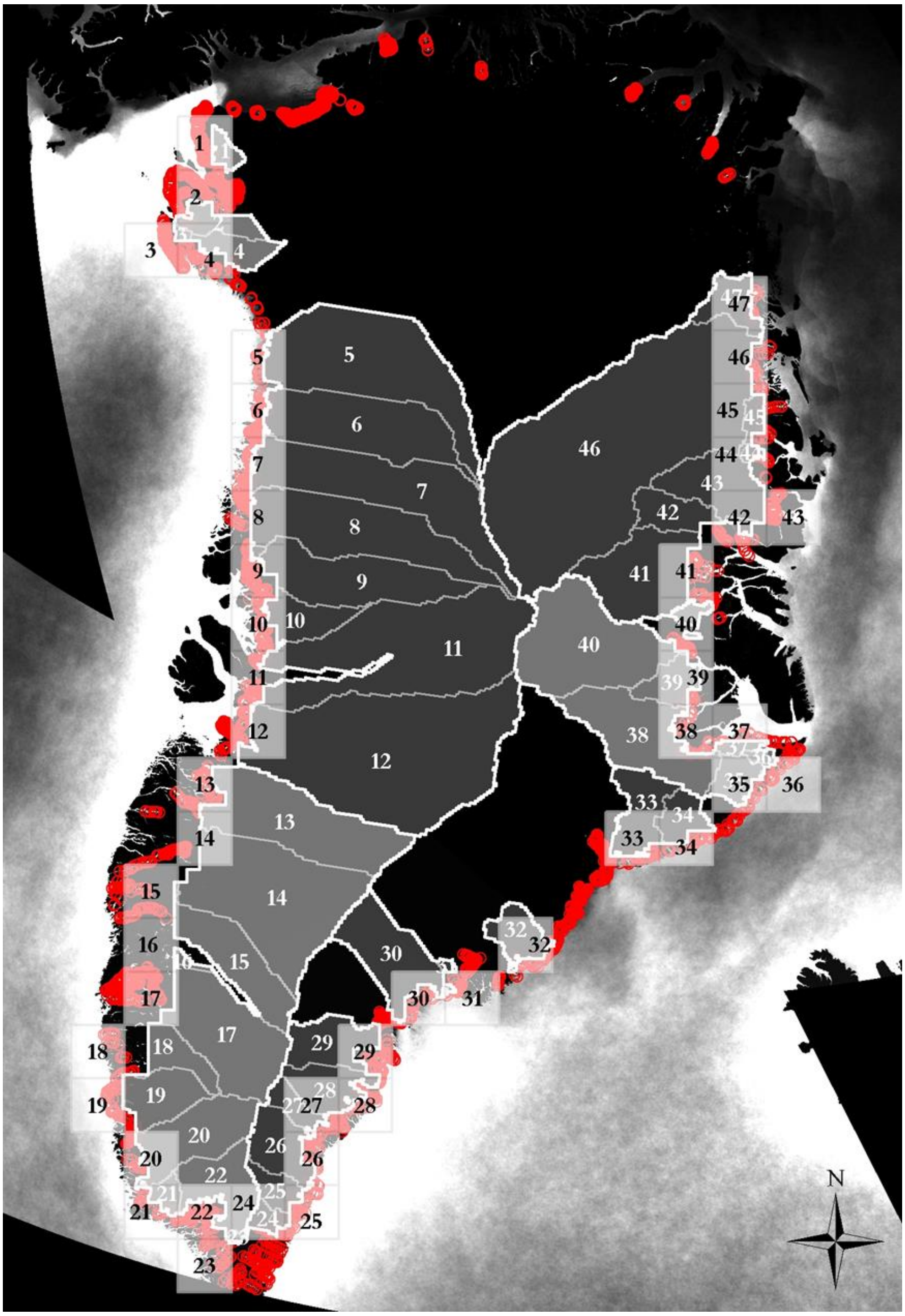

Figure 2-3. Coastal 100 km gridcells and their corresponding ice sheet drainage basins are overlaid onto an image showing data density (DD_{500m}) for 10 years of MODIS 500 m data, representing the number of open water days classified for each pixel out of a total of 1531 available and ranging from 0 – 40.6%. Regions of interest (ROIs, red circles) are manually drawn to restrict open water data to fjords draining the ice sheet. Gridcells are grouped into six regions for summary analysis: Northwest (NW), West (W), Southwest (SW), Southeast (SE), East ©, and Northeast (NE). The north/northeast and a swath along the southeast contain very low frequencies of detected open water days due to the presence of sea ice and glaciers heavily calving icebergs.

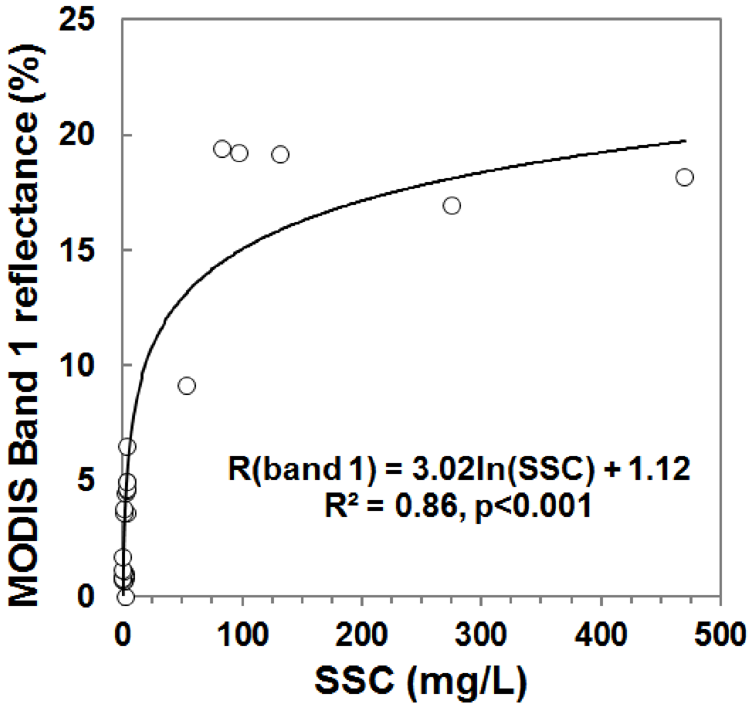

Figure 2-4. Empirical relationship between field SSC and simultaneous MODIS band 1 reflectance, with 22 samples from Kangerlussuaq Fjord, a land-terminating glacier outlet, and 3 samples from Equip Sermia, a marine-terminating glacier outlet ($R^2 = 0.86$, $p<0.001$).

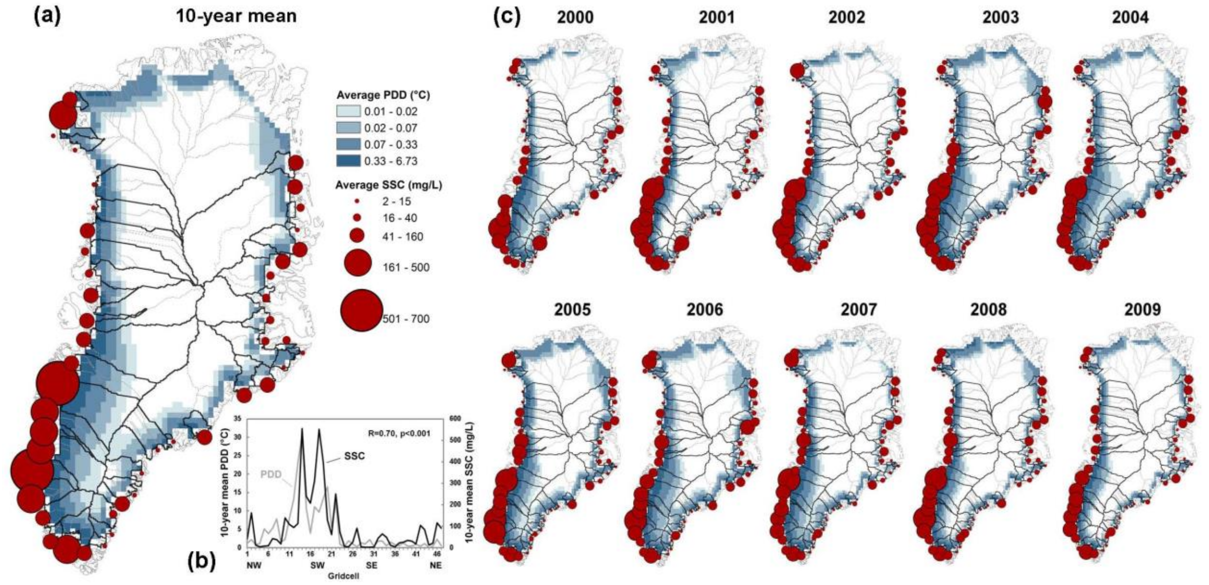

Figure 2-5. (a) Map of 10-year mean ice sheet PDD (blue) and fjord plume SSC (red circles). (b) Spatial variation of 10-year mean PDD (grey line) and SSC (black line), starting in the northwest and going counterclockwise towards the northeast (R=0.70, p<0.001). (c) Map of mean yearly SSC (red circles) and PDD (blue) for 2000-2009.

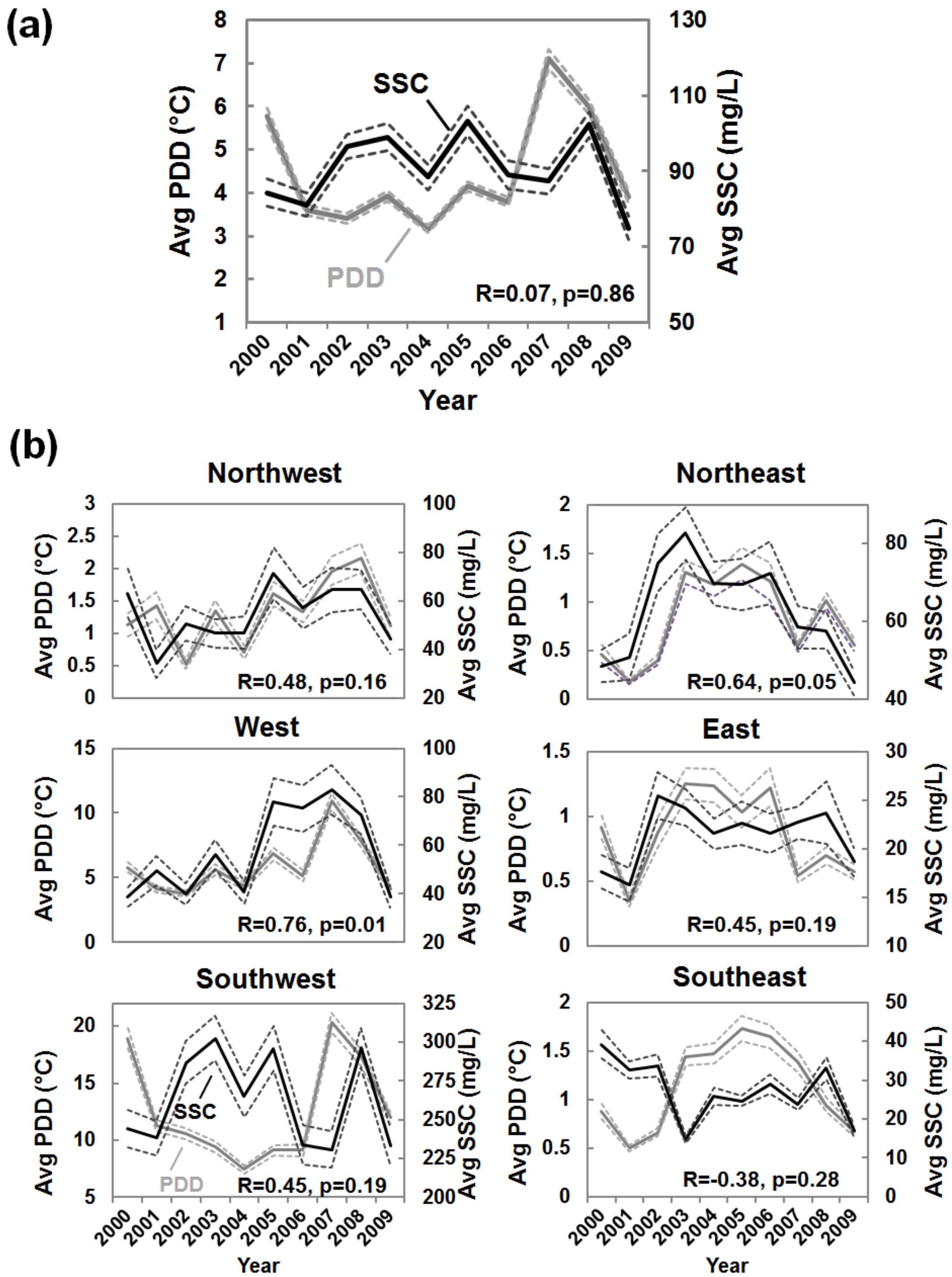

Figure 2-6. Interannual variations of ice sheet PDD and plume SSC for the (a) entire ice sheet and for (b) each of the six regions from 2000-2009, with 95% confidence intervals. The West and Northeast regions track each other rather well, while the Southwest and Southeast regions are fairly anti-correlated.

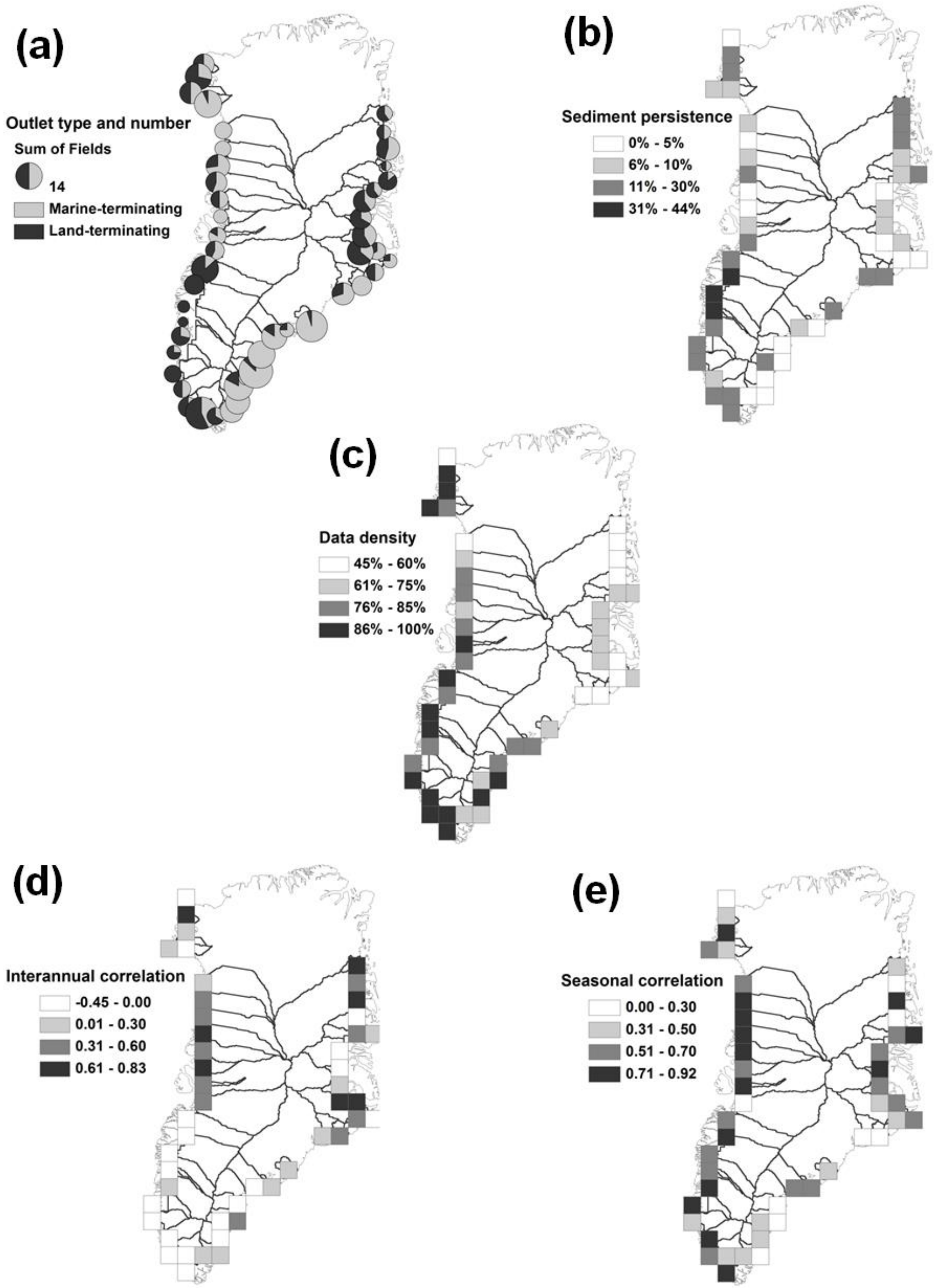

Figure 2-7. Maps of parameters and analyses for each of the 47 gridcells. (a) Glacier outlet type shows the number and proportion of outlets in each gridcell that is land-terminating (N_L) or marine-terminating (N_M), with the size of the circle representing the total number of outlets reaching the fjord. (b) Sediment persistence (F_{SSC}) shows the fraction of open water days with sediment-rich water detected. (c) Data density (DD_{100km}) shows the fraction of total days with open water detected (free of ice and clouds) for the aggregated 100 km data. (d) Correlation between interannual averages of PDD and SSC over 2000-2009. © Correlation between mean seasonal cycles of PDD and SSC.

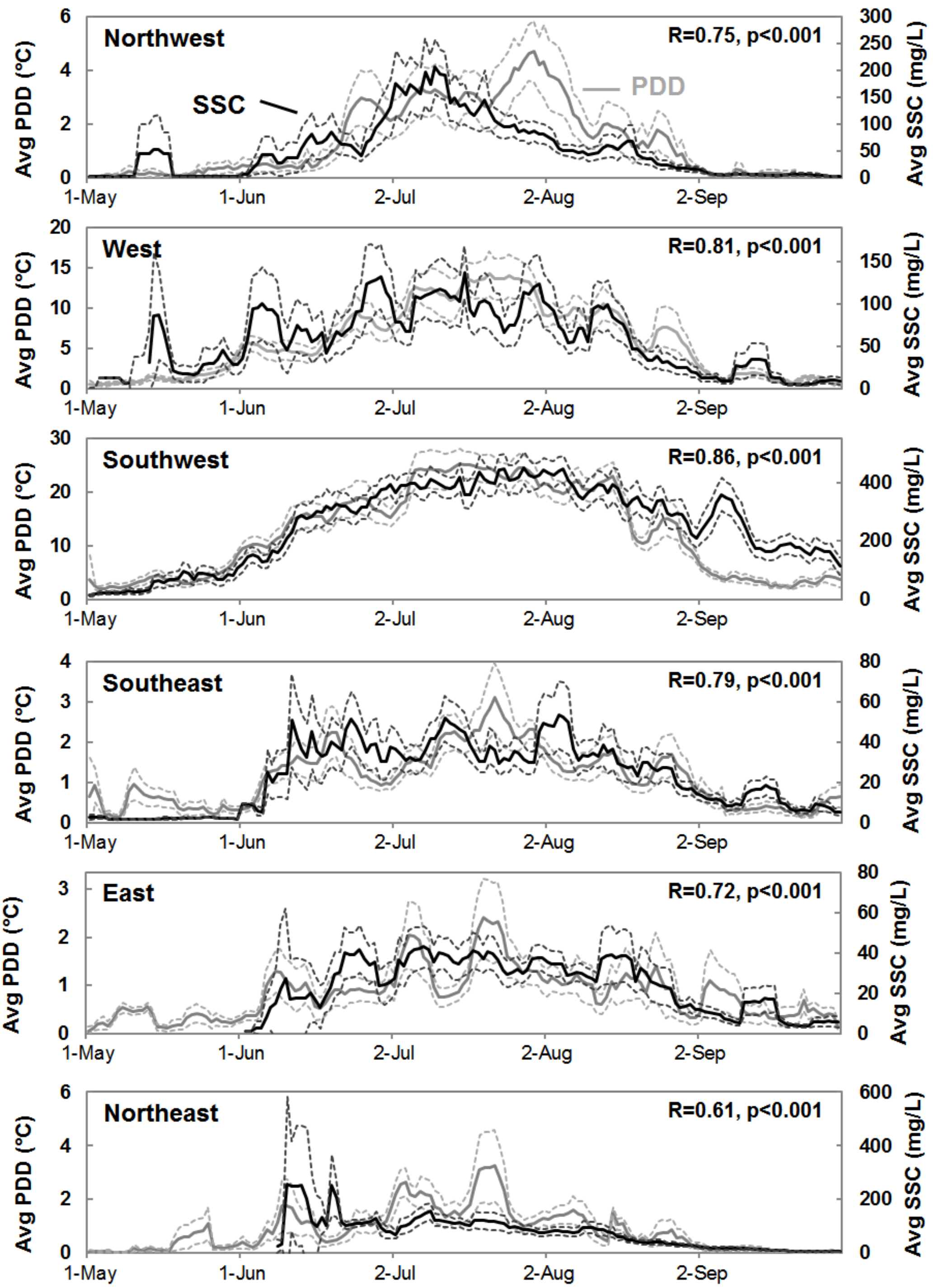

Figure 2-8. Mean seasonal development of ice sheet PDD and downstream fjord SSC for each of the six regions. A seasonal climatology is calculated by taking day-of-year averages over 2000-2009, with 95% confidence intervals. Seasonal cycles broadly coincide with plume onset coincident with or after surface melt onset, though the East and Northeast regions show difficulty detecting onset due to presence of sea ice. High SSCs persist in the Southwest region during the waning of the melt season.

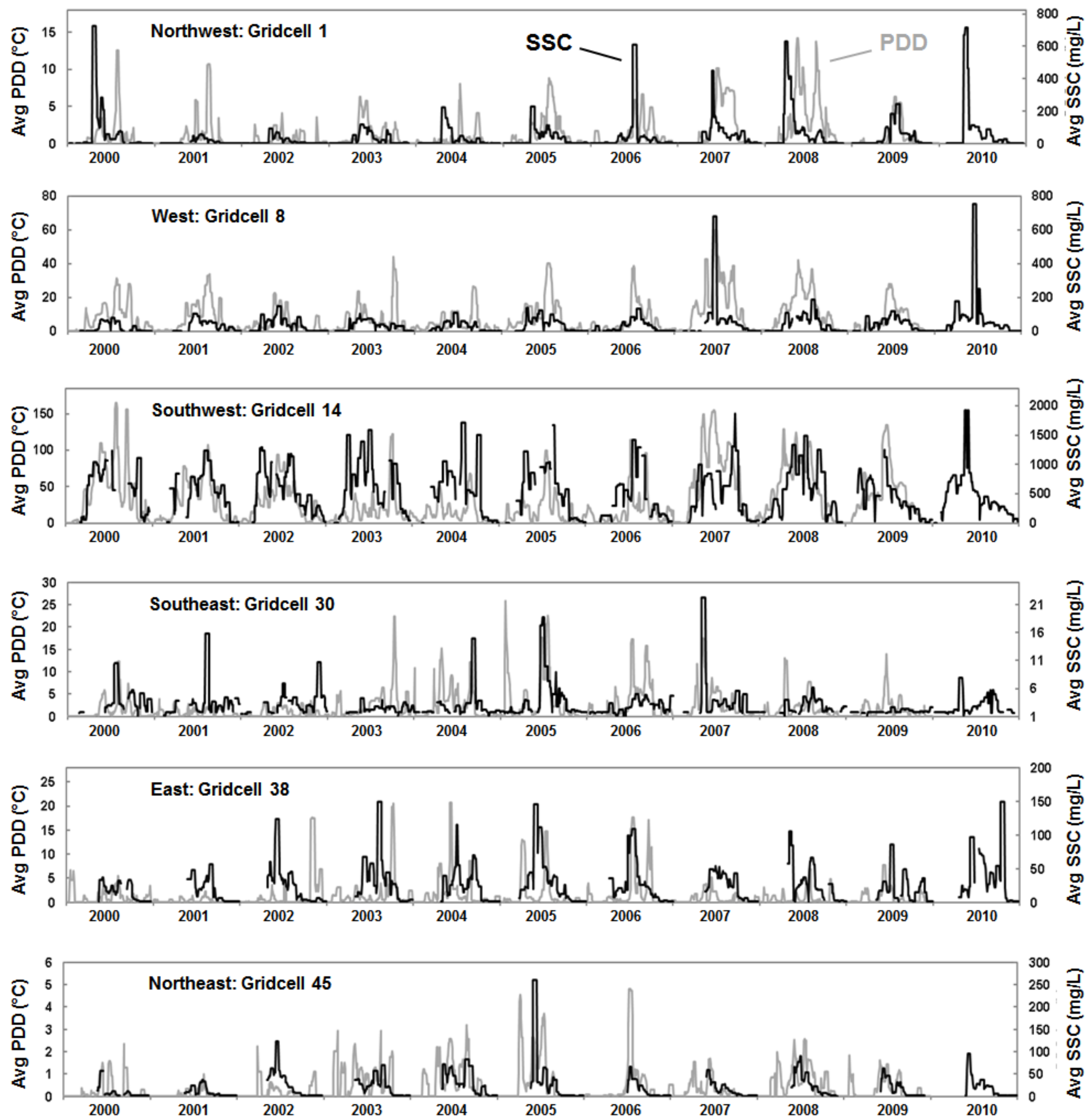

Figure 2-9. Examples of high frequency time series of SSC and PDD for one gridcell in each of the six regions from 2000-2009. SSC is displayed for 2010 but not used in analysis due to PDD only being available up to 2009.

2.8 Tables

Point	Location	Date	Time (local)	Lat	Long	Secchi Depth (cm)	Water Temp (°C)	Salinity (%)	MODIS Band 1 Reflectance (%)	SSC (mg/L)
1	Kangerlussuaq	June 3, 2008	13:40	66.8483	-51.2261	581.5	12	1.52	0.8	2.9
2	Kangerlussuaq	June 3, 2008	14:04	66.8537	-51.2145	619	10.4	1.75	0.67	1.3
3	Kangerlussuaq	June 3, 2008	14:49	66.8598	-51.2062	649	10.8	1.82	0.68	1.5
4	Kangerlussuaq	June 3, 2008	15:02	66.8647	-51.1871	520	11.4	1.68	0.7	0.6
5	Kangerlussuaq	June 3, 2008	15:12	66.8684	-51.1681	506	9.8	1.8	0.84	0.9
6	Kangerlussuaq	June 3, 2008	15:17	66.8728	-51.1482	531	9.9	1.82	0.79	0.2
7	Kangerlussuaq	June 3, 2008	15:31	66.8778	-51.1294	576	9.9	1.85	1.1	1.7
8	Kangerlussuaq	June 3, 2008	15:41	66.8832	-51.1117	326.5	10.4	1.61	1.16	0.9
9	Kangerlussuaq	June 3, 2008	15:52	66.8892	-51.0945	196	13.7	0.69	1.72	0.7
10	Kangerlussuaq	June 3, 2008	16:01	66.8950	-51.0768	178.5	13.7	0.65	3.62	1.6
11	Kangerlussuaq	June 3, 2008	16:09	66.9010	-51.0581	134	13	0.79	3.82	1.1
12	Kangerlussuaq	June 3, 2008	16:18	66.9065	-51.0382	97	12.4	0.46	4.49	2.6
13	Kangerlussuaq	June 3, 2008	16:52	66.9130	-51.0146	117.5	11.9	0.55	6.52	4.0
14	Kangerlussuaq	June 3, 2008	17:00	66.9180	-50.9929	102.5	13.5	0.33	4.59	3.9
15	Kangerlussuaq	June 3, 2008	17:10	66.9228	-50.9723	94.5	13.4	0.49	4.98	3.9
16	Kangerlussuaq	June 3, 2008	17:18	66.9296	-50.9536	107.5	14.5	0.34	4.63	3.7
17	Kangerlussuaq	June 3, 2008	17:25	66.9355	-50.9347	91	13.7	0.46	4.95	3.3
18	Kangerlussuaq	June 3, 2008	17:37	66.9418	-50.9112	5.5	14.1	0	16.94	275.6
19	Kangerlussuaq	June 3, 2008	17:48	66.9477	-50.8935	7.5	10.2	0.29	19.22	98.0
20	Kangerlussuaq	June 3, 2008	18:07	66.9504	-50.8741	7.5	10.7	0.2	19.12	132.5
21	Kangerlussuaq	June 3, 2008	17:58	66.9527	-50.8787	11	10.3	0.26	19.4	83.5
22	Kangerlussuaq	June 3, 2008	18:15	66.9544	-50.8544	5	7.9	0.11	18.17	470.0
23	Equip Sermia	July 4, 2007	10:45	69.8454	-50.3774	--	--	--	3.59	4.4
24	Equip Sermia	July 4, 2007	11:35	69.7965	-50.3094	--	--	--	9.16	53.9
25	Equip Sermia	July 4, 2007	12:45	69.7821	-50.6376	--	--	--	0	2.8
26	Equip Sermia	July 4, 2008	16:23	69.2415	-51.1155	--	--	--	0.99	3.1

Table 2-1. Field dataset of surface water samples from both Kangerlussuaq Fjord and Equip Sermia.

Gridcell	10yr Avg SSC (mg/L)	Max SSC (mg/L)	Min SSC (mg/L)	Sediment persistence	10yr Avg PDD (°C)	Max PDD (°C)	Drainage basin size (km2)	Avg melt area (km2)	Avg % drainage basin melting	Avg inland melt depth (km)	Ice edge length (km)	# marine-terminating glaciers	# land-terminating glaciers	Data density 100km (%)	Interannual Correlation	Seasonal Correlation
1	40	723	0.8	13.67%	1.23	14.13	2,847	830	29.2%	5.9	141	6	3	92%	0.61	0.48
2	162	1,784	1.0	16.02%	2.23	27.69	6,587	1,720	26.1%	8.1	212	4	10	86%	0.26	0.75
3	13	377	0.8	6.56%	0.78	7.41	711	310	43.6%	4.2	73	5	5	89%	0.02	0.63
4	4	65	0.9	9.07%	1.10	12.38	6,711	1,041	15.5%	5.5	189	14	1	75%	-0.18	0.46
	55			**11.33%**	**1.34**		**4,214**	**975**	**28.6%**	**5.9**	**154**	7	**5**	**85.6%**	**0.18**	**0.58**
5	8	226	0.7	9.03%	5.09	42.46	55,652	4,531	8.1%	21.9	207	6	0	58%	0.17	0.54
6	10	112	1.0	3.59%	3.81	28.73	36,968	3,176	8.6%	14.9	212	5	0	67%	0.33	0.74
7	42	686	0.9	6.10%	5.29	44.24	46,506	3,645	7.8%	17.8	204	8	3	82%	0.58	0.87
8	38	677	0.8	12.81%	7.86	59.84	41,373	4,721	11.4%	39.0	121	5	4	84%	0.83	0.89
9	18	215	1.0	1.81%	1.50	23.43	30,978	1,763	5.7%	11.9	148	3	3	74%	0.42	0.81
10	140	1,925	1.1	4.27%	2.30	29.15	10,166	2,089	20.5%	10.3	203	4	0	79%	0.83	0.55
11	109	1,553	0.9	5.01%	7.74	49.37	72,190	5,495	7.6%	32.3	170	5	1	91%	0.32	0.76
12	93	1,616	0.9	10.41%	13.25	88.72	99,210	9,863	9.9%	44.1	224	4	3	80%	0.46	0.08
	57			**6.63%**	**5.85**		**49,131**	**4,410**	**10.0%**	**24.0**	**186**	**5**	**2**	77%	**0.49**	**0.65**
13	112	1,149	0.8	19.09%	23.12	113.25	39,964	10,551	26.4%	40.9	258	2	13	94%	-0.09	0.62
14	555	1,875	1.7	44.29%	30.79	164.93	55,891	16,277	29.1%	111.9	146	0	8	78%	-0.08	0.92
15	238	1,568	1.1	33.33%	10.76	65.63	21,152	6,725	31.8%	60.7	111	0	3	90%	-0.09	0.65
16	207	939	1.9	32.82%	3.93	20.56	1,200	1,200	100.0%	30.9	39	0	2	91%	-0.23	0.61
17	312	1,887	0.9	20.46%	11.10	82.69	33,462	7,803	23.3%	58.0	135	2	5	82%	0.19	0.81
18	552	1,887	1.0	21.33%	9.64	57.70	8,603	4,314	50.1%	31.8	135	1	3	85%	-0.25	0.82
19	397	1,772	0.8	17.00%	13.39	72.97	12,796	4,926	38.5%	31.0	159	0	6	91%	-0.01	0.35
20	129	1,820	0.8	9.44%	16.55	86.57	21,386	6,272	29.3%	25.6	245	3	3	87%	-0.21	0.81
21	61	443	0.8	13.40%	5.53	23.93	3,134	1,384	44.2%	10.6	131	1	7	93%	-0.10	0.52
22	250	1,925	1.0	12.22%	12.19	74.05	15,793	6,219	39.4%	18.4	338	9	12	94%	-0.45	0.31
23	72	623	0.7	11.80%	0.96	6.13	553	349	63%	9.8	35	2	4	93%	-0.26	0.85
	262			**21.38%**	**12.54**		**19,449**	**6,002**	**43%**	**39.0**	**157**	**2**	**6**	**89%**	**-0.14**	**0.66**
24	6	133	1.1	1.34%	0.30	3.12	3,052	176	5.8%	2.4	74	10	1	61%	0.12	0.42
25	4	62	1.2	0.99%	1.94	27.41	5,344	1,196	22.4%	13.1	92	12	0	69%	0.04	0.28
26	26	704	0.8	1.19%	1.05	23.29	11,994	891	7.4%	3.9	227	14	3	100%	-0.39	0.46
27	91	1,838	0.9	10.16%	0.27	5.88	4,808	227	4.7%	1.8	125	4	0	68%	-0.32	0.32
28	5	373	0.9	3.50%	1.27	14.78	11,014	963	8.7%	2.8	344	20	3	89%	-0.23	0.10
29	3	49	1.0	0.56%	1.04	11.73	13,047	1,026	7.9%	5.6	184	15	0	82%	-0.37	0.09
30	3	22	0.9	8.25%	2.14	25.77	22,121	2,590	11.7%	8.2	318	11	2	78%	-0.01	0.64
31	2	11	0.9	2.09%	0.30	2.41	753	219	29.1%	2.0	110	3	1	81%	0.00	0.63
32	44	679	0.9	11.81%	1.84	17.58	8,391	1,542	18.4%	6.2	250	19	1	67%	0.20	0.40
33	64	697	1.3	15.64%	1.78	25.66	13,117	1,472	11.2%	4.9	302	7	3	57%	0.05	0.30
34	49	806	0.9	13.20%	0.56	8.53	6,917	635	9.2%	3.2	197	8	0	51%	0.43	0.09
	27			**6.25%**	**1.13**		**9,142**	**994**	**12.4%**	**4.9**	**202**	**11**	**1**	73%	**-0.04**	**0.34**
35	11	108	1.0	0.00%	1.51	21.38	6,235	1,111	17.8%	8.8	126	3	3	57%	0.41	0.33
36	4	22	0.7	0.00%	0.83	8.03	1,464	363	24.8%	5.9	62	3	1	63%	-0.15	0.66
37	23	211	0.8	7.06%	0.67	7.96	1,884	318	16.9%	2.7	117	4	2	54%	0.62	0.54
38	26	149	1.1	3.79%	1.34	20.75	29,747	1,462	4.9%	5.2	283	5	9	66%	0.68	0.44
39	35	185	0.7	7.56%	0.42	8.66	7,563	302	4.0%	1.8	170	5	7	65%	0.17	0.55
40	31	350	0.8	9.31%	0.45	9.36	44,694	490	1.1%	1.6	310	3	6	63%	-0.11	0.72
	22			**4.62%**	**0.87**		**15,264**	**674**	**11.6%**	**4.3**	**178**	**4**	**5**	**61%**	**0.27**	**0.54**
41	17	333	0.9	4.16%	0.91	28.13	27,790	841	3.0%	3.5	242	4	6	65%	-0.25	0.66
42	104	1,579	0.9	7.51%	0.47	9.89	10,232	501	4.9%	2.8	178	2	3	66%	0.46	0.57
43	84	603	1.0	10.40%	1.13	19.23	17,528	1,273	7.3%	7.5	170	1	6	66%	0.18	0.76
44	13	362	0.9	5.73%	0.05	1.10	1,165	32	2.7%	0.3	96	1	1	51%	-0.20	0.18
45	21	260	0.9	16.16%	0.41	4.80	2,790	231	8.3%	1.7	138	6	5	58%	0.75	0.79
46	115	1,497	1.0	26.76%	2.29	56.98	142,175	2,675	1.9%	16.3	164	2	2	54%	0.32	0.30
47	91	396	1.4	10.76%	0.88	10.37	8,043	437	5.4%	2.4	180	2	3	45%	0.61	0.49
	63			**11.64%**	**0.88**		**29,960**	**856**	**4.8%**	**4.9**	**167**	**3**	**4**	**58%**	**0.27**	**0.54**

Table 2-2. All parameters for each of the 47 gridcells, which are grouped and averaged into six regions. 10-year mean SSC ± standard deviation (*s*), 10-year median SSC, and 10-year mean PDD ± *s* are shown with standard deviations, and region averages are shown with standard deviations of gridcell averages within the region. *B* is drainage basin size (with medians summarizing regions), *I* is horizontal ice edge length, A_{PDD} is melt area within each drainage basin, F_{PDD} is percent of drainage basin actively melting, D_{PDD} is melt penetration distance, N_M is number of marine-terminating glacier outlets, F_M is the fraction of marine-terminating outlets, N_L is number of land-terminating glacier outlets, F_L is the fraction of land-terminating outlets, DD_{500m} is average data density of open water from raw 500 m data, DD_{100km} is data density of open water from aggregated 100 km gridcells, F_{SSC} is sediment persistence (fraction of high-SSC days from total open water days), *R(interannual)* is the correlation between interannual variations of SSC and PDD over 2000-2009, and *R(seasonal)* is the correlation between 10-year mean seasonal cycles, with significant correlations ($p<0.05$) in bold.

2.9 References

Abdalati, W. and K. Steffen (1997). Snowmelt on the Greenland ice sheet as derived from passive microwave satellite data. *Journal of Climate, 10*(2), 165-175.

Amundson, J. M., Truffer, M., Lüthi, M. P., Fahnestock, M., West, M., and Motyka, R. J. (2008). Glacier, fjord, and seismic response to recent large calving events, Jakobshavn Isbræ, Greenland. *Geophysical Research Letters*, 35(22), 1–5. doi:10.1029/2008GL035281

Andersen, M. L., Larsen, T. B., Nettles, M., Elósegui, P., van As, D., Hamilton, G. S., Stearns, L. A., Davis, J. L., Ahlstrøm, A. P., de Juan, J., Ekström, G., Stenseng, L., Khan, S. A., Forsberg, R., and Dahl-Jensen, D. (2010). Spatial and temporal melt variability at Helheim Glacier, East Greenland, and its effect on ice dynamics. *Journal of Geophysical Research*, 115(F4), 1–18. doi:10.1029/2010JF001760

Andrews, J. T., Milliman, J. D., Jennings, A. E., Rynes, N., and Dwyer, J. (1994). Sediment Thicknesses and Holocene glacial marine sedimentation rates in three East Greenland fjords (ca. 68°N). *Journal of Geology*, 102(6), 669–683.

Azetsu-Scott, K. and J. P. M. Syvitski (1999). Influence of melting icebergs on distribution, characteristics and transport of marine particles in an East Greenland fjord. *Journal of Geophysical Research-Oceans*, 104(C3), 5321-5328.

Bartholomew, I. D., Nienow, P., Mair, D., Hubbard, A. L., King, M. A., and Sole, A. (2010). Seasonal evolution of subglacial drainage and acceleration in a Greenland outlet glacier. *Nature Geoscience*, 3(6), 408–411. doi:10.1038/ngeo863

Bhattacharya, I., Jezek, K. C., Wang, L., and Liu, H. (2009). Surface melt area variability of the Greenland ice sheet: 1979–2008. *Geophysical Research Letters*, 36(20), 1–6. doi:10.1029/2009GL039798

Bøggild, C. E., Knudby, C. J., Knudsen, M. B., and Starzer, W. (1999). Snowmelt and runoff modelling of an Arctic hydrological basin in west Greenland. *Hydrological Processes*, *13*(12), 1989–2002. doi:10.1002/(SICI)1099-1085(199909)13:12/13<1989::AID-HYP848>3.0.CO;2-Y

Bougamont, M., Bamber, J. L., Ridley, J. K., Gladstone, R. M., Greuell, W., Hanna, E., Payne, A. J., and Rutt, I. (2007). Impact of model physics on estimating the surface mass balance of the Greenland ice sheet. *Geophysical Research Letters*, *34*(17), 1–5. doi:10.1029/2007GL030700

Bowers, D. G., Boudjelas, S., and Harker, G. E. L. (1998). The distribution of fine suspended sediments in the surface waters of the Irish Sea and its relation to tidal stirring. *International Journal of Remote Sensing*, *19*(14), 2789–2805. doi:10.1080/014311698214514

Box, J. E., Bromwich, D. H., Veenhuis, B. A., Bai, L.-S., Stroeve, J. C., Rogers, J. C., Steffen, K., Haran, T., and Wang, S.-H. (2006). Greenland Ice Sheet surface mass balance variability (1988 – 2004) from calibrated Polar MM5 output. *Journal of Climate*, *19*, 2783–2800. doi:10.1175/JCLI3738.1

Box, J. E. and Ski, K. (2007). Remote sounding of Greenland supraglacial melt lakes: implications for subglacial hydraulics. *Journal of Glaciology*, *53*(181), 257–265. doi:10.3189/172756507782202883

Box, J. E., Yang, L., Bromwich, D. H., and Bai, L.-S. (2009). Greenland Ice Sheet surface air temperature variability: 1840–2007. *Journal of Climate*, *22*(14), 4029–4049. doi:10.1175/2009JCLI2816.1

Burgess, E. W., Forster, R. R., Box, J. E., Mosley-Thompson, E., Bromwich, D. H., Bales, R. C., and Smith, L. C. (2010). A spatially calibrated model of annual accumulation rate on the Greenland Ice Sheet (1958–2007). *Journal of Geophysical Research*, *115*(F2), 1–14. doi:10.1029/2009JF001293

Busskamp, R. and B. Hasholt (1996). Coarse bed load transport in a glacial valley, Sermilik, South East Greenland. *Zeitschrift Fur Geomorphologie*, *40*(3), 349-358.

Castaing, P. and Allen, G. P. (1981). Mechanisms controlling seaward escape of suspended sediment from the Gironde: a macrotidal estuary in France. *Marine Geology*, *40*, 101–118.

Catania, G. A. and Neumann, T. A. (2010). Persistent englacial drainage features in the Greenland Ice Sheet. *Geophysical Research Letters*, *37*(2), 1–5. doi:10.1029/2009GL041108

Chen, J. L., Wilson, C. R., and Tapley, B. D. (2006). Satellite gravity measurements confirm accelerated melting of Greenland ice sheet. *Science*, *313*(5795), 1958–60. doi:10.1126/science.1129007

Chu, V. W., Smith, L. C., Rennermalm, A. K., Forster, R. R., Box, J. E., and Reeh, N. (2009). Sediment plume response to surface melting and supraglacial lake drainages on the Greenland ice sheet. *Journal of Glaciology*, *55*(194), 1072–1082. doi:10.3189/002214309790794904

Colgan, W., Rajaram, H., Anderson, R. S., Steffen, K., Phillips, T., Joughin, I., Zwally, H. J., and Abdalati, W. (2011). The annual glaciohydrology cycle in the ablation zone of the Greenland ice sheet: Part 1. Hydrology model. *Journal of Glaciology*, *57*(204), 697–709. doi:10.3189/002214311797409668

Curran, P. J. and E. M. M. Novo (1988). The relationship between suspended sediment concentration and remotely sensed spectral radiance - A review. *Journal of Coastal Research*, *4*(3), 351-368.

Das, S. B., Joughin, I., Behn, M. D., Howat, I. M., King, M. A., Lizarralde, D., and Bhatia, M. P. (2008). Fracture propagation to the base of the Greenland Ice Sheet during supraglacial lake drainage. *Science*, *320*(5877), 778–81. doi:10.1126/science.1153360

Dowdeswell, J. A. and Cromack, M. (1991). Behavior of a glacier-derived suspended sediment plume in a small inlet. *Journal of Geology*, *99*, 111–123.

Doxaran, D., Froidefond, J., Lavender, S., and Castaing, P. (2002). Spectral signature of highly turbid waters Application with SPOT data to quantify suspended particulate matter concentrations, *81*, 149–161.

Ettema, J., van den Broeke, M. R., van Meijgaard, E., van de Berg, W. J., Bamber, J. L., Box, J. E., and Bales, R. C. (2009). Higher surface mass balance of the Greenland ice sheet revealed by high-resolution climate modeling. *Geophysical Research Letters*, *36*(12), 1–5. doi:10.1029/2009GL038110

Fettweis, X. (2007). Reconstruction of the 1979 – 2006 Greenland ice sheet surface mass balance using the regional climate model MAR. *The Cryosphere*, *1*, 21–40.

Fettweis, X., Hanna, E., and Gall, H. (2008). Estimation of the Greenland ice sheet surface mass balance for the 20th and 21st centuries. *The Cryosphere*, *2*, 117–129. doi:10.5194/tc-2-117-2008

Georgiou, S., Shepherd, A., McMillan, M., and Nienow, P. (2009). Seasonal evolution of supraglacial lake volume from ASTER imagery. *Journal of Glaciology*, *50*(52), 95–100. doi:10.3189/172756409789624328

Gurnell, A., Hannah, D., and Lawler, D. (1996). Suspended sediment yield from glacier basins, (236), 97–104.

Hall, D. K., Williams, R. S., Luthcke, S. B., and DiGirolamo, N. E. (2008). Greenland ice sheet surface temperature, melt and mass loss: 2000 – 06. *Journal of Glaciology*, *54*(184), 81–93. doi:10.3189/002214308784409170

Hallet, B., Hunter, L., and Bogen, J. (1996). Rates of erosion and sediment evacuation by glaciers: A review of field data and their implications. *Global and Planetary Change*, *12*(1-4), 213–235. doi:10.1016/0921-8181(95)00021-6

Halverson, M. J. and Pawlowicz, R. (2008). Estuarine forcing of a river plume by river flow and tides. *Journal of Geophysical Research*, *113*(C9), 1–15. doi:10.1029/2008JC004844

Hammer, K. M. and Smith, N. D. (1983). Sediment production and transport in a proglacial stream: Hilda Glacier, Alberta, Canada. *Boreas1*, *12*(2), 91–106.

Hanna, E., Huybrechts, P., Steffen, K., Cappelen, J., Huff, R., Shuman, C. A., Irvine-Fynn, T. D. L., Wise, S., and Griffiths, M. (2008). Increased runoff from melt from the Greenland Ice Sheet: A response to global warming. *Journal of Climate*, *21*(2), 331–341. doi:10.1175/2007JCLI1964.1

Hasholt, B. (1996). Sediment transport in Greenland. *Response*, (236), 105–114.

Hasholt, B., Bobrovitskaya, N., Bogen, J., McNamara, J., Mernild, S. H., Milburn, D., and Walling, D. E. (2006). Sediment transport to the Arctic Ocean and adjoining cold oceans. *Nordic Hydrology*, *37*(4), 413–432.

Hasholt, B. and Mernild, S. H. (2001). Hydrology, sediment transport and water resources of Ammassalik Island, SE Greenland. *Geografisk Tidsskrift - Danish Journal of Geography*, *108*(1), 73–96.

Hock, R. (2003). Temperature index melt modelling in mountain areas. *Journal of Hydrology*, *282*(1-4), 104–115. doi:10.1016/S0022-1694(03)00257-9

Holland, D. M., Thomas, R. H., de Young, B., Ribergaard, M. H., and Lyberth, B. (2008). Acceleration of Jakobshavn Isbræ triggered by warm subsurface ocean waters. *Nature Geoscience*, *1*(10), 659–664. doi:10.1038/ngeo316

Howat, I. M., Joughin, I., and Scambos, T. A. (2007). Rapid changes in ice discharge from Greenland outlet glaciers. *Science*, *315*(5818), 1559–61. doi:10.1126/science.1138478

Hu, C., Chen, Z., Clayton, T. D., Swarzenski, P., Brock, J. C., and Muller–Karger, F. E. (2004). Assessment of estuarine water-quality indicators using MODIS medium-resolution bands: Initial results from Tampa Bay, FL. *Remote Sensing of Environment*, *93*(3), 423–441. doi:10.1016/j.rse.2004.08.007

Joughin, I., Das, S. B., King, M. A., Smith, B. E., Howat, I. M., and Moon, T. (2008). Seasonal speedup along the western flank of the Greenland Ice Sheet. *Science*, *320*(5877), 781–3. doi:10.1126/science.1153288

Joughin, I., Smith, B. E., Howat, I. M., Scambos, T. A., and Moon, T. (2010). Greenland flow variability from ice-sheet-wide velocity mapping. *Journal of Glaciology*, *56*(197), 415–430. doi:10.3189/002214310792447734

Joughin, I., Tulaczyk, S., Fahnestock, M., and Kwok, R. (1996). A mini-surge on the Ryder Glacier, Greenland, observed by satellite radar interferometry. *Science*, *274*(5285), 228–230.

Khan, S. A., Wahr, J., Bevis, M., Velicogna, I., and Kendrick, E. (2010). Spread of ice mass loss into northwest Greenland observed by GRACE and GPS. *Geophysical Research Letters*, *37*(6), 1–5. doi:10.1029/2010GL042460

Knudsen, N. T., Yde, J. C., and Gasser, G. (2003). Suspended sediment transport in glacial meltwater during the initial quiescent phase after a major surge event at Kuannersuit Glacier, Greenland. *Geografisk Tidsskrift - Danish Journal of Geography*, *107*(1), 1–8.

Krabill, W. B. (2004). Greenland Ice Sheet: Increased coastal thinning. *Geophysical Research Letters*, *31*(24), 2–5. doi:10.1029/2004GL021533

Lewis, S. M. and Smith, L. C. (2009). Hydrologic drainage of the Greenland Ice Sheet. *Hydrological Processes*, *23*(May 2009), 2004–2011. doi:10.1002/hyp

Lihan, T., Saitoh, S.-I., Iida, T., Hirawake, T., and Iida, K. (2008). Satellite-measured temporal and spatial variability of the Tokachi River plume. *Estuarine, Coastal and Shelf Science*, *78*(2), 237–249. doi:10.1016/j.ecss.2007.12.001

Lund-Hansen, L. C., Andersen, T. J., Nielsen, M. H., and Pejrup, M. (2010). Suspended matter, Chl-a, CDOM, grain sizes, and optical properties in the Arctic fjord-type estuary, Kangerlussuaq, West Greenland during summer. *Estuaries and Coasts*, *33*(6), 1442–1451. doi:10.1007/s12237-010-9300-7

Luthcke, S. B., Zwally, H. J., Abdalati, W., Rowlands, D. D., Ray, R. D., Nerem, R. S., Lemoine, F. G., McCarthy, J. J., and Chinn, D. S. (2006). Recent Greenland ice mass loss by drainage system from satellite gravity observations. *Science*, *314*(5803), 1286–1289. doi:10.1126/science.1130776

McGrath, D., Steffen, K., Overeem, I., Mernild, S. H., Hasholt, B., and Van den Broeke, M. R. (2010). Sediment plumes as a proxy for local ice-sheet runoff in Kangerlussuaq Fjord, West Greenland. *Journal of Glaciology*, *56*(199), 813–821. doi:10.3189/002214310794457227

Mernild, S. H. and Hasholt, B. (2009). Observed runoff, jökulhlaups and suspended sediment load from the Greenland ice sheet at Kangerlussuaq, West Greenland, 2007 and 2008. *Journal of Glaciology*, *55*(193), 855–858.

Mernild, S. H., Howat, I. M., Ahn, Y., Liston, G. E., Steffen, K., Jakobsen, B. H., Hasholt, B., Fog, B., and van As, D. (2010a). Freshwater flux to Sermilik Fjord, SE Greenland. *The Cryosphere*, *4*(4), 453–465. doi:10.5194/tc-4-453-2010

Mernild, S. H., Liston, G. E., Hiemstra, C. A., Christensen, J. H., Stendel, M., and Hasholt, B. (2011). Surface mass balance and runoff modeling using HIRHAM4 RCM at Kangerlussuaq (Søndre Strømfjord), West Greenland, 1950–2080. *Journal of Climate*, *24*(3), 609–623. doi:10.1175/2010JCLI3560.1

Mernild, S. H., Liston, G. E., Steffen, K., Van den Broeke, M. R., and Hasholt, B. (2010b). Runoff and mass-balance simulations from the Greenland Ice Sheet at Kangerlussuaq (Søndre Strømfjord) in a 30-year perspective, 1979–2008. *The Cryosphere*, *4*(2), 231–242. doi:10.5194/tc-4-231-2010

Miller, R. L. and McKee, B. A. (2004). Using MODIS Terra 250 m imagery to map concentrations of total suspended matter in coastal waters. *Remote Sensing of Environment*, *93*(1-2), 259–266. doi:10.1016/j.rse.2004.07.012

Mote, T. L. (2007). Greenland surface melt trends 1973–2007: Evidence of a large increase in 2007. *Geophysical Research Letters*, *34*(22), 1–5. doi:10.1029/2007GL031976

Mugford, R. I. and Dowdeswell, J. A. (2010). Modeling iceberg-rafted sedimentation in high-latitude fjord environments. *Journal of Geophysical Research*, *115*(F3), 1–21. doi:10.1029/2009JF001564

Mugford, R. I. and Dowdeswell, J. A. (2011). Modeling glacial meltwater plume dynamics and sedimentation in high-latitude fjords. *Journal of Geophysical Research*, *116*(F1), 1–20. doi:10.1029/2010JF001735

Mulder, T. and Syvitski, J. P. M. (1995). Turbidity currents generated at river mouths during exceptional discharges to the world oceans. *Journal of Geology*, *103*(3), 285–299.

Ohmura, A. (2001). Physical basis for the temperature-based melt-index method. *Journal of Applied Meteorology, 40*(4), 753-761.

Palmer, S., Shepherd, A., Nienow, P., and Joughin, I. (2011). Seasonal speedup of the Greenland Ice Sheet linked to routing of surface water. *Earth and Planetary Science Letters*, *302*, 423–428. doi:10.1016/j.epsl.2010.12.037

Pfeffer, W. T., Harper, J. T., and O’Neel, S. (2008). Kinematic constraints on glacier contributions to 21st-century sea-level rise. *Science*, *321*(5894), 1340–1343. doi:10.1126/science.1159099

Powell, R. D. and Molnia, B. F. (1989). Glacimarine sedimentary processes, facies and morphology of the South-Southeast Alaska shelf and fjords. *Marine Geology*, *85*, 359–390. doi:10.1016/0025-3227(89)90160-6

Pritchard, H. D., Arthern, R. J., Vaughan, D. G., and Edwards, L. A. (2009). Extensive dynamic thinning on the margins of the Greenland and Antarctic ice sheets. *Nature*, *461*(7266), 971–5. doi:10.1038/nature08471

Rasch, M., Elberling, B., Jakobsen, B. H., and Hasholt, B. (2011). High-resolution measurements of water discharge, sediment, and solute transport in the river Zackenbergelven, Northeast Greenland. *Arctic and Alpine Research*, *32*(3), 336–345.

Reeh, N., Mayer, C., and Miller, H. (1999). Present and past climate control on fjord glaciations in Greenland: Implications for IRD-deposition in the sea. *Geophysical Research Letters*, *26*(8), 1039–1042.

Rennermalm, A. K., Smith, L. C., Chu, V. W., Fortner, S. K., Box, J. E., and Hagedorn, B. (2012). Proglacial river stage, discharge, and temperature datasets from the Akuliarusiarsuup Kuua River northern tributary, Southwest Greenland, 2008–2011. *Earth System Science Data*, *4*(1), 1–12. doi:10.5194/essd-4-1-2012

Rignot, E. (2004). Rapid ice discharge from southeast Greenland glaciers. *Geophysical Research Letters*, *31*(10), 2–5. doi:10.1029/2004GL019474

Rignot, E., Box, J. E., Burgess, E. W., and Hanna, E. (2008). Mass balance of the Greenland ice sheet from 1958 to 2007. *Geophysical Research Letters*, *35*(20), 1–5. doi:10.1029/2008GL035417

Rignot, E. and Kanagaratnam, P. (2006). Changes in the velocity structure of the Greenland Ice Sheet. *Science*, *311*(5763), 986–90. doi:10.1126/science.1121381

Rignot, E. and Steffen, K. (2008). Channelized bottom melting and stability of floating ice shelves. *Geophysical Research Letters*, *35*(2), 2–6. doi:10.1029/2007GL031765

Russell, A. J. (2007). Controls on the sedimentology of an ice-contact jökulhlaup-dominated delta, Kangerlussuaq, west Greenland. *Sedimentary Geology*, *193*(1-4), 131–148. doi:10.1016/j.sedgeo.2006.01.007

Schneider, T., Bronge, C., Geografiska, S., Series, A., and Geography, P. (2008). Suspended sediment transport in the Storglaciaren drainage basin. *Geografiska Annaler*, *78*(2/3), 155–161.

Schoof, C. (2010). Ice-sheet acceleration driven by melt supply variability. *Nature*, *468*(7325), 803–6. doi:10.1038/nature09618

Shepherd, A., Hubbard, A. L., Nienow, P., King, M. A., McMillan, M., and Joughin, I. (2009). Greenland ice sheet motion coupled with daily melting in late summer. *Geophysical Research Letters*, *36*(1), 2–5. doi:10.1029/2008GL035758

Smith, L. C. (2003). Melting of small Arctic ice caps observed from ERS scatterometer time series. *Geophysical Research Letters*, *30*(20), 20–23. doi:10.1029/2003GL017641

Sole, A., Mair, D. W. F., Nienow, P. W., Bartholomew, I. D., King, M. A., Burke, M. J., and Joughin, I. (2011). Seasonal speedup of a Greenland marine-terminating outlet glacier forced by surface melt–induced changes in subglacial hydrology. *Journal of Geophysical Research*, *116*(F3), 1–11. doi:10.1029/2010JF001948

Stott, T. A. and Grove, J. R. (2001). Short-term discharge and suspended sediment fluctuations in the proglacial Skeldal River, north-east Greenland. *Hydrological Processes*, *423*(15), 407–423.

Straneo, F., Hamilton, G. S., Sutherland, D. A., Stearns, L. A., Davidson, F., Hammill, M. O., Stenson, G. B., and Rosing-Asvid, A. (2010). Rapid circulation of warm subtropical waters in a major glacial fjord in East Greenland. *Nature Geoscience*, *3*(3), 182–186. doi:10.1038/ngeo764

Stumpf, R. P., Gelfenbaum, G., and Pennock, J. R. (1993). Wind and tidal forcing of a buoyant plume, Mobile Bay, Alabama. *Continental Shelf Research*, *13*(11), 1281–1301. doi:10.1016/0278-4343(93)90053-Z

Sundal, A. V., Shepherd, A., Nienow, P., Hanna, E., Palmer, S., and Huybrechts, P. (2009). Evolution of supra-glacial lakes across the Greenland Ice Sheet. *Remote Sensing of Environment*, *113*(10), 2164–2171. doi:10.1016/j.rse.2009.05.018

Syvitski, J. P. M., Andrews, J. T., and Dowdeswell, J. A. (1996). Sediment deposition in an iceberg-dominated glacimarine environment, East Greenland: basin fill implications. *Global and Planetary Change*, *12*, 251–270.

Syvitski, J. P. M., Asprey, K. W., Clattenburg, D. A., and Hodge, G. D. (1985). The prodelta environment of a fjord: suspended particle dynamics. *Sedimentology*, *32*, 83–107. doi:10.1111/j.1365-3091.1985.tb00494.x

Tedesco, M. (2007). Snowmelt detection over the Greenland ice sheet from SSM/I brightness temperature daily variations. *Geophysical Research Letters*, *34*(2), 1–6. doi:10.1029/2006GL028466

Tedesco, M., Serreze, M. C., and Fettweis, X. (2008). Diagnosing the extreme surface melt event over southwestern Greenland in 2007. *The Cryosphere*, *2*, 159–166. doi:10.5194/tc-2-159-2008

Thomas, A. and Weatherbee, R. (2006). Satellite-measured temporal variability of the Columbia River plume. *Remote Sensing of Environment*, *100*(2), 167–178. doi:10.1016/j.rse.2005.10.018

Thomas, R. H., Abdalati, W., Frederick, E., Krabill, W. B., Manizade, S., and Steffen, K. (2003). Investigation of surface melting and dynamic thinning on Jakobshavn Isbræ, Greenland. *Journal of Glaciology*, *49*(165), 231–239. doi:10.3189/172756503781830764

Thomas, R. H., Frederick, E., Krabill, W. B., Manizade, S., and Martin, C. (2009). Recent changes on Greenland outlet glaciers. *Journal of Glaciology*, *55*(189), 147–162. doi:10.3189/002214309788608958

Van de Wal, R. S. W., Boot, W., van den Broeke, M. R., Smeets, C. J. P. P., Reijmer, C. H., Donker, J. J. A., and Oerlemans, J. (2008). Large and rapid melt-induced velocity changes in the ablation zone of the Greenland Ice Sheet. *Science*, *321*(5885), 111–3. doi:10.1126/science.1158540

Van den Broeke, M. R., Bamber, J. L., Ettema, J., Rignot, E., Schrama, E. J. O., van de Berg, W. J., van Meijgaard, E., Velicogna, I., and Wouters, B. (2009). Partitioning recent Greenland mass loss. *Science*, *326*(5955), 984–6. doi:10.1126/science.1178176

Van den Broeke, M. R., Smeets, P., Ettema, J., van der Veen, C. J., van de Wal, R. S. W., and Oerlemans, J. (2008). Partitioning of melt energy and meltwater fluxes in the ablation zone of the west Greenland ice sheet. *The Cryosphere*, *2*, 178–189. doi:10.5194/tc-2-179-2008

Velicogna, I. (2009). Increasing rates of ice mass loss from the Greenland and Antarctic ice sheets revealed by GRACE. *Geophysical Research Letters*, *36*(19), 5–8. doi:10.1029/2009GL040222

Vermote, E. F., El Saleous, N. Z., and Justice, C. O. (2002). Atmospheric correction of MODIS data in the visible to middle infrared: First results. *Remote Sensing of Environment*, *83*, 97–111. doi:10.1016/S0034-4257(02)00089-5

Whitney, M. M. (2005). Wind influence on a coastal buoyant outflow. *Journal of Geophysical Research*, *110*(C3), 1–15. doi:10.1029/2003JC002261

Willis, I. C., Richards, K. S., and Sharp, M. J. (1996). Links between proglacial stream suspended sediment dynamics, glacier hydrology and glacier motion at Midtdalsbreen, Norway. *Hydrological Processes*, *10*, 629–648. doi:10.1002/(SICI)1099-1085(199604)10:4

Yin, J., Overpeck, J. T., Griffies, S. M., Hu, A., Russell, J. L., and Stouffer, R. J. (2011). Different magnitudes of projected subsurface ocean warming around Greenland and Antarctica. *Nature Geoscience2*, *4*, 524–528. doi:10.1038/nphys1189

Zwally, H. J., Abdalati, W., Herring, T., Larson, K., Saba, J. L., and Steffen, K. (2002). Surface melt-induced acceleration of Greenland ice-sheet flow. *Science*, *297*(218), 218–222. doi:10.1126/science.1072708

Chapter 3

Adaptation of the Manning Equation for Remote Estimation of Supraglacial River Discharge Using GIS Modelling and WorldView-2 Satellite Imagery

3.1 Abstract

Increasing surface melting on the Greenland ice sheet and associated concerns over rising runoff and sea level have heightened the need for improved understanding of meltwater transfer from the ice sheet surface to the ocean. Summertime field observations and high-resolution satellite imagery reveal extensive supraglacial river networks across the southwestern ablation zone transporting large volumes of meltwater to moulins, yet these features remain poorly mapped and their discharges unquantified. A GIS modelling framework is developed to estimate supraglacial river discharge, by adapting the Manning equation for use with available geospatial datasets calibrated with limited in situ hydraulic measurements. The framework incorporates high-resolution visible/near-infrared WorldView-2 (WV2) satellite imagery, the Greenland Ice Mapping Project digital elevation model (GIMP DEM), a field-calibrated WV2 river bathymetry retrieval algorithm, and limited in situ estimates of channel roughness (Manning's n) collected on the ice sheet. GIS modelled river discharges are mapped for ~1 million cross sectional vectors orthogonal to river centerlines, with attributes of instantaneous flow width, depth, velocity, slope, wetted perimeter, and hydraulic radius. Moulin discharges (mean value 9.1 m^3/s, σ=5.3 m^3/s) are retrieved for 465 river networks, helping to quantify instantaneous meltwater flux into the ice sheet. The described GIS modelling framework demonstrates novel integration of geospatial datasets with in situ measurements to provide scientifically useful water flux estimates for a scientifically interesting, logistically difficult polar environment.

3.2 Introduction

Climate warming has been linked to rising runoff of terrestrial water to the Arctic ocean (Peterson et al., 2002; McClelland et al., 2006; Rawlins et al., 2010), thus contributing to rising global sea level. This trend is projected to continue (Holland et al., 2007; Kattsov et al., 2007), including increased meltwater runoff from the Greenland Ice Sheet (Fettweis et al., 2013; van Angelen et al., 2013; Vizcaíno et al., 2014). This projected increase in meltwater runoff from the ice sheet is important because of its anticipated impact on ice sliding velocity, i.e. outlet glacier speedups (Shannon et al., 2013; Hoffman & Price, 2014), in addition to its direct contribution to the ocean. Much of the meltwater produced on the ice surface is first transported through supraglacial rivers before entering the subglacial environment through moulins (sinkholes) and reaching the ocean (Lampkin and VanderBerg, 2013; Rennermalm et al., 2013; Chu, 2014; Smith et al., 2015). Yet it is exceedingly difficult to collect direct measurements of flow in these features. Satellite remote sensing in the visible/near-infrared spectrum offers the ability to map supraglacial rivers from space (Colgan et al., 2011; McGrath et al., 2011; Yang & Smith, 2013), and even estimate river bathymetry (Legleiter et al., 2014), but not discharge. However, through integration of field and geospatial datasets, successful remote estimation of river discharge has been demonstrated in terrestrial rivers using various remote-sensing algorithms (Smith et al., 1996; Bjerklie et al., 2005; LeFavour and Alsdorf, 2005; Smith and Pavelsky, 2008; Tarpanelli et al., 2011, 2013; Durand et al., 2014).

This paper proposes to develop such an algorithm for the Greenland ice sheet, through adaption of the Manning equation (Manning, 1891) within a GIS framework. The Manning equation is a commonly used empirical method for calculating open channel discharge and is a function of channel shape, slope, and roughness. It has been adapted to be used with remotely sensed datasets because its components of channel shape and slope can potentially be measured remotely, and roughness has traditionally been tabulated based on field-based categorizations of the channel environment (Barnes, 1967; Hicks and Mason, 1991).

A GIS modelling framework is developed to estimate river discharge by spatially adapting the Manning equation for use with remotely sensed river properties. The input geospatial datasets are visible/near-infrared satellite imagery, a digital elevation model, and a limited collection of in situ field measurements for calibration. This framework produces vector outputs of cross-sectional and reach-averaged discharges at regular postings along river centerlines, and also attributes discharges to moulins (termination points). A cross-validation is performed to test the sensitivity of the Manning roughness coefficient parameter required by the model. This paper concludes with some discussion of the advances that might be achieved by integrating geospatial datasets into a GIS model.

3.3 Geospatial and field datasets

3.3.1 Study area

The study region is located in southwest Greenland between 66°35'N and 67°35'N near the town of Kangerlussuaq (Figure 3-1). In this region the upper limit of the ablation zone is typically ~1500 m and can reach up to ~1800 m elevation in warmer years (Box et al., 2006; Fettweis, 2007). This study uses geospatial and field data from the summer of 2012, coincident with an extreme melt event on July 11-13 where 97% of the ice sheet experienced some degree of melting (Tedesco et al., 2013). Hundreds of river networks form in this region to efficiently transport meltwater off the surface of the ice sheet (Smith et al., 2015), making it an important region for estimating river discharge. A field campaign to collect hydraulic data was carried out during July 20 – August 20, 2012 along a transect from the ice edge to 1500 m elevation. These data were used in conjunction with high-resolution multispectral WorldView-2 (WV2) imagery acquired within the field campaign time period in a GIS modelling framework to estimate supraglacial discharge for July 2012. The resulting mapped supraglacial river discharge area, bounded by the region with available WV2 imagery, spans 900-1680 m elevation.

3.3.2 In situ data

In an extensive field campaign on the Greenland ice sheet during 20 July – 20 August 2012, in situ hydraulic data were collected to characterize supraglacial river discharge and calibrate a Manning's equation parameter of channel roughness. Measurements of cross-sectional flow area (A) and velocity (v) were converted to discharge (Q) using the velocity-area method for 73 cross sections, with 54 cross sections from extended ice camp sites focusing on smaller rivers and 19 cross sections from day sites targeting larger rivers (Figure 3-1). For ice camp sites with rivers < 5 m wide, cross-sectional areas were measured using surveying rods and steel probes, and surface velocities were measured using a FloWav Phaser portable Doppler radar. For day sites with rivers > 5 m wide, cross-sectional areas and surface velocities were measured using a Sontek Acoustic Doppler Current Profiler (ADCP) along a cross-sectional cableway. Manning roughness coefficient (n) was calculated from:

$$n = \frac{1}{v}(R)^{2/3}S^{1/2} \tag{3-1}$$

where *R* is hydraulic radius, and *S* is water surface slope, measured at each cross section. *R* is defined as *R* = *A*/*P*, where *P* is wetted perimeter calculated from cross-sectional depth measurements. Typically in Manning's equation, hydraulic radius is approximated by depth; however, for smaller width/depth ratios like those in smaller streams, the approximation of *R* = *d* breaks down. A detailed description of instruments and data collected in this field campaign can be found in Smith et al. (2015).

Longitudinal velocity data were also collected from three autonomous precision GPS river drifters. These data provided downstream velocities from large, fast rivers that we were not able to safely measure using helicopter-aided cable cross sections. The drifters obtained GPS location measurements over 14.4 km of three large rivers (Figure 3-1).

3.3.3 WorldView-2 satellite images

Thirty-two high-resolution multispectral WorldView-2 (WV2) satellite images were obtained from DigitalGlobe through the University of Minnesota's Polar Geospatial Center (PGC) over southwestern Greenland on July 18, 21, and 23, 2012, creating a 5,328 km^2 mosaic. WV2 provides 8 bands in the visible to near-infrared (2 m resolution) and a panchromatic band (0.5 m resolution). Images were orthorectified using the Greenland Ice Mapping Project (GIMP) DEM (Howat et al., 2014) and projected to a polar stereographic coordinate system using code from the PGC. Radiance was calculated using radiometric coefficients included in the WV2 metadata for each band (Updike and Comp, 2010). Atmospheric correction was performed using ENVI's Fast Line-of-sight Atmospheric Analysis of Hypercubes (FLAASH) module, incorporating the MODTRAN4 radiation transfer code. Inputs to FLAASH included the WV2 radiance image, scene date and location, ground elevation and sensor altitude, spectral band configuration, visibility (40 km), and standard models for the atmosphere (sub-arctic summer) and aerosols (rural) to produce apparent surface reflectance images.

3.3.4 Elevation data

The GIMP DEM (Howat et al., 2014) was used to calculate longitudinal channel bank slope within the WV2 mapped area. The DEM has a spatial resolution of 30 m and an average elevation RMSE over ice-covered areas of ±8.5 m. We assumed that longitudinal channel bank slopes calculated using ice surface elevations can adequately approximate water surface slope, which is a parameter of the Manning equation for calculating discharge.

3.4 GIS modelling framework

The goal of this paper is to produce estimates of supraglacial river discharge as vector outputs using a GIS modelling framework that incorporates reflectance imagery, elevation data, and field-derived parameters using semi-automated procedures (Figure 3-2). This section describes that framework through the steps of raster and vector processing, application of the Manning equation to extract discharge, filtering and reach averaging, and finally attribution to termination points, which represent meltwater input to the ice sheet from individual river networks. Cross-validation of the Manning roughness coefficient model parameter and calculation of discharge uncertainties are also described.

3.4.1 Raster processing

3.4.1.1 Water feature classification

Supraglacial river network water features were classified using a simple ratio of WV2 Band 2 (blue, 450-510 nm) and Band 8 (NIR, 860-1040 nm), with a size filter to remove slush regions. This water feature extraction method, a simplified version of the algorithm introduced by Yang and Smith (2013), identified contiguous pixel areas greater than a band ratio threshold of 1.25 and less than a size of 500 pixels. The resulting raster river mask represented all channelized, connected, and actively flowing meltwater rivers visible in 2 m resolution imagery.

Additionally, individual river networks were separated by termination points. For the southwestern Greenland supraglacial region ~20 km inland from the ice margin, all termination points represented moulins. Moulins are vertical channels that divert meltwater from supraglacial river networks into the ice sheet. These termination points were manually digitized from WV2 panchromatic imagery. They were defined as the final downstream drainage accumulation point of a continuous river network. There were occasions of multiple termination points within a river network at the downstream end where a river splits and encounters multiple moulins.

3.4.1.2 Water depth retrieval

Supgraglacial river depths were retrieved using the dataset and algorithm of Legleiter et al. (2014), which derives lake and river bathymetry from WV2 band ratios calibrated by *in situ* water depths and simultaneous WV2 images for three sites on the ice sheet (Cold Creek, Olsen River, and Lake Napoli, Legleiter et al., 2014). The current methodology and dataset are identical to Legleiter et al. (2014), except supraglacial river reflectances only are used (Cold Creek, Olsen River). This yields a depth-retrieval algorithm optimally calibrated for relating WV2 spectral reflectance to river depths:

$$d = 1.89 - 4.03X + 3.31X^2, \quad R^2 = 0.67 \qquad (3\text{-}2)$$

where X is the quantity $\ln\left(\frac{B2}{B4}\right)$, *B2* is WV2 Band 2 (blue, 450-510 nm), and *B4* is WV2 Band 4 (yellow, 585-625 nm). The RMSE accuracy of the retrieved depths using this rivers-only dataset is ±0.32 m. The algorithm was applied to atmospherically corrected WV2 surface reflectance imagery within the river mask to produce a raster image of river bathymetry.

3.4.1.3 Path distance

Path distance was defined as the distance upstream of the termination point for every pixel, constrained by the water mask. Path distance rasters were computed from river masks using ArcGIS 10.2, which calculates the least cost accumulated distance from the termination point to each raster pixel within the river mask.

3.4.2 Vector processing

3.4.2.1 River centerlines and orthogonal cross sections

Input rasters were processed to produce river centerlines and orthogonal cross sections along the river. Rivwidth version 0.4 (Pavelsky and Smith, 2008) is a software tool in the IDL programming language that automates the calculation of river widths using raster-based classifications of inundation extent. Rivwidth inputs are a channel mask (showing all channels and islands, Figure 3-3a) and a river mask (showing areas within the river boundary including islands), which is used to derive a river centerline. Rivwidth was modified to also read in a river bathymetry mask (Figure 3-3b) and a DEM for analysis. Independent continuous river networks, identified by termination points manually verified, were processed separately. Orthogonal cross sections were simulated as polylines at a 2 m interval (the WV2 spatial resolution) along river centerlines. Locations where islands exist were flagged with the number of channels crossed by the polyline.

3.4.2.2 River segment order

Resulting cross section points within each river network were split into individual river segments. River segments were defined as continuous reaches where consecutive points were no more than 3 m apart. Continuous segments that spanned more than one river tributary branch (as artefacts of Rivwidth processing) were manually separated. Points within segments were reordered in an upstream direction according to path distance upstream from the moulin.

Stream order was designated for each river segment based on Strahler's ordering scheme (Strahler, 1957). Breaks exist in the river network due to ice bridges across rivers preventing full extraction of active river channels. Segments downstream of breaks were treated as new tributaries with an order of 1 to preserve the fragmented nature of river networks visible in satellite imagery.

3.4.3 Discharge from the Manning equation

The Manning equation is a commonly used empirical method for calculating open channel discharge and is a function of channel shape, slope, and roughness. It has been adapted to be used with remotely sensed datasets because its components of channel shape and slope can potentially be measured remotely, and roughness has traditionally been tabulated based on field-based categorizations of the channel environment. It has previously been adapted for use in terrestrial rivers using remotely sensed channel or water surface slopes and widths, calibrated by field data (e.g., Birkinshaw et al. 2014; Bjerklie et al. 2005; LeFavour and Alsdorf 2005).

The Manning equation for calculating velocity (v) is defined as:

$$v = \frac{1}{n}(R)^{2/3}S^{1/2} \tag{3-3}$$

and combining with cross section area ($A = wd$) to produce discharge (Q):

$$Q = \frac{1}{n}wdR^{2/3}S^{1/2} \tag{3-4}$$

Requirements for the Manning equation include roughness coefficient (n), flow width (w) in meters, average flow depth (d) in meters, hydraulic radius (R) in meters, and water surface slope (S) in meters per meter. Hydraulic radius (R) is defined as cross-sectional area divided by wetted perimeter (P), $R = A/P$. Of these parameters, width, depth, wetted perimeter, and slope are remotely sensed, and the Manning roughness coefficient is a calibration parameter derived from *in situ* discharge (Figure 3-2). This section will describe how each parameter is obtained, along with their associated uncertainties. Note that for parameters that are a combination of other parameters, uncertainties are defined through error propagation (Taylor, 1997), and determination of total discharge uncertainty using two methods is described in the Appendix. At this point in the GIS modelling framework, the dataset consists of a river centerline and orthogonal cross sections along that centerline represented as both polylines and points.

3.4.3.1 Width

Within the modified Rivwidth tool, widths were calculated from orthogonal cross sections over the channel mask at each pixel along river centerlines. Widths were added to the attributes of the output point dataset which included number of channels in each cross section. Width uncertainty from Rivwidth (δw) was defined as $\delta w = ½rc$, where r is the pixel resolution of 2 m, and c represents the number of riverbanks crossed by the orthogonal segment along which the width is calculated (Pavelsky and Smith, 2008). Only single-channel portions ($c = 2$) were used in the final discharge calculation, and therefore the uncertainty associated each width measurement was defined as $\delta w = \pm 2$ m.

3.4.3.2 Depth and wetted perimeter

Average flow depth was extracted for each cross section from the river bathymetry masks and modified to prevent overestimation of depth from the presence of bank shadows. Water depth values from the river bathymetry mask were extracted if they intersected the orthogonal polyline. To minimize influence from shadows, cross sections were divided in half, and depths were averaged for each half. The shallower half was mirrored to produce a conservative estimate of average cross-sectional water depth (d). Depth uncertainty (δd) for each measurement was defined as δd = ±0.32 m using the RMSE accuracy assessment for the depth retrieval algorithm.

Cross-sectional area, wetted perimeter, and hydraulic radius were calculated and added as cross section point attributes. Cross-sectional area was defined as the product of width and average depth, $A = wd$. Wetted perimeter (P) was calculated as the sum of the wetted distance in the cross section, again using a conservative shadow-free bathymetric cross section:

$$P = \sqrt{{h_i}^2 + {d_i}^2} + \sqrt{{h_{i+1}}^2 + {d_{i+1}}^2} + \cdots + \sqrt{{h_n}^2 + {d_n}^2} \tag{3-5}$$

with h defined as the horizontal distance between consecutive points along the cross section for a total of n river pixels. An assumption is made that the river banks are represented by the pixels immediately outside the river mask and have a depth of 0.

3.4.3.3 Slope

Slope (S) was calculated for each point along river segments with a linear regression fit over a reach length centered on each point using the 30 m GIMP DEM. A reach length (L) of 1 km was designated as ideal for capturing the driving slope at each cross section. For river segments shorter than 1 km, or when the moving reach length encounters segment ends and produces a reach also shorter than 1 km, L was then defined as the longest available reach. This approach allows slope to be calculated regardless of river segment length, though slopes calculated from reaches shorter than 1 km are deemed more uncertain by using a dynamic uncertainty that increases as L decreases.

The dynamic slope uncertainty (δS) was defined as δS = ±8.5 m/L for each point measurement, with $L \leq$ 1000 m and ±8.5 m as the overall RMS error of the GIMP DEM over ice-covered terrain (Howat et al., 2014). The lowest slope uncertainties are obtained by points with a 1 km reach, producing a static uncertainty of 0.0085, and higher uncertainties are acquired as L decreases. Elevation at each point was also included as an attribute.

3.4.3.4 Manning roughness coefficient

A distribution of Manning roughness coefficient was calculated from field-derived discharge and used to calibrate the Manning equation. The Manning roughness coefficient is a unitless empirical coefficient tabulated according to factors that affect roughness and typically chosen from ranges given in Chow (1959), Henderson (1966), and Streeter (1971). Here, Manning roughness coefficient was calculated using Equation (3-1) from both *in situ* discharge and remote sensing-aided discharge datasets. 73 measurements of Manning roughness coefficient were derived from *in situ* measurements, representing cross sections from smaller or slower rivers. A remote sensing-aided discharge dataset was derived from *in situ* longitudinal velocity measurements paired with remotely sensed cross-sectional area extracted from WV2 imagery within hours to 3 days of drifter data collection and slope calculated from the GIMP DEM using the methods described above. These points were filtered to simulated cross sections with widths < 50 m, adding 125 remote sensing-aided estimates of n representing larger, faster rivers to the 73 measurements of n derived solely from *in situ* data.

The median (second quartile) of the Manning roughness coefficient distribution from the combined dataset (n =0.030, sample size of 198 points) was applied to discharge calculations as a static parameter (Figure 3-4). For the uncertainty analysis, the first quartile was used as the lower bound of n ($n_{\downarrow}$ = 0.019), producing upper bound velocities, and the third quartile was used as the upper bound of n ($n_{\uparrow}$ = 0.062), producing lower bound velocities. Uncertainty in Manning roughness coefficient was defined as $\delta n = n_{\uparrow} - n_{\downarrow}$.

3.4.4 Filtering

High quality discharge measurements were defined as single channel river segments that remained relatively narrow and channelized. Errors in calculated discharge arise from cross sections with multiple channels (i.e., islands), wide river sections including lakes ($w \geq 20$m), and/or slopes ≤ 0. Points were filtered out if they met any of these three conditions. Additionally, a longitudinal filter threshold was defined as 10m on each side of any point that met multiple channel or width thresholds and those points were also filtered out to minimize influence from problem areas.

3.4.5 Reach-averaging

Remaining cross-sectional points representing narrow, single-thread channels were spatially averaged within continuous 1 km reaches (Gleason and Smith, 2014). Reaches were dynamic and centered on each cross-sectional point measurement, with attributes averaged over all available high quality points within the reach. This produced attributes of reach-averaged discharge ($\overline{Q}$), width ($\overline{w}$), depth ($\overline{d}$), wetted perimeter ($\overline{P}$), hydraulic radius ($\overline{R}$), slope ($\overline{S}$), velocity ($\overline{v}$).

3.4.6 Attribution to termination points

Each stream network has a termination point representing a moulin, where supraglacial river runoff enters the ice sheet. Each termination point was attributed a reach averaged discharge value $\overline{Q}$ closest to 1 km upstream of the termination to avoid supercritical flows near the moulin. These moulin discharges represent an instantaneous snapshot of total supraglacial discharge penetrating the ice sheet.

3.5 Cross-validation of Manning roughness coefficient model parameter

Cross validation was performed on the parameter determined from field data, Manning roughness coefficient (*n*), using repeated random sub-sampling validation with varying proportions of the training/validation split. Because the dataset contains two different sources of data, with 73 measurements of *in situ* discharge and 125 measurements of remote sensing-aided discharge, the validation data was only drawn from the *in situ* population.

A varying percentage of data, from 10% to 80%, were randomly sampled from the *in situ* dataset to act as validation data, and the remaining data were designated as training data. Manning roughness coefficient was then calculated using the training data measurements of discharge, channel cross-sectional area, and slope. The median of that derived dataset was used as the new Manning roughness coefficient to be combined with validation data measurements of channel cross-sectional area and slope to calculate a validation discharge. The average validation discharge was then compared with the average testing discharge to test the sensitivity of discharge to changes in the Manning roughness coefficient parameter.

3.6 Results

3.6.1 Mapping of reach-averaged supraglacial discharge

Table 3-1 shows summary attributes of reach-averaged cross-sectional points. A total of 1,020,574 reach-averaged points were retrieved with attributes of width, depth, wetted perimeter, hydraulic radius, velocity, slope, and discharge. This represents 63% of the total point dataset, after low quality points are removed through filtering and smoothed through reach-averaging. Reach-averaged widths range from 2 – 18 m, constricted by the width filter, and average 5.7 ± 2.1 m (with standard deviation shown). Depths average 0.9 ± 0.1 m with a small range between 0.6 and 1.7 m. Velocities are on average 1.9 ± 0.7 m/s and vary between

0.7 to 7.7 m s-1. Reach-averaged discharge estimates range from 0.01 – 54.5 m^3/s and average 9.2 ± 4.4 m^3/s. Uncertainties for total discharge using the two methods average 24.1 m3/s using error propagation and 27.7 m^3/s using min-max propagation. While the error propagation method produces a lower average uncertainty, it also produces a much larger range of values with a standard deviation of 20.9 m^3/s compared to 10.0 m^3/s for the min-max method.

Figure 3-5 maps extracted components of reach-averaged width, depth, slope, velocity, and discharge for an example river network. Component values are shown as colored points grouped in equal intervals, with the termination point moulin represented as a larger green point at the downstream end, and locations with no data show the underlying vector centreline in black. Higher widths are shown in the main trunk river, with highest values farther downstream in the highest order segment, and lowest values along low order upstream tributaries. Depths show a smaller range without a distinct spatial pattern compared to widths. Both velocity and slope is shown, with slope being the main driver of velocity variations based on the Manning equation, and therefore very similar spatial patterns. These two components show generally higher values along the higher ordered trunk rivers. The final discharge map shows that combining the components of width, depth, and velocity, highest discharge is estimated for the highest ordered river segment within two km of the termination point.

The inclusion of a 30 m DEM is the coarsest resolution input to the GIS model, and it also represents a dataset fixed in time rather than responding to the changing ice sheet surface topography. The coarseness means that slopes from a 1 km reach length have a maximum of 33 pixels for slope to be calculated, and even less for river networks with survival lengths shorter than 1 km. This leads to many poor quality slopes from shorter reach lengths (producing higher slope uncertainties propagating to higher discharge uncertainties), or slopes that are negative or zero and are filtered out.

3.6.2 Mapping of moulin (termination point) discharges

Separating reach-averaged results into individual river networks, discharge is estimated for 465 river networks out of a total 523 mapped networks, producing an instantaneous discharge of 4,213 m^3/s over a 5,328 km^2 WV2 mosaic area. The remaining 11% of mapped networks do not produce estimates that passed quality control measures. Mapped rivers have a survival length (maximum continuous length) of 3.2 km (range of 0.05 – 29.6 km) and a total length (including all tributaries) of 8 km (range of 0.04 – 141.7 km). These rivers are mapped between 907 – 1644 m in elevation a.s.l., and on average are comprised of 2,195 reach-averaged cross-sectional points.

Termination points are attributed using the reach-averaged point closest to 1 km upstream of mapped moulins to avoid incised canyons with supercritical flow. These summary termination points represent the instantaneous meltwater flux input to the ice sheet's subglacial environment through moulins. On average these summary termination points are found 0.9 km upstream of moulins, but they could be found as close as 0.05 km upstream in ver short rivers, or as far as 8.5 km upstream in rivers without enough high quality points closer to the moulin.

Table 3-2 summarizes attributes for each individual river network, showing an average discharge of 9.1 ± 5.3 m^3/s (with standard deviation shown) and the distribution of discharges for the 465 networks is presented in Figure 3-6. Widths average 6.1 ± 2.6 m, depths average 0.9 ± 0.1 m, and velocities average 1.8 ± 0.7 m/s. Uncertainties for total discharge are much higher than average discharge, averaging 29.6 ± 34.2 m^3/s with error propagation and 28.9 ± 12.4 m^3/s with min-max propagation. While these two methods produce similar average uncertainties, the error propagation method varies much more widely as seen with the full dataset of reach-averaged points.

3.6.3 Sensitivity of discharge retrieval to Manning roughness coefficient

For varying proportions of the validation/training split from 255 field measurements of Manning roughness coefficient, the average discharge calculated using the Manning roughness coefficient derived from the training set is 155% of average discharge calculated using the coefficient derived from the validation set, with an average 4.01 m^3/s for the training set and an average 2.58 m^3/s for the validation set. The validation and training sets show little sensitivity to the different proportions sampled as shown by the standard deviations of 0.21 m^3/s for the training set discharge and 0.02 m^3/s for the validation set.

3.7 Discussion and conclusion

This paper provides a first geospatial adaptation of the Manning equation to supraglacial rivers on the Greenland ice sheet, by developing a GIS modelling framework to integrate available datasets on ice surface topography, river depth, and river width. Owing to their dense, extensive development across the southwestern ablation zone, supraglacial river networks are a prime example of a hydrologic system that can benefit from a broad spatial mapping of discharge. Despite the importance of these networks for delivering water to the subglacial hydrologic system and ultimately, the global ocean, estimates of supraglacial river discharge are currently absent from the scientific literature. Therefore, while uncertainties remain large (Table 3-2), the GIS modelling approach described here can help to quantify river discharges for a logistically challenging part of the world, while also adding to a small but growing literature on geospatial discharge algorithms (e.g., Bjerklie et al. 2005; Durand et al. 2014; Gleason and Smith 2014).

The GIS modelling framework described here successfully retrieved discharge estimates for 63% of mapped cross section vectors and 89% of moulin-terminating river networks. For the remaining cross sections and networks, complex river morphologies posed the greatest challenge to discharge retrieval, as the method requires strict quality control measures in order to apply the Manning equation. These measures include filtering and/or removal of islands, lakes, and wide (> 20 m) river sections, negative or zero slope values, and buffering around affected cross sections. Complex river channel morphology also requires detailed manual checks after topological processing, to separate river segments and reorder points in an upstream direction.

Cross-validation of the Manning roughness coefficient for different subsamples of the field dataset suggests little sensitivity of modeled discharge to choice of roughness coefficient. The low standard deviations of the validation and training modeled discharges means there is little difference in the distribution of field discharges used for calculating Manning roughness coefficient, where the median of the distribution is used as an input to the model. This lends support to our use of two different datasets to calculate Manning roughness coefficients, with the two distributions combined to yield a Manning roughness coefficient of 0.030 for discharge retrieval (Figure 3-4). Because the *in situ* discharge dataset represents discharges from smaller streams (mean discharge 2.6 m^3/s) and the remote sensing-aided discharges were derived from longitudinal drifters in larger rivers (mean discharge 25.2 m^3/s), this single value spans a range of channel scales. However, more *in situ* field estimates of Manning roughness coefficient are needed, to either confirm representativeness of this single value or (more likely) build a lookup table of varying roughness values for differing channel morphologies, discharges, and/or slopes.

Perhaps the greatest weakness of the described approach is its use of an ice surface DEM to estimate river water surface slope. Most Greenland DEMs are too coarse to capture supraglacial rivers and thus represent the surrounding ice surface, not the free water surface. This problem is mitigated by using a long 1 km reach length in calculating channel slopes, which may be more useful in estimating the hydraulic slope associated with a particular discharge and channel geometry than a spatially and temporally varying water surface (Bjerklie et al., 2003). The assumption that an ice surface slope can approximate water surface slope is also complicated by rivers that become more incised as they flow downstream, making the water surface slope steeper than the channel bank slope. The method would nonetheless benefit from finer-scale DEMs, the growing availability of WV2 DEMs (http://www.pgc.umn.edu/elevation/stereo/) that offer a much higher spatial and temporal resolution to better align with the extraction of instantaneous snapshots of river discharge. Furthermore, more field surveys are needed to better characterize water surface slopes in relation to available DEMs of ice surface topography.

The GIS modelling framework presented here holds promise for retrieving estimates of river discharge in a logistically challenging environment. Through fusion of sparse *in situ* measurements and geospatial datasets in a vector GIS, we are able to estimate instantaneous supraglacial river discharge flowing across the ice sheet, and entering the ice sheet through moulins, for a large (5,328 km^2) study area in southwestern Greenland. While uncertainties remain large, key advantages of the method include ease of application, and new availability of a field-based *in situ* Manning roughness coefficent (n = 0.030) presented here. Additional field campaigns, preferably in larger supraglacial rivers across a range of discharges, would lend further confidence to the value for this roughness coefficient reported here. While this study is hampered by lack of field data, we show that standard GIS tools are able to provide a framework for retrieving river discharges from a study region where mapping meltwater flux is becoming more important for understanding Greenland’s contributions to sea level rise.

3.8 Figures

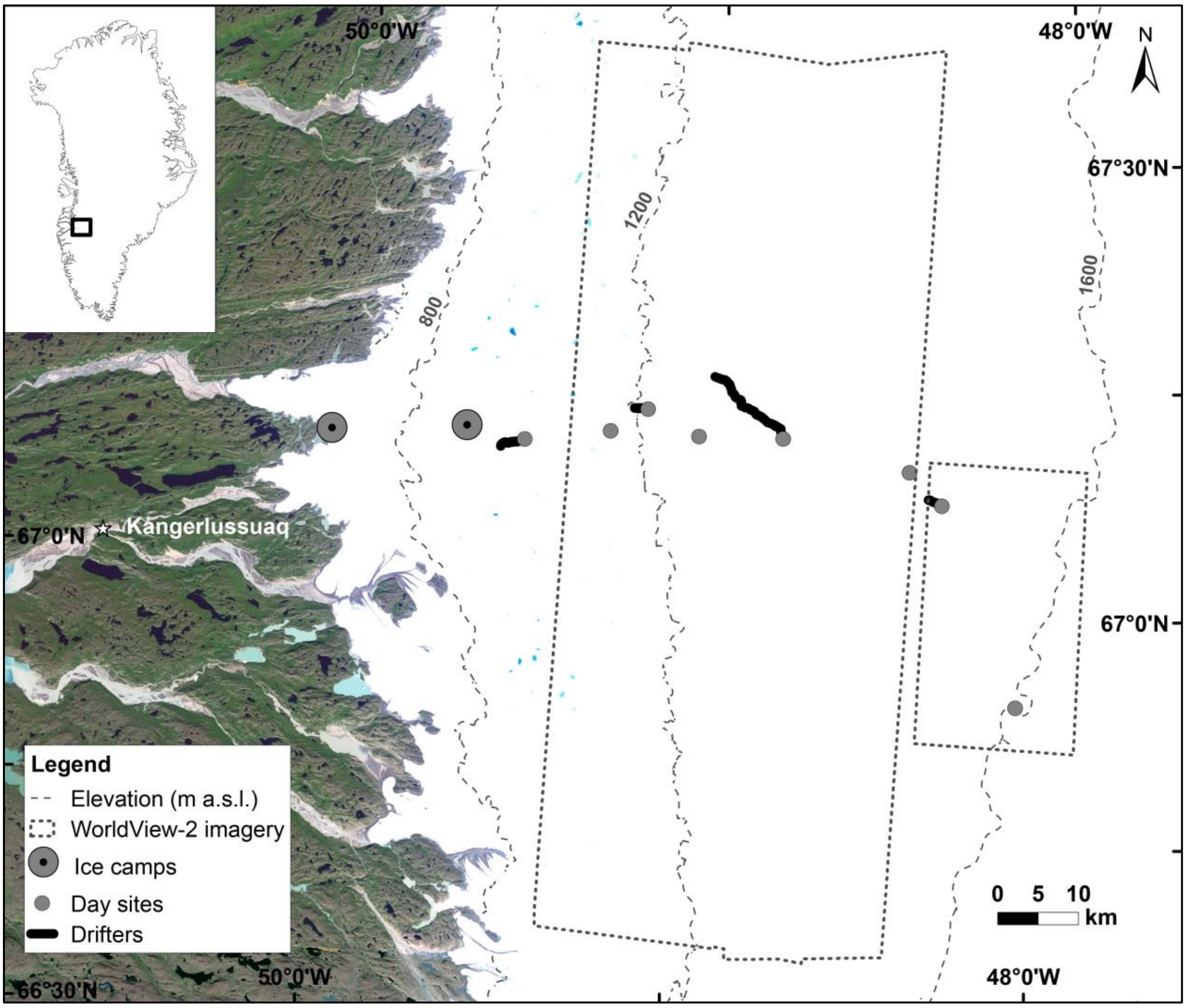

Figure 3-1. The southwestern Greenland study area showing the WorldView-2 mapped region (July 18-23, 2012) and field measurement locations (July 20 - August 20, 2012).

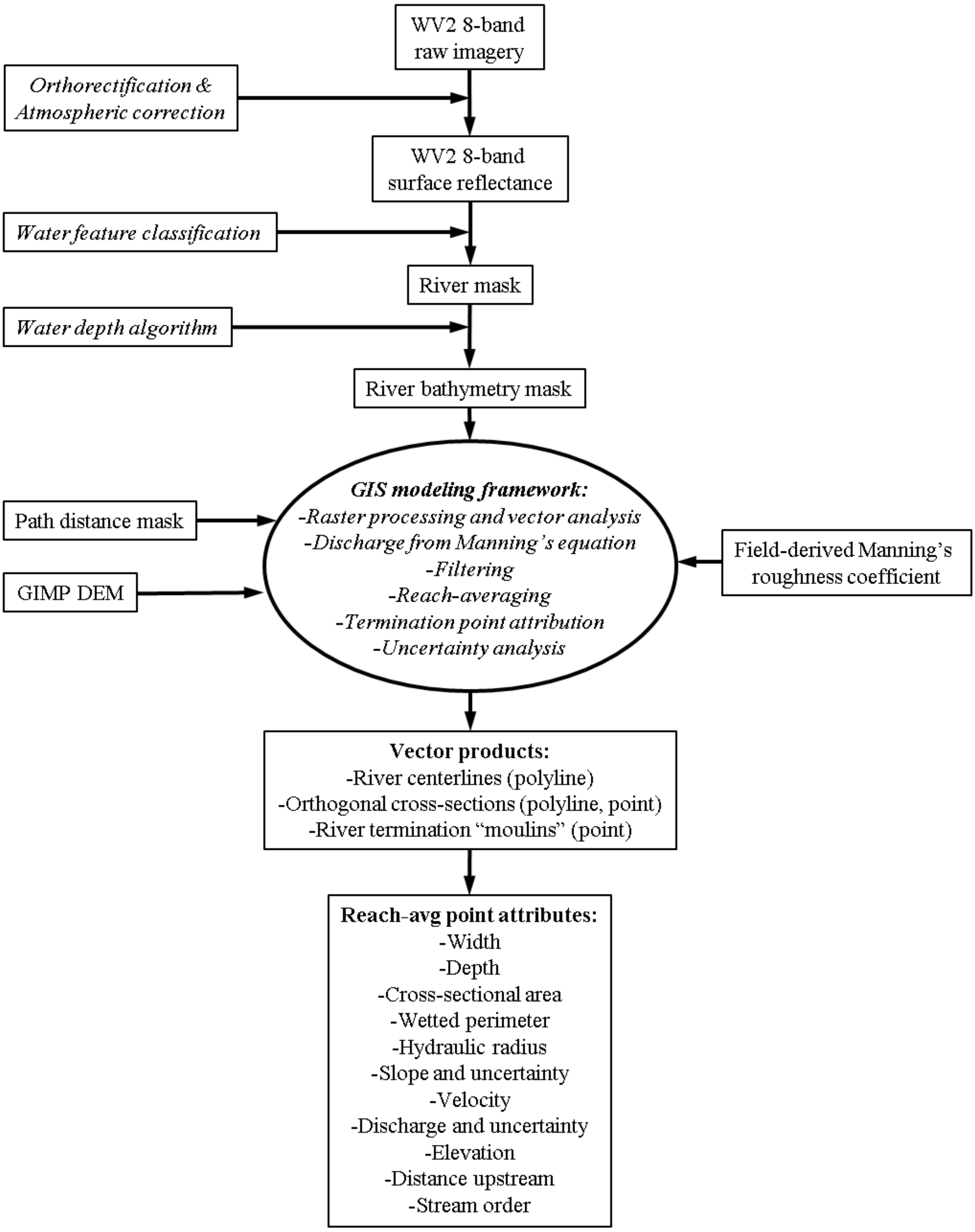

Figure 3-2. Methodology flowchart, with italicized boxes indicating processes and non-italicized boxes indicating objects and attributes. WorldView-2 imagery were processed to produce surface reflectance. Water feature classification and application of a depth retrieval algorithm produced a river bathymetry mask. The GIS modelling framework calculated discharge from the Manning equation using the river bathymetry mask, DEM, and field-calibrated Manning roughness coefficient. Resulting discharge was output as filtered and reach-averaged points along river centerlines as well as attributed to river termination "moulin" points.

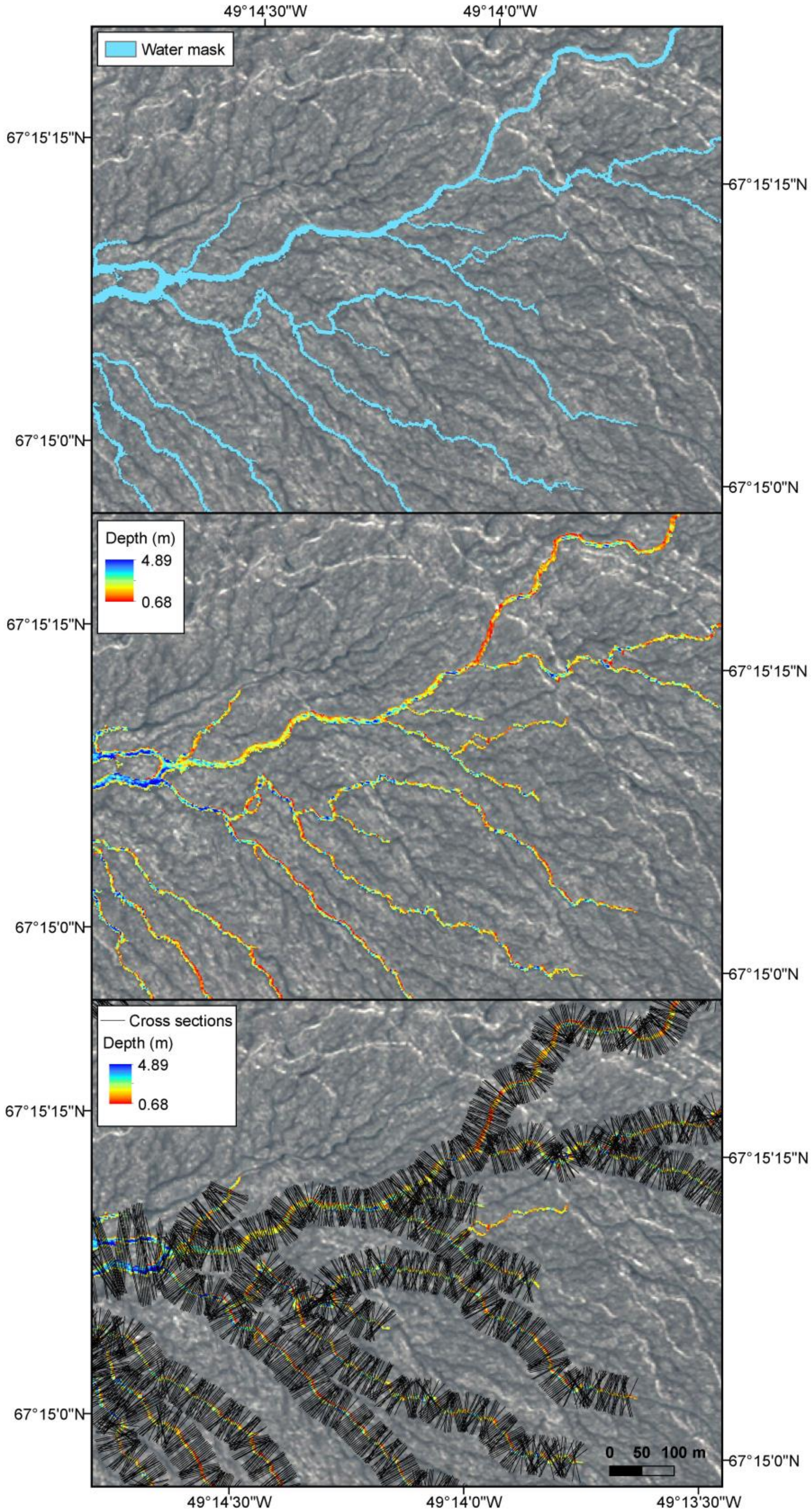

Figure 3-3. Examples of a river water mask, water depths, and orthogonal cross sections underlaid with WorldView-2 imagery.

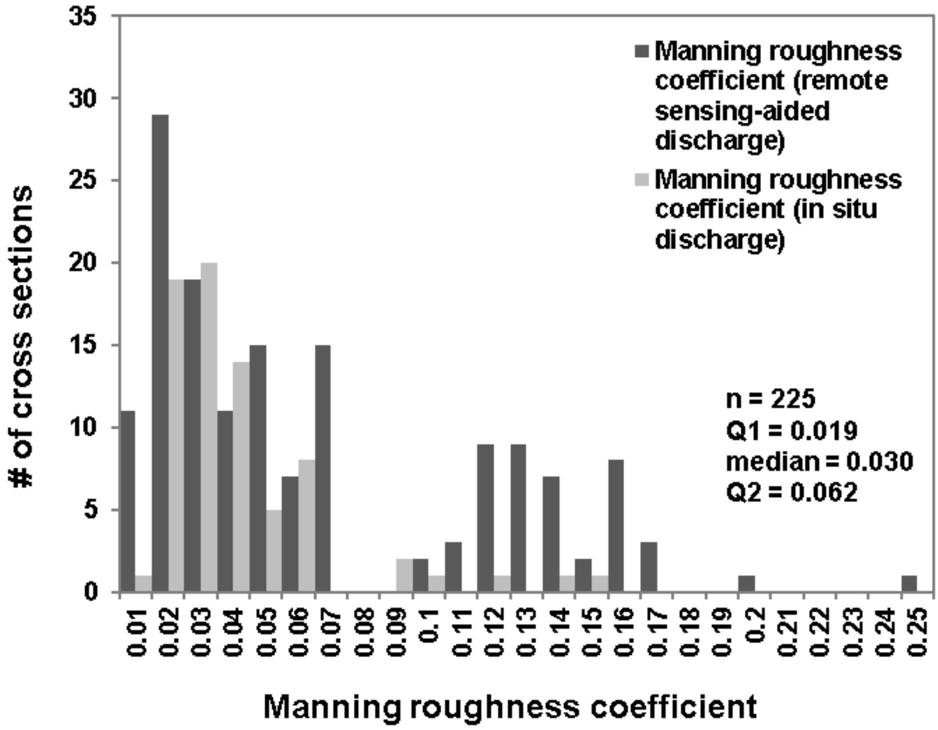

Figure 3-4. Manning roughness coefficient calculated from field data. The dataset consists of coefficients calculated from *in situ* discharge and those calculated from *in situ* velocities combined with remotely sensed cross-sectional area and slope, designated as "remote sensing-aided" discharge.

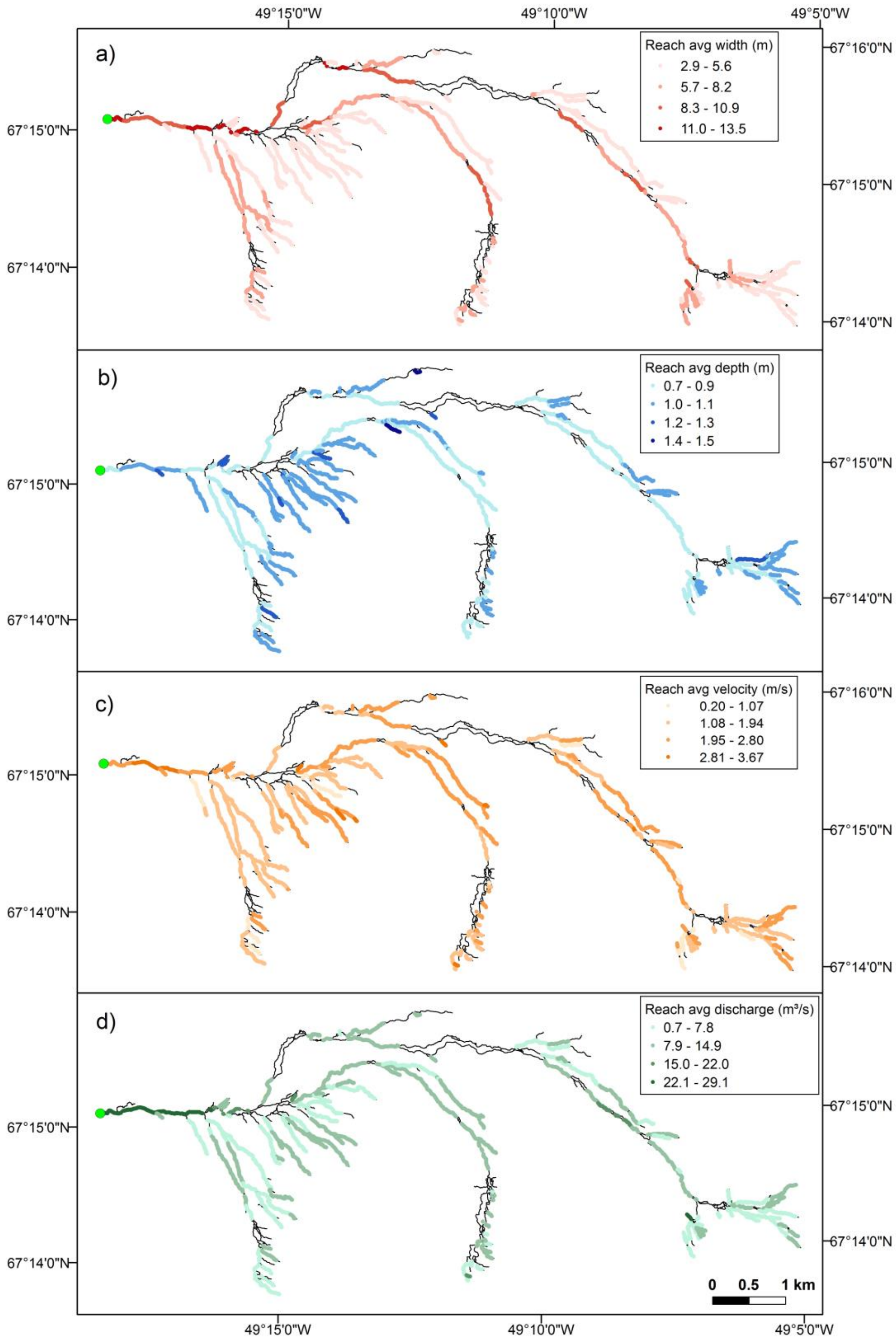

Figure 3-5. An example river network showing reach-averaged points of width, depth, slope, velocity, and discharge. Moulin termination points are shown as a large green point, and vector centerlines of river networks are underlaid in black.

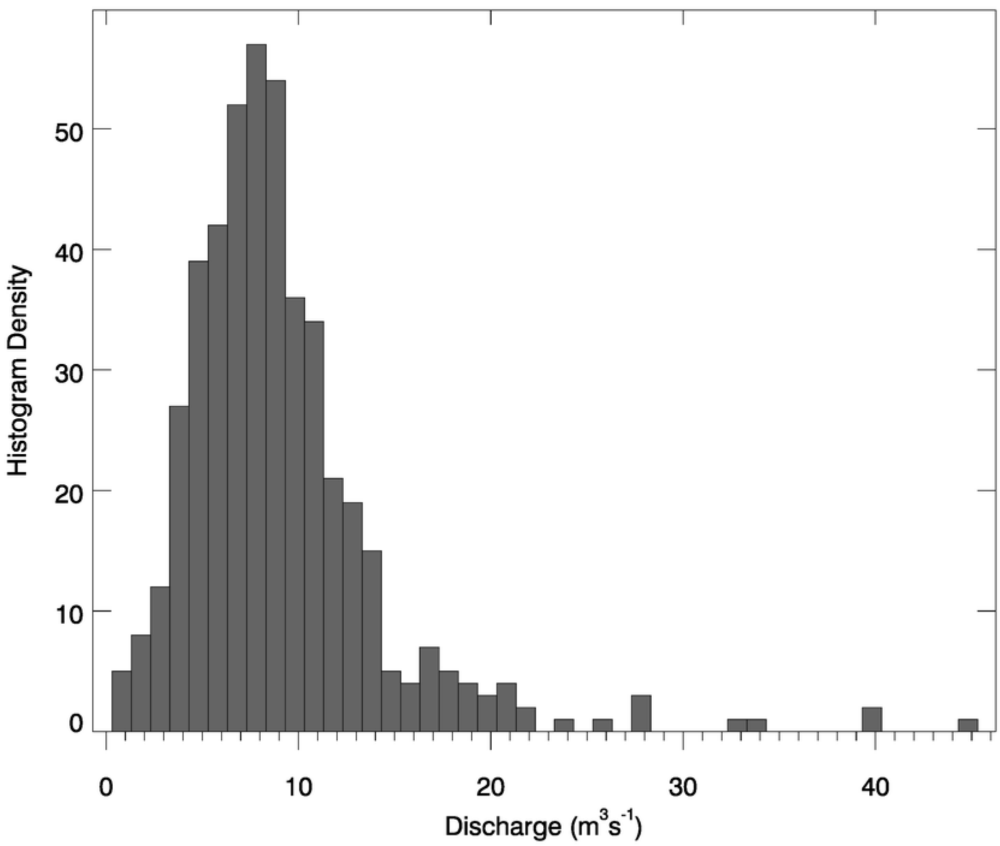

Figure 3-6. Distribution of GIS modeled moulin (termination point) discharges for all 465 river networks.

3.9 Tables

	Width (m)	Depth (m)	Wetted perimeter (m)	Hydraulic radius (m)	Slope (m/km)	Velocity (m/s)	Discharge (m^3/s)	Uncertainty – min-max (m^3/s)	Uncertainty – err. prop. (m^3/s)
Avg	5.65	0.89	7.98	0.62	7.95	1.91	9.16	27.66	24.11
Std dev	2.07	0.13	5.91	0.09	5.46	0.65	4.40	9.95	20.93
Max	17.86	1.71	703.64	1.18	183.39	7.70	54.54	182.57	1,856.90
Min	2.00	0.56	4.33	0.00	0.01	0.01	0.01	0.11	0.18
Median	5.04	0.87	7.40	0.62	6.82	1.88	8.42	25.84	19.59

Table 3-1. Attributes from reach-averaged cross-sectional points. A total of 1,629,502 reach-averaged points were retrieved including attributes of width, depth, velocity, slope, and discharge.

	Width (m)	Depth (m)	Wetted per. (m)	Hydraulic radius (m)	Slope (m/km)	Velocity (m/s)	Discharge (m^3/s)	Uncer. – min-max (m^3/s)	Uncer. – err prop (m^3/s)	# of reach-avg points	Elevation (m)	Max length (m)	Total length (m)	Max order
Avg	6.13	0.88	8.60	0.62	7.02	1.76	9.06	28.86	29.57	2,195	1,267	3,222	8,078	2.3
Std dev	2.55	0.13	6.48	0.11	5.52	0.68	5.29	12.37	34.15	4,839	164	4,357	18,244	1.0
Max	16.43	1.71	139.26	1.15	51.27	4.38	44.75	100.43	582.55	40,002	1,644	29,564	141,718	5.0
Min	2.00	0.68	5.42	0.01	0.03	0.11	0.31	1.44	1.19	16	907	59	41	1.0
Median	5.33	0.86	7.77	0.62	5.96	1.73	8.10	25.98	21.48	517	1,260	1,576	1,962	2.0

Table 3-2. Attributes from 465 river networks characterized by the reach-averaged point 1 km upstream of each network termination point.

3.10 Appendix: Discharge uncertainty

Uncertainty in the supraglacial discharge retrievals was characterized using two methods: propagating parameter uncertainties as standard error and propagating upper and lower bound parameter uncertainties to discharge. A dynamic uncertainty system was employed to retain as much of the raw data as possible while still reflecting varying quality levels, i.e., higher uncertainties reflect a lower quality level and vice versa.

Uncertainty from error propagation

Treating parameter uncertainties as standard error, uncertainties in all parameters were propagated to discharge uncertainty following error propagation rules (Taylor, 1997). δw and δd were defined as constants (δw = 2 m and δd = 0.32 m), δd was defined as a dynamic quantity, $\delta S = \pm 8.5$ m/L. Uncertainties in cross-sectional area and wetted perimeter were both defined by propagating δw and δd:

$$\delta A = wd\sqrt{\left(\frac{\delta w}{w}\right)^2 + \left(\frac{\delta d}{d}\right)^2} \tag{6}$$

$$\delta P = P\sqrt{\left(\frac{\delta w}{w}\right)^2 + \left(\frac{\delta d}{d}\right)^2} \tag{7}$$

Uncertainty in hydraulic radius was defined by propagating δA and δP:

$$\delta R = \frac{A}{P}\sqrt{\left(\frac{\delta A}{A}\right)^2 + \left(\frac{\delta P}{P}\right)^2} \tag{8}$$

and propagating Equations (6), (7), and (8) through the Equation (3) results in:

$$\delta v = v\sqrt{\left(\frac{n_3 - n_1}{n_2}\right)^2 + \left(\frac{2}{3}\frac{\delta R}{R}\right)^2 + \left(\frac{1}{2}\frac{\delta S}{S}\right)^2} \tag{9}$$

with total discharge uncertainty defined as:

$$\delta Q = 0.64v\sqrt{\left(\frac{n_3 - n_1}{n_2}\right)^2 + \left(\frac{2}{3}\frac{\delta R}{R}\right)^2 + \left(\frac{1}{2}\frac{\delta S}{S}\right)^2} \tag{10}$$

Uncertainty from min-max propagation

A second method for estimating uncertainty is calculating the discharge uncertainty due to each individual parameter uncertainty range. Each parameter uncertainty was propagated through the discharge calculation with an upper bound and lower bound one at a time, yielding associated discharge uncertainties for each parameter (in units of m^3s^{-1}). Using width as an example, the discharge uncertainty associated with width uncertainty for each point (δQ_w) was defined as:

$$\delta Q_w = Q_{\uparrow w} - Q_{\downarrow w} \tag{11}$$

with $Q_{\uparrow w}$ and $Q_{\downarrow w}$ defined as upper and lower bound discharge due to width uncertainty. $Q_{\uparrow w}$ was calculated using Equation (4) with w substituted by upper bound width ($w + \delta w$), and $Q_{\downarrow w}$ was similarly calculated by substituting w with lower bound width ($w - \delta w$):

$$Q_{\uparrow w} = \frac{1}{(n)}(w + \delta w)(d)\left(\frac{(w+\delta w)(d)}{P}\right)^{2/3}(S)^{1/2} \tag{12}$$

$$Q_{\downarrow w} = \frac{1}{(n)}(w - \delta w)(d)\left(\frac{(w-\delta w)(d)}{P}\right)^{2/3}(S)^{1/2} \tag{13}$$

This is done for each of the four parameters, w, d, S, and n. Note that while δw and δd are fixed quantities, δS is a dynamic quantity, changing with L. Also note that n is fixed and the upper and lower bounds are calculated using $n_{\uparrow}$ and $n_{\downarrow}$ defined in section 3.2.4. The following equations define discharge uncertainty associated with the remaining three parameters.

Depth:

$$\delta Q_d = Q_{\uparrow d} - Q_{\downarrow d} \tag{14}$$

$$Q_{\uparrow d} = \frac{1}{(n)}(w)(d + \delta d)\left(\frac{(w)(d+\delta d)}{P}\right)^{2/3}(S)^{1/2} \tag{15}$$

$$Q_{\downarrow d} = \frac{1}{(n)}(w)(d - \delta d)\left(\frac{(w)(d-\delta d)}{P}\right)^{2/3}(S)^{1/2} \tag{16}$$

Slope:

$$\Delta Q_S = Q_{\uparrow S} - Q_{\downarrow S} \tag{17}$$

$$Q_{\uparrow S} = \frac{1}{(n)} wd \left(\frac{wd}{P}\right)^{2/3} (S + \delta S)^{1/2} \tag{18}$$

$$Q_{\downarrow S} = \frac{1}{(n)} wd \left(\frac{wd}{P}\right)^{2/3} (S - \delta S)^{1/2} \tag{19}$$

Manning roughness coefficient:

$$\delta Q_n = Q_{\uparrow n} - Q_{\downarrow n} \tag{20}$$

$$Q_{\uparrow n} = \frac{1}{(n_{\downarrow})} wd \left(\frac{wd}{P}\right)^{2/3} (S)^{1/2} \tag{21}$$

$$Q_{\downarrow n} = \frac{1}{(n_{\uparrow})} wd \left(\frac{wd}{P}\right)^{2/3} (S)^{1/2} \tag{22}$$

These independent parameter uncertainties were aggregated to yield a conservative estimate of the total uncertainty in discharge at each cross-sectional point, calculated by:

$$\delta Q = \sqrt{\delta {Q_w}^2 + \delta {Q_d}^2 + \delta {Q_n}^2 + \delta {Q_S}^2} \tag{23}$$

Reach-averaged uncertainty

Discharge uncertainties were also reach-averaged ($\overline{\delta Q}$) for *x* number of available points, δQ_1, …, δQ_n, within a moving 1 km reach centered on each pixel:

$$\overline{\delta Q} = \sqrt{\frac{(\delta Q_1)^2 + \cdots + (\delta Q_n)^2}{x}} \tag{24}$$

3.11 Appendix: Field and remote sensing-aided dataset of Manning’s n and hydraulic properties

A dataset of river hydraulic properties from both field measurements (73 cross-sections) and remote sensing-aided measurements (152 cross-sections). Fields include date and time of measurement (date and time of image acquisition for the remote sensing-aided measurements), latitude, longitude, elevation, width, depth, cross-section area, wetted perimeter, hydraulic radius, slope, discharge, and Mannning’s n.

Point	Site	Date	Time (local)	Lat	Long	Elevation (m)	Width (m)	Depth (m)	Cross-section area (m^2)	Wetted perimeter (m)	Hydraulic radius (m)	Slope (m/km)	Velocity (m/s)	Discharge (m^3/s)	Manning's n
								Field dataset							
1	A16	7/23/12	10:28	67.167	-49.650	877	2.32	0.14	0.32	2.54	0.13	20.76	0.68	0.22	0.053
2	A17	7/23/12	10:15	67.167	-49.649	880	3.58	0.13	0.43	3.21	0.13	12.04	0.56	0.24	0.052
3	A18	7/23/12	11:11	67.167	-49.649	881	1.26	0.14	0.16	1.43	0.11	16.06	1.36	0.22	0.022
4	A19	7/23/12	11:25	67.166	-49.647	882	1.78	0.13	0.22	1.91	0.11	20.79	1.29	0.28	0.026
5	A21	7/23/12	11:53	67.166	-49.647	881	0.8	0.13	0.09	0.93	0.10	24.13	1.75	0.16	0.019
6	A22	7/23/12	12:12	67.166	-49.646	879	1.54	0.20	0.28	1.75	0.16	10.73	1.21	0.33	0.025
7	A24	7/23/12	14:20	67.165	-49.646	882	0.65	0.09	0.28	0.72	0.38	22.46	0.96	0.26	0.082
8	A25	7/23/12	14:31	67.165	-49.646	881	1.9	0.19	0.34	2.02	0.17	12.09	1.20	0.40	0.028
9	A26	7/23/12	14:48	67.164	-49.644	885	1.2	0.15	0.18	1.25	0.14	18.63	1.90	0.33	0.019
10	A27	7/23/12	14:59	67.165	-49.644	883	0.51	0.11	0.06	0.64	0.09	14.71	0.92	0.05	0.026
11	A28	7/23/12	15:13	67.163	-49.642	887	0.84	0.26	0.21	1.29	0.16	31.46	1.67	0.35	0.031
12	A29	7/23/12	15:27	67.163	-49.640	889	0.94	0.21	0.19	1.32	0.14	16.91	1.60	0.30	0.022
13	A30	7/23/12	15:40	67.162	-49.639	890	0.5	0.40	0.16	1.19	0.13	21.52	1.22	0.19	0.031
14	A31	7/23/12	15:53	67.162	-49.639	893	0.77	0.18	0.13	0.97	0.13	39.78	1.85	0.24	0.028
15	A33	7/23/12	16:09	67.162	-49.637	897	0.8	0.19	0.13	1.06	0.12	20.75	1.51	0.20	0.024
16	A34	7/23/12	16:18	67.162	-49.637	896	0.95	0.13	0.12	1.08	0.11	20.41	1.41	0.17	0.023
17	A36	7/23/12	16:24	67.161	-49.635	897	0.5	0.14	0.06	0.64	0.09	21.43	0.92	0.05	0.031
18	A37	7/23/12	16:46	67.161	-49.635	898	0.82	0.12	0.09	0.90	0.09	24.26	0.97	0.08	0.033
19	A39	7/23/12	17:05	67.158	-49.631	904	0.38	0.08	0.03	0.44	0.06	6.65	0.75	0.02	0.016
20	A40	7/23/12	17:12	67.158	-49.631	904	0.31	0.07	0.01	0.35	0.04	15.06	1.13	0.02	0.013
21	E1	7/24/12	16:13	67.174	-48.999	1204	0.94	0.17	0.14	1.11	0.12	5.65	0.74	0.10	0.025
22	B4	7/24/12	17:35	67.174	-49.249	1082	2.42	0.17	0.40	2.56	0.16	1.28	0.58	0.23	0.018
23	B5	7/24/12	17:43	67.174	-49.249	1080	0.7	0.11	0.07	0.79	0.09	4.54	0.32	0.02	0.041
24	N1	8/9/12	8:41	67.153	-50.035	511	0.95	0.05	0.05	1.00	0.05	7.50	0.48	0.02	0.024
25	N2	8/9/12	9:08	67.152	-50.035	499	1.24	0.08	0.10	1.37	0.07	7.37	0.40	0.04	0.037
26	N3	8/9/12	9:24	67.152	-50.034	504	1.22	0.13	0.14	1.35	0.11	7.58	0.52	0.07	0.038
27	N4	8/9/12	9:41	67.152	-50.034	505	0.89	0.05	0.04	0.93	0.04	9.83	0.56	0.02	0.021
28	N5	8/9/12	9:48	67.152	-50.034	504	0.96	0.10	0.09	1.05	0.09	7.58	0.56	0.05	0.031
29	N6	8/9/12	9:58	67.152	-50.034	500	1.15	0.07	0.07	1.24	0.06	7.70	0.45	0.03	0.029
30	N7	8/9/12	10:10	67.152	-50.034	503	0.58	0.03	0.01	0.59	0.02	7.70	0.40	0.01	0.018
31	N8	8/9/12	12:12	67.151	-50.032	506	0.88	0.15	0.12	1.02	0.12	36.50	0.76	0.09	0.060
32	N9	8/9/12	12:22	67.151	-50.032	505	0.71	0.07	0.05	0.76	0.06	30.46	2.06	0.10	0.014
33	N10	8/9/12	12:30	67.151	-50.032	505	1.975	0.06	0.12	2.04	0.06	31.70	0.60	0.07	0.044
34	N11	8/9/12	12:00	67.151	-50.032	507	1.05	0.09	0.09	1.14	0.08	18.70	0.80	0.08	0.032
35	N15	8/9/12	13:18	67.150	-50.030	520	0.765	0.08	0.06	0.82	0.07	58.96	1.54	0.09	0.028
36	N16	8/9/12	13:30	67.150	-50.029	518	0.39	0.05	0.01	0.42	0.03	82.44	1.74	0.02	0.017
37	N17	8/9/12	13:39	67.150	-50.029	519	0.73	0.07	0.05	0.77	0.06	88.27	0.96	0.05	0.050
38	N18	8/9/12	13:50	67.150	-50.029	518	0.2	0.07	0.01	0.21	0.04	37.95	2.60	0.02	0.009
39	N19	8/9/12	13:56	67.150	-50.029	521	1.245	0.06	0.07	1.29	0.05	46.17	0.67	0.05	0.046
40	N20	8/9/12	14:11	67.149	-50.028	530	1.07	0.07	0.07	1.12	0.06	27.65	0.70	0.05	0.036

41	N21	8/9/12	14:24	67.148	-50.026	534	0.51	0.07	0.04	0.59	0.06	61.48	0.74	0.03	0.052
42	N22	8/9/12	15:00	67.153	-50.035	503	1.61	0.09	0.14	1.66	0.08	13.75	0.67	0.09	0.034
43	N23	8/15/12	10:47	67.154	-50.041	496	0.95	0.09	0.06	1.02	0.06	50.85	1.24	0.08	0.029
44	N24	8/15/12	12:05	67.154	-50.040	498	0.86	0.16	0.13	1.02	0.12	47.11	2.00	0.25	0.027
45	N25	8/15/12	12:25	67.154	-50.039	500	1.65	0.14	0.22	1.74	0.13	32.09	1.49	0.33	0.030
46	N26	8/15/12	12:46	67.154	-50.038	500	2.2	0.15	0.29	2.38	0.12	21.41	1.36	0.39	0.027
47	N27	8/15/12	13:07	67.153	-50.036	506	3.84	0.09	0.35	3.87	0.09	12.16	1.07	0.37	0.021
48	N28	8/15/12	13:24	67.153	-50.035	508	2.5	0.13	0.29	4.21	0.07	7.95	1.09	0.31	0.014
49	S1	8/20/12	13:21	67.153	-50.040	494	1.25	0.09	0.11	1.32	0.08	30.59	2.08	0.23	0.016
50	S2	8/20/12	13:43	67.153	-50.039	500	1.69	0.10	0.16	1.79	0.09	17.60	1.46	0.24	0.018
51	S3	8/20/12	14:01	67.152	-50.038	500	1.03	0.08	0.08	1.13	0.07	58.67	1.42	0.12	0.030
52	S4	8/20/12	14:17	67.152	-50.038	500	0.75	0.07	0.05	0.80	0.06	62.78	1.54	0.08	0.026
53	S5	8/20/12	14:25	67.152	-50.038	502	0.93	0.08	0.07	1.00	0.07	52.10	1.36	0.10	0.029
54	S6	8/20/12	14:35	67.151	-50.038	500	0.78	0.08	0.06	0.85	0.07	28.24	1.48	0.09	0.019
55	1_0322	7/20/12	14:07	67.120	-48.331	1485	18.96	1.64	20.61	16.94	1.22	3.64	0.48	9.99	0.142
56	1_5900	7/20/12	14:02	67.120	-48.331	1485	19.94	1.59	23.77	18.82	1.26	3.64	0.53	12.55	0.134
57	1_1452	7/20/12	14:17	67.119	-48.331	1485	19.24	1.65	26.73	25.67	1.04	2.43	0.54	14.46	0.094
58	1_2736	7/20/12	17:29	67.119	-48.331	1486	18.96	1.67	28.82	26.73	1.08	2.43	0.47	13.54	0.110
59	1_1838	7/20/12	17:20	67.119	-48.330	1485	17.37	2.14	33.05	55.95	0.59	0.67	0.45	14.95	0.040
60	1_1635	7/20/12	17:18	67.119	-48.330	1485	17.37	1.84	29.00	20.11	1.44	0.67	0.41	11.77	0.082
61	1_1441	7/20/12	16:17	67.119	-48.330	1449	15.13	1.94	25.29	16.19	1.56	0.27	0.43	10.77	0.052
62	1_1948	7/20/12	16:21	67.119	-48.330	1485	15.13	1.96	27.77	27.90	1.00	0.27	0.39	10.79	0.042
63	1_2532	7/20/12	16:27	67.119	-48.330	1485	15.13	1.92	26.28	32.73	0.80	0.27	0.45	11.77	0.032
64	1_2853	7/20/12	16:31	67.119	-48.330	1485	15.13	2.21	30.19	52.49	0.58	0.27	0.35	10.42	0.033
65	1_3522	7/20/12	16:36	67.119	-48.330	1485	15.13	1.89	25.52	16.72	1.53	0.27	0.38	9.75	0.057
66	1_3821	7/20/12	16:40	67.119	-48.330	1485	15.13	2.00	26.14	20.91	1.25	0.27	0.38	10.00	0.050
67	3_4731	7/23/12	11:49	67.201	-49.160	1197	8.346	0.54	3.36	8.09	0.42	1.78	1.73	5.80	0.014
68	3_4427	7/23/12	11:46	67.201	-49.160	1197	8.214	0.48	3.20	8.29	0.39	1.78	1.72	5.50	0.013
69	3_5628	7/23/12	11:58	67.201	-49.160	1197	8.417	0.59	3.75	8.16	0.46	1.78	1.83	6.85	0.014
70	3_5345	7/23/12	11:55	67.201	-49.160	1197	8.417	0.59	3.59	7.74	0.46	1.78	1.79	6.42	0.014
71	3_2418	7/23/12	11:26	67.201	-49.158	1197	7.193	0.51	3.08	8.20	0.38	1.78	1.49	4.57	0.015
72	3_3008	7/23/12	11:32	67.201	-49.158	1197	7.202	0.50	3.05	7.73	0.39	1.78	1.64	5.00	0.014
73	3_3317	7/23/12	11:35	67.201	-49.158	1197	7.272	0.54	3.30	9.35	0.35	1.78	1.70	5.61	0.012
Remote sensing-aided dataset															
1	4620	7/23/12	14:08	67.183	-48.766	1297	15	0.86	12.87	16.46	0.78	0.88	1.22	15.69	0.021
2	4620	7/23/12	14:08	67.184	-48.767	1297	14	1.00	13.94	12.86	1.08	1.67	0.91	12.75	0.047
3	4620	7/23/12	14:08	67.184	-48.767	1297	11	0.81	8.95	8.26	1.08	2.15	1.22	10.91	0.040
4	4620	7/23/12	14:08	67.185	-48.768	1297	12	0.95	11.36	12.33	0.92	1.05	1.83	20.78	0.017
5	4620	7/23/12	14:08	67.187	-48.771	1285	7	0.80	5.58	8.43	0.66	13.04	9.45	52.77	0.009
6	4620	7/23/12	14:08	67.188	-48.771	1282	12	0.75	8.95	12.30	0.73	6.21	3.66	32.73	0.017
7	4620	7/23/12	14:08	67.188	-48.771	1282	18	0.72	13.04	20.27	0.64	4.66	2.44	31.79	0.021
8	4620	7/23/12	14:08	67.188	-48.771	1280	36	0.67	24.18	36.24	0.67	3.68	1.52	36.85	0.030
9	4620	7/23/12	14:08	67.189	-48.772	1280	41	0.71	29.00	44.56	0.65	3.05	0.91	26.52	0.045
10	4620	7/23/12	14:08	67.189	-48.772	1277	43	0.69	29.82	40.31	0.74	2.66	0.91	27.27	0.046
11	4620	7/23/12	14:08	67.189	-48.773	1282	49	0.71	34.61	52.56	0.66	2.49	0.61	21.10	0.062
12	4620	7/23/12	14:08	67.193	-48.796	1284	12	0.87	10.44	12.33	0.85	1.03	3.35	35.00	0.009
13	4620	7/23/12	14:08	67.195	-48.808	1285	21	0.71	14.96	20.23	0.74	3.01	3.35	50.15	0.013
14	4620	7/23/12	14:08	67.198	-48.817	1283	25	0.68	17.11	20.25	0.84	3.81	2.44	41.71	0.023
15	4620	7/23/12	14:08	67.198	-48.820	1280	27	0.73	19.76	24.41	0.81	4.23	3.66	72.29	0.015
16	4620	7/23/12	14:08	67.199	-48.821	1281	17	0.72	12.23	16.27	0.75	4.06	2.44	29.82	0.022
17	4620	7/23/12	14:08	67.199	-48.822	1281	20	0.70	13.92	16.25	0.86	3.65	2.13	29.69	0.026
18	4620	7/23/12	14:08	67.199	-48.823	1281	21	0.72	15.18	20.33	0.75	3.22	2.13	32.38	0.022
19	4620	7/23/12	14:08	67.199	-48.824	1281	17	0.72	12.17	16.29	0.75	3.86	2.74	33.38	0.019
20	4620	7/23/12	14:08	67.199	-48.824	1280	12	0.74	8.93	12.23	0.73	4.36	3.96	35.39	0.014
21	4620	7/23/12	14:08	67.199	-48.824	1279	16	0.68	10.90	12.22	0.89	2.81	3.66	39.88	0.013
22	4620	7/23/12	14:08	67.200	-48.826	1278	17	0.75	12.67	16.45	0.77	2.89	3.35	42.49	0.013
23	4620	7/23/12	14:08	67.200	-48.826	1279	31	0.72	22.19	32.49	0.68	2.30	2.13	47.35	0.017
24	4620	7/23/12	14:08	67.200	-48.827	1278	28	0.70	19.53	28.30	0.69	1.04	2.74	53.58	0.009
25	4620	7/23/12	14:08	67.200	-48.828	1278	15	0.80	11.94	16.58	0.72	0.51	3.35	40.03	0.005
26	4620	7/23/12	14:08	67.200	-48.828	1277	30	0.68	20.39	24.23	0.84	0.66	3.05	62.13	0.008

27	4620	7/23/12	14:08	67.200	-48.828	1277	43	0.70	30.07	36.46	0.82	1.00	1.83	54.99	0.015
28	4620	7/23/12	14:08	67.200	-48.829	1278	25	0.69	17.28	20.22	0.85	2.29	2.44	42.12	0.018
29	4620	7/23/12	14:08	67.201	-48.830	1278	22	0.73	16.08	24.48	0.66	2.97	2.74	44.11	0.015
30	4620	7/23/12	14:08	67.201	-48.830	1275	12	0.73	8.74	12.36	0.71	2.91	4.88	42.60	0.009
31	4620	7/23/12	14:08	67.201	-48.831	1275	21	0.71	14.85	20.36	0.73	3.61	1.22	18.10	0.040
32	4620	7/23/12	14:08	67.201	-48.831	1277	17	0.73	12.35	16.23	0.76	5.35	3.05	37.64	0.020
33	4620	7/23/12	14:08	67.201	-48.832	1276	18	0.76	13.60	20.51	0.66	6.88	3.35	45.60	0.019
34	4620	7/23/12	14:08	67.201	-48.833	1276	24	0.69	16.47	24.30	0.68	8.25	1.52	25.10	0.046
35	4620	7/23/12	14:08	67.201	-48.833	1272	10	0.71	7.11	8.22	0.86	10.14	4.27	30.34	0.021
36	4620	7/23/12	14:08	67.202	-48.835	1271	15	0.72	10.87	12.29	0.89	11.37	5.18	56.34	0.019
37	4620	7/23/12	14:08	67.202	-48.835	1267	10	0.83	8.32	8.45	0.98	8.23	4.57	38.04	0.020
38	4620	7/23/12	14:08	67.202	-48.836	1264	14	0.74	10.36	16.34	0.63	5.83	4.88	50.50	0.012
39	4620	7/23/12	14:08	67.202	-48.838	1263	14	0.77	10.75	12.22	0.88	4.85	3.35	36.03	0.019
40	4620	7/23/12	14:08	67.202	-48.841	1262	12	0.74	8.84	12.35	0.72	3.88	3.66	32.32	0.014
41	4620	7/23/12	14:08	67.203	-48.843	1263	20	0.76	15.16	20.53	0.74	2.42	3.96	60.07	0.010
42	4620	7/23/12	14:08	67.204	-48.845	1263	20	0.73	14.65	16.33	0.90	2.16	3.35	49.12	0.013
43	4620	7/23/12	14:08	67.205	-48.846	1261	20	0.75	14.99	20.46	0.73	3.12	3.66	54.83	0.012
44	4620	7/23/12	14:08	67.206	-48.848	1261	16	0.83	13.26	12.43	1.07	3.01	3.35	44.47	0.017
45	4620	7/23/12	14:08	67.206	-48.850	1260	14	0.80	11.14	12.28	0.91	2.55	3.66	40.74	0.013
46	4620	7/23/12	14:08	67.207	-48.852	1260	15	0.79	11.79	16.45	0.72	2.69	3.05	35.94	0.014
47	4620	7/23/12	14:08	67.207	-48.854	1259	12	0.75	9.05	12.24	0.74	1.75	2.74	24.83	0.012
48	4620	7/23/12	14:08	67.207	-48.856	1258	12	0.71	8.52	12.28	0.69	1.29	6.40	54.51	0.004
49	4620	7/23/12	14:08	67.208	-48.860	1257	12	0.81	9.68	12.31	0.79	1.96	4.27	41.30	0.009
50	4620	7/23/12	14:08	67.208	-48.862	1257	12	0.70	8.41	12.23	0.69	2.21	3.96	33.31	0.009
51	4620	7/23/12	14:08	67.209	-48.865	1257	19	0.77	14.57	16.23	0.90	3.00	2.13	31.08	0.024
52	4620	7/23/12	14:08	67.209	-48.867	1259	28	0.70	19.64	20.26	0.97	3.56	0.30	5.99	0.192
53	4620	7/23/12	14:08	67.209	-48.870	1259	25	0.69	17.15	20.22	0.85	3.70	0.91	15.68	0.060
54	4620	7/23/12	14:08	67.209	-48.872	1259	27	0.72	19.38	24.37	0.80	3.88	1.22	23.63	0.044
55	4620	7/23/12	14:08	67.209	-48.875	1258	14	0.74	10.30	12.22	0.84	4.02	1.52	15.69	0.037
56	4620	7/23/12	14:08	67.210	-48.876	1257	11	0.79	8.65	8.27	1.05	3.91	3.66	31.65	0.018
57	4620	7/23/12	14:08	67.210	-48.879	1257	33	0.72	23.82	28.32	0.84	4.21	3.35	79.85	0.017
58	4620	7/23/12	14:08	67.226	-48.916	1254	29	0.74	21.32	28.64	0.74	1.47	3.66	77.96	0.009
59	4620	7/23/12	14:08	67.227	-48.916	1248	10	0.88	8.83	12.53	0.70	0.39	7.01	61.88	0.002
60	4620	7/23/12	14:08	67.228	-48.917	1248	16	0.77	12.39	12.26	1.01	3.10	3.96	49.11	0.014
61	5700	7/18/12	13:53	67.118	-48.320	1468	48	0.80	38.24	48.32	0.79	1.91	0.61	23.31	0.061
62	5700	7/18/12	13:53	67.118	-48.321	1464	48	0.80	38.52	48.49	0.79	1.92	0.61	23.48	0.062
63	5700	7/18/12	13:53	67.118	-48.321	1468	44	0.83	36.58	44.40	0.82	1.93	0.67	24.53	0.058
64	5700	7/18/12	13:53	67.118	-48.321	1448	38	0.86	32.77	36.29	0.90	1.93	0.64	20.97	0.064
65	5700	7/18/12	13:53	67.118	-48.321	1448	35	0.91	31.80	36.36	0.87	1.94	0.76	24.24	0.053
66	5700	7/18/12	13:53	67.118	-48.322	1470	35	0.94	32.73	36.41	0.90	1.94	0.67	21.95	0.061
67	5700	7/18/12	13:53	67.118	-48.322	1474	33	0.95	31.43	32.41	0.97	1.93	0.64	20.12	0.067
68	5700	7/18/12	13:53	67.118	-48.322	1458	33	0.93	30.53	32.56	0.94	1.93	0.64	19.54	0.066
69	5700	7/18/12	13:53	67.118	-48.323	1460	29	0.94	27.34	28.50	0.96	1.92	0.61	16.67	0.070
70	5700	7/18/12	13:53	67.118	-48.323	1465	27	1.02	27.57	28.57	0.97	1.82	0.64	17.65	0.065
71	5700	7/18/12	13:53	67.118	-48.324	1483	25	1.01	25.29	24.40	1.04	1.73	0.64	16.19	0.067
72	5700	7/18/12	13:53	67.119	-48.325	1484	25	0.98	24.38	24.40	1.00	1.68	0.61	14.86	0.067
73	5700	7/18/12	13:53	67.119	-48.325	1492	25	1.01	25.13	24.65	1.02	1.66	0.67	16.85	0.062
74	5700	7/18/12	13:53	67.119	-48.325	1466	22	0.91	19.97	24.45	0.82	1.53	0.64	12.78	0.053
75	5700	7/18/12	13:53	67.119	-48.325	1492	23	1.03	23.80	24.66	0.97	1.42	0.67	15.96	0.055
76	5700	7/18/12	13:53	67.119	-48.326	1496	20	0.97	19.47	20.47	0.95	1.11	0.73	14.24	0.044
77	5700	7/18/12	13:53	67.119	-48.326	1486	23	1.03	23.69	24.45	0.97	1.06	0.76	18.05	0.042
78	5700	7/18/12	13:53	67.119	-48.327	1480	20	0.96	19.13	20.29	0.94	0.93	0.70	13.41	0.042
79	5700	7/18/12	13:53	67.119	-48.327	1494	22	0.80	17.58	24.25	0.72	1.02	0.76	13.39	0.034
80	5700	7/18/12	13:53	67.119	-48.328	1463	14	1.18	16.59	17.06	0.97	1.15	0.67	11.12	0.050
81	5700	7/18/12	13:53	67.119	-48.328	1454	14	1.08	15.13	16.81	0.90	1.16	0.55	8.30	0.058
82	5700	7/18/12	13:53	67.119	-48.328	1455	16	1.09	17.46	12.71	1.37	5.32	0.58	10.11	0.156
83	5700	7/18/12	13:53	67.119	-48.329	1449	18	1.13	20.31	20.50	0.99	5.29	0.70	14.24	0.103
84	5700	7/18/12	13:53	67.119	-48.329	1456	12	1.15	13.85	12.45	1.11	5.20	0.61	8.45	0.127
85	5700	7/18/12	13:53	67.119	-48.329	1459	14	1.04	14.52	12.85	1.13	5.14	0.67	9.73	0.116
86	5700	7/18/12	13:53	67.119	-48.329	1453	14	1.03	14.39	12.38	1.16	5.11	0.67	9.65	0.118

87	5700	7/18/12	13:53	67.119	-48.330	1452	17	1.17	19.82	16.38	1.21	5.15	0.70	13.89	0.116
88	5700	7/18/12	13:53	67.119	-48.330	1457	14	1.14	16.02	12.41	1.29	5.29	0.70	11.23	0.123
89	5700	7/18/12	13:53	67.119	-48.330	1447	17	1.12	19.06	16.72	1.14	5.38	0.70	13.36	0.114
90	5700	7/18/12	13:53	67.119	-48.330	1453	17	1.10	18.62	16.33	1.14	5.46	0.70	13.05	0.115
91	5700	7/18/12	13:53	67.119	-48.330	1450	20	1.08	21.67	16.41	1.32	5.49	0.73	15.85	0.122
92	5700	7/18/12	13:53	67.119	-48.330	1455	20	1.09	21.78	16.43	1.33	5.51	0.70	15.27	0.128
93	5700	7/18/12	13:53	67.119	-48.331	1456	20	1.17	23.41	16.89	1.39	5.53	0.76	17.84	0.121
94	5700	7/18/12	13:53	67.120	-48.331	1450	20	1.04	20.83	16.34	1.27	5.54	0.70	14.60	0.125
95	5700	7/18/12	13:53	67.120	-48.331	1458	23	0.96	22.02	24.25	0.91	5.53	0.76	16.78	0.092
96	5700	7/18/12	13:53	67.120	-48.331	1450	21	0.97	20.40	20.26	1.01	5.57	0.73	14.93	0.103
97	5700	7/18/12	13:53	67.120	-48.332	1454	21	1.02	21.36	20.36	1.05	5.71	0.70	14.97	0.111
98	5700	7/18/12	13:53	67.120	-48.332	1453	27	1.02	27.45	24.32	1.13	5.71	0.67	18.41	0.122
99	5700	7/18/12	13:53	67.120	-48.332	1455	25	1.00	24.89	24.26	1.03	5.71	0.67	16.69	0.115
100	5700	7/18/12	13:53	67.120	-48.332	1457	30	0.92	27.61	24.27	1.14	5.71	0.76	21.04	0.108
101	5700	7/18/12	13:53	67.120	-48.333	1448	38	0.90	34.38	32.33	1.06	5.71	0.61	20.96	0.129
102	5700	7/18/12	13:53	67.120	-48.333	1448	43	0.84	35.94	36.32	0.99	5.71	0.52	18.62	0.145
103	5700	7/18/12	13:53	67.120	-48.333	1453	48	0.84	40.24	40.31	1.00	5.71	0.55	22.08	0.138
104	5700	7/18/12	13:53	67.120	-48.333	1459	50	0.82	41.17	44.29	0.93	5.71	0.52	21.33	0.139
105	5700	7/18/12	13:53	67.121	-48.337	1457	50	0.82	40.95	52.56	0.78	5.71	0.40	16.23	0.162
106	5700	7/18/12	13:53	67.121	-48.338	1460	48	0.81	38.84	48.56	0.80	5.71	0.43	16.57	0.153
107	5700	7/18/12	13:53	67.121	-48.338	1455	43	0.83	35.84	44.36	0.81	5.71	0.46	16.39	0.143
108	5700	7/18/12	13:53	67.121	-48.338	1453	41	0.82	33.71	40.49	0.83	5.71	0.43	14.39	0.157
109	5700	7/18/12	13:53	67.121	-48.338	1457	41	0.82	33.71	40.49	0.83	5.71	0.40	13.36	0.169
110	5700	7/18/12	13:53	67.121	-48.338	1459	37	0.85	31.39	36.63	0.86	5.68	0.43	13.39	0.159
111	5700	7/18/12	13:53	67.121	-48.338	1465	37	0.90	33.34	36.63	0.91	5.66	0.43	14.23	0.166
112	5700	7/18/12	13:53	67.121	-48.338	1453	31	0.87	26.97	32.39	0.83	5.60	0.49	13.15	0.136
113	5700	7/18/12	13:53	67.121	-48.339	1451	29	0.88	25.53	28.43	0.90	5.55	0.52	13.23	0.134
114	5700	7/18/12	13:53	67.121	-48.339	1451	27	0.86	23.10	28.28	0.82	5.58	0.58	13.38	0.113
115	5700	7/18/12	13:53	67.121	-48.339	1458	27	0.93	25.20	28.62	0.88	5.62	0.55	13.83	0.126
116	5700	7/18/12	13:53	67.121	-48.339	1445	27	0.99	26.70	28.77	0.93	5.63	0.55	14.65	0.130
117	5700	7/18/12	13:53	67.121	-48.339	1452	20	1.00	20.09	20.31	0.99	5.69	0.67	13.47	0.112
118	5700	7/18/12	13:53	67.121	-48.340	1456	17	1.07	18.16	16.57	1.10	5.75	0.34	6.09	0.240
119	5700	7/18/12	13:53	67.121	-48.340	1451	18	1.21	21.70	20.38	1.06	5.77	0.52	11.24	0.153
120	5700	7/18/12	13:53	67.121	-48.340	1458	14	1.01	14.18	12.57	1.13	5.84	0.52	7.35	0.160
121	5700	7/18/12	13:53	67.121	-48.340	1451	14	1.04	14.51	12.64	1.15	5.84	0.55	7.96	0.153
122	5700	7/18/12	13:53	67.121	-48.340	1453	14	1.02	14.28	12.64	1.13	5.85	0.61	8.71	0.136
123	5700	7/18/12	13:53	67.121	-48.340	1454	14	1.17	16.44	12.47	1.32	5.85	0.61	10.02	0.151
124	5700	7/18/12	13:53	67.121	-48.341	1456	16	0.88	14.09	12.36	1.14	6.03	0.61	8.59	0.139
125	1440	7/23/12	14:08	67.201	-49.158	1174	10	0.86	8.60	12.65	0.68	7.29	2.90	24.91	0.023
126	1440	7/23/12	14:08	67.201	-49.158	1168	8	0.80	6.44	8.31	0.78	7.44	2.13	13.74	0.034
127	1440	7/23/12	14:08	67.201	-49.159	1163	12	0.75	9.03	12.24	0.74	8.08	1.92	17.34	0.038
128	1440	7/23/12	14:08	67.201	-49.160	1176	10	0.74	7.43	12.24	0.61	8.25	1.65	12.22	0.040
129	1440	7/23/12	14:08	67.201	-49.161	1167	12	0.72	8.64	12.26	0.70	9.00	2.77	23.95	0.027
130	1440	7/23/12	14:08	67.201	-49.166	1160	10	0.85	8.49	12.26	0.69	8.99	5.67	48.15	0.013
131	1440	7/23/12	14:08	67.201	-49.166	1159	12	0.82	9.86	12.37	0.80	9.14	2.87	28.26	0.029
132	1440	7/23/12	14:08	67.201	-49.167	1163	14	0.70	9.83	12.23	0.80	9.24	2.87	28.17	0.029
133	1440	7/23/12	14:08	67.201	-49.168	1171	10	0.72	7.17	12.29	0.58	9.22	2.23	15.95	0.030
134	1440	7/23/12	14:08	67.201	-49.168	1158	10	0.68	6.76	8.22	0.82	9.43	3.44	23.28	0.025
135	1440	7/23/12	14:08	67.201	-49.169	1161	16	0.69	11.01	12.25	0.90	9.22	4.42	48.67	0.020
136	1440	7/23/12	14:08	67.201	-49.170	1155	10	0.76	7.56	12.30	0.61	8.24	1.89	14.29	0.035
137	1440	7/23/12	14:08	67.201	-49.172	1160	10	0.70	7.04	8.23	0.86	7.40	3.69	25.98	0.021
138	1440	7/23/12	14:08	67.201	-49.173	1150	12	0.76	9.06	12.24	0.74	6.86	2.38	21.55	0.029
139	1440	7/23/12	14:08	67.201	-49.173	1151	12	0.72	8.66	12.23	0.71	6.76	1.71	14.78	0.038
140	1440	7/23/12	14:08	67.201	-49.173	1160	10	0.70	7.05	12.22	0.58	6.25	2.47	17.40	0.022
141	1440	7/23/12	14:08	67.201	-49.175	1160	12	0.79	9.51	12.48	0.76	5.36	1.46	13.92	0.042
142	1440	7/23/12	14:08	67.201	-49.176	1163	12	0.83	9.90	12.38	0.80	5.28	1.10	10.86	0.057
143	1440	7/23/12	14:08	67.201	-49.177	1160	10	0.75	7.52	12.35	0.61	5.12	1.28	9.62	0.040
144	1440	7/23/12	14:08	67.201	-49.177	1169	12	0.79	9.53	12.46	0.76	5.08	1.25	11.90	0.048
145	1440	7/23/12	14:08	67.201	-49.177	1151	14	0.89	12.42	16.51	0.75	5.04	1.46	18.17	0.040
146	1440	7/23/12	14:08	67.201	-49.177	1153	12	0.77	9.27	12.25	0.76	4.99	0.85	7.91	0.069

147	1440	7/23/12	14:08	67.201	-49.178	1161	17	0.83	14.12	16.54	0.85	4.96	0.64	9.03	0.099
148	1440	7/23/12	14:08	67.201	-49.178	1157	20	0.76	15.25	20.24	0.75	4.88	1.16	17.67	0.050
149	1440	7/23/12	14:08	67.201	-49.179	1157	14	0.76	10.67	16.30	0.65	4.82	0.85	9.10	0.061
150	1440	7/23/12	14:08	67.201	-49.179	1159	14	0.83	11.57	16.23	0.71	4.76	0.82	9.52	0.067
151	1440	7/23/12	14:08	67.201	-49.179	1159	14	0.85	11.91	16.69	0.71	4.64	1.52	18.15	0.036
152	1440	7/23/12	14:08	67.201	-49.179	1153	12	0.71	8.51	12.23	0.70	5.68	2.71	23.08	0.022

3.12 Appendix: Moulin discharge results

A dataset of 465 moulin discharges and associated river network properties resulting from the GIS modeling framework. Fields include width, depth, wetted perimeter, hydraulic radius, slope, velocity, discharge, discharge uncertainty calculated using the min-max method, discharge uncertainty calculated using error propagation, number of reach-averaged points in each network, elevation, maximum stream network length, and maximum stream order.

Point	Width (m)	Depth (m)	Wetted perimeter (m)	Hydraulic radius (m)	Slope (m/km)	Velocity (m/s)	Discharge (m3/s)	Uncer.-min-max (m3/s)	Uncer.-err prop (m3/s)	# reach avg points	Elevation (m)	Max length (m)	Max stream order
1	7.20	0.73	9.93	0.53	14.05	2.60	14.03	32.46	24.54	3502	1175	5420	3
2	4.70	0.95	6.90	0.64	3.95	1.34	5.27	18.51	12.86	850	1180	2284	1
3	3.90	0.99	6.47	0.60	10.61	2.21	7.99	23.92	15.53	1102	1160	2760	2
4	7.74	0.74	10.79	0.53	16.82	2.89	16.61	37.30	28.36	5234	1126	6548	3
5	4.50	0.87	6.67	0.59	12.15	2.40	9.23	27.04	17.99	274	1292	658	1
6	4.32	0.91	6.81	0.58	10.62	2.26	8.74	24.91	16.62	602	1275	1136	3
7	6.77	0.77	8.51	0.61	7.40	2.04	10.85	31.45	22.22	7516	1295	9504	3
8	5.03	0.85	7.04	0.61	1.96	0.98	3.91	21.57	41.90	303	1121	719	2
9	4.16	1.06	7.26	0.61	9.92	2.24	8.89	27.78	17.16	919	1271	2538	2
10	9.12	0.82	9.08	0.83	1.31	1.03	8.15	28.96	42.52	7073	1136	15751	4
11	8.41	0.72	9.15	0.67	3.21	1.39	8.53	25.83	59.29	7281	1287	10798	3
12	5.68	0.89	7.93	0.64	8.57	2.17	11.25	35.90	26.69	178	1205	747	1
13	4.98	0.78	8.44	0.46	1.72	0.81	3.16	14.20	29.18	96	1184	993	2
14	5.48	0.87	8.90	0.54	1.34	0.80	4.12	19.42	25.19	241	1117	558	1
15	4.64	0.92	6.68	0.64	2.79	1.19	4.77	19.52	20.84	168	1044	435	1
16	3.22	0.84	6.03	0.45	8.10	1.68	4.69	17.58	11.09	287	1033	753	1
17	3.26	1.26	5.83	0.70	3.77	1.43	5.09	18.38	13.74	761	1537	2419	1
18	9.73	0.75	10.30	0.71	2.84	1.36	10.18	31.56	24.92	13541	1562	14044	4
19	3.90	1.01	6.09	0.65	6.78	1.85	6.73	24.08	17.87	213	1135	709	2
20	12.15	0.71	11.90	0.72	6.69	2.16	18.68	50.40	36.51	8442	1489	20329	4
21	7.80	0.74	7.93	0.73	2.11	1.19	7.02	23.77	22.55	863	1481	2280	1
22	4.71	0.89	6.92	0.61	3.09	1.21	4.94	16.29	16.33	1091	1486	2973	3
23	5.57	0.87	8.51	0.57	2.03	0.99	5.07	19.74	22.58	244	1494	572	2
24	4.10	0.89	6.24	0.58	0.03	0.11	0.40	22.59	582.55	40	1505	857	1
25	4.07	1.05	8.19	0.52	1.80	0.89	3.74	18.47	26.35	194	1370	386	3
26	3.90	1.01	6.47	0.61	11.11	2.35	8.78	24.74	16.33	783	1511	1379	2
27	5.35	0.96	7.56	0.68	20.48	3.42	16.91	50.45	34.27	168	1352	1008	2
28	5.35	0.90	11.86	0.41	0.42	0.35	1.88	15.97	89.35	17	1336	59	1
29	8.66	0.73	8.69	0.73	16.60	3.36	21.17	47.84	36.05	10960	1365	10108	4
30	4.91	0.89	10.35	0.42	51.27	4.38	20.37	63.33	44.79	33	1375	177	1
31	3.52	1.21	7.10	0.60	19.97	3.11	12.62	43.59	27.39	144	1357	1170	3
32	4.13	1.05	6.75	0.64	14.31	2.72	11.15	30.38	21.09	435	1367	1333	2
33	4.55	0.84	8.38	0.46	6.39	1.57	5.82	21.45	19.10	245	1066	622	1
34	5.36	0.80	9.21	0.47	0.46	0.42	1.84	10.67	32.18	819	916	2834	2
35	2.99	0.99	5.45	0.54	22.15	3.14	9.60	28.68	19.22	1084	1408	2737	3
36	4.03	1.01	7.17	0.57	1.98	0.95	3.61	14.78	15.68	328	1459	779	2
37	4.68	0.92	6.60	0.65	6.37	1.81	7.00	22.31	14.40	261	1507	803	1
38	5.60	0.83	7.92	0.59	8.33	2.04	9.62	29.79	20.21	237	1509	587	3
39	4.98	0.80	6.67	0.60	12.45	2.48	10.00	25.73	18.32	750	1348	3127	2

40	6.03	0.79	7.92	0.61	13.03	2.63	12.75	30.22	22.33	3211	1139	3315	3
41	4.40	0.92	6.55	0.62	9.17	2.10	8.14	24.93	16.65	415	1259	1050	1
42	4.85	0.83	6.85	0.59	6.82	1.74	6.73	20.20	13.56	1301	1245	1828	2
43	5.24	0.85	8.87	0.50	3.91	1.28	5.84	20.02	16.98	248	1158	668	2
44	2.17	1.71	5.42	0.68	0.54	0.55	2.02	13.71	39.60	29	1437	904	1
45	4.14	1.05	6.39	0.68	8.71	2.16	8.61	26.87	16.76	1914	1465	4381	2
46	7.21	0.72	8.61	0.60	0.41	0.48	2.60	14.82	31.38	362	1458	3016	1
47	5.09	0.98	6.68	0.75	6.50	2.13	10.67	34.16	29.30	357	1468	2609	1
48	9.85	0.81	10.15	0.78	1.40	1.00	8.71	32.07	30.33	1381	1352	2926	2
49	5.59	0.84	7.31	0.64	6.18	1.75	8.31	24.46	17.64	1661	1354	4592	2
50	10.21	1.20	10.60	1.15	7.98	3.23	40.17	90.16	67.17	16584	1357	21501	4
51	6.98	0.77	8.36	0.64	4.39	1.55	8.09	23.28	16.44	1072	1487	1908	2
52	4.26	1.00	6.57	0.65	4.37	1.49	5.85	20.34	14.26	316	1468	838	1
53	4.63	0.96	6.74	0.66	3.16	1.30	5.25	16.81	12.03	2054	1471	3901	3
54	5.78	0.88	7.73	0.66	2.21	1.11	5.34	17.89	15.27	851	1454	2170	2
55	3.96	1.17	6.41	0.72	1.74	1.01	4.23	17.84	20.11	238	1453	749	1
56	4.02	1.06	6.39	0.67	2.78	1.23	4.85	18.35	16.90	221	1492	508	1
57	9.07	0.74	10.17	0.66	7.29	2.12	14.15	36.96	25.06	3523	1440	8064	3
58	12.25	0.68	11.82	0.71	3.78	1.60	13.53	38.51	29.60	21393	1387	22862	4
59	5.01	0.93	7.82	0.60	5.92	1.69	7.31	21.97	17.40	1195	1385	2382	3
60	9.33	0.72	9.56	0.70	3.60	1.56	10.63	30.87	23.60	347	1479	838	1
61	9.21	0.71	10.09	0.65	1.21	0.86	5.75	23.21	33.12	284	1469	984	2
62	5.07	0.94	8.11	0.59	3.83	1.35	5.88	19.91	14.77	243	1480	815	2
63	4.52	1.20	7.61	0.71	4.44	1.57	7.19	26.88	22.09	687	1455	2459	2
64	4.79	1.01	6.76	0.72	4.78	1.67	7.46	24.32	17.70	255	1437	634	1
65	7.61	0.76	8.59	0.67	4.81	1.72	10.30	29.28	20.53	1702	1445	4616	3
66	5.84	0.86	8.29	0.61	6.45	1.85	9.30	25.89	17.59	2006	1418	5681	3
67	10.82	0.70	11.96	0.63	0.27	0.38	2.89	18.60	65.20	5689	1413	13347	3
68	4.67	0.97	6.73	0.67	3.93	1.45	6.29	20.47	14.22	940	1388	2023	2
69	4.36	0.99	6.58	0.66	6.74	1.92	8.18	30.17	27.06	238	1386	919	1
70	5.99	0.94	8.68	0.65	5.34	1.73	9.41	28.51	20.74	261	1380	1199	1
71	3.45	1.26	6.10	0.71	4.79	1.61	6.03	22.08	14.14	344	1473	827	1
72	5.90	0.85	7.77	0.64	3.81	1.44	7.05	21.61	15.50	503	1487	1714	2
73	5.88	0.84	7.41	0.66	2.71	1.24	6.06	21.62	20.03	473	1489	1824	2
74	4.45	1.07	7.38	0.64	6.10	1.77	7.83	26.39	17.82	366	1441	943	3
75	4.85	0.94	6.65	0.69	6.31	1.93	8.63	24.61	16.37	2922	1410	7347	2
76	5.74	0.86	8.14	0.61	1.95	0.94	4.63	17.37	20.68	252	1398	689	2
77	13.19	0.74	14.38	0.68	7.48	2.24	21.64	53.01	36.92	3416	1423	5518	4
78	3.76	1.24	6.26	0.74	1.35	0.86	3.53	15.91	21.12	258	1417	1378	1
79	6.82	0.86	8.98	0.65	10.82	2.47	13.99	34.98	26.73	2391	1368	5018	2
80	3.25	1.20	5.96	0.66	2.44	1.05	3.61	15.84	36.80	125	1376	1043	2
81	5.53	0.85	7.18	0.66	2.56	1.14	5.14	19.27	29.71	1029	1383	3587	2
82	10.77	0.71	11.06	0.69	3.41	1.50	11.65	33.94	26.18	2372	1348	9352	3
83	4.76	0.97	7.45	0.62	4.02	1.45	6.57	23.88	21.95	232	1359	409	2
84	3.84	1.18	6.28	0.72	16.68	3.11	12.80	36.31	24.12	383	1364	1068	1
85	3.31	1.11	6.14	0.60	1.59	0.86	2.89	15.90	26.21	1048	1468	1784	3
86	5.99	0.76	7.18	0.63	2.86	1.27	5.80	18.84	15.68	1220	1479	2292	2
87	3.33	1.26	5.78	0.72	6.12	1.88	6.90	23.60	14.86	1114	1471	3778	2
88	4.22	1.07	6.38	0.71	5.36	1.74	7.30	24.18	16.55	329	1465	900	1
89	4.40	0.93	6.37	0.64	6.02	1.80	7.18	21.29	14.76	683	1470	1900	3
90	4.32	0.98	7.72	0.55	3.97	1.36	5.45	18.79	14.34	288	1474	949	1
91	15.15	0.68	15.31	0.67	0.50	0.54	5.62	27.66	63.04	264	1357	1832	2
92	5.41	0.91	6.82	0.72	0.51	0.51	2.19	16.04	88.83	44	1429	123	3
93	5.94	0.84	7.57	0.66	0.55	0.55	2.88	17.79	39.15	1140	1434	3778	2
94	5.64	0.78	7.42	0.59	2.66	1.17	5.23	16.67	13.02	3304	1414	6591	3
95	5.35	0.95	7.41	0.69	1.31	0.82	4.14	18.34	32.72	282	1384	1127	1
96	6.23	0.81	8.75	0.58	2.44	1.01	4.64	17.39	71.62	1336	1350	2943	3
97	4.02	1.15	6.44	0.72	5.70	1.83	7.91	28.51	21.99	327	1374	828	2
98	5.21	0.91	7.15	0.66	6.30	1.88	8.62	26.32	18.43	219	1488	1293	2
99	3.72	1.06	6.30	0.63	5.34	1.67	6.23	20.58	14.66	218	1403	522	2

100	6.59	0.75	8.01	0.62	9.87	2.36	11.94	31.23	21.09	4544	1405	7278	4
101	15.50	0.71	14.29	0.77	3.70	1.69	18.55	99.37	223.94	3043	1390	4337	4
102	5.02	0.93	7.05	0.66	5.82	1.69	7.85	24.06	19.44	602	1391	1644	1
103	6.22	0.91	8.07	0.70	11.61	2.62	13.84	49.91	49.77	51	1457	397	1
104	8.19	0.70	8.88	0.64	7.25	2.09	11.97	31.00	20.68	8176	1442	18622	4
105	7.54	0.73	8.85	0.62	2.94	1.27	6.85	21.33	19.32	2330	1438	7126	3
106	5.12	0.99	7.01	0.72	2.55	1.17	5.22	22.79	26.37	69	1432	1842	1
107	3.72	1.12	6.11	0.68	2.35	1.14	4.34	16.72	15.51	251	1440	594	2
108	5.17	0.94	7.15	0.68	4.43	1.61	7.81	27.19	23.76	125	1403	493	1
109	6.36	0.78	7.44	0.67	13.94	2.92	14.74	33.19	25.05	3101	1350	6199	3
110	4.33	1.08	7.33	0.64	6.80	1.88	8.09	25.72	16.67	1552	1353	1261	2
111	5.74	0.86	8.36	0.59	3.68	1.37	6.77	21.76	16.71	577	1498	1229	2
112	10.42	0.72	10.76	0.70	1.91	1.08	7.79	29.80	39.23	621	1468	2932	2
113	8.00	0.73	9.06	0.64	12.96	2.80	16.60	36.76	27.84	1695	1446	3458	3
114	15.95	0.69	14.16	0.78	2.87	1.50	16.55	46.28	35.68	3878	1404	4738	3
115	4.46	0.92	6.63	0.62	9.89	2.21	8.36	27.32	19.35	198	1410	1306	2
116	5.53	0.93	7.55	0.68	4.36	1.54	8.16	28.28	21.04	238	1402	1363	1
117	6.32	0.88	8.36	0.67	0.19	0.32	1.80	18.94	85.58	28	1421	158	1
118	4.59	0.91	7.10	0.59	8.84	2.12	9.02	23.93	16.79	2650	1458	6283	2
119	4.38	0.93	6.71	0.60	6.38	1.82	7.26	21.04	13.83	494	1461	1138	2
120	8.96	0.80	10.75	0.66	10.77	2.44	17.64	57.34	44.80	1315	1474	2729	2
121	6.75	0.92	9.21	0.67	3.23	1.35	8.07	34.64	43.55	88	1453	531	2
122	4.47	1.03	7.23	0.64	1.06	0.69	3.27	16.68	40.98	178	1451	1146	1
123	5.03	0.88	6.75	0.66	3.76	1.44	6.21	18.89	13.68	1953	1395	3469	3
124	4.30	0.94	10.83	0.37	15.74	2.14	9.60	35.78	28.57	441	1400	513	3
125	11.88	0.69	11.96	0.68	7.07	2.15	17.61	45.03	30.44	9606	1418	10507	4
126	5.18	0.92	7.22	0.66	5.48	1.71	8.29	25.77	17.73	431	1468	1541	2
127	3.88	0.97	6.10	0.61	5.64	1.60	5.74	19.21	22.34	925	1353	1523	4
128	6.38	0.90	8.82	0.65	5.65	1.76	10.51	42.33	42.76	107	1335	283	1
129	5.02	0.82	6.92	0.59	17.81	2.93	11.67	30.77	21.39	116	1476	217	3
130	6.99	0.86	9.84	0.61	5.23	1.69	10.36	38.49	35.88	95	1489	1316	2
131	5.28	0.80	7.96	0.53	5.87	1.59	6.76	19.80	13.52	1544	1495	2426	3
132	2.42	0.87	10.24	0.20	22.68	1.83	4.27	21.37	21.27	49	1431	482	2
133	6.78	0.85	8.73	0.66	4.00	1.48	7.75	23.30	17.72	501	1442	1544	2
134	7.35	0.71	8.18	0.64	1.22	0.79	4.27	17.01	29.16	892	1444	4302	3
135	9.61	0.71	9.27	0.73	1.85	1.13	7.76	25.68	34.56	5977	1353	7991	3
136	7.14	0.85	8.20	0.74	6.71	2.09	12.23	39.94	32.10	80	1358	334	2
137	5.54	0.95	6.99	0.75	4.33	1.74	9.40	32.07	30.81	288	1351	1128	2
138	7.31	0.78	8.55	0.67	6.32	1.89	10.52	28.52	20.83	1451	1345	2635	3
139	4.09	1.14	6.93	0.67	7.26	2.01	8.65	28.69	19.67	200	1349	1239	1
140	5.88	0.81	7.61	0.63	8.78	2.21	10.74	26.92	18.85	2281	1337	5169	3
141	3.98	0.98	6.39	0.61	10.33	2.29	8.77	25.23	16.44	1719	1326	2121	1
142	5.20	0.92	7.23	0.66	3.75	1.44	6.99	22.21	15.93	566	1317	1897	1
143	5.37	0.89	7.43	0.64	0.22	0.32	1.55	13.39	65.63	78	1316	1096	2
144	7.60	0.75	8.73	0.66	4.16	1.55	9.04	26.48	20.39	1424	1306	4850	3
145	5.66	0.91	7.55	0.69	8.93	2.30	12.17	35.14	24.23	324	1400	866	1
146	9.10	0.76	10.29	0.67	8.89	2.34	16.12	43.49	30.40	13043	1387	11147	5
147	4.57	1.03	6.62	0.71	11.32	2.62	13.41	46.08	33.69	109	1397	348	1
148	6.23	0.91	8.70	0.65	8.00	2.20	12.82	38.07	28.32	149	1397	455	1
149	4.94	0.98	7.10	0.68	2.77	1.24	5.47	23.66	30.25	110	1457	475	1
150	7.04	0.74	7.88	0.66	0.68	0.55	2.87	15.77	49.66	618	1459	2176	3
151	11.15	0.73	12.51	0.65	1.47	0.87	6.71	25.45	36.35	5367	1456	5328	3
152	2.00	0.70	139.26	0.01	21.00	0.22	0.31	1.44	1.19	4140	1411	4600	4
153	5.56	0.79	7.54	0.58	15.99	2.86	12.73	29.82	21.70	5306	1419	7433	3
154	5.17	0.80	7.01	0.59	6.24	1.76	7.11	20.28	13.35	2148	1495	3592	3
155	3.70	1.13	6.05	0.69	11.96	2.49	8.98	27.72	17.32	1347	1487	2662	3
156	6.34	0.73	7.75	0.59	10.07	2.29	10.57	27.17	18.61	2064	1478	4636	3
157	5.26	0.91	7.33	0.65	9.80	2.32	10.63	28.48	19.83	736	1436	2013	2
158	6.23	0.82	8.04	0.63	5.34	1.65	8.23	25.13	20.35	424	1257	2040	3
159	5.11	0.99	7.57	0.67	7.12	1.96	9.21	28.76	19.39	677	1266	1832	3

160	5.94	0.88	7.92	0.66	10.18	2.35	11.72	31.84	21.65	943	1293	1803	3
161	4.43	1.11	6.95	0.71	6.91	1.95	8.51	28.65	19.60	179	1281	678	1
162	2.48	1.09	12.86	0.21	45.43	2.71	8.72	46.89	30.11	25	1316	287	1
163	4.57	1.08	6.88	0.72	4.95	1.73	8.10	28.93	25.98	143	1318	465	1
164	4.44	1.06	6.73	0.70	16.28	3.04	13.25	39.36	25.30	181	1334	428	1
165	9.59	0.75	9.98	0.72	4.22	1.65	12.23	35.11	28.71	5861	1339	8386	5
166	8.62	0.74	8.75	0.73	8.15	2.38	15.56	39.27	27.50	11477	1336	15461	4
167	6.38	0.92	7.94	0.74	10.43	2.61	15.01	48.17	39.99	68	1281	299	1
168	4.71	1.05	7.17	0.69	7.09	2.02	9.52	30.25	21.51	204	1285	563	2
169	5.14	0.99	9.02	0.56	0.61	0.54	2.75	33.96	161.43	59	1414	198	2
170	5.33	0.87	7.17	0.65	14.42	2.78	12.44	31.15	22.38	1433	1321	3808	4
171	6.88	0.88	16.39	0.37	9.61	1.74	13.85	68.47	83.86	16	1307	572	1
172	4.07	1.07	6.42	0.68	0.62	0.57	2.33	13.62	31.80	217	1365	927	3
173	6.35	0.85	8.58	0.63	3.97	1.44	7.80	25.07	18.61	401	1395	1576	2
174	4.32	0.94	6.70	0.61	7.85	1.99	8.26	23.82	16.93	729	1394	1026	2
175	3.64	1.08	6.11	0.65	18.10	3.09	11.36	32.09	21.29	255	1398	1134	1
176	8.87	0.73	9.78	0.66	6.43	1.96	12.56	33.44	23.15	8057	1308	14449	4
177	6.09	1.02	7.99	0.77	9.99	2.37	11.98	34.46	22.76	619	1302	1940	3
178	9.19	0.72	9.60	0.69	3.31	1.45	9.69	28.70	22.44	449	1429	1123	3
179	8.55	0.77	11.25	0.58	1.90	0.95	5.99	25.62	32.88	426	1449	1245	3
180	12.45	0.73	11.99	0.76	9.02	2.64	24.07	55.54	39.79	3457	1450	9244	4
181	8.04	0.75	9.40	0.64	3.04	1.28	8.04	25.81	20.98	857	1282	2435	3
182	4.17	0.95	6.17	0.64	17.48	2.93	10.64	32.91	21.10	1137	1290	3879	1
183	4.53	0.84	6.65	0.57	1.78	0.91	3.65	17.59	24.53	146	1292	398	1
184	5.28	0.85	7.66	0.59	6.80	1.83	8.47	28.74	22.67	148	1290	366	1
185	5.08	0.87	7.40	0.60	10.27	2.30	10.70	31.94	22.05	191	1291	455	1
186	4.27	0.90	6.58	0.58	5.47	1.61	5.95	20.02	14.50	290	1261	508	2
187	5.89	0.80	8.12	0.58	1.04	0.71	3.43	16.73	31.03	519	1266	772	2
188	9.08	0.80	10.31	0.70	5.03	1.73	12.31	37.25	28.93	2937	1191	5329	4
189	4.62	0.97	7.97	0.56	6.71	1.73	7.46	25.98	17.01	387	1155	1020	2
190	5.41	0.86	8.01	0.58	10.43	2.28	10.59	29.83	19.85	802	1148	2508	2
191	12.89	0.90	12.37	0.93	5.55	2.32	27.41	67.85	49.99	24620	1151	23925	5
192	3.45	0.96	6.45	0.52	6.13	1.60	5.21	20.22	16.18	163	1147	362	2
193	9.44	0.74	10.80	0.65	8.55	2.26	16.19	63.83	78.14	1504	1143	4212	3
194	5.13	0.88	7.93	0.57	7.09	1.86	8.69	29.50	22.35	150	1147	386	1
195	8.53	0.71	9.07	0.66	3.29	1.38	8.47	25.97	20.59	1530	1133	2373	3
196	6.21	0.86	10.13	0.53	2.59	1.10	5.66	19.42	16.43	572	1139	1284	2
197	5.62	0.82	7.41	0.62	15.15	2.79	12.41	31.34	22.17	2044	1120	4427	3
198	5.91	0.86	8.49	0.60	5.02	1.57	7.82	26.58	20.27	346	1167	648	2
199	5.91	0.82	9.39	0.52	2.10	0.99	4.95	19.87	19.67	646	1165	904	2
200	5.29	0.77	7.07	0.57	0.38	0.39	1.64	11.40	35.36	575	1266	2739	2
201	4.37	0.89	6.51	0.60	1.81	0.92	3.50	14.50	15.16	386	1266	1864	2
202	7.42	0.84	11.79	0.53	5.05	1.57	10.32	40.06	43.38	170	1227	695	3
203	4.46	0.90	6.76	0.59	2.20	1.02	4.06	16.70	17.38	1035	1141	1622	2
204	5.38	0.88	8.64	0.55	5.21	1.54	7.07	25.95	23.38	531	1136	821	3
205	5.29	0.89	9.99	0.47	1.36	0.74	3.75	24.85	53.35	110	1103	325	2
206	5.04	0.90	7.33	0.62	10.66	2.29	10.14	32.59	21.27	784	1085	1181	3
207	5.05	0.88	7.15	0.62	7.08	1.89	8.09	25.05	17.04	445	1115	1253	2
208	4.43	0.89	6.99	0.57	14.16	2.58	9.81	26.04	18.05	977	1093	2243	3
209	3.98	1.14	6.42	0.71	7.09	1.98	7.98	27.83	18.74	178	1089	782	2
210	5.59	0.82	8.16	0.56	11.65	2.40	11.15	30.00	20.66	927	1087	2197	2
211	11.68	0.79	11.21	0.82	6.24	2.28	20.76	51.02	36.27	18879	1255	21628	4
212	4.20	1.02	6.47	0.66	15.66	2.83	10.95	33.41	21.38	420	1258	1642	1
213	6.02	0.87	8.37	0.63	6.68	1.86	9.30	27.85	18.60	445	1262	1661	2
214	13.19	0.91	12.34	0.98	7.23	2.74	32.84	75.70	54.73	21254	1264	18194	5
215	6.20	0.81	7.91	0.64	0.48	0.52	2.63	20.01	61.35	164	1268	398	1
216	4.33	0.84	6.99	0.52	4.88	1.45	5.28	19.21	16.50	191	1260	424	2
217	8.93	0.72	8.91	0.72	0.90	0.78	5.10	20.97	29.18	1712	1264	4093	3
218	14.32	0.86	13.67	0.90	10.56	3.17	39.42	92.26	65.98	21051	1274	15316	4
219	11.79	0.74	12.83	0.68	3.90	1.41	12.48	38.48	35.19	5064	1244	8977	4

220	4.67	0.85	6.70	0.60	13.39	2.43	9.31	25.17	18.07	1612	1221	2174	3
221	8.58	0.75	9.44	0.68	3.95	1.53	10.00	30.65	22.06	1362	1205	3983	3
222	6.58	0.99	7.83	0.83	4.34	1.56	8.68	33.45	28.92	5754	1152	12421	4
223	6.85	0.79	7.97	0.68	17.49	3.18	16.53	41.35	29.51	3537	1127	9112	3
224	5.11	0.79	6.89	0.58	2.04	0.97	3.92	15.99	20.80	245	1142	747	1
225	4.25	0.98	7.53	0.55	10.68	2.24	8.83	26.46	17.08	517	1151	2166	3
226	6.52	0.83	8.27	0.66	2.56	1.16	6.41	21.93	25.65	1382	1124	3884	3
227	14.30	0.95	14.86	0.91	6.89	2.51	34.27	83.04	61.74	28615	1175	14655	4
228	4.26	1.07	6.77	0.67	6.57	1.83	7.36	25.49	16.04	309	1179	922	2
229	4.97	0.83	7.07	0.59	9.75	2.16	8.68	23.36	15.96	915	1185	2037	1
230	8.75	0.71	9.93	0.62	7.22	2.08	13.20	35.06	23.64	2122	1184	3241	3
231	3.42	1.20	5.91	0.69	4.51	1.51	5.49	21.86	14.55	231	1171	786	1
232	13.20	0.74	13.83	0.70	0.33	0.45	4.41	26.57	179.37	4345	1155	4758	3
233	6.11	0.75	8.40	0.55	7.92	1.92	8.79	24.21	16.30	2892	1162	4407	3
234	5.15	0.98	7.40	0.68	4.89	1.57	6.84	23.09	16.49	207	1163	774	1
235	3.79	0.98	6.13	0.60	9.25	2.12	7.40	22.66	14.38	420	1161	1021	1
236	9.01	0.72	9.56	0.68	6.31	2.01	13.56	36.97	25.45	5434	1103	4189	3
237	3.62	0.94	5.82	0.58	7.33	1.82	5.89	19.32	12.28	438	1082	1182	2
238	9.75	0.73	9.94	0.72	7.90	2.32	16.71	40.91	29.31	5843	1078	7668	3
239	6.35	0.71	7.87	0.57	6.64	1.81	8.32	23.06	15.70	1012	1072	2035	2
240	9.17	0.82	9.52	0.79	5.61	2.12	16.13	43.10	32.03	4305	1045	6655	3
241	4.63	0.91	6.70	0.63	9.47	2.15	8.77	26.34	17.56	638	1044	1555	1
242	3.83	0.90	6.79	0.51	11.86	2.20	7.62	27.06	19.08	734	1024	1211	2
243	4.60	0.94	7.22	0.60	9.40	2.12	9.14	29.31	19.35	363	1015	946	2
244	9.02	0.70	9.43	0.67	4.70	1.73	10.93	31.57	24.40	2378	1071	4043	3
245	4.11	0.91	6.28	0.60	9.68	2.15	7.86	24.42	15.74	261	1043	1021	1
246	4.99	0.80	7.76	0.52	9.71	2.01	7.87	22.25	15.17	521	1049	1505	2
247	11.47	0.81	10.95	0.84	1.91	1.17	10.97	38.77	66.40	40002	1270	23271	5
248	3.39	0.94	5.68	0.56	6.43	1.71	5.38	17.71	11.53	268	1269	723	1
249	14.52	0.97	13.41	1.05	0.52	0.78	11.11	54.01	109.76	23676	1249	8331	5
250	9.54	0.94	9.38	0.96	4.13	1.85	17.75	51.61	76.14	24284	1262	29564	5
251	4.13	1.01	6.53	0.64	6.44	1.83	7.15	22.03	14.44	691	1244	1691	5
252	4.64	0.80	6.52	0.57	17.20	2.81	10.42	26.83	18.95	798	1248	2347	1
253	14.46	1.04	13.56	1.11	6.91	2.94	44.75	100.43	74.54	35462	1190	25961	5
254	16.23	0.85	16.36	0.84	1.96	1.31	18.06	52.84	48.68	27915	1107	9115	5
255	16.00	0.95	16.57	0.92	0.37	0.60	9.18	47.49	105.21	18524	1063	8283	5
256	8.19	0.72	10.01	0.59	2.94	1.25	7.46	22.57	17.35	1416	1039	2866	3
257	11.61	0.74	17.50	0.49	2.37	0.99	8.60	25.36	20.94	4664	1058	7004	4
258	8.49	0.83	9.00	0.78	10.25	2.79	20.50	46.50	35.71	14325	1065	10426	4
259	4.05	0.91	6.15	0.60	8.63	2.06	7.39	21.46	14.17	495	1129	1291	1
260	4.26	0.98	6.56	0.63	5.80	1.71	6.73	23.29	16.72	197	1302	539	1
261	6.40	0.78	7.92	0.63	9.39	2.23	11.08	29.06	20.49	2516	1288	4634	2
262	4.64	0.94	7.09	0.61	9.44	2.17	8.90	26.77	17.41	272	1294	763	2
263	5.97	0.74	7.72	0.58	17.36	2.90	13.03	31.54	23.32	1801	1293	4520	3
264	4.89	0.86	7.59	0.55	13.26	2.44	10.34	28.46	20.08	335	1288	1885	3
265	4.00	1.02	6.30	0.65	25.82	3.61	13.74	54.31	46.07	131	1189	754	2
266	6.22	0.72	8.12	0.55	10.71	2.26	10.35	26.34	18.92	1746	1196	2370	3
267	16.43	0.69	12.81	0.89	1.21	1.05	11.95	50.89	81.76	8120	1200	7257	4
268	7.44	0.86	10.37	0.62	2.41	1.10	7.37	41.52	71.31	87	1237	830	2
269	4.71	1.03	7.00	0.69	4.25	1.51	6.50	25.59	25.39	287	1235	1318	2
270	4.96	0.89	7.47	0.59	14.72	2.68	11.65	34.77	22.94	348	1236	729	2
271	5.60	0.86	11.27	0.43	2.27	0.91	4.34	17.49	18.42	299	1166	637	2
272	5.34	0.77	7.33	0.56	10.85	2.27	9.46	24.18	17.13	2297	1115	3957	3
273	4.68	0.88	7.08	0.58	7.65	1.90	8.50	31.56	24.56	128	1330	311	1
274	6.32	0.76	7.84	0.61	14.33	2.63	12.19	31.90	22.67	2822	1324	4931	3
275	12.77	0.79	13.00	0.78	4.83	1.95	19.97	56.12	44.46	22647	1173	14107	5
276	3.16	1.06	5.49	0.61	8.77	2.08	6.69	21.85	13.44	255	1235	875	2
277	6.02	0.85	9.11	0.56	4.98	1.58	7.90	33.02	43.10	57	1230	201	2
278	4.26	1.00	6.97	0.61	13.93	2.68	10.80	30.06	19.72	409	1237	576	2
279	5.23	0.84	7.89	0.56	9.73	2.14	9.40	27.82	18.49	1015	1235	910	2

280	5.17	0.83	7.52	0.57	13.46	2.56	11.32	34.33	23.57	265	1246	367	2
281	5.89	0.82	7.77	0.62	1.75	0.93	4.61	18.88	19.66	359	1248	1041	1
282	4.58	0.86	6.71	0.59	5.64	1.67	6.68	20.87	14.86	267	1250	1146	1
283	8.99	0.72	9.93	0.65	2.93	1.33	8.82	26.15	20.31	1058	1234	1996	3
284	5.42	0.96	8.50	0.61	14.81	2.82	14.11	49.61	46.65	36	1169	299	1
285	9.90	0.75	10.60	0.70	10.27	2.59	19.40	44.65	33.80	6476	1147	6484	4
286	4.76	1.09	6.97	0.74	13.77	2.83	12.90	36.43	24.18	453	1146	1085	1
287	10.41	0.93	12.08	0.80	11.13	2.91	27.54	58.76	46.21	17574	1145	12114	5
288	4.26	0.95	6.63	0.61	1.50	0.87	3.52	17.14	25.39	247	1175	813	3
289	6.28	0.80	8.82	0.57	15.38	2.77	13.98	33.23	24.94	4359	1110	5072	3
290	4.79	0.84	11.63	0.35	6.14	1.34	5.62	26.04	39.10	207	1095	516	3
291	4.96	0.89	7.39	0.60	1.95	1.00	4.34	16.33	16.97	387	1301	1891	2
292	8.17	0.80	9.02	0.73	2.55	1.29	8.71	30.78	29.13	135	1300	897	1
293	5.58	0.79	7.36	0.60	1.52	0.81	3.42	14.97	26.35	250	1336	1061	2
294	3.00	1.05	7.07	0.44	23.19	2.81	9.69	47.55	47.41	19	1260	153	1
295	4.50	0.97	7.31	0.60	1.24	0.80	3.43	20.18	42.51	121	1251	346	1
296	4.40	1.01	6.78	0.65	1.86	0.96	3.98	16.50	34.79	356	1252	1048	2
297	6.87	0.76	8.57	0.61	6.71	1.91	10.12	28.23	19.09	2800	1212	4011	3
298	10.57	0.75	11.22	0.70	8.21	2.37	18.91	45.36	32.23	6481	1204	10769	4
299	4.62	0.91	7.00	0.60	2.07	0.99	4.01	16.10	38.11	267	1191	693	3
300	7.19	0.92	9.38	0.71	6.76	1.96	11.55	32.36	22.55	11782	1148	9538	4
301	5.56	0.91	7.86	0.64	4.50	1.59	8.12	25.51	19.93	380	1171	644	3
302	6.28	0.86	7.97	0.68	4.91	1.70	9.35	37.58	43.24	88	1219	482	1
303	5.67	0.84	8.35	0.57	1.85	0.93	4.32	18.28	20.59	261	1277	673	1
304	5.09	0.98	8.04	0.62	10.30	2.22	9.06	26.88	17.63	473	1279	1755	2
305	5.24	0.84	8.07	0.54	4.83	1.52	6.93	23.73	19.13	191	1193	713	2
306	5.74	0.85	8.24	0.59	3.20	1.27	6.20	23.76	24.50	129	1176	434	2
307	8.39	0.71	9.50	0.63	4.17	1.56	9.45	28.03	20.90	2649	1107	4279	3
308	3.47	0.84	5.81	0.50	0.28	0.32	0.96	9.60	51.28	290	1105	1267	2
309	4.69	0.92	6.89	0.62	14.18	2.67	11.07	30.15	21.35	1335	1105	2803	2
310	4.20	1.05	7.37	0.60	9.93	2.23	9.26	32.85	25.22	501	1095	1279	2
311	4.14	1.01	6.85	0.61	3.02	1.20	4.86	20.15	18.80	423	1282	1232	2
312	8.77	0.77	9.50	0.71	14.92	3.22	22.23	50.43	38.12	18390	1213	12689	3
313	8.97	0.71	9.70	0.66	4.19	1.61	10.49	29.41	20.94	5585	1171	6526	4
314	5.47	0.83	7.64	0.59	2.89	1.21	5.50	17.54	13.29	582	1209	1837	2
315	7.99	0.75	8.98	0.67	7.43	2.13	13.38	40.22	29.26	3776	1198	5973	4
316	6.55	0.82	8.41	0.64	3.17	1.19	5.81	20.86	39.39	607	1137	1731	2
317	13.26	0.76	14.13	0.72	1.67	0.99	9.83	34.03	46.31	8622	1133	8430	5
318	7.55	0.75	8.90	0.64	5.08	1.65	9.88	29.41	24.32	1009	1166	3116	2
319	4.00	1.09	6.54	0.66	11.70	2.47	9.63	30.83	18.95	216	1168	501	2
320	5.35	0.81	7.37	0.59	9.15	2.11	8.83	24.94	16.44	1067	1122	3070	2
321	5.17	0.85	7.29	0.60	11.02	2.29	9.37	27.22	17.52	1134	1275	6202	2
322	4.89	0.97	6.83	0.69	5.39	1.72	7.70	39.19	60.07	46	1269	586	1
323	3.79	1.02	6.18	0.63	13.77	2.66	9.64	26.25	17.60	799	1282	1758	2
324	6.91	0.77	8.85	0.60	11.25	2.47	13.45	32.69	24.19	2987	1300	4640	3
325	11.81	0.79	12.62	0.74	11.45	2.91	27.67	64.53	46.98	12726	1291	16766	4
326	4.72	0.98	6.74	0.69	7.41	1.85	7.02	23.36	15.68	2344	1250	4223	3
327	5.74	0.77	7.45	0.59	14.67	2.72	12.07	29.81	21.48	1995	1228	4847	4
328	8.85	0.76	9.33	0.72	11.64	2.81	19.33	44.16	33.43	5568	1160	7857	4
329	4.21	0.94	6.74	0.59	11.36	2.29	9.49	34.46	25.27	80	1206	416	2
330	10.38	0.88	10.89	0.84	8.85	2.74	25.47	57.64	43.69	9410	1212	12100	4
331	5.81	0.85	8.10	0.61	2.65	1.17	5.73	19.81	17.36	753	1185	1194	2
332	3.31	0.93	5.59	0.55	19.04	2.87	8.91	26.70	17.72	997	1194	1382	2
333	9.68	0.72	11.19	0.62	9.32	2.36	16.53	43.12	29.64	3482	1002	7559	3
334	5.30	0.85	9.11	0.49	7.15	1.73	8.53	27.61	19.68	183	1048	603	2
335	4.29	0.91	8.26	0.47	5.93	1.50	5.92	22.82	18.25	162	1004	399	2
336	5.90	0.84	8.31	0.60	10.64	2.32	11.94	32.65	22.92	346	990	1946	2
337	4.68	0.91	6.70	0.64	10.27	2.37	9.97	25.75	18.10	1698	1279	3406	2
338	8.32	0.72	8.86	0.68	9.26	2.19	12.49	32.09	26.48	5292	1258	9623	3
339	6.57	0.72	8.08	0.59	9.44	2.20	10.80	29.89	20.21	5570	979	9179	3

340	7.09	0.74	8.37	0.62	5.05	1.67	8.70	24.78	16.99	2262	1066	5080	2
341	10.69	0.70	11.42	0.65	1.47	0.95	7.30	25.45	27.32	587	1059	1343	3
342	7.61	0.72	9.79	0.56	5.84	1.47	6.66	22.13	58.09	1608	1039	5022	2
343	5.63	0.75	8.59	0.49	5.88	1.57	6.59	19.84	13.40	1169	1151	2459	3
344	8.45	0.73	9.03	0.68	6.95	2.06	13.08	34.17	25.51	10710	1270	16737	4
345	10.22	0.70	10.13	0.71	5.23	1.89	13.82	39.21	28.16	4073	1260	6823	3
346	4.78	0.84	6.70	0.60	8.36	1.91	7.27	21.09	15.93	665	1264	2385	2
347	4.36	0.97	6.60	0.64	5.96	1.78	7.37	22.74	15.63	288	1290	834	1
348	4.79	0.98	7.31	0.64	8.83	2.15	10.31	34.73	24.93	165	1289	922	2
349	5.23	0.83	7.65	0.57	8.13	2.02	8.95	25.18	17.06	759	1282	1621	3
350	4.89	0.86	9.97	0.42	5.29	1.40	6.06	38.17	87.45	30	1267	568	2
351	4.97	0.92	7.61	0.60	5.83	1.72	7.50	23.28	16.26	340	1258	652	2
352	6.70	0.87	9.57	0.61	3.47	1.34	7.44	36.36	61.26	476	1191	2085	2
353	5.10	0.77	6.89	0.57	17.20	2.84	10.89	29.33	19.98	706	1127	2762	2
354	4.34	0.98	6.88	0.62	7.58	1.91	7.43	23.75	14.99	436	1157	906	3
355	6.37	0.85	9.26	0.58	15.10	2.77	14.93	47.57	35.87	71	1157	189	1
356	5.78	0.85	9.14	0.54	1.09	0.70	3.27	17.56	33.03	491	1158	1116	2
357	4.28	0.98	6.56	0.64	7.12	1.90	7.27	23.23	15.14	240	1157	700	1
358	3.87	0.82	5.84	0.54	12.40	2.33	7.48	22.06	14.42	732	1139	2373	1
359	4.42	0.91	6.61	0.61	7.69	1.94	7.32	22.31	14.41	339	1123	1023	1
360	5.26	0.85	7.34	0.61	13.22	2.64	12.08	32.23	22.98	389	1158	875	2
361	7.67	0.87	8.80	0.76	3.83	1.53	9.41	33.26	28.82	192	1176	702	1
362	4.15	0.94	6.38	0.61	7.54	1.90	6.85	20.68	13.18	1114	1181	3163	2
363	3.52	1.02	5.79	0.62	8.07	1.98	6.91	22.63	14.51	857	1196	1860	2
364	7.39	0.72	9.35	0.57	3.11	1.24	6.67	20.99	16.53	1543	1186	2278	3
365	4.09	1.07	6.41	0.68	3.37	1.36	5.40	19.66	16.55	217	1216	531	1
366	4.96	1.03	7.29	0.70	5.06	1.66	7.85	27.19	20.50	233	1211	608	2
367	6.96	0.71	8.17	0.61	8.83	2.19	11.15	28.18	19.74	1054	1213	2237	2
368	6.73	0.78	7.89	0.67	4.97	1.58	7.99	25.52	21.60	716	1201	2808	3
369	3.89	1.06	6.54	0.63	7.36	1.94	7.36	24.70	16.26	345	1204	2019	2
370	4.61	0.92	6.87	0.62	6.64	1.84	7.57	22.84	15.01	744	1209	1938	1
371	4.88	1.14	6.89	0.81	4.65	1.68	7.86	27.23	20.10	261	1205	607	2
372	4.31	0.92	6.89	0.57	4.41	1.46	5.90	25.84	30.05	68	1205	296	1
373	3.54	0.94	7.45	0.45	6.98	1.57	5.28	18.11	12.15	106	1199	1148	2
374	5.95	0.91	7.76	0.70	1.39	0.87	4.96	41.70	123.31	21	1195	217	1
375	5.83	0.85	8.06	0.62	8.75	2.12	10.48	39.34	34.65	161	1184	719	2
376	5.35	0.96	7.26	0.71	1.70	0.96	4.57	18.12	23.55	295	1178	890	2
377	7.88	0.83	11.29	0.58	3.27	1.30	8.66	56.93	150.68	57	1180	361	1
378	9.79	0.72	10.59	0.66	10.29	2.60	18.76	48.77	33.34	36	1130	1051	2
379	4.28	0.94	6.62	0.61	13.48	2.58	10.05	30.56	19.74	202	1178	552	2
380	7.19	0.81	8.86	0.66	3.91	1.49	8.49	26.78	20.50	1443	1170	2767	2
381	5.12	0.93	11.08	0.43	2.87	1.04	5.50	32.44	57.01	66	1138	213	2
382	4.39	0.86	7.68	0.49	29.69	3.46	13.04	46.31	33.89	201	1116	900	3
383	5.48	0.87	8.18	0.58	9.76	2.22	10.78	29.24	20.74	526	1086	1454	2
384	3.79	0.85	6.08	0.53	5.83	1.57	5.16	17.67	12.14	233	1114	628	2
385	4.22	0.91	6.44	0.60	9.28	2.08	7.75	24.34	15.59	612	1096	1370	1
386	6.17	0.79	8.11	0.60	11.31	2.25	11.00	30.03	30.50	1078	1019	2172	3
387	3.72	0.83	7.31	0.42	17.90	2.41	8.03	35.56	32.85	25	1033	300	2
388	5.72	0.87	7.41	0.67	2.63	1.20	5.73	31.28	55.26	65	1028	530	1
389	2.00	0.77	29.32	0.05	18.21	0.64	0.99	4.65	4.13	17	974	760	1
390	6.17	0.79	8.43	0.58	4.11	1.43	6.93	21.14	14.82	651	1039	3101	2
391	4.94	0.93	7.47	0.62	9.70	2.19	9.87	34.76	25.41	121	1039	696	2
392	4.56	0.86	9.62	0.41	3.33	1.07	4.34	21.19	30.50	90	1038	228	2
393	3.84	0.97	6.11	0.61	5.06	1.54	5.32	19.30	13.71	203	994	597	1
394	3.51	0.91	5.72	0.56	7.17	1.76	5.57	20.71	14.50	147	992	759	1
395	4.03	0.85	6.41	0.53	10.36	2.11	7.16	21.31	13.89	558	993	1401	1
396	7.18	0.73	8.69	0.60	3.23	1.25	6.41	20.52	21.05	1029	1090	2731	3
397	5.73	0.87	8.81	0.56	18.52	3.01	15.09	42.76	28.74	319	1091	1524	2
398	4.48	0.93	8.72	0.48	2.69	1.02	4.20	21.99	31.21	111	1054	297	2
399	5.19	0.85	7.57	0.59	5.00	1.54	6.80	24.46	19.68	181	1031	644	1

400	4.78	0.89	7.99	0.53	11.27	2.22	9.71	33.16	22.53	152	1026	342	2
401	7.99	0.71	8.81	0.65	5.56	1.77	10.14	29.42	20.78	1876	932	5548	3
402	4.33	0.88	7.41	0.52	6.47	1.65	6.42	21.82	14.71	354	940	1633	1
403	5.91	0.75	9.11	0.48	8.52	1.89	8.63	25.63	17.08	598	943	1459	2
404	4.43	0.89	8.17	0.48	8.04	1.74	7.01	28.55	23.75	266	924	601	2
405	4.39	0.90	6.47	0.61	17.00	2.83	10.97	30.35	20.94	1044	1096	2514	1
406	10.87	0.71	12.58	0.62	8.38	2.24	17.36	46.05	31.77	2688	1176	6910	3
407	5.75	0.96	7.66	0.72	3.16	1.31	6.31	22.88	18.79	182	1166	1527	2
408	7.06	0.81	8.35	0.69	5.63	1.79	9.84	36.98	36.57	180	1194	479	2
409	9.68	0.77	9.37	0.79	2.12	1.22	9.52	32.04	29.81	2500	1177	3986	3
410	4.48	0.89	6.71	0.59	5.12	1.53	5.79	21.35	15.93	193	1175	682	2
411	10.02	0.76	12.65	0.60	3.35	1.26	10.28	35.71	34.23	175	1145	644	2
412	8.47	0.74	9.60	0.65	7.24	2.06	13.18	36.48	24.92	331	1112	1368	2
413	4.94	0.90	7.47	0.60	14.70	2.76	12.04	33.05	22.71	172	1141	1292	2
414	5.51	0.78	7.43	0.58	7.97	1.85	7.40	21.40	24.37	1466	1120	3325	3
415	7.30	0.76	8.67	0.64	4.19	1.56	8.75	25.08	17.76	882	1068	2637	2
416	7.78	0.72	9.29	0.60	2.78	1.17	7.03	24.20	30.21	232	1099	1352	1
417	4.17	1.00	7.66	0.54	3.21	1.19	4.82	21.51	22.50	175	1129	351	2
418	4.53	0.90	7.88	0.52	5.96	1.61	6.70	23.77	17.04	152	1111	543	1
419	4.37	1.05	6.93	0.66	9.61	2.19	8.82	29.89	18.05	507	1165	1716	1
420	5.49	0.84	7.21	0.64	7.60	1.93	8.71	25.26	17.81	774	1168	2030	2
421	3.64	0.85	6.25	0.50	20.44	2.82	8.79	25.89	17.41	444	1033	1140	1
422	3.55	0.80	5.56	0.51	5.49	1.48	4.43	15.35	10.26	690	1015	1652	2
423	5.51	0.80	8.25	0.54	7.64	1.86	8.38	23.32	16.04	833	1002	1375	2
424	4.24	0.89	6.80	0.55	9.11	1.97	7.05	33.73	41.08	37	1000	851	2
425	2.90	0.88	10.98	0.23	15.62	1.74	5.08	27.30	33.70	21	1048	279	1
426	4.35	0.83	7.80	0.47	2.63	1.03	3.85	16.28	17.09	179	991	490	2
427	8.11	0.72	10.54	0.55	12.15	2.47	15.19	39.66	28.22	2305	951	4418	3
428	4.14	0.86	7.22	0.49	13.94	2.36	7.98	32.79	35.96	272	936	935	2
429	6.43	0.80	9.01	0.57	5.33	1.61	7.96	24.58	17.30	494	916	764	1
430	5.53	0.81	7.66	0.58	5.00	1.50	6.74	20.94	16.19	429	907	1868	2
431	4.91	0.89	7.00	0.62	5.59	1.66	6.98	25.23	18.66	182	918	812	1
432	7.73	0.80	9.48	0.65	7.25	1.99	11.96	39.80	30.25	113	916	384	1
433	4.64	0.78	6.67	0.55	11.87	2.30	8.45	25.00	16.15	341	924	855	1
434	4.65	0.82	6.73	0.57	2.10	0.96	3.64	14.39	14.99	370	939	1937	2
435	3.79	0.91	6.38	0.54	7.26	1.78	5.99	20.60	13.61	194	970	469	1
436	3.96	0.86	8.68	0.39	1.33	0.64	2.23	11.32	13.06	387	949	811	2
437	4.14	0.91	6.38	0.59	4.33	1.39	4.91	15.96	11.72	1183	1563	3359	1
438	4.22	0.94	7.14	0.56	3.73	1.32	4.97	18.60	17.71	151	1564	385	2
439	4.74	0.88	8.81	0.47	3.96	1.28	5.49	21.40	21.14	145	1563	610	2
440	10.62	0.69	10.13	0.72	0.62	0.64	4.68	26.50	88.79	5721	1559	11383	4
441	9.33	0.69	9.56	0.67	0.07	0.19	1.23	16.47	181.87	1586	1553	4670	2
442	9.80	0.70	10.34	0.67	2.93	1.38	9.65	28.38	21.52	1033	1578	3014	3
443	4.98	0.85	11.53	0.37	8.00	1.61	6.93	31.80	41.48	631	1548	716	3
444	6.06	0.81	8.01	0.61	1.29	0.76	3.48	15.66	36.23	236	1529	1055	2
445	7.40	0.82	20.61	0.30	7.53	1.31	7.90	34.81	46.03	59	1514	692	1
446	4.91	1.03	6.48	0.78	10.84	2.49	12.68	45.25	32.03	263	1520	2323	2
447	4.16	0.85	6.56	0.54	7.69	1.86	6.48	19.90	13.12	1201	1519	5230	2
448	3.41	1.34	6.28	0.73	4.03	1.47	5.70	25.25	23.42	99	1525	571	2
449	2.89	1.19	5.45	0.63	3.24	1.28	4.10	15.41	11.53	770	1533	2752	1
450	5.96	0.77	7.76	0.59	3.57	1.32	5.98	18.65	14.02	2636	1529	4866	2
451	3.48	1.14	5.92	0.67	4.00	1.46	5.20	18.28	12.83	305	1531	777	1
452	8.87	0.69	8.73	0.70	7.69	2.27	14.06	36.24	24.61	4566	1527	6365	3
453	7.46	0.70	8.14	0.64	3.92	1.52	8.10	23.29	16.48	12488	1536	15757	3
454	7.14	0.77	8.91	0.61	10.60	2.42	13.20	32.54	23.90	668	1544	2250	2
455	3.63	0.92	5.91	0.56	1.52	0.78	2.43	11.23	22.23	142	1562	2284	1
456	8.14	0.79	9.15	0.70	1.19	0.83	5.14	20.44	36.75	328	1565	1636	2
457	4.83	0.88	7.25	0.59	6.31	1.73	7.19	22.38	15.15	539	1556	1957	1
458	8.02	0.72	8.73	0.66	2.82	1.25	7.10	22.53	31.40	11277	1569	17055	4
459	4.41	0.97	6.67	0.64	2.67	1.17	4.60	17.93	17.35	278	1562	3615	1

460	5.19	0.87	7.09	0.64	5.90	1.79	7.91	23.44	16.29	276	1577	681	1
461	7.52	0.70	8.23	0.64	5.08	1.73	9.25	25.69	17.51	5178	1587	11513	4
462	6.05	0.74	7.60	0.59	3.23	1.23	5.50	17.67	15.94	912	1586	1906	2
463	4.10	1.00	6.20	0.66	7.17	1.92	6.92	21.91	13.72	1616	1596	4461	4
464	4.74	0.88	6.99	0.60	2.17	1.02	3.98	13.72	10.99	2185	1640	3093	2
465	3.02	1.23	5.67	0.66	4.01	1.47	4.99	17.36	11.50	1037	1644	1433	3

3.13 References

Barnes, H. H. (1967). Roughness characteristics of natural channels. *U.S. Geological Survey Water-Supply Paper*. doi:10.1016/0022-1694(69)90113-9

Bjerklie, D. M., Lawrence Dingman, S., Vorosmarty, C. J., Bolster, C. H., and Congalton, R. G. (2003). Evaluating the potential for measuring river discharge from space. *Journal of Hydrology*, *278*(1-4), 17–38. doi:10.1016/S0022-1694(03)00129-X

Bjerklie, D. M., Moller, D., Smith, L. C., and Dingman, S. L. (2005). Estimating discharge in rivers using remotely sensed hydraulic information. *Journal of Hydrology*, *309*(1-4), 191–209. doi:10.1016/j.jhydrol.2004.11.022

Box, J. E., Bromwich, D. H., Veenhuis, B. A., Bai, L.-S., Stroeve, J. C., Rogers, J. C., Steffen, K., Haran, T., and Wang, S.-H. (2006). Greenland Ice Sheet surface mass balance variability (1988 – 2004) from calibrated Polar MM5 output. *Journal of Climate*, *19*, 2783–2800. doi:10.1175/JCLI3738.1

Chu, V. W. (2014). Greenland ice sheet hydrology: A review. *Progress in Physical Geography*, *38*(1), 19–54. doi:10.1177/0309133313507075

Colgan, W., Steffen, K., McLamb, W. S., Abdalati, W., Rajaram, H., Motyka, R. J., Phillips, T., and Anderson, R. S. (2011). An increase in crevasse extent, West Greenland: Hydrologic implications. *Geophysical Research Letters*, *38*(18), 1–7. doi:10.1029/2011GL048491

Durand, M., Neal, J., Rodríguez, E., Andreadis, K. M., Smith, L. C., and Yoon, Y. (2014). Estimating reach-averaged discharge for the River Severn from measurements of river water surface elevation and slope. *Journal of Hydrology*, *511*, 92–104. doi:10.1016/j.jhydrol.2013.12.050

Fettweis, X. (2007). Reconstruction of the 1979 – 2006 Greenland ice sheet surface mass balance using the regional climate model MAR. *The Cryosphere*, *1*, 21–40.

Fettweis, X., Franco, B., Tedesco, M., van Angelen, J. H., Lenaerts, J. T. M., van den Broeke, M. R., and Gallée, H. (2013). Estimating the Greenland ice sheet surface mass balance contribution to future sea level rise using the regional atmospheric climate model MAR. *The Cryosphere*, *7*(2), 469–489. doi:10.5194/tc-7-469-2013

Gleason, C. J. and Smith, L. C. (2014). Toward global mapping of river discharge using satellite images and at-many-stations hydraulic geometry. *Proceedings of the National Academy of Sciences of the United States of America*, 1–4. doi:10.1073/pnas.1317606111

Hicks, D. M. and Mason, P. D. (1991). Roughness characteristics of New Zealand Rivers: A handbook for assigning hydraulic roughness coefficients to river reaches by the “visual comparison” approach. *Water Resources Survey*.

Hoffman, M. and Price, S. (2014). Feedbacks between coupled subglacial hydrology and glacier dynamics. *Journal of Geophysical Research: Earth Surface*, 414–436. doi:10.1002/2013JF002943.Received

Holland, M. M., Finnis, J., Barrett, A. P., and Serreze, M. C. (2007). Projected changes in Arctic Ocean freshwater budgets. *Journal of Geophysical Research*, *112*(G4), G04S55. doi:10.1029/2006JG000354

Howat, I. M., Negrete, a., and Smith, B. E. (2014). The Greenland Ice Mapping Project (GIMP) land classification and surface elevation data sets. *The Cryosphere*, *8*(4), 1509–1518. doi:10.5194/tc-8-1509-2014

Kattsov, V. M., Walsh, J. E., Chapman, W. L., Govorkova, V. a., Pavlova, T. V., and Zhang, X. (2007). Simulation and Projection of Arctic Freshwater Budget Components by the IPCC AR4 Global Climate Models. *Journal of Hydrometeorology*, *8*(3), 571–589. doi:10.1175/JHM575.1

Lampkin, D. J. and VanderBerg, J. (2013). Supraglacial melt channel networks in the Jakobshavn Isbræ region during the 2007 melt season. *Hydrological Processes*. doi:10.1002/hyp.10085

LeFavour, G. and Alsdorf, D. (2005). Water slope and discharge in the Amazon River estimated using the shuttle radar topography mission digital elevation model. *Geophysical Research Letters*, *32*(17), L17404. doi:10.1029/2005GL023836

Legleiter, C. J., Tedesco, M., Smith, L. C., Behar, a. E., and Overstreet, B. T. (2014). Mapping the bathymetry of supraglacial lakes and streams on the Greenland ice sheet using field measurements and high-resolution satellite images. *The Cryosphere*, *8*(1), 215–228. doi:10.5194/tc-8-215-2014

Manning, R. (1891). On the flow of water in open channels and pipes. *Transactions, Institution of Civil Engineers of Ireland*, *20*, 161–207.

McClelland, J. W., Déry, S. J., Peterson, B. J., Holmes, R. M., and Wood, E. F. (2006). A pan-arctic evaluation of changes in river discharge during the latter half of the 20th century. *Geophysical Research Letters*, *33*(L06715), 1–4. doi:10.1029/2006GL025753

McGrath, D., Colgan, W., Steffen, K., Lauffenburger, P., and Balog, J. (2011). Assessing the summer water budget of a moulin basin in the Sermeq Avannarleq ablation region, Greenland ice sheet. *Journal of Glaciology*, *57*(205), 954–964. doi:10.3189/002214311798043735

Noh, M. and Howat, I. M. (2015). Automated stereo-photogrammetric DEM generation at high latitudes: Surface Extraction from TIN-Based Search Minimization (SETSM) validation and demonstration over glaciated regions. *GIScience & Remote Sensing*, *52*(2), 198–217. doi:10.1080/15481603.2015.1008621

Pavelsky, T. M. and Smith, L. C. (2008). RivWidth: A Software Tool for the Calculation of River Widths From Remotely Sensed Imagery. *IEEE Geoscience and Remote Sensing Letters*, *5*(1), 70–73. doi:10.1109/LGRS.2007.908305

Peterson, B. J., Holmes, R. M., McClelland, J. W., Vörösmarty, C. J., Lammers, R. B., Shiklomanov, A. I., Shiklomanov, I. a, and Rahmstorf, S. (2002). Increasing river discharge to the Arctic Ocean. *Science*, *298,* 2171–3. doi:10.1126/science.1077445

Rawlins, M. a., Steele, M., Holland, M. M., Adam, J. C., Cherry, J. E., Francis, J. a., Groisman, P. Y., Hinzman, L. D., Huntington, T. G., Kane, D. L., Kimball, J. S., Kwok, R., Lammers, R. B., Lee, C. M., Lettenmaier, D. P., McDonald, K. C., Podest, E., … Zhang, T. (2010). Analysis of the Arctic System for Freshwater Cycle Intensification: Observations and Expectations. *Journal of Climate*, *23*(21), 5715–5737. doi:10.1175/2010JCLI3421.1

Rennermalm, A. K., Moustafa, S. E., Mioduszewski, J., Chu, V. W., Fortner, S. K., Hagedorn, B., Harper, J. T., Mote, T. L., Robinson, D. A., Shuman, C. A., Smith, L. C., and Tedesco, M. (2013). Understanding Greenland ice sheet hydrology using an integrated multi-scale approach. *Environmental Research Letters*, *8*(1), 1–14. doi:10.1088/1748-9326/8/1/015017

Shannon, S. R., Payne, A. J., Bartholomew, I. D., Broeke, M. R. Van Den, Edwards, T. L., Sole, A. J., Wal, R. S. W. Van De, and Zwinger, T. (2013). Enhanced basal lubrication and the contribution of the Greenland ice sheet to future sea-level rise. *Proceedings of the National Academy of Sciences of the United States of America*, *110*(35), 14156–14161.

Smith, L. C., Chu, V. W., Yang, K., Gleason, C. J., Pitcher, L. H., and Rennermalm, A. K. (2015). Efficient meltwater drainage through supraglacial streams and rivers on the southwest Greenland ice sheet. *Proceedings of the National Academy of Sciences*, *112*(4), 1001–1006. doi:10.1073/pnas.1413024112

Smith, L. C., Isacks, B. L., Bloom, A. L., and Murray, A. B. (1996). Estimation of discharge from three braided rivers using synthetic aperture radar satellite imagery: Potential application to ungaged basins. *Water Resources Research*, *32*(7), 2021–2034.

Smith, L. C. and Pavelsky, T. M. (2008). Estimation of river discharge, propagation speed, and hydraulic geometry from space: Lena River, Siberia. *Water Resources Research*, *44*(3), 1–11. doi:10.1029/2007WR006133

Strahler, A. N. (1957). Quantitative analysis of watershed geomorphology. *Transactions, American Geophysical Union*, *38*(6), 913–920.

Tarpanelli, A., Barbetta, S., Brocca, L., and Moramarco, T. (2013). River discharge estimation by using altimetry data and simplified flood routing modeling. *Remote Sensing*, *5*, 4145–4162. doi:10.3390/rs5094145

Tarpanelli, A., Brocca, L., Lacava, T., Faruolo, M., Melone, F., Moramarco, T., Pergola, N., and Tramutoli, V. (2011). River discharge estimation through MODIS data. *Proceedings of SPIE - The International Society for Optical Engineering*, *8174*, 817408. doi:10.1117/12.898201

Taylor, J. R. (1997). *An Introduction to Error Analysis: The Study of Uncertainties in Physical Measurements* (2nd ed.). Sausalito, CA: University Science Books.

Tedesco, M., Fettweis, X., Mote, T. L., Wahr, J., Alexander, P., Box, J. E., and Wouters, B. (2013). Evidence and analysis of 2012 Greenland records from spaceborne observations, a regional climate model and reanalysis data. *The Cryosphere*, *7*(2), 615–630. doi:10.5194/tc-7-615-2013

Updike, T. and Comp, C. (2010). *Radiometric Use of WorldView-2 Imagery Technical Note*.

van Angelen, J. H., Lenaerts, J. T. M., van den Broeke, M. R., Fettweis, X., and van Meijgaard, E. (2013). Rapid loss of firn pore space accelerates 21st century Greenland mass loss. *Geophysical Research Letters*, *40*, 2109–2113. doi:10.1002/grl.50490

Vizcaíno, M., Lipscomb, W. H., Sacks, W. J., and van den Broeke, M. (2014). Greenland Surface Mass Balance as Simulated by the Community Earth System Model. Part II: Twenty-First-Century Changes. *Journal of Climate*, *27*(1), 215–226. doi:10.1175/JCLI-D-12-00588.1

Yang, K. and Smith, L. C. (2013). Supraglacial streams on the Greenland Ice Sheet delineated from combined spectral – shape information in high-resolution satellite imagery. *IEEE Geoscience and Remote Sensing Letters*, *10*(4), 801–805.

Chapter 4

Assessing Southwestern Greenland Ice Sheet Moulin Distribution and Formation from High-Resolution WorldView-1/2 Remote Sensing

4.1 Abstract

River moulins represent connections between surface meltwater generated on the Greenland ice sheet and subglacial drainage networks, where increased meltwater can enhance ice sliding dynamics. A new high-resolution moulin map for a 12,534 km^2 area of southwest Greenland near Russell Glacier created from WorldView-1/2 imagery acquired during the 2012 record melt year is used to assess physical controls on moulin location. A total of 1236 moulins are mapped up to 1787 m elevation, with 43% found in crevasse fields, 17% found along a single ice fracture, 25% found within drained lake basins, and 14 % with no formation mechanism visible from high-resolution satellite imagery. Approximately 40% of the mapped moulins are located in crevasse fields below 1300 m elevation and less than 1000 m ice thickness. However, 11% of moulins are found above 1600 m elevation, which is higher than any previously mapped moulin and where glaciological theory suggests few moulins should form. These high-elevation stream/river moulins are found predominately in drained lake basins (65%) and along single fractures (30%). Our study observes moulins forming in both extensional and compressional ice flow regimes (with only 28% of moulins found in areas of high extensional strain rate >0.005 yr-1), showing that strain rates are not a strong indicator of the likelihood for moulin formation. A multiple regression shows that moulin density increases with higher bed elevation, thinner ice, lower surface slope, higher velocity, and higher strain rate. In sum, moulins are most common in crevassed, thinner ice near the ice sheet edge, but non trivial quantities also develop at high elevations, indicating

that future inland expansion of melting may create hydrologic connections between the surface and the bed in higher elevations than previously thought.

4.2 Introduction

Current projections of global sea level rise are primarily based on surface mass balance, and do not account for enhanced ice motion from surface meltwater entering the ice-bedrock interface on the Greenland ice sheet. GPS and radar remote sensing observations have shown short-term ice flow speedups following increased meltwater production in both slow-moving portions of the ice sheet (Bartholomew et al., 2010; Palmer et al., 2011; Doyle et al., 2013) and fast-moving outlet glaciers (Joughin, et al., 2008a; Shepherd et al., 2009; Andersen et al., 2011). In particular, supraglacial lake drainage events have been observed to cause local uplift and ice speedup (Das et al., 2008; Tedesco, et al., 2013a), owing to surface melt-induced basal lubrication (Zwally et al., 2002). This basal lubrication mechanism is a spatially and temporally varying process, with the subglacial drainage system becoming increasingly efficient as hydraulic connections between the ice surface and bedrock are established further inland over the melt season (Bartholomew et al., 2011). While lake drainages are important for transient uplift, supraglacial stream/river moulins dominate total meltwater flux (Smith et al., 2015). The hydraulic connections between the supraglacial and subglacial systems are dominated by river moulins, vertical conduits that divert large quantities of surface meltwater streams and rivers into the ice sheet.

Moulins are formed when water-filled fractures propagate down through the ice sheet. Fractures open and close due to the stress and strain of glacier movement, and larger moulin conduits can form where surface water is concentrated into point sources of high water flux flowing into a fracture (Fountain et al., 2005; van der Veen, 2007). Hydrofracturing therefore requires a water-filled crack, where the local tensile stress at the crack tip exceeds the fracture toughness of the surrounding ice, forcing the crack downward, and propagation can continue with the density of the water offsetting the overburden stress (Alley et al., 2005; Krawczynski et al., 2009; Lampkin et al., 2013). Both supraglacial rivers and lakes can provide the water supply necessary for a moulin to form. Moulins are typically classified as within a drained lake basin (formed during a drainage event) or outside of a lake basin where overflow streams and rivers intersect existing cracks (Lampkin & VanderBerg, 2013; Poinar et al., 2015). A study comparing the ice dynamic effects of both types of moulins show that a lake rapidly draining into a moulin that formed at the bottom of a lake during the event resulted in twice the speedup and uplift of a lake slowly draining into another moulin via a stream (Tedesco, et al., 2013a).

While most attention has been paid to rapid supraglacial lake drainages and associated ice dynamic effects (Das et al., 2008; Selmes et al., 2011; Doyle et al., 2013; Johansson et al., 2013), once lakes have drained, river networks occupy the basin so that all moulins act as termination points for river networks (Smith et al., 2015). Furthermore, most moulins are formed by supraglacial streams and rivers, not lakes (Smith et al., 2015). Unlike abrupt lake drainages, river moulins inject a seasonally and diurnally controlled influx of meltwater into the ice sheet. The subglacial system also responds differently to fast local drainage through moulins compared to slower distributed drainage through crevasses (McGrath et al., 2011).

Previous mapping studies of moulin locations have either focused on small geographic areas using field observations and/or high-resolution aerial/satellite imagery, or on larger areas using medium-resolution satellite imagery. Catania et al. (2008) mapped moulin locations using ice-penetrating radar surveys and modeled along-flow tensile stress, finding an area of elevated tensile stress (~100 kPa) and thinner ice moving over a bedrock ridge that is coincident with moulin observations. Phillips et al. (2011) attempted to model moulin locations based on the relationship between moulin presence and topographical characteristics such as elevation, slope, and aspect, but did not incorporate information on physical processes controlling crevasse formation. One study also finds that modelled timing and location of delivery of meltwater to the bed through moulins match well with observed temporal and spatial patterns of ice surface speed-ups (Clason et al., 2014). Other studies have produced principal strain rate datasets to identify positive (i.e., extensional) strain rate regimes (Lampkin et al., 2013) and suggest a threshold for crevasse formation (0.005 yr^{-1}, Poinar et al., 2015; Joughin et al., 2013) and thus potential moulin formation. Poinar et al. (2015) showed that lower ice surface elevations are more susceptible to crevassing (e.g., at 1100-1200 m elevation 17% of the surface area is susceptible to fracture formation), and propose that ~1600 m elevation is the upper limit for likely crevasse and moulin formation. Altogether moulin studies suggest melt production, ice thickness, strain rate, ice velocity, surface elevation, and bedrock elevation should be influential factors that contribute to moulin distribution. However, this is difficult to test empirically, without explicit mapping of observed moulin locations. Absence of such mapping capacity also preclude direct modelling of hydraulic connections between surface meltwater production and subglacial drainage systems.

In this paper, we expand on the remotely sensed river moulin dataset of Smith et al. (2015), to produce a geographically extensive, high-resolution moulin map in the southwestern Greenland ablation zone. For a 12,534 km^2 area, all active moulins terminating supraglacial meltwater streams and rivers are mapped from panchromatic and multispectral WorldView-1/2 imagery acquired between July 10 and August 12, 2012. Because this mapping period captures a 2012 record melt event (Nghiem et al., 2012; Tedesco et al., 2013b), the resultant moulin dataset may therefore be considered an end-member snapshot of an unusually active period for surface meltwater transport, and possibly an analogue of future years if Greenland meltwater production continues to increase (Fettweis et al., 2013;

Vizcaíno et al., 2014). Moulins are classified by visible formation mechanism including crevasse fields, single fractures, and drained lakes, and moulin distribution in each class is examined with geophysical datasets such as surface elevation, bed elevation, ice thickness, ice velocity, and strain rate. The new dataset thus allows study of moulin distribution, and testing whether strain rate can be used to represent the physical processes controlling moulin formation.

4.3 Study area

The study area is located near the town of Kangerlussuaq, southwest Greenland, extending 135 km inland (up to 1870 m elevation) and spanning 66°30’-67°30’N latitude (115 km) of the ice sheet ablation zone (Figure 4-1). Southwest Greenland is dominated by melting and runoff, rather than ice discharge, and contains the highest proportion of land-terminating glaciers in Greenland. While ice dynamic changes have been more associated with fast-moving marine-terminating glaciers, land-terminating glaciers have also experienced speedups as high as 50% because of meltwater-induced sliding enhancement (Joughin et al., 2008b). This region is also characterized by a well-developed supraglacial hydrologic network of rivers and lakes, including the majority of rapidly-draining lakes associated with moulins (Selmes et al., 2011), and therefore is a prime area for studying supraglacial meltwater transfer to the ice sheet bed.

This dataset captures the record melt event on 11-13 July 2012, where 97% of the ice sheet experienced some degree of melting (Nghiem et al., 2012; Tedesco et al., 2013b). The equilibrium line altitude (ELA) separating the accumulation zone from the ablation zone reached 2687 m a.s.l. in the study area in 2012 compared to a mean ELA of 1553 m a.s.l. over 1990-2011 (van de Wal et al., 2012; Box et al., 2013). This expanded ablation zone in 2012 increases the area where hydrologic connections can be made between the surface and the bed, and provides an opportunity for exploring how and where these connections occur via river moulins.

4.4 Geophysical datasets

4.4.1 Optical satellite imagery

High-resolution WorldView-1 (WV1) and WorldView-2 (WV2) satellite images were obtained from DigitalGlobe through the University of Minnesota's Polar Geospatial Center (PGC) between 10 July and 17 August 2012 (Figure 4-1). WV1 provides a panchromatic visible band with 0.5 m spatial resolution, and WV2 provides 8 bands in the visible to near-infrared with 2.0 m resolution as well as a panchromatic band (0.5 m resolution). Images were orthorectified using the Greenland Ice Mapping Project (GIMP) DEM (Howat et al., 2014) and projected to a polar stereographic coordinate system using code from the PGC. Thirty-two WV2 images comprised the main dataset from July 18, 21, and 23 covering 1000-1600 m elevation (5,328 km^2), where moulins were extracted as river termination points using a semi-automated algorithm (Yang & Smith, 2013; Smith et al., 2015). Seventy-four WV1 images were used to complete the study area, using manual methods, at lower (100-1000 m) and higher (1600-1870 m) elevations not covered by WV2, thus increasing the total WV1/WV2 mapped areas from 5,328 km^2 to 11,909 km^2 addition.

Multispectral Advanced Spaceborne Thermal Emission and Reflection Radiometer (ASTER) images acquired on 16 July and 19 August 2012 (downloaded from the NASA Land Processes Distributed Active Archive Center, USGS/Earth Resources Observation and Science Center) were used to fill a narrow gap (625 km^2) between the WV1/2 swaths (Figure 4-1), yielding a final, total mapping area of 12,534 km^2.

4.4.2 Digital elevation models

The Greenland Ice Mapping Project (GIMP) 30 m resolution digital elevation model (DEM) was used for ice sheet surface topography (Howat et al., 2014) and for calculating surface slope. While a more widely used DEM for the Greenland ice sheet is a 1 km dataset created from a combination of radar altimeter and stereo-photogrammetric data (Bamber et al., 2001), its lower spatial resolution was deemed too poor to capture steep margins and high-relief periphery. The GIMP DEM enhances the resolution and accuracy of that DEM by integrating photogrammetric topography data and registering the DEM to elevations acquired by the Geoscience Laser Altimeer System (GLAS) on the Ice, Cloud, and land Elevation Satellite (ICESat).

BedMachine Greenland is a new 150 m resolution ice thickness and bed topography dataset created using a novel mass conservation approach (Morlighem et al., 2011; Morlighem et al., 2014). Ice thickness is traditionally interpolated from airborne radar sounding surveys using geostatistical techniques such as kriging, but the resulting product tends to be inconsistent with ice flow dynamics. BedMachine Greenland instead combines ice thickness data from airborne radar surveys with high-resolution satellite mapping of ice velocity from synthetic-aperture interferometry to produce and ice thickness map that conserves mass. Bed topography, also provided by BedMachine Greenland, is then created by subtracting the ice thickness from the GIMP DEM resampled to 150 m resolution, and was used to calculate bed slope.

4.4.3 Ice velocity and strain rate

Ice velocity products for the winters of 2000-2001, 2005-2006, 2006-2007, and 2007-2008 gridded at 500 m resolution were acquired from the NASA Making Earth System Data Records for Use in Research Environments (MEaSUREs) program (Joughin et al., 2010). The speed magnitude from each image was averaged to provide a 2000-2008 average velocity dataset.

Principal strain rates provided by Poinar et al. (2015) were produced from RADARSAT-derived velocity data representing an average over 2007-2010. The data are provided at a 250 m resolution, with positive values indicating extension and negative values indication compression. Poinar et al. (2015) note that these strain rates are calculated from wintertime velocities, which are lower than summertime velocities, and can underestimate strain rates (extensional strain rates reach their maximum in the summer).

4.5 Methods

4.5.1 Moulin location dataset

4.5.1.1 Moulin classification

To aid in the classification of moulins formed by lake drainages, drained lake basin scars visible in WV1 imagery were manually identified and digitized, also at a 1:20,000 scale (Figure 4-2c). Within the WV1 swath gap, lakes were clearly visible in ASTER imagery so the same method was applied there. The much larger size of supraglacial lakes compared to streams/rivers lends confidence to the completeness of the drained lakes identified in ASTER data.

Moulins were defined as visible sinkholes terminating actively flowing supraglacial rivers (Yang & Smith, 2013; Smith et al., 2015) as here detected in WV1/WV2/ASTER satellite imagery. Inactive moulins, typically found downstream of active ones, were not inventoried in this study. Moulins were mapped semi-automatically (WV2 imagery) and manually (WV1 imagery and ASTER). A semi-automatic algorithm for extracting supraglacial river networks requiring multispectral WV2 imagery produced river network termination points that were manually verified as moulins using the panchromatic WV2 imagery (Yang & Smith, 2013; Smith et al., 2015). This semi-automatic method maps only larger continuous meltwater channels ("rivers") with widths > 2 m because of the use of 2 m resolution imagery, and misses smaller meltwater channels ("streams") that appear discontinuous.

In the WV1 mapping area (Figure 4-1) moulin locations were digitized manually as follows. A scale of 1:15,000 was use to systematically identify and record stream/river termination points as moulins. This method does notably identify moulins from rivers that are smaller and narrower than the ones mapped using the semi-automated method. To prevent bias between the WV1 and WV2 mapped areas, a manual pass was taken over the WV2 area at a 1:15,000 scale to identify moulins from rivers seen in 0.5 m resolution imagery but missed by the automated 2 m resolution extraction.

Next, moulin formation mechanism was classified by visual inspection within a 500 m radius of each mapped moulin. This was performed visually at 1:2,000 scale with each moulin assigned to one of four categories: "crevasse field" (characterized by parallel crevassing patterns and/or numerous fractures visible on the ice surface; Figure 4-2a); "fracture" (a single fracture intersecting the supraglacial stream/river to create a moulin, Figure 4-2b); "drained lake" (located within a lake basin scar, Figure 4-2c); and "undetermined" (no observable mechanism for moulin formation, Figure 4-2d). This follows the same attribution method as the Smith et al. (2015) study.

In the ASTER images, moulins were identified by following streams/rivers originating in adjacent, higher resolution WV1 imagery and terminating in the lower resolution ASTER imagery. Due to the coarser 15 m resolution of ASTER, moulin formation mechanism was classified as 'undetermined' unless it was within a drained lake basin scar.

While ASTER imagery were available for much higher elevations, only moulins connected to streams identified in high-resolution WV1 imagery were considered for confirming active moulins draining supraglacial streams.

The final moulin dataset is a shapefile containing the following attributes (see Appendix): visible moulin formation type, surface elevation (m), bed elevation (m), ice thickness (m), surface slope (degrees), bed slope (degrees), ice velocity (m/yr), and principal surface strain rate (yr-1).

4.5.2 Moulin density

The moulin location dataset was interpolated to a 500 m grid to produce a moulin density dataset as follows. First, the Kernel Density function in ArcGIS 10.2 was used with inputs of moulin locations to create a moulin density grid, using a circular search radius of 4000 m and quadratic distance weighting. This produces a gridded surface based on a quadratic formula with the highest value at the point location and tapering to zero at the search radius distance. The resulting moulin density grid (number of moulins / km^2) represents the likelihood of moulin occurrence for each pixel over the entire study area. To sample between geophysical datasets at varying resolutions, this grid was converted to a point dataset, with one point at every 500 m pixel, and the geophysical datasets were attributed to each point using nearest neighbour resampling. To distinguish this derivative product from the "moulin location" dataset (1,236 points), it is referred to as the "moulin density" dataset (50,132 points), containing the same attributes of surface elevation, bed elevation, ice thickness, surface slope, bed slope, ice velocity, principal strain rate, as well as moulin density.

4.5.3 Moulin distribution analysis

To test whether the distribution of moulin location attributes is different from the distribution of background attributes within the study area, a Wilcoxon-Rank Sum test was performed. This non-parametric test determines whether two samples come from the same population, and is a useful alternative to the Student's-t test when data appear to arise from non-normal distributions.

The moulin density point dataset was used to run an ordinary least squares multiple regression, with moulin density as the dependent variable. Candidate independent variables were bed elevation, ice thickness, surface slope, bed slope, ice velocity, and principal strain rate. Before running a multiple regression, the possibility of multicollinearity (high correlations between independent variables in a linear regression) between independent variables of surface elevation, bed elevation, ice thickness, surface slope, bed slope, ice velocity, and principal strain rate was tested by examining a correlation matrix (Table 4-1). For any variable pair having a correlation higher than 0.8, one of those variables was removed at a time and tested in an exploratory regression. Table 4-1 shows that surface elevation and ice thickness are highly correlated, indicating a redundancy between the two variables.

An exploratory regression was performed on the moulin density dataset to find properly specified ordinary least squares linear regression model. Exploratory regression is a form of stepwise multiple regression, which finds the best combination of predictor variables by adding independent variables to the regression equation one at a time until none of the possible additions can significantly improve the R2. All variables were standardized by subtracting the mean and dividing by the standard deviation before running the regression. The best combination of independent variables was determined by the R2, and used to run the multiple regression model. Of the two correlated independent variables, surface elevation and ice thickness, inclusion of ice thickness in the exploratory regression generated a better fit model, so surface elevation was removed from the final multiple regression model.

4.6 Results

4.6.1 Moulin location and moulin density datasets

A new comprehensive dataset of 1,236 actively flowing moulins visible in the summer of 2012 within a 12,534 km^2 area was created from high-resolution WorldView-1/2 imagery, together with attribution of visible formation mechanisms. Of these 1,236 moulins, 535 (43%) were found in crevasse fields, 215 (17%) were found where a supraglacial stream/river intersects an isolated fracture, 294 (24%) were found inside drained lake basins, and 192 (16%) had an undetermined formation mechanism (Table 4-2, Figure 4-3a). The 625 km^2 gap in WV1/2 imagery was bridged by 15 m resolution ASTER imagery within the same time period and yielded 8 moulins. Four of these were located within three drained lake basins, and four were assigned an undetermined formation mechanism. Moulins are located primarily in crevasse fields below 1250 m elevation, and within drained lake basins above 1400 m elevation. 141 moulins (11%) were found in high elevations greater than 1600 m, and these moulins are almost exclusively due to lake drainages (87 moulins) and single fractures (40 moulins) rather than crevasse fields.

A moulin density grid at a 500 m resolution created from moulin point locations shows hotspots of moulin locations below 1200 m elevation to the north and the south of the major land-terminating outlet glaciers in the region (Figure 4-3b). The northwest hotspot is situated near at the edge of the ice sheet, where the ice is thin with a very high bed elevation, though this region is dominated by low ice velocity and negative strain rates indicating ice compression (Figure 4-4).

4.6.2 Drained lakes

While 83 out of 91 total lakes (91%) contain at least one active moulin, only 25% of all moulins were found within drained lake basins (Figure 4-3a). The drained lake basins comprised a total area of 280 km^2 (representing 2% of the study area), and are found between 1053 m and 1791 m elevation. On average, lakes contained 3.4 moulins per basin, with two basins notably containing 11 and 14 moulins at 1713 m and 1600 m elevation, respectively. Of particular note is the one at 1713 m elevation, the highest lake mapped that shows a typical configuration: multiple river networks converging in a radial pattern into the lake basin depression, and moulins forming right at the edge of the drained lake scar. However, the majority of mapped moulins (75%) were found outside of drained lake basins.

4.6.3 Statistical significance

Results from the Wilcoxon-Rank Sum test shows that moulin locations have a significantly different mean than the overall distribution of each geophysical variable ($p<0.001$). Moulins form in areas of thinner ice, higher velocity and extensional strain rate, as well as lower surface elevation and slope, and higher bed elevation and slope. For example, Figure 4-5 shows background strain rates with a mean of -0.0001 and moulin location strain rates with a mean of 0.001, a significantly ($p<0.001$) higher positive strain rate indicating moulins form in areas of compression. However, 69 % of moulins form in areas of extension, and using a typical strain rate threshold of extension necessary for crevasse formation and therefore moulin formation (0.005 yr^{-1}, Joughin et al., 2013; Poinar et al., 2015), only 8% of mapped moulins should have formed. Thus, far more moulins are observed on the ice surface than would be predicted from the use of strain rate thresholds alone.

4.6.4 Influence of geophysical variables on moulin distribution

The distribution and classification of moulins is presented in two ways (Figure 4-6). The first column (Figure 4-6a) presents the frequency of moulins within bins of selected geophysical variables, and the second column (Figure 4-6b) presents the frequency of moulins normalized by the area covered in each bin, the moulin density (moulins / km^2). These moulin density histograms differ from the moulin density grid in Figure 4-3b, which calculates density based on a standard circular search radius; these results show moulins normalized differently according to each geophysical variable and are useful for identifying how geophysical variables control moulin distribution. The raw frequency of moulin location binned by elevation shows a large number forming above 1000 m elevation (Figure 4-6a), but moulin density is higher below 1000 m after normalizing by the total surface area within each elevation bin (Figure 4-6b). Moulin frequency with bed elevation shows a fairly normal distribution (Figure 4-6c), moulin density normalized by the area within each elevation bin shows that moulins located in crevasse fields occupy lower and higher bed elevations, and moulins located in drained lake basins preferring bed elevations in between.

Table 4-2 summarizes moulin distributions for the four different visible moulin attribution types. Moulins located in crevasse fields are most frequent (n=535) and on average show the highest moulin density (0.2 km^{-2}), lowest surface elevation (967 m), highest bed elevation (412 m), lowest ice thickness (555 m), highest surface slope (1.05 degrees), and highest bed slope (4.26 degrees). The second most frequent type of moulin are those located in drained lake basins (n=307), and in contrast with those found in crevasse fields, these moulins show the highest surface elevation (1532 m), lowest bed elevation (270 m), highest ice thickness (1254 m), lowest surface slope (0.40 degrees), and lowest bed slope (2.43 degrees). The third most frequent type of moulin is occurs along isolated cracks or fractures (n=212), and on average show relatively higher surface elevation (1417 m), lower bed elevation (287 m), higher ice thickness (1127 m), lower surface slope (0.51 degrees), and lower bed slope (2.58 degrees).

4.6.5 Moulin density correlation with bed elevation, ice thickness, surface slope, velocity, and strain rate

Application of ordinary least squares regression to the moulin density point dataset indicates that five out of the six independent variables are significant ($p<0.001$) predictors of moulin density variability (Table 4-3). These five significant variables are bed elevation, velocity, and strain rate (positively correlated, with higher values associated with greater abundance and/or density of observed moulins); ice thickness, and surface slope (negatively correlated), with bed slope not significant ($p=0.135$). A total of 50,132 observations were used in the regression model, yielding an adjusted R2 of 0.36 and a statistically significant overall model as given by the F-statistic ($p<0.001$). With surface elevation not included in the regression model due to multicollinearity, all remaining Variable Inflation Factors (VIFs) are between 1.00 and 2.53, indicating that the standard errors of the predictor variables are 1-2.5 times as large as they would be if the variable were uncorrelated with the other predictor variables (large VIF values > 7.5 indicate redundancy among explanatory variables).

The regression coefficients show that moulin density increases with higher bed elevation, thinner ice, lower surface slope, higher velocity, and higher strain rate. Due to the input variables being standardized, these regression coefficients indicate how a change in each variable would result in a change in moulin density in units of standard deviation. For example, ice thickness shows the highest coefficient, indicating that a 0.489 standard deviation decrease in thickness would increase moulin density by one standard deviation. Notably different from results in Section 5.3 is the bed slope parameter, which shows moulin density increasing with lower bed slopes, but the parameter is not significant and should not be used as a predictor variable in this regression model.

4.7 Discussion and conclusion

This study presents the most comprehensive high-resolution moulin dataset in southwestern Greenland, mapping 1,236 moulins up to 1788 m elevation between 10 July and 17 August 2012, a record melt year. Of these observed, actively flowing stream/river moulins, 133 (11%) were found above 1600 m elevation, higher than any previously mapped moulins and where very few moulins are expected to form (Poinar et al., 2015). While satellite imagery within the study area are only available up to 1872 m elevation, there is a distinct decrease in the distribution of moulins above 1700 m elevation, and ASTER imagery available in elevations higher than the study area (Figure 4-1) also indicate a lack of moulins and instead show long river networks terminating at lower elevations, a finding consistent with Poinar et al. (2015).

The largest group of moulins by formation type is located in crevasse fields (43%), and primarily below 1250 m elevation, where the subglacial hydrologic environment is expected to be dominated by a largely arborescent network of channels that are effective at accommodating large meltwater fluxes from moulins (Lampkin & VanderBerg, 2013). The second largest group of moulins is located within drained lake basins (24%), primarily above 1400 m elevation, where the subglacial network may take on more of a distributed drainage pattern of linked cavities, causing glacier speedup when meltwater input exceeds the hydraulic capacity at the beginning of the season (Sundal et al., 2011; Bartholomew et al., 2012). Subglacial water pressure and ice velocity are thought to remain elevated until the switch from distributed to channelized drainage in these regions where the drainage system is closed by ice deformation over winter (Cowton et al., 2013). This evolution from distributed to channelized drainage occurs later in the season and more slowly for inland areas, and regions with surface elevation above ~1200 m (or ice thicker than 1 km) are expected to be beyond the upper limit of efficient drainage (Chandler et al., 2013). Therefore, high elevation moulins (54% > 1200 m elevation, 11% >1600 m elevation) are exceedingly important to melt-induced speedup.

High moulin density hotspots are found near the ice margin outside of the faster moving outlet glaciers that have deep bedrock trenches (Figure 4-4b), features expected to efficiently route subglacial meltwater to the ice margin (Bamber et al., 2013). This indicates that moulins forming outside of these deep trenches are less likely to have existing well-developed subglacial networks to efficiently channel meltwater, and may have a greater impact on ice dynamic changes.

Of the geophysical datasets analyzed here, ice thickness has the greatest influence on moulin density and distribution, with the strongest significant coefficient in the multiple regression model (Figure 4-6f, Table 4-3). This is broadly consistent with the findings of Catania et al. (2008), who observe an increased frequency of moulins in regions with ice thickness less than ~800 m. While this study shows a smoothly decreasing moulin density of values in each ice thickness bin, there is a distinct transition from moulins formed in crevasse fields below 800 m ice thickness, and an overall decrease in moulin density below 950 m elevation (Figure 4-6f). However, moulins formed from lake drainages are found in ice thicknesses greater than 950 m. This indicates these two moulin formation types occupy different regions of the ice sheet, with crevasse moulins typical of thinner ice near the margin, and drained lake moulins hydraulically connecting thicker ice areas further inland of the ice sheet.

Principal surface strain rate, which is often cited as an important control on crevasse and moulin formation (Lampkin et al., 2013; Joughin et al., 2013; Poinar et al., 2015), appears to be less important for moulin formation than ice thickness. While moulin locations do show a significantly higher distribution in higher strain rates than the rest of the study area (Figure 4-5), they are found in both extensional and compressional ice flow regimes (as indicated by positive and negative principal surface strain rates, respectively Figure 4-6j). Indeed, using any type of threshold would exclude a large proportion of moulins: 72% of moulins are located outside of high-strain rate (0.005 yr^{-1}) areas, and 31% of moulins are located in negative strain rate (compression) areas. Similarly, Harper et al. (1998) found crevasses in both positive and negative strain rate areas in an Alaskan glacier, with splaying crevasses found in compressing flow where surface deformation is dominated by shear strain, and transverse crevasses found in extending flow. Doyle et al. (2013) also observed fractures caused by a lake drainage that are evidence of both compressional (reverse dip-slip fault) and extensional (normal fault with a dropped graben) strain regimes. Our study observes moulins forming in both extensional and compressional ice flow regimes, showing that strain rates are not a strong indicator of the likelihood for moulin formation.

In addition to areas of relatively thinner ice, moulins are expected to form at lower elevations where meltwater is more plentiful (Catania et al., 2008). The idea is that a certain amount or rate of meltwater influx into a crevasse is needed to initiate hydrofracturing to form a connection with the bed. While van der Veen (2007) shows that the water-filling rate is the most important factor controlling fracture propagation and moulin formation, an existing fracture must first exist from a high enough tensile stress from ice flow or thermal contraction (Alley et al., 2005). The amount of water flowing through stream/river networks in the southwestern Greenland ablation zone is not tested but mapped distributions of supraglacial river discharge are not as systematic as other geophysical controls like ice thickness. Smith et al. (2015) map moulin discharge in 2012 up to 1644 m elevation and find a wide distribution of discharges at varying elevations. Furthermore, catchment area does not increase lower in elevation; in fact river networks are longer high in elevation as meltwater travels farther before reaching a moulin (Poinar et al., 2015). Therefore, while river discharge as a control of moulin formation needs to be explored to understand whether increases in surface melting will affect moulin formation higher in elevation, the existence of a fracture is still necessary for moulin formation.

Our current ability to study temporal and spatial dynamics of moulin formation and distribution is limited by existing geospatial datasets and techniques for mapping and modeling these features. The small size of these features means that the use of 15-30 m resolution satellite imagery like Landsat (Lampkin & VanderBerg, 2013; Poinar et al., 2015) miss a large number of smaller supraglacial stream/river networks that terminate in moulins on the ice surface. High-resolution panchromatic imagery (WorldView-1) discriminates these fine scale structures well but requires manual digitizing, an arduous task that has previously been applied only to small areas of the ice sheet. In the present study, even those 523 moulins derived using a semi-automated method and multispectral WV2 data, required manual confirmation of stream termination points as moulins.

The time-intensive nature of deriving moulin maps from high-resolution satellite imagery is likely offset by their useful lifetime, which is likely several years or more. Though new moulins are created when new crevasses intersect rivers or during lake drainage events, moulins often persist for multiple years (average ~11 years, Catania and Neumann, 2010), and the river networks feeding moulins are relatively stable year after year (Smith et al., 2015). That said, future work should focus on constraining temporal dynamics of moulin formation, in particular the ability of new moulins to form at higher elevations in years with an expanded ablation zone as occurred in 2012.

In sum, a new high-resolution dataset of moulin location and density for a 12,534 km^2 area of the southwestern Greenland ablation shows that moulins predominately form in crevassed regions in thinner ice, but are also common in higher elevations as well, with locations quite observable in high-resolution satellite imagery but difficult to model from other geophysical datasets, such as surface topography and strain rate. Traditional indicators of fracture formation that can also be derived from remotely sensed imagery, notably as surface strain rates, are limited as predictors of moulin location. Finally, the significant proportion of moulins mapped above 1600 m elevation in the 2012 record melt year indicate that future inland expansion of melting may create hydrologic connections between the surface and the bed at higher elevations than previously expected (Poinar et al., 2015).

4.8 Figures

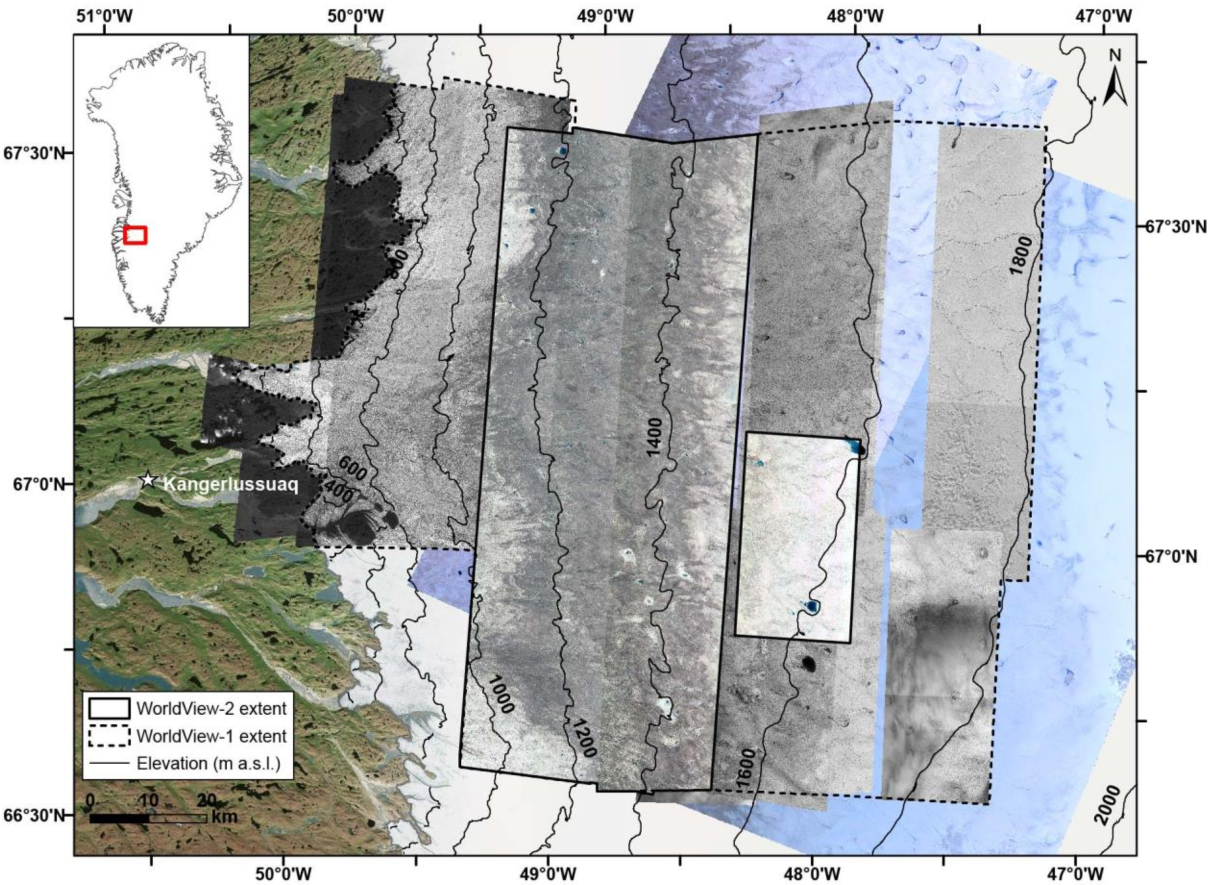

Figure 4-1. The study area is located in the ablation zone of southwest Greenland (inset map). Optical satellite imagery used for mapping moulins are shown over a Google Earth background image, with panchromatic WorldView-1 imagery, multispectral WorldView-2 imagery, and ASTER imagery.

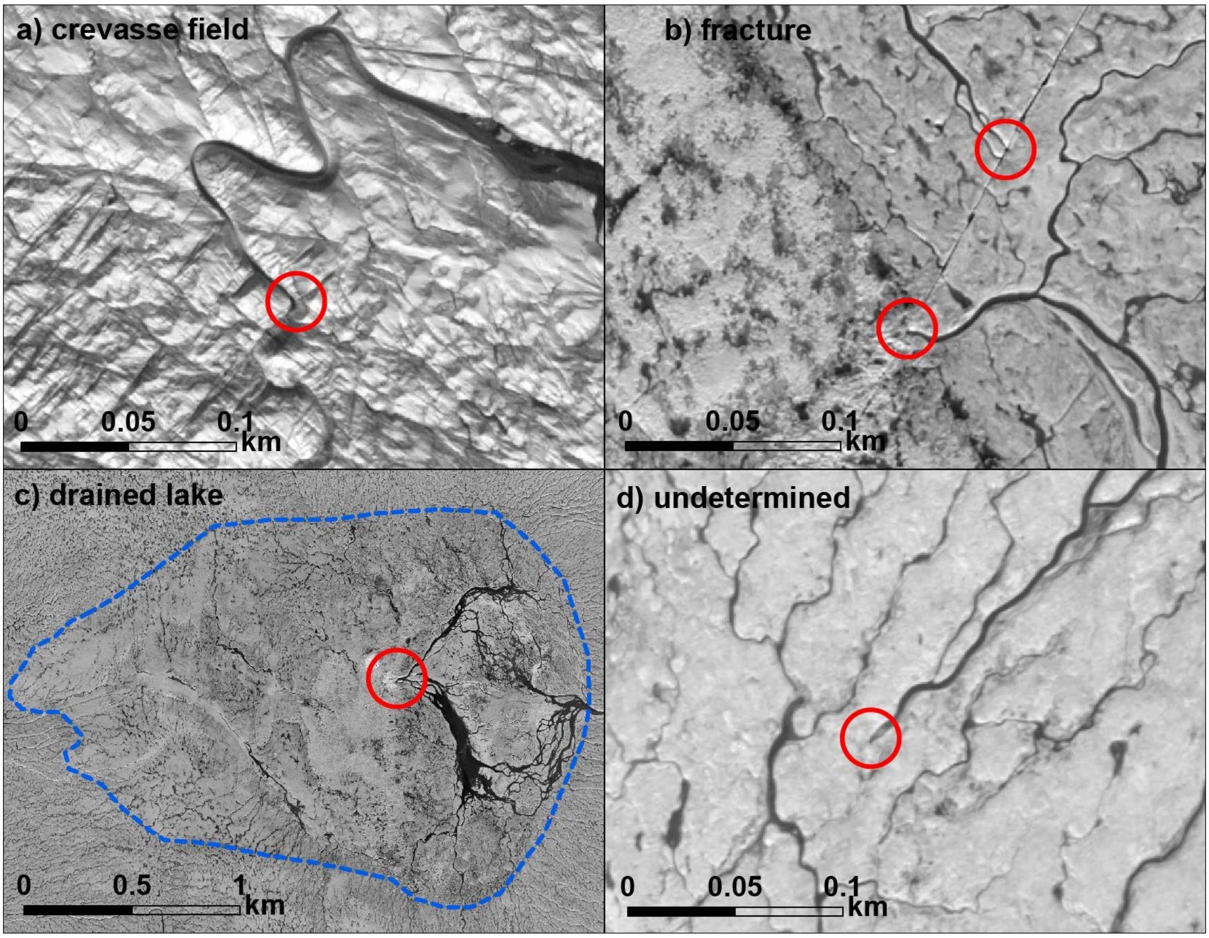

Figure 4-2. Examples of the four different moulin formation types identified from visual inspection of WorldView-1 imagery, with moulins outlined by red circles: (a) crevasse field, (b) fracture, (c) drained lake (with drained lake scar outlined in blue stippled line), or (d) undetermined.

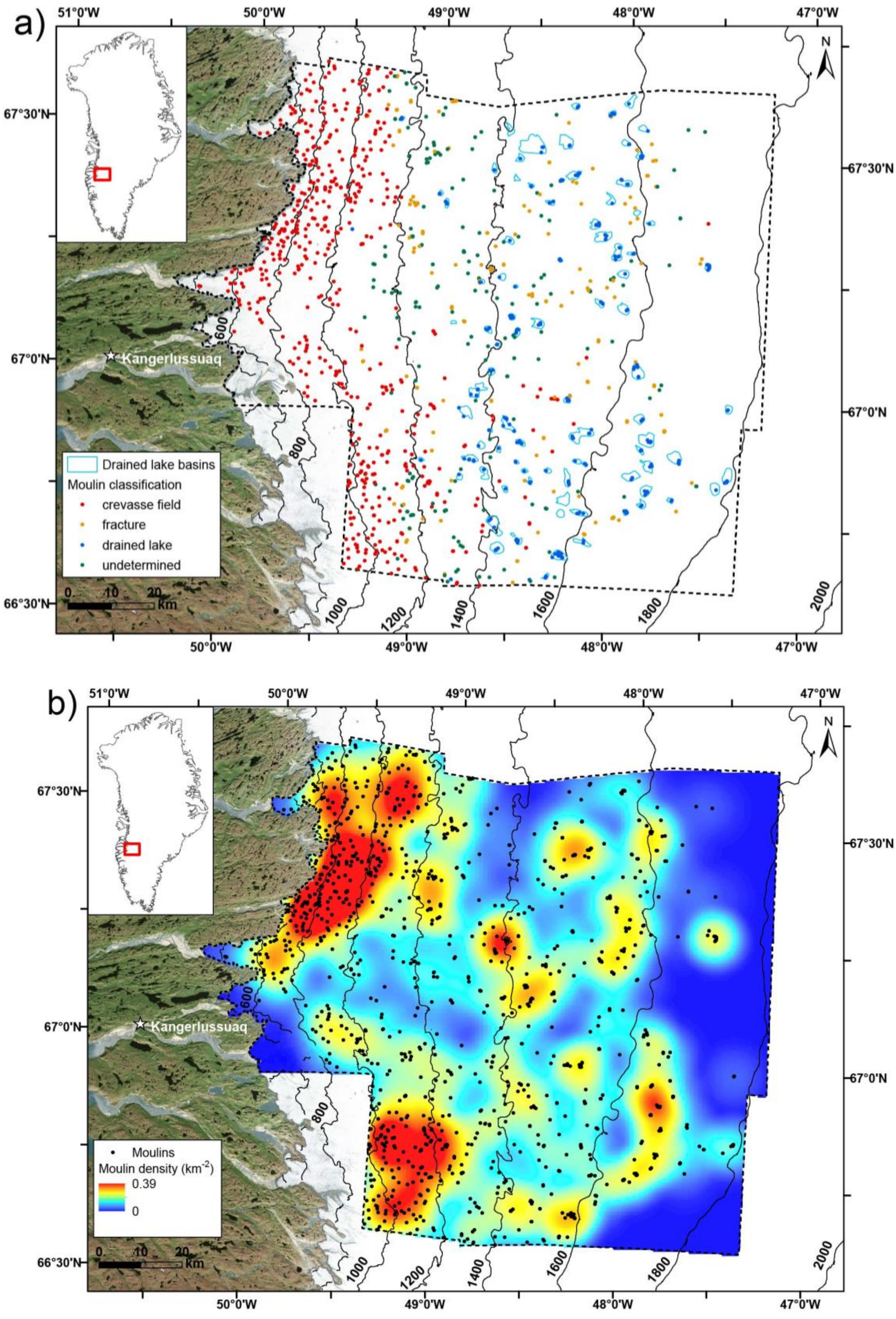

Figure 4-3. Moulin locations within the southwest Greenland study area. (a) Colored points indicate moulin classification by visible formation mechanism (i.e., crevasse field, fracture, drained lake, or undetermined), and drained lake basins are shown in blue outlines. (b) Moulin density grid created from observed moulin locations.

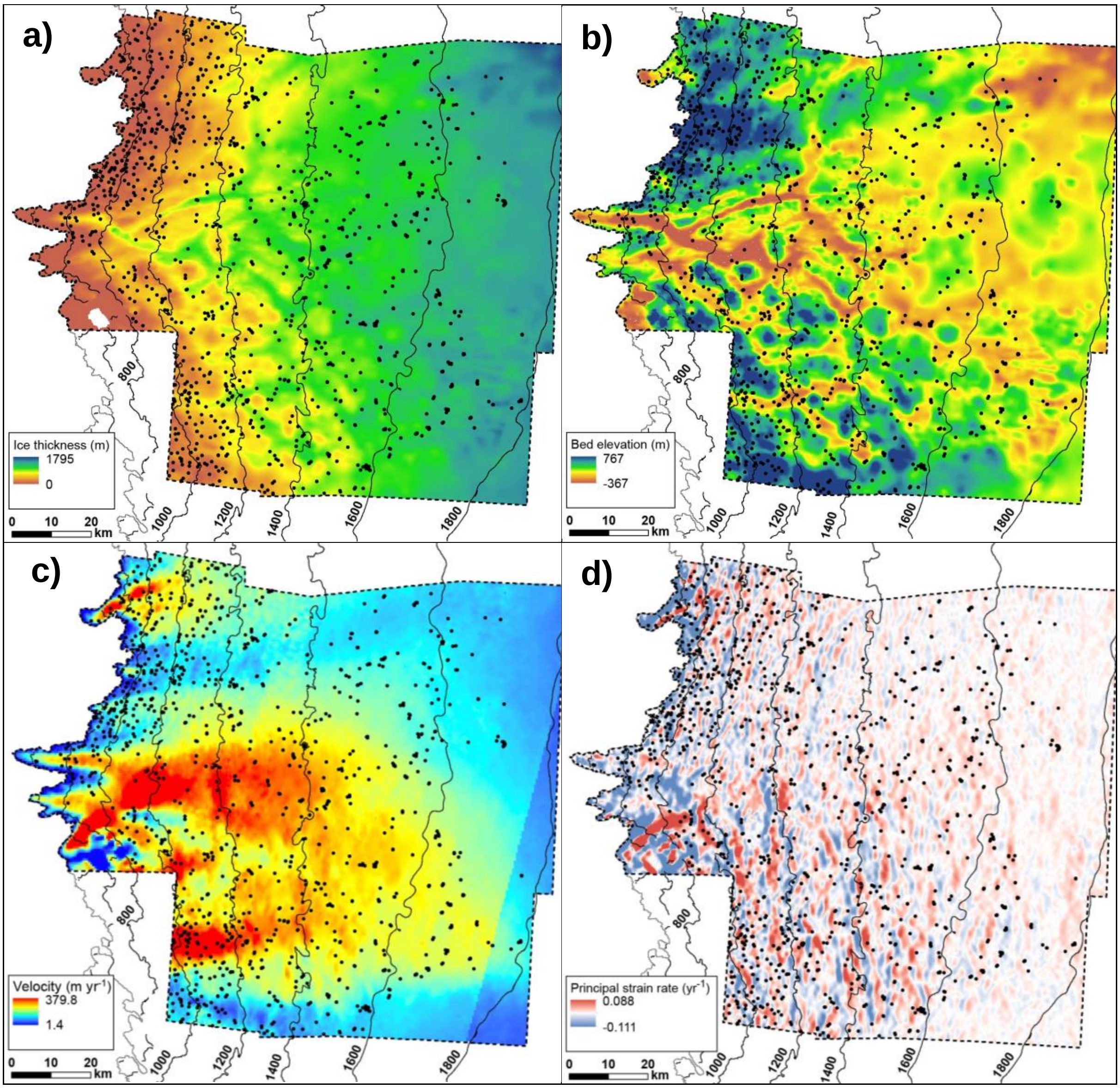

Figure 4-4. Gridded geospatial datasets within the study region with surface elevation contours (black lines) and moulin locations (black dots): (a) ice thickness, (b) bed elevation, (c) velocity, and (d) principal strain rate.

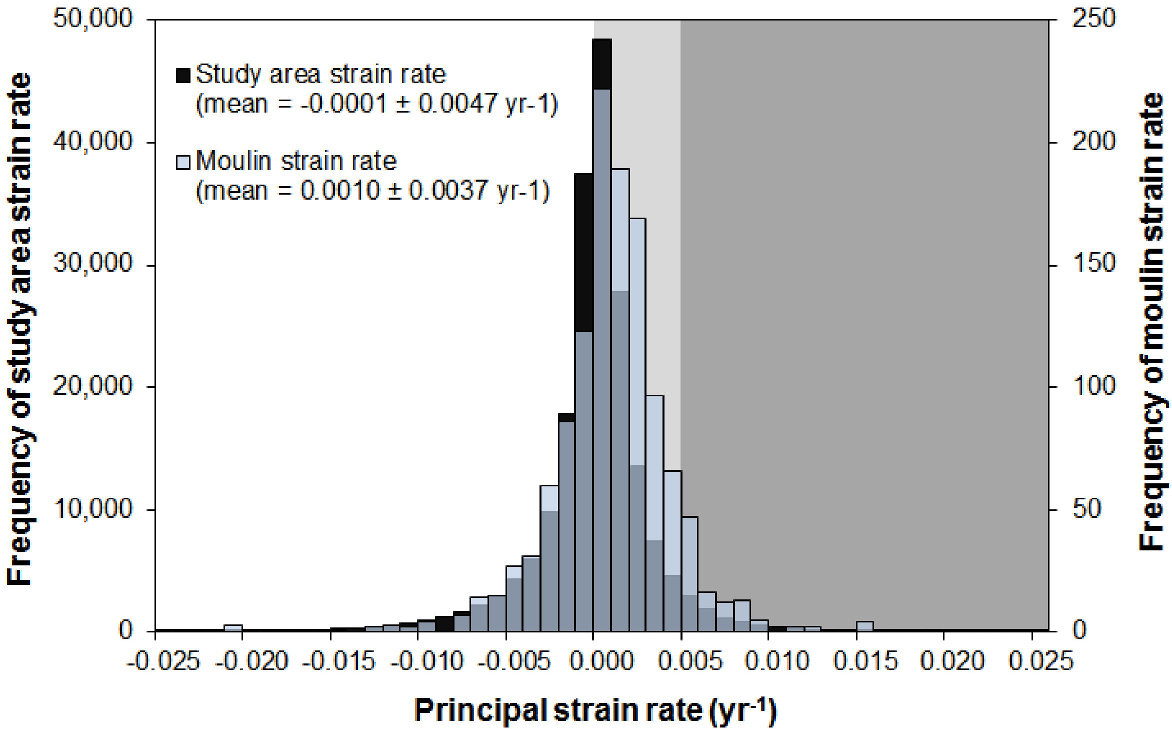

Figure 4-5. Principal strain rates of mapped moulins (transparent blue bars) compared to those of the entire study area (black bars). Dark grey areas indicate strain rates greater than 0.005 yr^{-1}, the expected threshold for crevasse and moulin formation, and light grey areas indicate positive strain rates representing ice extension where crevasses and moulins may also form.

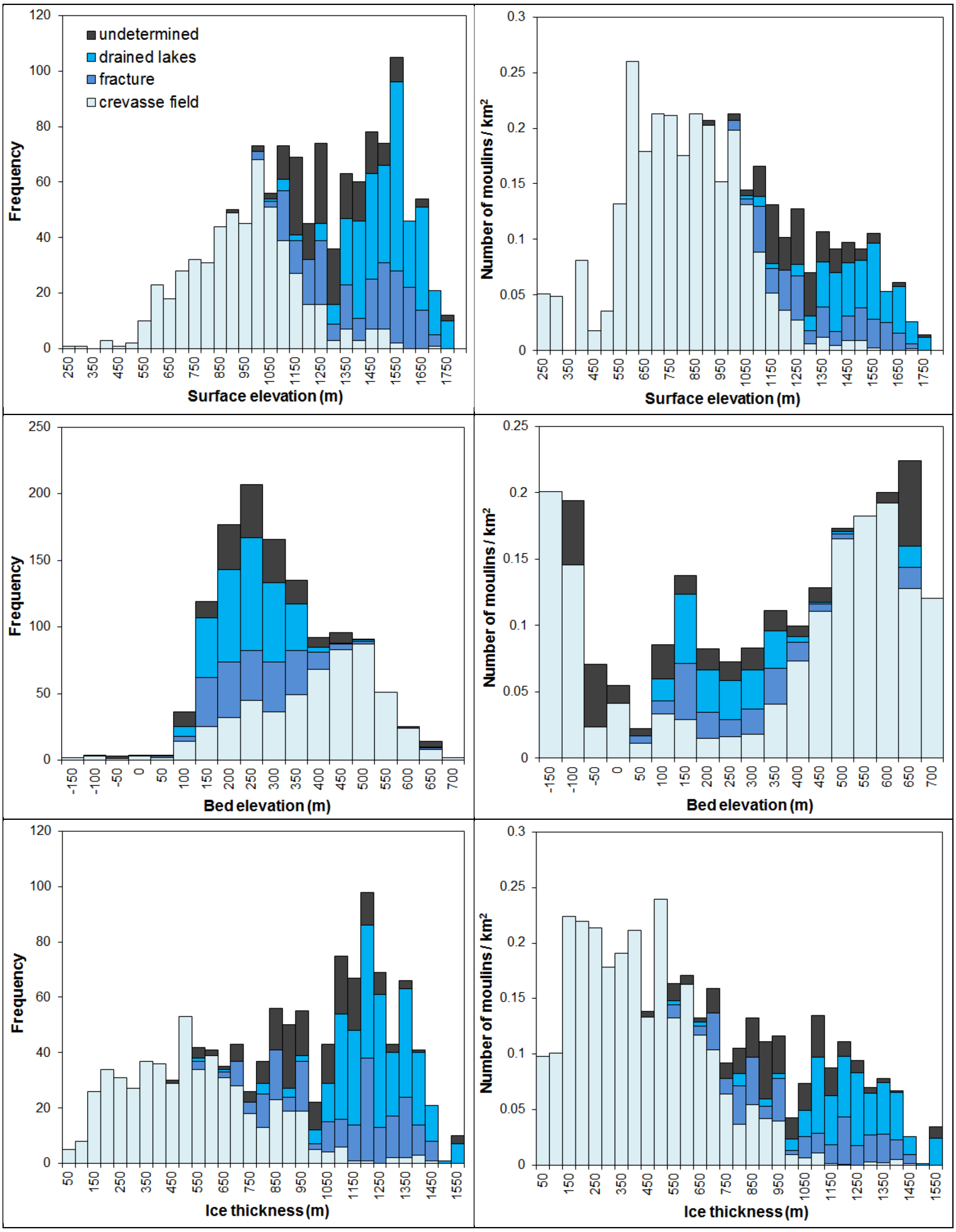
undetermined
drained lakes
fracture
crevasse field
Frequency
Surface elevation (m)
Number of moulins / km²
Surface elevation (m)
Frequency
Bed elevation (m)
Number of moulins / km²
Bed elevation (m)
Frequency
Ice thickness (m)
Number of moulins / km²
Ice thickness (m)

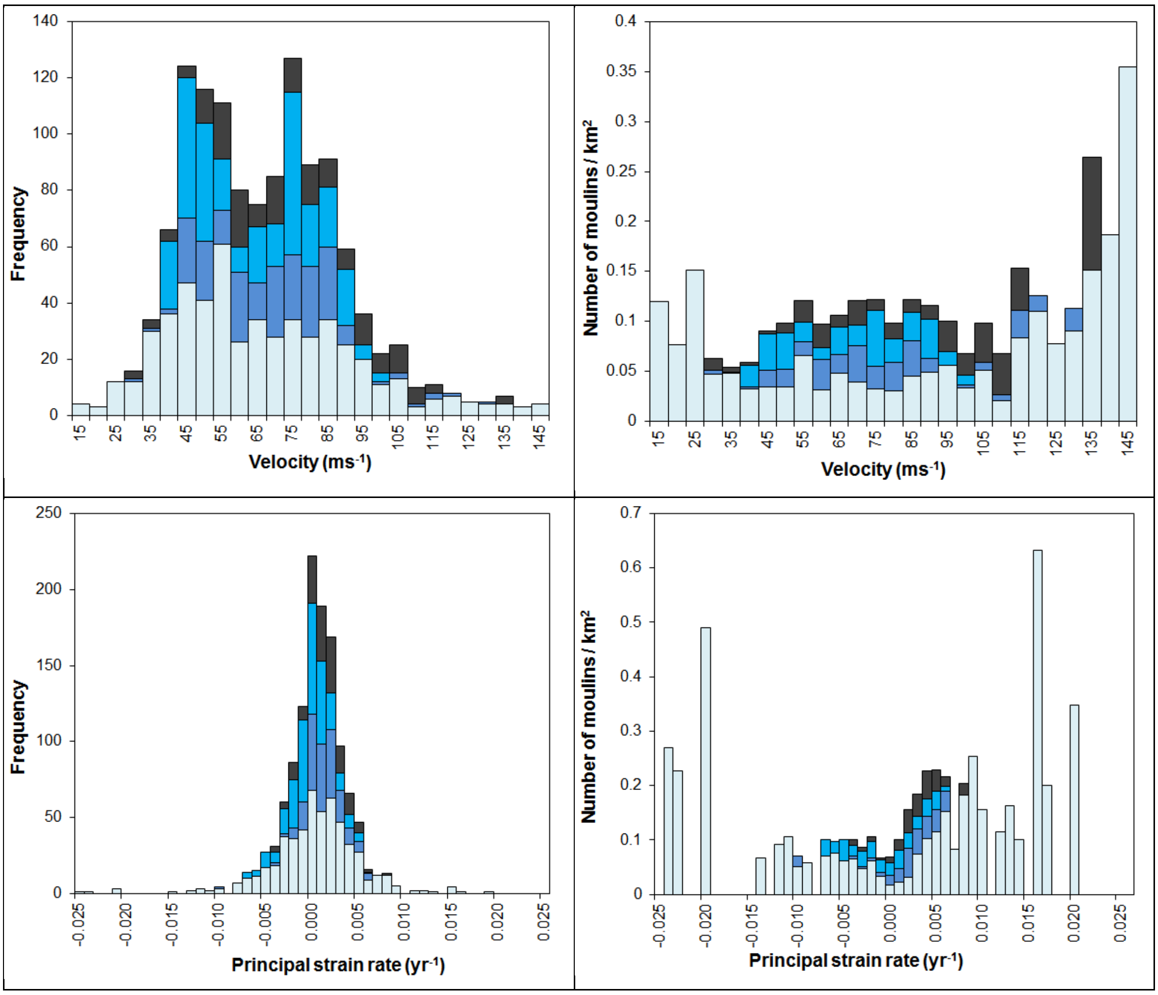

Figure 6. Distribution of moulins with visible formation mechanism indicated by color. The left column shows the frequency of moulins for selected geospatial variables, and the right column shows the frequency of moulins normalized by the area covered within each bin. Geospatial variables include: (a) surface elevation, (c) bed elevation, (e) ice thickness, (g) velocity, and (i) principal strain rate.

4.9 Tables

	Surface elevation (m)	Bed elevation (m)	Ice thickness (m)	Surface slope (deg)	Bed slope (deg)	Velocity ($m\ s^{-1}$)
Bed elevation (m)	-0.29					
Ice thickness (m)	0.95	-0.56				
Surface slope (deg)	-0.57	0.33	-0.60			
Bed slope (deg)	-0.48	0.07	-0.44	0.41		
Velocity ($m\ s^{-1}$)	-0.27	-0.18	-0.17	0.02	0.28	
Strain rate (yr^{-1})	0.20	-0.05	0.19	-0.23	-0.09	0.03

Table 4-1. Correlation matrix between independent geospatial variables. Higher R values indicate multicollinearity between variables (red values).

Group	Statistic	Moulin density (km^{-2})	Surface elevation (m)	Bed elevation (m)	Ice thickness (m)	Surface slope (deg)	Bed slope (deg)	Velocity (m s^{-1})	Strain rate (yr^{-1})
All moulins (n = 1236)	**Avg**	0.16	1,238	336	899	0.72	3.34	69.3	0.0010
	Std dev	0.08	307	136	382	0.63	2.71	22.2	0.0037
	Min	0.00	282	-139	80	0.00	0.00	15.1	-0.0249
	Max	0.39	1,788	713	1,594	6.00	27.12	148.9	0.0268
	Median	0.15	1,257	316	951	0.54	2.73	67.9	0.0010
Crevasse field (n = 535)	**Avg**	0.20	967	412	555	1.05	4.26	68.5	0.0009
	Std dev	0.09	216	147	267	0.75	3.12	26.2	0.0050
	Min	0.00	282	-139	80	0.07	0.21	15.1	-0.0249
	Max	0.39	1,721	713	1,475	6.00	27.12	148.9	0.0268
	Median	0.20	985	441	526	0.88	3.70	64.8	0.0011
Fracture (n = 212)	**Avg**	0.14	1,417	287	1,127	0.51	2.58	70.6	0.0017
	Std dev	0.05	185	89	225	0.34	2.08	16.5	0.0019
	Min	0.05	1,034	87	571	0.00	0.00	34.3	-0.0094
	Max	0.30	1,748	683	1,495	2.20	10.84	130.1	0.0068
	Median	0.14	1,462	273	1,198	0.41	2.03	72.6	0.0016
Drained lake (n = 307)	**Avg**	0.14	1,532	270	1,254	0.40	2.43	66.3	0.0002
	Std dev	0.04	130	72	146	0.34	1.97	16.7	0.0023
	Min	0.02	1,054	112	594	0.00	0.14	41.4	-0.0065
	Max	0.23	1,788	661	1,559	2.69	9.32	100.2	0.0062
	Median	0.13	1,552	271	1,252	0.28	1.77	68.5	0.0004
Undetermined (n = 174)	**Avg**	0.13	1,321	288	1,030	0.56	3.14	76.4	0.0017
	Std dev	0.06	150	119	196	0.34	2.29	22.0	0.0021
	Min	0.00	936	-96	493	0.00	0.00	30.5	-0.0036
	Max	0.30	1,753	687	1,594	1.79	12.42	138.2	0.0082
	Median	0.12	1,297	281	1,035	0.49	2.68	73.0	0.0017

Table 4-2. Summary of moulin attributes for all moulins and for each visible moulin formation type.

	Coefficient	Std. error	t-statistic	p-value	VIF
Intercept	0.000	0.0036	0.00	0.999	---
Bed elevation	0.224	0.0047	47.57	<0.001	1.73
Ice thickness	-0.489	0.0057	-85.95	<0.001	2.53
Surface slope	-0.153	0.0047	-32.82	<0.001	1.70
Bed slope	-0.006	0.0043	-1.50	0.135	1.42
Velocity	0.058	0.0037	15.55	<0.001	1.07
Strain rate	0.165	0.0040	41.45	<0.001	1.24

Table 4-3. Results of the multiple regression using standardized independent geospatial variables and the moulin density dataset as the dependent variable.

4.10 Appendix: Moulin dataset

This moulin dataset of 1236 moulin locations and visible formation mechanism is created from high-resolution WorldView-1/2 imagery. Fields include latitude, longidude, formation mechanism, surface elevation, bed elevation, ice thickness, surface slope, bed slope, velocity, and strain rate.

Point	Lat	Long	Moulin formation type	Surface elevation (m)	Bed elevation (m)	Ice thickness (m)	Surface slope (deg)	Bed slope (deg)	Velocity (m/yr)	Strain rate (yr^{-1})
1	67.413	-49.215	crevasses	1176	539	637	1.48	3.37	44.35	0.0009
2	66.716	-49.021	fracture	1174	304	870	0.45	3.39	58.33	-0.0008
3	66.762	-49.068	unknown	1147	338	809	0.43	2.03	80.66	0.0008
4	66.913	-49.179	fracture	1121	238	883	0.41	1.00	80.07	-0.0012
5	67.405	-48.988	drained lake	1283	197	1086	0.74	2.75	44.37	0.0028
6	67.326	-49.064	fracture	1270	409	861	0.62	3.76	72.85	0.0061
7	67.171	-49.052	unknown	1252	116	1136	0.61	1.63	109.98	0.0007
8	67.002	-49.216	crevasses	1119	217	902	0.90	1.07	85.37	0.0002
9	66.973	-48.957	crevasses	1264	392	872	0.92	5.82	91.67	0.0026
10	66.902	-49.209	crevasses	1134	334	800	1.69	9.85	72.10	0.0036
11	66.759	-48.840	unknown	1281	175	1106	0.75	5.44	71.98	0.0044
12	66.771	-48.911	unknown	1259	341	918	0.39	8.61	82.31	0.0016
13	66.845	-48.969	crevasses	1206	229	977	1.41	5.59	95.23	-0.0046
14	66.845	-49.068	crevasses	1182	315	867	1.20	5.70	90.08	0.0029
15	66.863	-49.194	crevasses	1115	488	627	0.51	3.57	80.49	-0.0024
16	66.811	-49.263	crevasses	1043	226	817	0.61	2.70	133.71	0.0022
17	66.754	-49.275	crevasses	1029	526	503	0.38	4.08	86.10	0.0049
18	66.624	-49.280	unknown	936	363	573	0.49	3.06	46.32	0.0029
19	67.009	-48.232	unknown	1532	156	1376	0.43	0.43	87.98	0.0006
20	67.030	-48.030	fracture	1576	200	1376	0.19	1.78	83.35	0.0035
21	67.039	-48.143	fracture	1558	167	1391	0.34	0.82	86.70	0.0010
22	67.039	-48.144	fracture	1558	167	1391	0.34	0.82	86.70	0.0010
23	67.039	-48.143	fracture	1558	167	1391	0.34	0.82	86.70	0.0010
24	67.039	-48.142	fracture	1558	167	1391	0.34	0.82	86.70	0.0008
25	66.991	-49.167	unknown	1133	216	917	0.77	2.11	92.72	0.0067
26	67.165	-49.176	crevasses	1177	359	818	0.75	2.27	122.46	-0.0019
27	67.136	-48.401	unknown	1479	230	1249	0.89	1.60	81.04	0.0013
28	67.583	-48.388	unknown	1481	388	1093	0.38	1.49	50.53	0.0010
29	66.934	-48.413	crevasses	1476	331	1145	0.53	0.88	81.70	0.0023
30	66.796	-48.435	crevasses	1460	339	1121	0.21	6.57	76.39	0.0041
31	66.782	-48.396	unknown	1472	321	1151	0.79	6.62	76.12	0.0031
32	66.786	-48.680	crevasses	1345	556	789	0.20	2.42	80.52	0.0016
33	66.693	-48.414	crevasses	1462	561	901	0.64	1.98	60.87	0.0008
34	66.693	-48.414	crevasses	1462	561	901	0.64	1.98	60.87	0.0008
35	66.867	-48.763	drained lake	1340	207	1133	1.48	3.41	91.31	0.0013
36	66.892	-48.769	crevasses	1345	371	974	1.60	5.38	84.43	0.0019
37	66.894	-48.764	crevasses	1338	348	990	0.45	3.24	84.03	-0.0006
38	66.942	-48.540	drained lake	1426	303	1123	0.81	2.53	88.75	-0.0025
39	66.999	-48.752	drained lake	1361	230	1131	0.90	3.93	76.66	-0.0021
40	66.970	-48.808	drained lake	1330	284	1046	0.15	0.67	84.97	-0.0001
41	67.165	-48.877	unknown	1335	168	1167	0.48	3.14	112.35	0.0055
42	67.010	-48.717	drained lake	1351	112	1239	0.60	3.99	78.93	0.0013
43	67.010	-48.717	drained lake	1351	112	1239	0.60	3.99	78.93	0.0013
44	66.987	-48.724	unknown	1366	283	1083	0.41	1.24	81.14	-0.0017

45	66.998	-48.721	drained lake; fracture	1351	228	1123	0.41	2.77	77.42	-0.0003
46	66.998	-48.720	drained lake; fracture	1351	228	1123	0.41	2.77	77.42	-0.0003
47	66.822	-49.225	crevasses	1061	344	717	0.64	4.43	117.57	0.0052
48	66.635	-49.349	crevasses	916	398	518	0.75	3.24	50.38	0.0009
49	66.610	-48.644	crevasses	1383	501	882	0.62	4.23	38.31	0.0008
50	66.702	-48.459	drained lake	1419	379	1040	0.54	6.68	64.34	0.0018
51	66.744	-48.404	crevasses	1467	458	1009	0.64	1.24	71.80	0.0029
52	66.742	-48.405	crevasses	1467	455	1012	0.58	0.86	70.14	0.0030
53	67.438	-48.867	unknown	1336	395	941	0.62	1.60	53.51	0.0027
54	67.205	-49.305	unknown	1129	291	838	1.01	0.68	104.73	0.0026
55	67.496	-49.072	unknown	1250	377	873	1.02	1.00	62.99	0.0024
56	67.474	-49.071	unknown	1233	338	895	1.08	1.67	52.50	0.0003
57	67.377	-49.282	crevasses	1156	480	676	0.41	4.24	57.05	0.0014
58	66.953	-48.555	drained lake	1431	277	1154	0.51	2.35	87.00	-0.0028
59	66.954	-48.556	drained lake	1431	277	1154	0.51	2.35	87.00	-0.0028
60	67.515	-48.450	drained lake	1459	333	1126	0.38	3.04	44.52	-0.0036
61	67.515	-48.455	drained lake	1458	326	1132	0.19	2.52	44.35	-0.0025
62	67.504	-48.458	drained lake	1462	309	1153	0.43	0.69	46.01	-0.0027
63	67.501	-48.829	unknown	1354	496	858	0.56	1.56	61.22	0.0010
64	67.526	-48.818	unknown	1344	393	951	0.73	1.97	58.99	0.0003
65	67.539	-48.787	unknown	1359	383	976	0.64	1.96	56.81	0.0044
66	67.485	-48.413	fracture	1480	272	1208	0.34	1.02	46.42	0.0002
67	67.484	-48.413	fracture	1480	272	1208	0.34	1.02	46.42	0.0002
68	67.484	-48.412	fracture	1480	272	1208	0.34	1.02	46.42	-0.0002
69	67.484	-48.413	fracture	1480	272	1208	0.34	1.02	46.42	0.0002
70	67.484	-48.412	fracture	1480	272	1208	0.34	1.02	46.42	-0.0002
71	67.484	-48.412	fracture	1480	272	1208	0.34	1.02	46.42	-0.0002
72	67.421	-48.470	unknown	1462	267	1195	0.34	0.00	57.26	-0.0004
73	67.418	-48.452	fracture	1466	267	1199	0.30	0.07	56.81	0.0010
74	67.433	-48.503	drained lake; fracture	1451	269	1182	0.15	0.34	53.94	0.0016
75	67.433	-48.502	drained lake; fracture	1451	268	1183	0.19	0.27	53.94	0.0016
76	67.432	-48.500	drained lake	1451	268	1183	0.19	0.27	53.94	0.0016
77	67.438	-48.395	unknown	1488	281	1207	0.21	0.21	53.64	0.0014
78	67.489	-48.569	drained lake	1434	336	1098	0.28	0.21	45.74	0.0017
79	67.420	-48.699	unknown	1395	222	1173	0.43	3.66	56.20	0.0009
80	67.462	-48.702	drained lake; fracture	1384	342	1042	1.57	1.64	48.81	0.0011
81	67.461	-48.704	drained lake; fracture	1393	352	1041	1.54	1.42	48.81	0.0011
82	67.405	-48.381	drained lake	1475	258	1217	0.15	0.34	54.68	-0.0006
83	67.401	-48.400	drained lake	1474	261	1213	0.19	0.38	55.34	-0.0004
84	67.401	-48.397	drained lake	1474	260	1214	0.19	0.34	55.34	-0.0011
85	67.365	-48.394	unknown	1475	257	1218	0.27	0.60	62.07	0.0004
86	67.374	-48.438	unknown	1466	267	1199	0.21	0.39	62.79	0.0013
87	67.337	-48.395	fracture	1477	258	1219	0.34	0.77	64.60	0.0017
88	67.382	-48.502	fracture	1450	266	1184	0.34	0.48	60.87	0.0038
89	67.333	-48.573	fracture	1432	288	1144	0.58	0.41	68.45	0.0003
90	67.328	-48.553	unknown	1437	294	1143	0.72	1.55	67.68	0.0007
91	67.320	-48.599	drained lake	1406	260	1146	1.01	1.18	68.56	0.0007
92	67.316	-48.631	unknown	1417	258	1159	0.76	1.78	69.63	0.0022
93	67.332	-48.719	fracture	1384	189	1195	0.85	0.24	70.35	0.0013
94	67.332	-48.720	fracture	1383	188	1195	0.94	0.27	70.35	0.0013
95	67.331	-48.761	unknown	1378	264	1114	1.52	3.06	76.25	0.0021
96	67.230	-48.456	unknown	1467	245	1222	0.34	1.57	85.56	0.0018
97	67.247	-48.420	unknown	1480	281	1199	0.27	0.90	83.20	0.0007
98	67.254	-48.404	unknown	1483	252	1231	0.43	1.15	81.11	0.0011
99	67.225	-48.554	drained lake	1433	249	1184	0.45	3.67	90.04	0.0015
100	67.243	-48.641	drained lake	1403	213	1190	1.67	2.71	86.68	0.0028
101	67.258	-48.682	fracture	1396	196	1200	1.00	2.00	85.44	0.0031
102	67.269	-48.623	fracture	1422	196	1226	0.34	1.75	83.27	0.0028
103	67.306	-48.670	fracture	1416	346	1070	0.15	6.59	76.35	0.0040
104	67.231	-48.738	drained lake; fracture	1372	237	1135	1.02	2.99	96.81	0.0036

105	67.238	-48.749	unknown	1375	239	1136	0.39	7.61	95.78	0.0022
106	67.234	-48.746	fracture	1375	279	1096	0.86	3.44	94.08	0.0028
107	67.237	-48.749	unknown	1374	258	1116	0.79	7.43	95.78	0.0022
108	67.285	-48.765	unknown	1386	254	1132	0.88	4.88	84.81	0.0000
109	67.292	-48.838	unknown	1346	254	1092	0.43	0.98	82.20	0.0033
110	67.271	-48.807	unknown	1356	324	1032	0.61	1.99	85.12	0.0033
111	67.246	-48.807	unknown	1353	195	1158	0.60	4.87	93.72	0.0027
112	67.213	-48.463	fracture	1463	214	1249	0.21	0.00	86.90	0.0029
113	67.193	-48.433	unknown	1475	226	1249	0.14	0.77	86.17	0.0013
114	67.208	-48.461	fracture	1465	205	1260	0.41	1.39	86.85	0.0026
115	67.211	-48.480	fracture	1460	221	1239	0.57	1.35	89.34	0.0026
116	67.154	-48.409	drained lake; fracture	1472	151	1321	0.19	5.98	80.90	0.0045
117	67.152	-48.409	drained lake; fracture	1471	166	1305	0.21	5.99	80.90	0.0040
118	67.152	-48.409	drained lake; fracture	1471	166	1305	0.21	5.99	80.90	0.0040
119	67.154	-48.409	drained lake; fracture	1472	151	1321	0.19	5.98	80.90	0.0045
120	67.135	-48.683	drained lake; fracture	1355	201	1154	0.82	7.94	95.52	-0.0054
121	67.162	-48.558	drained lake; fracture	1428	173	1255	0.19	4.12	90.23	0.0057
122	67.190	-48.563	unknown	1432	261	1171	0.45	1.09	96.74	0.0017
123	67.200	-48.647	unknown	1410	292	1118	0.51	2.09	98.40	0.0050
124	67.212	-48.703	unknown	1387	273	1114	0.34	5.84	100.31	0.0037
125	67.148	-48.812	unknown	1347	246	1101	0.51	9.64	104.95	0.0041
126	67.147	-48.809	fracture	1344	263	1081	0.43	10.84	104.95	0.0041
127	67.212	-48.765	unknown	1367	268	1099	0.48	4.56	105.29	0.0028
128	67.080	-48.407	unknown	1485	250	1235	0.47	2.11	86.95	0.0046
129	67.051	-48.646	drained lake	1403	181	1222	0.53	2.66	83.50	-0.0048
130	67.050	-48.659	drained lake; fracture	1401	183	1218	0.28	2.73	80.74	-0.0007
131	67.050	-48.659	drained lake; fracture	1401	183	1218	0.28	2.73	80.74	-0.0007
132	67.105	-48.631	drained lake; fracture	1386	199	1187	0.36	4.11	92.62	0.0014
133	67.100	-48.677	unknown	1383	209	1174	0.24	5.79	91.03	0.0048
134	67.079	-48.535	unknown	1453	236	1217	0.58	2.60	94.49	0.0021
135	67.122	-48.542	unknown	1437	227	1210	0.29	6.66	87.59	0.0001
136	67.135	-48.533	drained lake; fracture	1439	222	1217	0.19	3.05	89.14	0.0017
137	67.126	-48.549	unknown	1436	241	1195	0.19	5.47	86.75	0.0004
138	67.139	-48.529	drained lake; fracture	1440	212	1228	0.19	3.65	89.14	0.0002
139	67.138	-48.524	drained lake; fracture	1441	228	1213	0.19	2.85	87.57	-0.0005
140	67.071	-48.685	unknown	1396	283	1113	0.61	1.09	89.21	-0.0005
141	67.102	-48.783	unknown	1346	267	1079	0.28	1.00	100.11	0.0002
142	67.117	-48.768	unknown	1350	249	1101	0.49	2.18	100.37	0.0037
143	67.003	-48.401	crevasses	1494	154	1340	0.34	2.15	86.35	0.0009
144	67.018	-48.389	crevasses	1490	144	1346	0.85	0.60	83.82	-0.0002
145	67.024	-48.481	crevasses	1466	285	1181	0.43	3.08	83.42	0.0019
146	67.041	-48.568	unknown	1433	265	1168	0.79	1.39	98.71	-0.0001
147	67.041	-48.564	unknown	1435	265	1170	0.67	1.44	98.10	0.0002
148	66.989	-48.642	fracture	1403	306	1097	0.00	1.76	82.67	0.0024
149	66.989	-48.642	fracture	1403	306	1097	0.00	1.76	82.67	0.0024
150	66.989	-48.641	fracture	1403	307	1096	0.07	1.95	82.67	0.0024
151	66.950	-48.627	crevasses	1395	394	1001	0.58	7.28	94.57	0.0114
152	66.958	-48.632	crevasses	1398	364	1034	0.39	7.11	90.73	0.0088
153	66.939	-48.572	drained lake	1414	298	1116	0.48	3.11	89.49	0.0006
154	66.955	-48.567	drained lake	1428	253	1175	0.73	2.57	86.57	-0.0002
155	66.930	-48.512	drained lake	1440	335	1105	0.97	4.62	85.41	-0.0024
156	66.930	-48.512	drained lake	1440	335	1105	0.97	4.62	85.41	-0.0024
157	66.910	-48.483	drained lake; fracture	1443	295	1148	0.51	1.42	84.55	-0.0009
158	66.905	-48.469	drained lake	1444	309	1135	0.73	3.11	85.61	-0.0012
159	66.907	-48.478	drained lake; fracture	1442	296	1146	0.60	2.11	85.82	-0.0009
160	66.907	-48.495	drained lake	1440	287	1153	0.47	2.27	84.48	0.0014
161	66.910	-48.637	unknown	1386	367	1019	0.54	3.46	96.74	0.0009
162	66.928	-48.644	drained lake; fracture	1382	406	976	1.30	0.70	98.25	0.0030
163	66.873	-48.628	unknown	1392	271	1121	0.20	4.08	95.85	0.0029
164	66.868	-48.495	drained lake; fracture	1435	285	1150	0.91	4.59	87.65	0.0006

165	66.867	-48.495	drained lake; fracture	1435	280	1155	0.81	3.74	87.65	0.0006
166	66.895	-48.695	drained lake; fracture	1341	231	1110	2.69	3.20	86.86	-0.0010
167	66.953	-48.782	drained lake	1328	184	1144	0.24	0.15	84.22	-0.0007
168	66.849	-48.448	drained lake; fracture	1446	371	1075	0.96	5.01	87.98	-0.0018
169	66.830	-48.442	fracture	1457	299	1158	0.34	2.42	82.78	0.0013
170	66.825	-48.414	drained lake; fracture	1459	380	1079	0.70	8.19	84.09	-0.0064
171	66.827	-48.414	drained lake; fracture	1460	387	1073	0.77	8.43	82.51	-0.0065
172	66.828	-48.413	drained lake; fracture	1461	392	1069	0.75	8.53	82.51	-0.0065
173	66.892	-48.589	drained lake; fracture	1402	312	1090	1.60	2.29	91.95	0.0001
174	66.826	-48.573	crevasses	1413	463	950	0.62	6.67	86.99	0.0119
175	66.811	-48.538	drained lake	1411	464	947	0.29	2.06	79.90	0.0006
176	66.846	-48.659	drained lake; fracture	1337	171	1166	0.82	5.79	97.32	-0.0044
177	66.848	-48.656	drained lake; fracture	1333	166	1167	0.36	6.00	100.19	-0.0040
178	66.863	-48.714	drained lake	1326	171	1155	1.58	4.56	92.92	-0.0028
179	66.865	-48.713	drained lake; fracture	1321	199	1122	0.27	6.08	91.21	-0.0049
180	66.865	-48.738	drained lake; fracture	1332	170	1162	1.30	2.26	91.31	0.0016
181	66.866	-48.736	drained lake	1327	172	1155	1.02	2.16	91.31	0.0003
182	66.844	-48.778	unknown	1319	164	1155	0.62	3.80	99.90	0.0023
183	66.834	-48.787	drained lake; fracture	1308	132	1176	1.13	2.06	94.52	0.0023
184	66.820	-48.822	fracture	1310	245	1065	0.34	6.93	88.49	0.0002
185	66.819	-48.804	unknown	1309	211	1098	0.60	3.29	89.48	0.0008
186	66.798	-48.826	unknown	1296	364	932	1.79	0.49	86.88	0.0056
187	66.744	-48.615	drained lake; fracture	1363	224	1139	0.43	1.03	68.07	0.0008
188	66.747	-48.609	drained lake; fracture	1360	234	1126	1.42	2.69	67.92	0.0000
189	66.748	-48.606	drained lake	1363	242	1121	1.02	2.78	67.92	0.0000
190	66.730	-48.585	drained lake	1363	187	1176	0.54	5.54	65.74	-0.0024
191	66.709	-48.467	drained lake	1421	331	1090	0.15	6.63	66.13	-0.0009
192	66.707	-48.468	drained lake; fracture	1422	316	1106	0.67	5.36	66.13	0.0006
193	66.706	-48.458	drained lake; fracture	1418	386	1032	0.10	7.71	64.78	-0.0021
194	66.688	-48.559	drained lake; fracture	1377	236	1141	0.75	6.86	52.80	-0.0039
195	66.685	-48.568	drained lake; fracture	1376	251	1125	0.21	5.43	45.09	-0.0014
196	66.685	-48.568	drained lake; fracture	1376	251	1125	0.21	5.43	45.09	-0.0014
197	66.684	-48.568	drained lake; fracture	1375	265	1110	0.21	5.76	45.09	-0.0014
198	66.684	-48.570	drained lake; fracture	1374	266	1108	0.14	6.03	45.09	-0.0014
199	66.684	-48.571	drained lake; fracture	1374	266	1108	0.14	6.03	45.09	-0.0014
200	66.683	-48.570	drained lake; fracture	1374	266	1108	0.14	6.03	45.09	-0.0014
201	66.683	-48.570	drained lake; fracture	1374	266	1108	0.14	6.03	45.09	-0.0014
202	66.664	-48.456	fracture	1457	399	1058	0.30	3.83	43.39	-0.0006
203	66.664	-48.457	fracture	1457	399	1058	0.30	3.83	43.39	-0.0006
204	66.645	-48.521	unknown	1448	436	1012	0.38	4.35	43.43	-0.0013
205	66.619	-48.473	fracture	1445	454	991	0.07	4.49	39.74	-0.0008
206	66.628	-48.594	unknown	1403	360	1043	0.88	1.42	36.22	-0.0005
207	66.629	-48.825	fracture	1254	683	571	1.00	0.82	34.32	-0.0036
208	66.625	-48.825	unknown	1259	686	573	0.69	0.70	34.32	-0.0036
209	66.618	-48.791	drained lake; crevasses	1255	661	594	1.13	2.48	44.80	-0.0064
210	66.613	-48.808	unknown	1273	687	586	1.05	1.02	41.76	-0.0004
211	66.612	-48.760	crevasses	1314	687	627	1.00	2.01	46.04	0.0042
212	66.610	-48.761	crevasses	1311	690	621	0.39	2.20	46.04	0.0028
213	66.635	-48.767	unknown	1314	680	634	1.19	3.75	35.20	0.0045
214	66.639	-48.758	unknown	1322	652	670	0.34	4.59	34.11	0.0052
215	66.676	-48.722	crevasses	1311	411	900	1.22	3.24	42.77	0.0005
216	66.676	-48.792	crevasses	1273	367	906	0.28	3.90	50.90	0.0001
217	66.676	-48.789	crevasses	1272	374	898	0.36	3.73	50.03	0.0013
218	66.627	-48.646	unknown	1392	469	923	0.43	9.75	39.73	0.0026
219	66.686	-48.742	unknown	1293	357	936	0.81	3.56	53.69	0.0001
220	66.689	-48.755	unknown	1295	329	966	0.43	2.88	53.52	0.0013
221	66.773	-48.690	crevasses	1346	518	828	1.89	6.26	75.40	0.0075
222	66.764	-48.645	unknown	1361	412	949	0.88	3.83	73.22	0.0019
223	66.733	-48.646	crevasses	1354	237	1117	1.00	3.99	72.34	0.0051
224	66.720	-48.648	crevasses	1354	247	1107	0.81	3.80	75.78	0.0060

225	66.696	-48.765	unknown	1293	317	976	1.03	2.16	61.23	0.0006
226	66.704	-48.792	unknown	1286	313	973	0.41	0.36	64.33	0.0018
227	67.266	-48.741	fracture	1394	288	1106	1.05	0.86	89.65	0.0028
228	67.118	-48.591	unknown	1425	155	1270	0.81	1.89	90.32	0.0023
229	67.393	-48.532	fracture	1444	260	1184	0.57	0.53	61.70	0.0026
230	66.954	-48.520	unknown	1437	341	1096	0.14	1.49	94.93	-0.0001
231	67.583	-48.988	unknown	1284	424	860	0.75	3.41	62.24	0.0020
232	67.597	-48.944	fracture	1290	330	960	0.19	2.06	62.08	0.0011
233	67.597	-48.947	fracture	1290	333	957	0.24	2.37	62.08	0.0007
234	67.596	-48.953	fracture	1290	337	953	0.41	2.77	61.90	0.0002
235	67.598	-48.935	fracture	1289	319	970	0.34	1.62	62.63	0.0007
236	67.599	-48.936	fracture	1289	319	970	0.34	1.62	62.63	0.0007
237	67.597	-48.945	fracture	1290	330	960	0.19	2.06	62.08	0.0007
238	67.599	-48.933	fracture	1289	319	970	0.34	1.62	62.63	0.0007
239	67.575	-49.021	fracture	1257	396	861	1.36	2.84	63.06	-0.0001
240	67.569	-48.998	unknown	1265	354	911	0.85	3.61	57.66	0.0060
241	67.568	-48.999	unknown	1265	354	911	0.85	3.61	56.64	0.0061
242	67.536	-49.181	unknown	1186	348	838	0.68	0.91	61.84	0.0014
243	67.527	-49.226	fracture	1147	318	829	1.52	2.62	58.08	0.0025
244	67.529	-49.227	fracture	1144	313	831	1.39	2.44	58.08	0.0030
245	67.498	-49.253	fracture	1146	226	920	0.68	0.82	59.65	0.0013
246	67.553	-49.255	fracture	1146	338	808	0.47	2.51	62.00	0.0028
247	67.552	-49.255	unknown	1146	338	808	0.00	3.44	62.00	0.0028
248	67.552	-49.255	unknown	1146	338	808	0.00	3.44	62.62	0.0029
249	67.555	-49.219	drained lake; fracture	1143	322	821	0.58	1.05	63.22	0.0005
250	67.553	-49.223	drained lake; fracture	1144	325	819	0.51	1.57	59.48	0.0001
251	67.554	-49.220	drained lake; fracture	1143	322	821	0.58	1.05	63.22	0.0005
252	67.556	-49.219	drained lake; fracture	1143	321	822	0.96	0.62	63.22	0.0005
253	67.572	-49.248	fracture	1136	379	757	0.81	4.68	63.27	0.0052
254	67.571	-49.249	fracture	1135	375	760	0.49	4.67	66.69	0.0054
255	67.580	-49.295	fracture	1112	430	682	0.47	3.44	75.20	0.0068
256	67.590	-49.177	fracture	1167	429	738	0.49	3.71	64.46	0.0030
257	67.592	-49.177	fracture	1167	431	736	0.53	3.29	64.93	0.0029
258	67.505	-49.036	unknown	1261	319	942	0.43	2.07	55.11	0.0021
259	67.489	-49.009	unknown	1264	305	959	0.34	0.54	53.74	0.0034
260	67.561	-49.089	unknown	1224	337	887	0.15	1.70	60.03	0.0013
261	67.516	-49.279	crevasses	1135	389	746	0.29	5.39	64.54	0.0031
262	67.517	-49.278	crevasses	1135	400	735	0.21	4.46	67.41	0.0042
263	67.572	-49.303	crevasses	1105	472	633	0.29	1.98	76.47	0.0046
264	67.519	-49.355	crevasses	1079	447	632	0.38	3.84	66.44	0.0036
265	67.519	-49.356	crevasses	1080	453	627	0.82	4.49	72.63	0.0057
266	67.543	-49.313	crevasses	1106	429	677	0.97	0.43	75.44	0.0004
267	67.531	-49.329	crevasses	1091	417	674	1.18	3.03	72.89	0.0040
268	67.526	-49.356	crevasses	1083	443	640	0.88	2.39	74.29	0.0011
269	67.544	-49.344	crevasses	1080	423	657	1.30	1.30	77.65	0.0010
270	67.543	-49.345	crevasses	1077	422	655	1.10	0.92	77.65	0.0010
271	67.543	-49.345	crevasses	1077	422	655	1.10	0.92	77.65	0.0010
272	67.468	-49.062	unknown	1245	336	909	0.77	3.26	49.00	0.0005
273	67.467	-49.070	unknown	1253	373	880	1.42	4.83	52.32	0.0009
274	67.477	-49.053	unknown	1253	341	912	1.75	2.08	57.29	-0.0014
275	67.486	-49.026	unknown	1266	315	951	0.20	2.10	54.25	0.0029
276	67.490	-49.019	unknown	1268	311	957	0.47	1.28	56.18	0.0023
277	67.485	-48.997	unknown	1264	310	954	0.48	0.54	52.25	0.0012
278	67.491	-49.031	fracture	1268	322	946	0.54	3.08	55.99	0.0010
279	67.509	-49.038	unknown	1258	328	930	0.49	3.58	56.88	0.0031
280	67.510	-49.038	unknown	1260	337	923	1.13	3.98	59.52	0.0035
281	67.500	-48.955	fracture	1269	304	965	0.58	1.51	54.93	0.0031
282	67.498	-48.961	unknown	1268	301	967	0.77	0.74	56.34	0.0025
283	67.395	-49.127	fracture	1233	464	769	0.73	3.11	49.72	0.0019
284	67.393	-49.191	crevasses	1205	514	691	0.20	1.37	54.04	0.0002

285	67.478	-49.166	unknown	1197	362	835	1.18	1.33	57.20	-0.0017
286	67.425	-49.274	crevasses	1130	544	586	1.56	1.88	44.55	0.0020
287	67.487	-49.316	crevasses	1116	358	758	1.69	4.82	57.83	0.0032
288	67.503	-49.298	crevasses	1138	362	776	1.10	5.74	65.41	0.0038
289	67.408	-49.269	crevasses	1149	554	595	0.15	1.37	47.56	0.0007
290	67.438	-49.300	crevasses	1107	463	644	0.15	2.02	42.89	0.0005
291	66.717	-49.023	unknown	1174	301	873	0.21	2.82	56.81	-0.0031
292	66.744	-49.017	unknown	1176	278	898	0.10	1.35	67.39	-0.0011
293	66.743	-49.020	unknown	1176	280	896	0.43	1.42	63.91	-0.0008
294	66.745	-49.008	unknown	1176	279	897	0.45	1.93	68.08	0.0005
295	66.751	-49.040	unknown	1169	289	880	0.49	1.90	67.70	0.0004
296	66.750	-49.041	unknown	1170	290	880	0.30	1.58	67.70	0.0004
297	66.765	-49.061	fracture	1153	315	838	0.73	3.03	78.98	0.0032
298	66.801	-49.074	fracture	1157	167	990	0.95	2.77	119.11	0.0055
299	66.801	-49.074	fracture	1157	167	990	0.95	2.77	119.11	0.0055
300	66.799	-49.079	fracture	1152	198	954	0.49	7.19	120.54	0.0053
301	66.794	-49.169	unknown	1095	173	922	0.91	1.70	138.19	-0.0029
302	66.801	-49.215	unknown	1072	232	840	0.92	6.76	135.02	0.0036
303	66.804	-49.219	crevasses	1068	212	856	0.41	3.19	137.58	0.0024
304	66.805	-49.219	crevasses	1068	212	856	0.41	3.19	137.63	0.0016
305	66.820	-49.273	fracture	1032	301	731	1.33	3.80	130.10	0.0048
306	66.821	-49.274	unknown	1028	309	719	1.18	3.83	119.63	0.0028
307	66.827	-49.294	crevasses	1021	356	665	0.85	6.26	117.74	0.0024
308	66.823	-49.297	crevasses	1018	316	702	0.58	5.29	125.10	0.0042
309	66.817	-49.312	crevasses	1003	264	739	0.75	4.63	139.90	0.0047
310	66.817	-49.312	crevasses	1003	264	739	0.75	4.63	139.90	0.0047
311	66.822	-49.234	crevasses	1061	346	715	1.00	5.38	124.12	0.0051
312	66.823	-49.271	crevasses	1028	323	705	1.21	4.54	119.63	0.0024
313	66.838	-49.262	crevasses	1046	455	591	0.64	4.40	105.29	0.0000
314	66.836	-49.259	crevasses	1046	443	603	0.62	3.74	105.29	-0.0005
315	67.260	-48.998	unknown	1266	132	1134	0.85	7.88	79.82	0.0018
316	67.260	-48.998	unknown	1266	132	1134	0.85	7.88	79.82	0.0018
317	67.298	-49.065	unknown	1250	139	1111	0.27	2.50	72.83	0.0028
318	67.298	-49.065	unknown	1250	139	1111	0.27	2.50	72.83	0.0028
319	67.376	-49.067	unknown	1261	322	939	1.10	3.33	57.40	0.0010
320	67.384	-49.102	fracture	1233	382	851	1.22	6.54	50.36	0.0010
321	67.383	-49.101	fracture	1230	365	865	0.84	5.61	53.19	0.0009
322	67.382	-49.103	fracture	1233	369	864	0.88	5.33	53.19	0.0018
323	67.382	-49.102	fracture	1230	365	865	0.84	5.61	53.19	0.0009
324	67.102	-49.148	unknown	1182	114	1068	0.75	3.27	111.04	-0.0018
325	67.141	-49.338	unknown	1101	-96	1197	0.28	0.21	117.55	0.0023
326	67.049	-49.236	crevasses	1102	260	842	0.38	6.85	77.64	0.0001
327	66.977	-49.344	crevasses	1035	155	880	0.88	4.24	117.34	0.0025
328	66.964	-49.275	crevasses	1063	214	849	0.90	2.92	99.58	0.0036
329	66.956	-49.286	crevasses	1058	274	784	0.14	3.63	85.18	0.0057
330	66.914	-49.179	fracture	1122	238	884	0.60	0.94	80.07	-0.0012
331	66.913	-49.181	fracture	1120	236	884	0.54	0.79	80.07	-0.0012
332	66.913	-49.181	fracture	1120	236	884	0.54	0.79	77.14	-0.0012
333	66.912	-49.183	fracture	1120	236	884	0.54	0.79	77.14	-0.0012
334	67.419	-48.923	unknown	1301	343	958	0.15	1.28	53.75	-0.0029
335	67.406	-48.985	drained lake; fracture	1282	203	1079	1.00	3.21	44.37	0.0031
336	67.390	-48.953	drained lake; fracture	1283	220	1063	1.54	7.65	53.34	-0.0044
337	67.389	-48.948	drained lake; fracture	1278	228	1050	1.07	9.32	53.34	-0.0044
338	67.386	-48.946	drained lake; fracture	1279	202	1077	0.36	4.59	55.71	-0.0044
339	67.392	-49.222	crevasses	1190	517	673	1.00	4.62	50.73	0.0030
340	67.382	-49.224	crevasses	1191	474	717	0.43	4.02	55.72	0.0018
341	67.335	-49.192	fracture	1197	504	693	0.53	1.47	72.14	0.0003
342	67.379	-49.112	fracture	1239	355	884	0.67	4.22	59.40	0.0016
343	67.384	-49.120	fracture	1240	398	842	0.49	3.69	56.63	-0.0001
344	67.389	-49.138	fracture	1233	426	807	0.24	4.10	54.08	0.0017

345	67.380	-49.142	fracture	1229	398	831	0.54	3.51	54.81	0.0026
346	67.380	-49.142	fracture	1229	398	831	0.54	3.51	54.81	0.0026
347	67.391	-49.264	crevasses	1165	545	620	0.86	3.32	52.55	0.0046
348	67.382	-49.350	crevasses	1107	534	573	0.67	0.95	49.58	0.0015
349	67.340	-48.854	unknown	1329	308	1021	0.45	1.93	71.30	0.0016
350	67.262	-48.878	fracture	1326	330	996	0.57	0.77	87.22	0.0033
351	67.270	-49.253	unknown	1171	205	966	0.10	5.52	77.86	0.0039
352	67.272	-49.254	unknown	1172	218	954	0.24	5.77	79.87	0.0046
353	67.311	-49.131	fracture	1228	270	958	0.34	9.12	78.37	0.0007
354	67.314	-49.122	fracture	1230	263	967	1.12	9.14	75.61	0.0047
355	67.314	-49.116	unknown	1228	295	933	0.88	9.31	72.78	0.0038
356	67.314	-49.115	unknown	1228	295	933	0.88	9.31	72.78	0.0038
357	67.314	-49.115	unknown	1228	295	933	0.88	9.31	72.78	0.0038
358	67.283	-49.103	fracture	1243	178	1065	0.54	7.21	79.79	0.0019
359	67.291	-49.101	fracture	1247	174	1073	0.20	5.71	75.89	0.0025
360	67.296	-49.076	fracture	1249	125	1124	0.73	1.16	73.32	0.0043
361	67.322	-49.062	fracture	1269	380	889	0.36	4.97	66.43	0.0043
362	67.330	-49.129	unknown	1234	486	748	0.85	3.38	73.71	0.0057
363	67.335	-49.237	crevasses	1168	462	706	0.64	1.50	67.56	0.0029
364	67.327	-49.291	crevasses	1129	412	717	1.78	2.80	69.58	-0.0054
365	67.252	-49.313	unknown	1133	-30	1163	0.41	5.49	81.27	0.0015
366	67.252	-49.305	unknown	1134	-41	1175	0.49	9.56	80.50	0.0016
367	67.289	-49.258	unknown	1172	285	887	0.68	3.36	77.61	-0.0012
368	67.307	-49.335	crevasses	1118	465	653	1.00	2.85	72.25	-0.0013
369	67.307	-49.360	crevasses	1094	426	668	0.15	3.58	66.20	0.0038
370	67.307	-49.361	crevasses	1094	426	668	0.15	3.58	66.20	0.0038
371	67.243	-49.000	fracture	1271	123	1148	0.21	8.21	86.83	0.0004
372	67.216	-48.962	unknown	1303	152	1151	0.24	1.89	104.41	0.0030
373	67.213	-48.967	unknown	1302	159	1143	0.24	2.44	109.26	0.0024
374	67.176	-48.883	fracture	1336	165	1171	0.48	2.23	109.15	0.0010
375	67.173	-48.883	fracture	1336	158	1178	0.43	1.78	110.29	0.0018
376	67.171	-49.073	unknown	1259	136	1123	0.53	3.99	109.36	0.0008
377	67.180	-49.074	unknown	1251	228	1023	0.00	6.15	112.32	0.0021
378	67.181	-49.072	unknown	1250	220	1030	0.27	5.81	112.32	0.0021
379	67.197	-49.162	unknown	1206	264	942	0.49	3.97	108.97	-0.0019
380	67.200	-49.188	unknown	1197	215	982	0.57	3.82	105.04	0.0034
381	67.196	-49.204	unknown	1189	207	982	0.36	2.60	111.34	0.0018
382	67.220	-49.303	unknown	1146	296	850	0.14	4.80	102.80	0.0045
383	67.197	-49.245	unknown	1168	245	923	0.38	4.52	105.81	0.0043
384	67.116	-49.073	unknown	1218	22	1196	0.77	2.72	96.67	0.0031
385	67.123	-48.970	crevasses	1277	279	998	0.19	5.24	107.71	0.0038
386	67.123	-48.970	crevasses	1277	279	998	0.19	5.24	107.71	0.0038
387	67.118	-48.961	crevasses	1278	288	990	0.36	3.84	104.32	0.0073
388	67.146	-49.168	unknown	1189	420	769	0.30	2.36	137.02	0.0082
389	67.085	-49.157	crevasses	1174	204	970	0.36	1.56	110.31	0.0015
390	67.052	-49.326	fracture	1101	111	990	1.03	5.05	79.37	-0.0036
391	67.050	-49.331	fracture	1096	87	1009	0.60	4.19	78.55	-0.0028
392	67.076	-49.342	fracture	1081	371	710	2.20	10.62	73.17	-0.0094
393	67.083	-49.342	crevasses	1081	448	633	1.35	3.97	86.26	-0.0059
394	67.029	-48.895	crevasses	1285	379	906	0.54	2.51	88.12	-0.0005
395	67.050	-49.033	unknown	1218	269	949	0.38	12.42	96.44	0.0010
396	67.027	-49.095	fracture	1174	206	968	0.77	7.17	73.89	0.0000
397	67.020	-49.044	unknown	1203	427	776	1.15	3.46	82.28	-0.0034
398	67.005	-49.035	fracture	1202	381	821	0.95	2.30	74.62	0.0061
399	67.005	-49.036	fracture	1202	381	821	0.95	2.30	74.62	0.0061
400	66.998	-49.165	crevasses	1133	200	933	0.27	1.11	94.36	0.0040
401	67.006	-49.174	crevasses	1136	198	938	0.51	2.20	94.29	0.0017
402	66.996	-49.194	crevasses	1128	206	922	0.77	1.02	96.96	-0.0007
403	67.015	-49.118	crevasses	1158	195	963	0.61	3.49	76.87	0.0024
404	67.019	-49.122	crevasses	1163	174	989	0.54	1.29	77.71	0.0057

405	67.002	-49.199	crevasses	1126	203	923	1.10	0.97	85.81	-0.0018
406	67.036	-49.289	crevasses	1101	148	953	1.16	3.78	75.71	0.0011
407	66.989	-49.209	crevasses	1110	175	935	0.77	1.90	98.22	-0.0010
408	66.966	-48.938	crevasses	1271	378	893	0.74	6.64	86.99	0.0056
409	66.966	-48.938	crevasses	1271	378	893	0.74	6.64	86.99	0.0056
410	66.970	-48.945	crevasses	1269	351	918	0.77	5.40	89.00	0.0060
411	66.973	-48.958	crevasses	1264	392	872	0.92	5.82	91.67	0.0026
412	66.982	-48.893	fracture	1299	370	929	0.39	4.28	82.11	0.0037
413	66.916	-48.935	fracture	1265	245	1020	0.61	5.87	94.20	0.0017
414	66.949	-48.971	crevasses	1250	531	719	0.14	3.73	89.15	0.0030
415	66.949	-48.971	crevasses	1250	531	719	0.14	3.73	89.15	0.0030
416	66.928	-49.034	crevasses	1205	289	916	1.62	5.53	88.26	-0.0098
417	66.955	-49.103	crevasses	1159	294	865	1.24	6.44	69.07	-0.0003
418	66.951	-49.021	crevasses	1209	513	696	0.48	2.59	95.84	0.0047
419	66.911	-49.034	crevasses	1208	263	945	0.58	1.91	92.59	-0.0040
420	66.914	-49.073	crevasses	1182	235	947	0.29	5.94	80.69	-0.0013
421	66.914	-49.072	crevasses	1182	235	947	0.29	5.94	80.69	-0.0013
422	66.899	-49.361	crevasses	995	486	509	0.70	7.29	86.42	0.0037
423	66.922	-49.317	crevasses	1042	491	551	0.97	2.71	85.14	0.0009
424	66.929	-49.362	crevasses	1001	504	497	0.07	2.01	86.50	0.0018
425	66.892	-49.318	crevasses	1025	538	487	2.57	1.89	73.96	0.0018
426	66.880	-49.350	crevasses	995	468	527	0.77	5.24	79.66	0.0002
427	66.843	-48.891	crevasses	1270	172	1098	0.30	5.15	103.25	0.0025
428	66.879	-48.937	fracture	1263	357	906	0.61	1.08	92.22	0.0029
429	66.879	-48.936	fracture	1263	361	902	0.24	2.06	92.22	0.0029
430	66.876	-48.969	crevasses	1236	363	873	1.49	3.01	89.59	-0.0107
431	66.768	-49.258	crevasses	1037	420	617	0.81	5.73	98.82	-0.0032
432	66.806	-49.354	crevasses	973	250	723	0.57	4.46	148.86	0.0037
433	66.738	-49.210	crevasses	1060	393	667	0.68	2.32	53.19	-0.0036
434	66.738	-49.213	crevasses	1059	408	651	0.85	6.30	53.19	0.0005
435	66.711	-49.207	crevasses	1047	498	549	0.92	3.91	49.79	0.0021
436	66.688	-49.083	crevasses	1145	481	664	1.51	4.17	50.76	0.0057
437	66.688	-49.083	crevasses	1145	481	664	1.51	4.17	50.76	0.0057
438	66.775	-48.850	crevasses	1268	166	1102	0.34	2.26	75.84	0.0015
439	66.791	-48.892	crevasses	1254	212	1042	0.97	7.33	94.02	-0.0019
440	66.789	-48.893	crevasses	1255	195	1060	1.00	0.91	94.02	-0.0024
441	66.757	-48.847	unknown	1287	218	1069	0.34	5.82	72.55	0.0050
442	66.758	-48.847	unknown	1286	210	1076	0.64	5.96	71.98	0.0053
443	66.737	-48.864	fracture	1279	418	861	1.11	4.16	75.37	-0.0018
444	66.756	-48.898	unknown	1268	365	903	0.19	4.79	78.89	0.0025
445	66.764	-48.915	crevasses	1254	400	854	0.43	4.31	78.25	0.0032
446	66.738	-48.959	fracture	1191	349	842	0.92	4.92	70.05	-0.0025
447	66.726	-49.133	crevasses	1115	503	612	0.70	2.72	65.99	-0.0029
448	66.731	-49.106	crevasses	1152	532	620	1.12	3.18	67.46	0.0040
449	66.735	-49.060	unknown	1158	361	797	1.18	5.25	59.90	0.0013
450	66.735	-49.060	unknown	1158	361	797	1.18	5.25	59.90	0.0013
451	66.751	-49.080	crevasses	1155	351	804	0.73	7.41	65.37	0.0018
452	66.764	-49.112	fracture	1128	403	725	1.05	5.37	87.65	0.0001
453	66.774	-49.138	crevasses	1110	309	801	1.00	8.10	109.80	0.0029
454	66.805	-49.105	crevasses	1146	187	959	1.22	3.14	130.49	0.0082
455	66.813	-49.046	unknown	1175	133	1042	0.75	1.53	112.39	0.0011
456	66.814	-49.050	unknown	1174	136	1038	0.64	1.72	117.94	0.0029
457	66.822	-49.023	unknown	1188	99	1089	0.57	0.36	107.59	-0.0022
458	66.820	-49.028	unknown	1185	104	1081	0.77	1.52	107.59	-0.0026
459	66.829	-49.041	unknown	1184	157	1027	0.24	5.25	108.61	-0.0030
460	66.806	-48.961	crevasses	1216	239	977	0.34	2.17	106.28	0.0082
461	66.812	-48.946	crevasses	1210	220	990	0.73	2.46	100.27	0.0088
462	66.811	-48.939	crevasses	1208	242	966	0.94	3.95	100.27	0.0082
463	66.816	-48.936	crevasses	1204	251	953	0.28	6.90	99.47	0.0064
464	66.815	-48.936	crevasses	1204	251	953	0.28	6.90	99.47	0.0066

465	66.816	-48.936	crevasses	1204	251	953	0.28	6.90	99.47	0.0064
466	66.815	-48.945	crevasses	1205	220	985	0.28	3.95	103.80	0.0090
467	66.825	-48.976	crevasses	1207	104	1103	0.61	0.82	109.93	0.0002
468	66.858	-48.990	drained lake; crevasses	1198	288	910	0.27	2.16	93.58	-0.0033
469	66.858	-48.990	drained lake; crevasses	1198	288	910	0.27	2.16	93.58	-0.0033
470	66.845	-49.027	crevasses	1197	308	889	0.75	2.43	96.93	0.0012
471	66.834	-49.058	crevasses	1183	238	945	0.61	5.81	97.02	-0.0027
472	66.842	-49.062	crevasses	1177	302	875	1.12	3.72	85.82	0.0011
473	66.848	-49.067	crevasses	1182	300	882	0.84	6.03	89.53	0.0016
474	66.849	-49.165	crevasses	1130	520	610	0.34	2.82	88.63	-0.0008
475	66.868	-49.038	crevasses	1172	288	884	0.64	7.44	78.64	-0.0040
476	66.869	-49.037	crevasses	1172	288	884	0.64	7.44	78.64	-0.0040
477	66.874	-49.074	crevasses	1170	292	878	0.21	9.46	79.27	-0.0026
478	66.868	-49.164	crevasses	1139	470	669	0.34	2.44	83.42	0.0025
479	66.872	-49.160	crevasses	1140	436	704	0.88	5.59	84.15	0.0024
480	66.863	-49.192	crevasses	1115	488	627	0.51	3.57	80.49	-0.0024
481	66.845	-49.234	crevasses	1073	538	535	0.81	3.74	85.28	0.0024
482	66.877	-49.220	crevasses	1110	465	645	0.28	3.70	88.72	0.0016
483	66.875	-49.261	crevasses	1090	512	578	0.94	5.86	91.17	0.0093
484	66.860	-49.319	crevasses	999	425	574	1.70	0.56	84.45	0.0033
485	66.841	-49.298	crevasses	1035	512	523	0.67	4.80	93.33	0.0043
486	66.846	-49.287	crevasses	1035	509	526	0.97	2.73	93.40	-0.0022
487	66.837	-49.353	crevasses	982	506	476	1.60	1.07	92.37	-0.0006
488	66.808	-49.286	crevasses	1032	275	757	0.54	3.96	144.90	0.0034
489	66.805	-49.274	crevasses	1036	253	783	0.24	4.48	140.19	0.0055
490	66.803	-49.270	crevasses	1038	256	782	0.48	3.34	132.68	0.0042
491	66.794	-49.358	crevasses	991	321	670	0.62	6.30	147.60	0.0064
492	66.800	-49.350	crevasses	986	273	713	0.94	2.86	148.42	0.0022
493	66.801	-49.348	crevasses	983	267	716	1.20	2.24	148.42	0.0022
494	66.776	-49.191	crevasses	1087	351	736	0.61	10.95	116.41	0.0067
495	66.758	-49.186	crevasses	1094	464	630	0.72	4.90	89.73	0.0021
496	66.754	-49.222	crevasses	1053	439	614	0.21	3.06	82.24	0.0016
497	66.779	-49.271	crevasses	1027	344	683	0.91	2.90	125.64	-0.0039
498	66.794	-49.274	crevasses	1022	262	760	0.90	2.55	133.78	0.0033
499	66.728	-49.333	crevasses	924	380	544	0.77	2.25	55.60	0.0035
500	66.716	-49.324	crevasses	935	465	470	0.27	3.55	45.50	0.0016
501	66.730	-49.315	crevasses	940	403	537	1.31	4.56	47.09	0.0010
502	66.740	-49.334	crevasses	926	472	454	0.70	5.35	86.82	-0.0011
503	66.728	-49.182	crevasses	1064	512	552	2.12	3.92	59.36	-0.0057
504	66.637	-48.979	crevasses	1148	476	672	1.55	2.12	35.09	-0.0043
505	66.632	-48.974	crevasses	1151	507	644	0.82	6.71	38.87	-0.0035
506	66.618	-48.922	crevasses	1193	518	675	0.94	11.47	48.80	0.0043
507	66.692	-49.031	fracture	1172	336	836	0.38	4.12	52.70	0.0003
508	66.688	-49.036	fracture	1172	388	784	0.15	6.32	49.03	0.0001
509	66.651	-49.034	crevasses	1149	593	556	1.39	3.34	33.75	0.0004
510	66.662	-49.089	crevasses	1117	678	439	2.96	5.95	26.36	0.0038
511	66.659	-49.052	crevasses	1141	639	502	2.07	5.58	26.92	0.0003
512	66.653	-49.074	unknown	1117	624	493	1.37	3.95	30.49	0.0041
513	66.645	-49.124	crevasses	1067	692	375	0.53	1.88	49.33	0.0016
514	66.622	-49.099	crevasses	1097	525	572	1.27	7.09	53.82	0.0004
515	66.632	-49.065	crevasses	1131	569	562	0.70	5.50	42.48	0.0024
516	66.673	-49.116	crevasses	1116	713	403	2.26	9.16	42.12	0.0042
517	66.706	-49.065	crevasses	1160	417	743	0.39	9.25	56.48	0.0035
518	66.704	-49.060	crevasses	1160	372	788	0.14	6.45	55.00	0.0029
519	66.698	-49.212	crevasses	1021	457	564	0.48	6.44	48.85	0.0034
520	66.690	-49.235	crevasses	1010	483	527	0.88	4.33	55.23	0.0035
521	66.686	-49.172	crevasses	1054	559	495	0.58	7.66	48.29	0.0032
522	66.665	-49.185	crevasses	996	550	446	1.60	1.97	39.30	-0.0020
523	66.664	-49.186	crevasses	992	545	447	1.03	1.35	39.30	-0.0008
524	66.678	-49.196	crevasses	1015	590	425	1.33	0.79	33.14	-0.0007

525	66.665	-49.141	crevasses	1053	704	349	1.08	2.68	39.19	-0.0032
526	66.668	-49.155	crevasses	1041	672	369	0.47	2.14	37.47	-0.0008
527	66.659	-49.191	crevasses	990	563	427	0.91	5.75	56.33	0.0022
528	66.644	-49.242	crevasses	953	451	502	0.20	2.50	46.48	-0.0021
529	66.626	-49.277	crevasses	935	375	560	0.54	3.45	46.85	0.0018
530	66.632	-49.268	crevasses	939	417	522	1.07	3.93	45.55	0.0037
531	66.647	-49.328	crevasses	916	486	430	2.23	8.50	43.21	0.0006
532	66.665	-49.332	crevasses	905	533	372	3.07	9.82	40.98	0.0059
533	66.685	-49.347	crevasses	905	371	534	0.81	3.37	41.68	0.0004
534	66.687	-49.310	crevasses	917	390	527	1.30	8.54	40.09	-0.0013
535	66.676	-49.295	crevasses	913	391	522	0.64	3.44	37.47	0.0026
536	66.674	-49.287	crevasses	916	411	505	0.64	2.08	37.48	-0.0020
537	66.669	-49.287	crevasses	919	433	486	0.39	3.72	42.90	0.0017
538	66.662	-49.279	crevasses	935	506	429	1.99	5.81	42.96	-0.0014
539	66.667	-49.239	crevasses	974	574	400	1.97	3.93	38.99	0.0086
540	66.659	-49.239	crevasses	966	575	391	1.28	3.68	51.94	-0.0028
541	66.696	-49.284	crevasses	950	480	470	0.36	2.50	41.91	-0.0030
542	67.126	-48.099	fracture	1561	325	1236	0.58	0.49	75.79	0.0016
543	67.125	-48.099	fracture	1561	325	1236	0.58	0.49	75.79	0.0016
544	67.123	-48.098	fracture	1562	327	1235	0.38	0.41	75.79	0.0014
545	67.107	-48.153	unknown	1553	343	1210	0.30	1.36	79.34	0.0047
546	67.088	-48.156	crevasses	1551	305	1246	0.28	1.24	83.90	0.0037
547	67.124	-48.026	unknown	1576	290	1286	0.24	0.95	73.47	0.0014
548	67.075	-48.197	fracture	1543	283	1260	0.36	1.48	83.04	0.0033
549	67.001	-48.311	crevasses	1518	106	1412	0.61	1.07	91.54	0.0016
550	67.001	-48.316	crevasses	1515	105	1410	0.69	0.49	91.54	0.0014
551	67.004	-48.311	fracture	1516	106	1410	0.54	1.97	90.26	0.0018
552	67.001	-48.328	crevasses	1511	115	1396	0.64	2.63	90.07	0.0005
553	66.999	-48.296	crevasses	1523	111	1412	0.41	2.16	89.21	0.0003
554	67.005	-48.237	fracture	1528	156	1372	0.54	1.69	86.46	0.0002
555	67.000	-48.238	drained lake; fracture	1524	173	1351	0.19	4.05	85.57	0.0011
556	66.999	-48.244	drained lake; fracture	1524	175	1349	0.34	4.27	85.87	0.0015
557	67.003	-48.246	drained lake	1526	153	1373	0.30	1.15	86.96	0.0008
558	66.999	-48.236	drained lake; fracture	1524	190	1334	0.21	4.73	84.98	0.0015
559	66.998	-48.237	drained lake; fracture	1524	190	1334	0.21	4.73	84.98	0.0015
560	66.998	-48.237	drained lake; fracture	1524	190	1334	0.21	4.73	84.98	0.0015
561	67.008	-48.233	fracture	1531	157	1374	0.39	0.82	86.46	0.0006
562	66.892	-48.308	crevasses	1518	425	1093	0.43	2.97	83.42	0.0024
563	66.922	-48.205	drained lake; fracture	1558	253	1305	0.21	4.67	75.97	0.0015
564	66.922	-48.203	drained lake; fracture	1557	244	1313	0.15	4.28	75.97	0.0013
565	66.926	-48.209	drained lake; fracture	1556	242	1314	0.34	4.03	77.25	0.0029
566	66.952	-48.204	crevasses	1549	189	1360	0.19	2.30	77.68	0.0024
567	66.934	-48.119	drained lake; fracture	1567	219	1348	0.51	1.57	79.13	-0.0010
568	66.934	-48.119	drained lake; fracture	1567	216	1351	0.49	1.49	78.13	0.0002
569	66.934	-48.122	drained lake; fracture	1567	216	1351	0.49	1.49	78.13	0.0002
570	66.934	-48.119	drained lake; fracture	1567	219	1348	0.51	1.57	79.13	-0.0010
571	66.942	-48.110	drained lake; fracture	1575	213	1362	0.48	2.39	79.06	-0.0017
572	66.871	-48.134	drained lake; fracture	1564	272	1292	0.41	2.02	75.83	0.0001
573	66.871	-48.135	drained lake; fracture	1563	267	1296	0.41	1.62	75.83	0.0001
574	66.869	-48.128	drained lake; fracture	1567	271	1296	0.54	2.97	75.64	-0.0007
575	67.074	-47.903	drained lake	1603	180	1423	0.20	0.54	74.58	0.0022
576	67.070	-47.904	drained lake	1603	186	1417	0.00	0.49	74.77	0.0024
577	66.876	-48.185	drained lake; fracture	1552	285	1267	0.07	2.97	75.39	0.0002
578	66.962	-47.927	fracture	1634	191	1443	0.21	2.05	80.59	0.0016
579	66.962	-47.927	fracture	1634	191	1443	0.21	2.05	80.59	0.0016
580	66.962	-47.927	fracture	1634	191	1443	0.21	2.05	80.59	0.0016
581	66.962	-47.927	fracture	1634	191	1443	0.21	2.05	80.59	0.0016
582	66.963	-47.926	fracture	1634	196	1438	0.19	2.31	80.59	0.0016
583	66.963	-47.926	fracture	1635	199	1436	0.43	2.33	80.59	0.0016
584	66.963	-47.925	fracture	1635	199	1436	0.43	2.33	80.59	0.0016

585	67.153	-49.641	crevasses	929	74	855	1.69	14.08	126.72	-0.0051
586	67.213	-49.639	crevasses	924	223	701	0.20	4.23	81.19	-0.0005
587	67.292	-49.377	crevasses	1088	453	635	0.21	8.10	65.18	0.0044
588	67.210	-49.514	crevasses	1017	87	930	1.15	8.51	86.05	-0.0038
589	67.163	-49.481	crevasses	1028	176	852	0.73	4.07	128.75	0.0002
590	67.115	-49.407	crevasses	1057	-22	1079	1.06	5.43	105.86	0.0007
591	67.111	-49.376	crevasses	1067	163	904	0.20	17.50	100.52	0.0009
592	66.994	-49.422	crevasses	998	218	780	0.88	9.08	88.97	-0.0020
593	66.983	-49.400	crevasses	1010	189	821	0.73	5.99	104.38	-0.0064
594	67.320	-49.440	drained lake; fracture	1055	383	672	0.62	0.30	67.97	-0.0012
595	67.358	-49.449	crevasses	1048	511	537	1.03	4.28	57.95	0.0024
596	67.375	-49.434	crevasses	1045	559	486	0.70	2.77	51.09	-0.0011
597	67.436	-49.367	crevasses	1091	556	535	0.54	3.81	48.50	0.0023
598	67.470	-49.391	crevasses	1075	500	575	1.55	3.29	55.03	0.0032
599	67.486	-49.371	crevasses	1083	452	631	1.12	7.36	57.04	0.0079
600	67.501	-49.379	crevasses	1087	478	609	0.43	3.86	68.98	0.0049
601	67.477	-49.539	crevasses	928	357	571	0.77	2.66	53.08	-0.0026
602	67.564	-49.397	crevasses	1042	500	542	1.24	3.07	77.34	0.0088
603	67.607	-49.429	crevasses	1003	457	546	0.34	1.75	66.99	0.0020
604	67.598	-49.403	crevasses	1030	450	580	0.34	1.96	71.44	0.0015
605	67.192	-49.855	crevasses	770	-119	889	1.28	7.60	98.28	0.0038
606	67.204	-49.870	crevasses	756	130	626	1.02	22.34	77.25	-0.0001
607	67.075	-47.885	drained lake; fracture	1605	185	1420	0.19	1.35	73.20	0.0014
608	67.075	-47.886	drained lake; fracture	1605	185	1420	0.19	1.35	73.20	0.0014
609	67.085	-47.896	fracture	1606	186	1420	0.34	1.03	72.24	0.0014
610	67.079	-47.888	drained lake; fracture	1604	179	1425	0.28	1.24	73.05	0.0006
611	67.234	-48.068	fracture	1556	225	1331	0.24	0.82	64.78	0.0030
612	67.241	-47.983	unknown	1571	206	1365	0.51	0.81	56.93	0.0021
613	67.216	-48.025	fracture	1566	245	1321	0.14	1.83	66.31	0.0024
614	67.190	-47.957	drained lake; fracture	1576	207	1369	0.34	0.28	64.93	0.0009
615	67.225	-48.156	unknown	1539	240	1299	0.51	0.91	71.86	0.0010
616	67.246	-48.159	fracture	1536	235	1301	0.15	0.75	67.51	0.0021
617	67.366	-48.129	drained lake; fracture	1545	286	1259	0.30	0.61	55.49	0.0014
618	67.449	-48.337	drained lake; fracture	1497	298	1199	0.15	0.47	51.02	-0.0003
619	67.445	-48.260	fracture	1518	277	1241	1.15	1.06	53.76	-0.0002
620	67.264	-47.977	drained lake	1570	203	1367	0.74	1.68	53.05	0.0016
621	67.302	-47.573	fracture	1706	343	1363	0.41	1.50	47.91	0.0020
622	67.285	-48.324	drained lake; fracture	1494	235	1259	0.07	1.40	68.83	0.0028
623	67.285	-48.324	drained lake; fracture	1495	240	1255	0.19	0.88	68.83	0.0028
624	67.191	-47.955	drained lake	1577	208	1369	0.34	0.28	64.93	0.0005
625	67.201	-48.087	drained lake; fracture	1554	306	1248	0.38	0.90	70.53	-0.0005
626	67.292	-47.948	unknown	1587	299	1288	0.43	1.58	54.93	0.0011
627	67.288	-47.893	fracture	1600	281	1319	0.43	1.44	53.82	0.0015
628	67.251	-48.051	unknown	1558	211	1347	0.15	0.15	60.55	0.0041
629	67.250	-48.038	fracture	1558	211	1347	0.15	0.15	58.79	0.0028
630	67.255	-48.036	unknown	1558	212	1346	0.19	0.43	57.27	0.0023
631	67.375	-47.545	crevasses	1718	243	1475	0.24	0.41	43.24	0.0002
632	67.379	-49.474	crevasses	1024	603	421	1.80	0.97	52.50	-0.0029
633	67.382	-49.462	crevasses	1028	604	424	0.94	1.30	53.36	-0.0001
634	67.269	-48.217	fracture	1526	294	1232	0.21	0.77	67.20	0.0047
635	67.382	-49.462	crevasses	1027	607	420	1.91	1.33	53.36	-0.0001
636	67.376	-49.461	crevasses	1032	590	442	0.43	1.92	52.95	0.0030
637	67.290	-49.383	crevasses	1091	449	642	0.73	8.03	70.66	0.0056
638	67.220	-48.251	fracture	1521	264	1257	0.24	0.68	80.48	0.0022
639	67.299	-48.035	drained lake	1567	316	1251	0.21	1.09	54.99	-0.0003
640	67.293	-48.030	drained lake; fracture	1567	301	1266	0.34	1.46	54.84	0.0007
641	67.299	-48.016	drained lake; fracture	1571	319	1252	0.21	1.22	55.11	0.0007
642	67.184	-49.989	crevasses	661	-139	800	0.67	11.18	106.87	0.0009
643	67.219	-49.806	crevasses	802	344	458	0.49	1.55	56.99	0.0009
644	67.291	-47.545	drained lake; fracture	1705	318	1387	0.34	1.15	46.52	0.0001

645	67.291	-47.539	drained lake	1708	315	1393	0.53	0.95	46.52	0.0006
646	67.289	-47.532	drained lake	1710	313	1397	0.57	0.88	46.48	0.0013
647	67.287	-47.530	drained lake	1710	315	1395	0.67	0.47	47.05	0.0012
648	67.284	-47.533	drained lake	1710	317	1393	0.58	0.61	46.89	0.0004
649	67.290	-47.535	drained lake	1709	313	1396	0.38	1.22	46.48	0.0013
650	67.286	-47.530	drained lake	1710	316	1394	0.62	0.54	47.05	0.0008
651	67.285	-47.531	drained lake	1710	316	1394	0.62	0.54	47.05	0.0008
652	67.282	-47.534	drained lake	1709	319	1390	0.53	0.49	46.89	0.0004
653	67.281	-47.539	drained lake	1708	321	1387	0.57	0.19	46.22	0.0000
654	67.303	-47.573	fracture	1706	343	1363	0.41	1.50	47.91	0.0020
655	67.293	-47.578	fracture	1700	345	1355	0.27	1.22	47.99	0.0023
656	67.307	-47.938	drained lake; fracture	1590	357	1233	0.68	1.72	55.76	0.0024
657	67.307	-47.938	drained lake; fracture	1590	353	1237	0.64	1.87	55.76	0.0024
658	67.307	-47.934	drained lake	1592	356	1236	0.54	1.88	55.76	0.0014
659	67.306	-47.938	drained lake; fracture	1590	353	1237	0.64	1.87	55.76	0.0024
660	67.300	-48.013	drained lake; fracture	1571	323	1248	0.34	1.47	55.11	0.0013
661	67.333	-48.090	drained lake; fracture	1548	342	1206	0.30	1.10	54.90	0.0013
662	67.334	-48.090	drained lake; fracture	1547	339	1208	0.21	0.96	54.90	0.0015
663	67.288	-48.327	drained lake; fracture	1494	228	1266	0.00	1.10	68.54	0.0029
664	67.287	-48.326	drained lake; fracture	1494	231	1263	0.00	1.30	68.54	0.0029
665	67.286	-48.329	drained lake; fracture	1494	235	1259	0.19	1.31	68.83	0.0028
666	67.215	-48.364	unknown	1494	207	1287	0.19	1.58	80.64	0.0031
667	67.200	-48.387	fracture	1482	215	1267	0.28	0.56	82.79	0.0007
668	67.192	-48.304	fracture	1504	263	1241	0.27	0.68	79.41	0.0025
669	67.192	-48.304	fracture	1503	264	1239	0.21	0.81	81.76	0.0019
670	67.199	-48.387	fracture	1481	213	1268	0.36	1.42	82.79	0.0007
671	67.231	-48.170	fracture	1533	232	1301	0.19	0.69	71.30	0.0012
672	67.227	-48.164	fracture	1535	233	1302	0.39	0.81	72.60	0.0013
673	67.228	-48.165	fracture	1534	233	1301	0.43	0.86	71.30	0.0013
674	67.202	-48.086	drained lake; fracture	1554	306	1248	0.38	0.90	70.53	-0.0005
675	67.204	-48.096	drained lake; fracture	1551	296	1255	0.28	1.41	70.38	0.0009
676	67.204	-48.096	drained lake; fracture	1551	296	1255	0.28	1.41	70.38	0.0009
677	67.227	-48.159	unknown	1537	237	1300	0.43	0.76	71.86	0.0012
678	67.227	-48.165	fracture	1535	233	1302	0.39	0.81	72.60	0.0013
679	67.291	-49.382	crevasses	1089	460	629	0.62	8.35	70.66	0.0056
680	67.245	-49.620	crevasses	935	415	520	0.81	5.69	58.05	0.0004
681	67.239	-49.691	crevasses	878	376	502	1.02	7.35	55.81	-0.0029
682	67.235	-49.711	crevasses	859	333	526	1.40	8.90	56.00	0.0032
683	67.229	-49.703	crevasses	853	291	562	1.02	1.50	57.52	0.0026
684	67.228	-49.707	crevasses	860	291	569	2.16	1.90	57.52	0.0042
685	67.220	-49.725	crevasses	862	319	543	1.84	8.30	68.81	-0.0033
686	67.221	-49.876	crevasses	748	452	296	0.28	5.70	44.51	-0.0047
687	67.201	-49.895	crevasses	749	26	723	0.49	14.29	97.45	0.0085
688	67.212	-49.896	crevasses	744	400	344	0.10	13.18	51.58	-0.0030
689	67.223	-49.904	crevasses	731	462	269	1.22	5.42	39.05	-0.0009
690	67.223	-49.950	crevasses	688	524	164	1.73	2.16	31.30	-0.0028
691	67.220	-49.963	crevasses	672	506	166	1.58	7.35	36.41	-0.0024
692	67.218	-49.982	crevasses	648	480	168	1.99	5.16	39.42	-0.0013
693	67.190	-49.998	crevasses	656	-94	750	1.30	13.13	105.37	0.0003
694	67.189	-50.033	crevasses	615	-75	690	1.30	10.48	97.25	-0.0029
695	67.188	-50.059	crevasses	589	-72	661	0.95	7.94	91.64	-0.0077
696	67.212	-50.056	crevasses	576	390	186	0.36	13.77	25.11	-0.0027
697	67.218	-50.043	crevasses	583	495	88	1.16	1.30	29.11	-0.0062
698	67.211	-50.011	crevasses	629	415	214	1.77	7.92	43.90	-0.0026
699	67.197	-50.083	crevasses	566	157	409	1.39	13.15	63.04	0.0000
700	67.177	-50.224	crevasses	423	196	227	2.56	4.43	44.74	-0.0023
701	67.172	-50.069	crevasses	569	196	373	0.88	7.99	48.58	0.0013
702	67.171	-50.022	crevasses	614	219	395	1.63	7.95	31.14	-0.0029
703	67.178	-49.575	crevasses	986	327	659	0.34	3.03	115.84	0.0042
704	67.175	-49.585	crevasses	982	333	649	1.08	1.56	123.03	0.0027

705	67.174	-49.528	crevasses	1004	307	697	0.30	5.32	122.67	0.0039
706	67.163	-49.511	crevasses	1014	185	829	0.48	4.23	128.10	0.0005
707	67.187	-49.495	crevasses	1030	278	752	0.61	3.48	110.05	0.0016
708	67.194	-49.482	crevasses	1045	278	767	1.15	3.92	101.28	0.0052
709	67.283	-47.532	drained lake	1711	319	1392	0.58	0.61	46.89	0.0004
710	67.172	-49.528	crevasses	1005	287	718	0.39	7.81	122.67	0.0039
711	67.177	-50.215	crevasses	433	167	266	1.17	8.75	47.67	-0.0028
712	67.287	-47.743		1642	251	1391	0.34	0.54	50.63	0.0004
713	67.250	-48.038	fracture	1558	211	1347	0.15	0.15	58.79	0.0029
714	67.250	-48.038	fracture	1558	211	1347	0.07	0.07	58.79	0.0029
715	67.384	-47.697		1662	263	1399	0.34	1.49	47.98	0.0006
716	67.385	-47.697		1662	262	1400	0.34	1.49	47.98	0.0006
717	67.369	-47.860	drained lake	1611	294	1317	0.38	0.38	50.20	0.0002
718	67.380	-47.926	fracture	1589	274	1315	0.34	1.27	50.01	-0.0008
719	67.422	-47.970	fracture	1585	226	1359	0.00	0.69	51.30	0.0018
720	67.447	-47.834	fracture	1622	241	1381	0.34	0.62	47.42	0.0005
721	67.447	-47.827		1624	244	1380	0.24	0.41	46.34	0.0009
722	67.482	-47.743		1649	216	1433	0.19	0.34	45.60	0.0002
723	67.533	-47.870	fracture	1624	154	1470	0.28	5.70	45.22	0.0002
724	67.564	-47.586	unknown	1685	121	1564	0.72	1.69	42.57	-0.0012
725	67.370	-47.963	fracture	1586	305	1281	0.20	1.27	51.76	0.0017
726	67.040	-47.757		1651	211	1440	0.15	1.96	67.24	0.0022
727	67.030	-47.766		1653	232	1421	0.30	1.08	69.26	0.0043
728	67.055	-47.877	drained lake; fracture	1609	227	1382	0.19	1.26	75.05	0.0020
729	67.056	-47.879	drained lake; fracture	1609	227	1382	0.19	1.26	75.05	0.0020
730	67.054	-47.877	drained lake; fracture	1609	227	1382	0.19	1.26	75.05	0.0020
731	66.922	-47.799	drained lake	1652	233	1419	0.34	0.73	76.48	0.0017
732	66.923	-47.797	drained lake; fracture	1653	235	1418	0.21	0.95	76.48	0.0017
733	66.924	-47.797	drained lake; fracture	1653	235	1418	0.21	0.95	76.48	0.0017
734	66.821	-47.803	drained lake; fracture	1677	289	1388	0.19	3.10	75.00	-0.0021
735	66.821	-47.803	drained lake; fracture	1677	289	1388	0.19	3.10	75.00	-0.0021
736	66.814	-47.811	drained lake; fracture	1675	296	1379	0.27	1.39	75.50	0.0009
737	66.792	-47.827	drained lake; fracture	1669	271	1398	0.19	0.43	74.95	0.0009
738	66.790	-47.831	drained lake; fracture	1670	272	1398	0.28	0.19	73.57	0.0000
739	66.753	-48.062	fracture	1590	316	1274	0.58	3.58	62.49	-0.0003
740	66.680	-48.234	drained lake	1559	358	1201	0.24	1.18	42.43	-0.0009
741	66.679	-48.233	drained lake; fracture	1559	359	1200	0.21	1.24	41.43	-0.0007
742	66.677	-48.226	drained lake; fracture	1561	368	1193	0.19	1.48	42.61	-0.0018
743	66.677	-48.226	drained lake; fracture	1561	368	1193	0.19	1.48	42.61	-0.0018
744	66.628	-48.387	drained lake	1504	517	987	0.21	1.48	46.70	0.0008
745	66.635	-48.304	drained lake; fracture	1530	438	1092	0.19	2.10	43.64	-0.0006
746	66.637	-48.303	drained lake; fracture	1530	429	1101	0.19	2.30	43.64	-0.0006
747	66.633	-48.305	drained lake; fracture	1531	445	1086	0.41	1.76	43.45	-0.0006
748	66.635	-48.257	unknown	1548	432	1116	0.75	0.64	44.13	0.0003
749	66.685	-48.231	drained lake; fracture	1559	360	1199	0.34	1.12	44.60	-0.0007
750	66.680	-48.245	drained lake	1557	352	1205	0.45	0.96	42.56	0.0012
751	66.677	-48.225	drained lake; fracture	1561	371	1190	0.24	1.45	42.61	-0.0018
752	66.677	-48.224	drained lake; fracture	1561	371	1190	0.24	1.45	42.61	-0.0018
753	66.683	-48.249	drained lake	1555	352	1203	0.41	0.30	42.56	0.0017
754	66.687	-48.247	drained lake; fracture	1552	350	1202	0.61	0.61	42.99	0.0004
755	66.686	-48.249	drained lake; fracture	1554	354	1200	0.68	0.58	42.99	0.0017
756	66.685	-48.232	drained lake; fracture	1559	360	1199	0.34	1.12	44.60	-0.0007
757	66.683	-48.264	drained lake	1551	360	1191	0.61	1.83	43.41	0.0042
758	66.676	-48.277	drained lake; fracture	1552	357	1195	0.43	2.18	45.14	0.0030
759	66.725	-48.357	fracture	1489	522	967	0.73	1.60	67.49	0.0020
760	66.686	-48.294	unknown	1545	444	1101	0.07	5.66	48.07	0.0003
761	66.709	-48.121	drained lake; fracture	1592	350	1242	0.28	2.30	50.60	0.0002
762	66.714	-48.118	drained lake; fracture	1590	329	1261	0.47	1.67	51.44	0.0010
763	66.728	-48.121	fracture	1581	345	1236	0.30	3.20	54.62	0.0005
764	66.727	-48.116	fracture	1582	338	1244	0.58	2.64	54.62	0.0010

765	66.726	-48.116	fracture	1582	338	1244	0.58	2.64	54.62	0.0010
766	66.783	-47.648	fracture	1724	259	1465	0.53	5.05	68.97	0.0005
767	66.769	-48.128	drained lake	1564	312	1252	0.07	3.05	65.77	0.0003
768	66.762	-47.978	fracture	1623	395	1228	0.58	2.38	64.76	0.0009
769	66.762	-47.977	fracture	1625	398	1227	0.77	2.37	64.76	0.0004
770	66.763	-47.975	fracture	1625	403	1222	0.73	1.56	64.76	0.0001
771	66.764	-47.973	fracture	1627	404	1223	0.79	1.35	64.76	0.0001
772	66.764	-47.972	fracture	1627	404	1223	0.79	1.35	65.85	-0.0006
773	66.765	-47.971	fracture	1628	408	1220	0.88	0.88	65.85	-0.0006
774	66.776	-47.903	drained lake; crevasses	1648	332	1316	0.14	2.82	68.55	0.0017
775	66.775	-47.905	drained lake; crevasses	1648	340	1308	0.15	3.13	68.55	0.0017
776	66.779	-47.907	drained lake; crevasses	1647	338	1309	0.15	2.81	68.60	0.0026
777	66.779	-47.917	drained lake; crevasses	1646	361	1285	0.15	4.07	68.60	0.0030
778	66.775	-47.906	drained lake; crevasses	1648	342	1306	0.15	3.52	67.31	0.0015
779	66.759	-47.942	fracture	1642	379	1263	0.53	4.62	64.21	0.0007
780	66.805	-47.673	drained lake; fracture	1717	284	1433	0.53	3.87	76.75	-0.0005
781	66.806	-47.672	drained lake; fracture	1719	283	1436	0.58	3.82	76.75	-0.0005
782	66.804	-47.675	drained lake; fracture	1717	274	1443	0.48	3.82	74.68	-0.0005
783	66.820	-47.805	drained lake; fracture	1677	289	1388	0.21	2.62	75.00	-0.0017
784	66.819	-47.801	drained lake; fracture	1677	294	1383	0.14	2.32	75.00	-0.0019
785	66.819	-47.803	drained lake; fracture	1677	289	1388	0.21	2.62	75.00	-0.0019
786	66.820	-47.805	drained lake; fracture	1677	289	1388	0.21	2.62	75.00	-0.0017
787	66.822	-47.816	drained lake; fracture	1676	267	1409	0.20	2.17	75.04	-0.0020
788	66.808	-47.922	unknown	1655	301	1354	0.10	2.65	75.93	0.0006
789	66.813	-48.163	unknown	1562	325	1237	1.19	1.52	77.18	0.0013
790	66.804	-48.157	fracture	1564	356	1208	0.88	5.85	75.16	0.0041
791	66.769	-48.154	drained lake; fracture	1561	272	1289	0.43	0.57	64.67	-0.0001
792	66.771	-48.150	drained lake; fracture	1563	278	1285	0.43	1.96	66.94	-0.0002
793	66.769	-48.160	drained lake; fracture	1559	272	1287	0.53	0.21	64.67	0.0004
794	66.811	-48.289	fracture	1510	208	1302	0.39	3.60	69.23	0.0031
795	66.775	-48.322	unknown	1507	241	1266	0.57	3.74	68.98	-0.0016
796	66.775	-48.321	unknown	1507	241	1266	0.57	3.74	70.48	-0.0010
797	66.776	-48.324	unknown	1505	228	1277	0.72	2.78	71.72	0.0009
798	66.853	-48.334	drained lake; fracture	1506	330	1176	0.64	4.68	82.19	-0.0009
799	66.827	-48.210	drained lake; fracture	1536	270	1266	0.64	1.30	77.46	-0.0053
800	66.831	-48.213	drained lake; fracture	1532	267	1265	0.49	1.34	76.61	-0.0048
801	66.829	-48.212	drained lake; fracture	1535	271	1264	0.75	1.40	77.46	-0.0047
802	66.834	-48.215	drained lake; fracture	1531	267	1264	0.34	2.63	76.61	-0.0050
803	66.844	-47.889	drained lake; fracture	1654	288	1366	0.21	2.02	74.62	0.0009
804	66.847	-47.885	drained lake	1654	275	1379	0.21	2.62	73.97	0.0030
805	66.873	-47.786	drained lake; fracture	1663	270	1393	0.34	4.59	75.48	-0.0045
806	66.872	-47.795	drained lake; fracture	1662	260	1402	0.27	4.15	73.52	-0.0014
807	66.872	-47.792	drained lake; fracture	1662	265	1397	0.34	4.35	75.48	-0.0026
808	66.877	-47.787	drained lake; fracture	1664	224	1440	0.27	7.02	75.70	-0.0041
809	66.843	-47.573	fracture	1738	243	1495	0.34	4.71	79.46	-0.0003
810	66.837	-47.550	unknown	1744	150	1594	0.34	3.20	61.73	-0.0001
811	66.837	-47.548	unknown	1744	150	1594	0.34	3.20	61.73	-0.0001
812	66.830	-47.445	drained lake	1770	247	1523	0.21	0.91	56.71	-0.0002
813	66.848	-47.393	drained lake; fracture	1785	227	1558	0.21	0.15	53.18	0.0011
814	66.849	-47.393	drained lake; fracture	1785	227	1558	0.21	0.15	53.18	0.0011
815	66.849	-47.391	drained lake; fracture	1785	227	1558	0.21	0.15	53.18	0.0010
816	66.849	-47.391	drained lake; fracture	1785	227	1558	0.21	0.15	53.18	0.0010
817	66.847	-47.391	drained lake; fracture	1785	226	1559	0.27	0.30	53.18	0.0011
818	66.847	-47.392	drained lake; fracture	1785	226	1559	0.27	0.30	53.18	0.0011
819	66.881	-47.644	drained lake; fracture	1695	269	1426	0.24	2.78	80.35	-0.0001
820	66.883	-47.647	drained lake; fracture	1694	261	1433	0.28	4.16	79.06	-0.0002
821	66.887	-47.645	drained lake; fracture	1694	251	1443	0.21	4.52	80.13	-0.0001
822	66.887	-47.644	drained lake; fracture	1694	262	1432	0.14	4.65	80.13	-0.0001
823	66.904	-47.847	drained lake; fracture	1651	156	1495	0.00	1.63	76.69	-0.0009
824	66.904	-47.846	drained lake; fracture	1651	153	1498	0.00	1.88	76.69	-0.0009

825	66.904	-47.846	drained lake; fracture	1651	153	1498	0.00	1.88	76.69	-0.0009
826	66.905	-47.844	drained lake; fracture	1651	159	1492	0.19	2.86	76.69	-0.0009
827	66.904	-47.844	drained lake; fracture	1651	159	1492	0.19	2.86	76.69	-0.0009
828	66.904	-47.846	drained lake; fracture	1651	153	1498	0.00	1.88	76.69	-0.0009
829	66.905	-47.844	drained lake; fracture	1651	159	1492	0.19	2.86	76.69	-0.0009
830	66.904	-47.845	drained lake; fracture	1651	159	1492	0.19	2.86	76.69	-0.0009
831	66.904	-47.845	drained lake; fracture	1651	153	1498	0.00	1.88	76.69	-0.0009
832	66.883	-48.390	fracture	1481	337	1144	0.39	1.26	87.26	0.0027
833	66.919	-48.357	fracture	1495	365	1130	0.39	0.43	83.66	0.0008
834	66.920	-48.358	fracture	1495	365	1130	0.39	0.43	83.66	0.0008
835	66.926	-47.814	drained lake	1655	230	1425	0.28	0.88	77.48	0.0008
836	66.922	-47.808	drained lake	1652	231	1421	0.36	0.14	76.57	0.0003
837	66.946	-47.730	fracture	1672	195	1477	0.20	1.24	73.01	0.0031
838	66.947	-47.727	fracture	1672	198	1474	0.21	0.94	73.01	0.0029
839	66.946	-47.727	fracture	1672	197	1475	0.24	1.51	73.01	0.0029
840	66.945	-47.730	fracture	1671	189	1482	0.21	2.12	73.01	0.0029
841	66.995	-47.401	drained lake; fracture	1760	310	1450	0.19	2.30	44.07	0.0017
842	66.994	-47.403	drained lake; fracture	1759	317	1442	0.34	2.83	44.07	0.0017
843	66.979	-47.748	fracture	1670	244	1426	0.49	1.78	67.76	0.0021
844	66.979	-47.748	fracture	1670	244	1426	0.49	1.78	67.76	0.0021
845	66.966	-47.851	drained lake	1643	210	1433	0.07	1.07	79.33	0.0040
846	66.965	-47.850	drained lake	1643	208	1435	0.21	1.36	79.33	0.0034
847	66.967	-47.845	drained lake; fracture	1643	213	1430	0.00	1.10	77.45	0.0040
848	66.968	-47.845	drained lake; fracture	1643	213	1430	0.00	1.10	77.45	0.0040
849	66.968	-47.845	drained lake; fracture	1643	213	1430	0.00	0.82	77.45	0.0040
850	67.012	-47.812	unknown	1650	226	1424	0.39	2.81	74.00	0.0035
851	67.038	-47.793	fracture	1649	275	1374	0.19	2.45	74.00	0.0033
852	67.038	-47.792	fracture	1649	275	1374	0.19	2.45	74.00	0.0033
853	67.038	-47.792	fracture	1649	268	1381	0.00	2.98	72.72	0.0043
854	67.039	-47.792	fracture	1649	265	1384	0.00	3.29	72.72	0.0043
855	67.361	-48.145	drained lake; fracture	1541	285	1256	0.34	0.54	55.55	0.0028
856	67.361	-48.145	drained lake; fracture	1541	285	1256	0.28	0.54	56.52	0.0030
857	67.362	-48.134	drained lake; fracture	1543	289	1254	0.34	0.61	56.38	0.0023
858	67.362	-48.130	drained lake; fracture	1544	290	1254	0.34	0.61	55.49	0.0015
859	67.362	-48.128	drained lake; fracture	1544	290	1254	0.34	0.61	54.83	0.0015
860	67.364	-48.131	drained lake; fracture	1545	290	1255	0.28	0.61	55.49	0.0015
861	67.343	-48.093	drained lake; fracture	1547	324	1223	0.14	0.73	54.06	-0.0004
862	67.340	-48.086	drained lake; fracture	1547	328	1219	0.21	0.62	53.87	-0.0004
863	67.340	-48.087	drained lake; fracture	1547	329	1218	0.21	0.70	53.87	-0.0004
864	67.318	-48.012	drained lake; fracture	1566	353	1213	0.20	1.63	54.95	0.0005
865	67.318	-48.014	drained lake; fracture	1566	353	1213	0.20	1.63	55.56	0.0009
866	67.401	-47.941	fracture	1588	238	1350	0.15	1.02	48.89	-0.0007
867	67.401	-47.941	fracture	1588	238	1350	0.15	1.02	48.89	-0.0007
868	67.408	-47.995	fracture	1578	244	1334	0.28	0.62	50.57	0.0022
869	67.407	-48.064	drained lake; fracture	1561	249	1312	0.19	0.60	53.05	0.0015
870	67.403	-48.229	fracture	1523	265	1258	0.34	0.90	56.43	0.0010
871	67.448	-48.349	drained lake	1496	294	1202	0.07	0.41	50.77	0.0009
872	67.450	-48.337	drained lake; fracture	1497	298	1199	0.15	0.47	51.02	-0.0003
873	67.449	-48.337	drained lake	1497	298	1199	0.15	0.47	51.02	0.0004
874	67.450	-48.340	drained lake; fracture	1496	296	1200	0.20	0.54	51.02	0.0004
875	67.448	-48.281	fracture	1514	293	1221	0.34	0.85	53.68	0.0007
876	67.461	-48.269	drained lake; fracture	1519	309	1210	0.19	1.11	52.13	0.0040
877	67.461	-48.261	drained lake; fracture	1519	306	1213	0.28	0.88	51.43	0.0044
878	67.461	-48.257	drained lake; fracture	1520	306	1214	0.07	0.95	51.43	0.0030
879	67.463	-48.255	drained lake; fracture	1519	307	1212	0.21	1.15	50.81	0.0028
880	67.465	-48.251	drained lake; fracture	1519	307	1212	0.21	1.22	51.18	0.0002
881	67.466	-48.250	drained lake; fracture	1519	305	1214	0.19	1.08	51.18	0.0002
882	67.466	-48.250	drained lake; fracture	1520	308	1212	0.19	1.08	51.18	0.0002
883	67.477	-48.178	fracture	1546	292	1254	0.21	1.43	50.00	0.0009
884	67.477	-48.179	fracture	1546	292	1254	0.21	1.43	50.00	0.0009

885	67.458	-48.023	drained lake; fracture	1574	230	1344	0.28	0.75	50.97	0.0002
886	67.457	-48.020	drained lake	1574	228	1346	0.27	0.58	51.31	0.0002
887	67.449	-47.987	drained lake; fracture	1577	215	1362	0.19	0.43	49.49	-0.0007
888	67.448	-47.986	drained lake; fracture	1577	213	1364	0.19	0.39	49.49	-0.0007
889	67.448	-47.986	drained lake; fracture	1577	213	1364	0.19	0.39	49.49	-0.0007
890	67.448	-47.990	drained lake; fracture	1577	215	1362	0.19	0.49	49.49	-0.0008
891	67.468	-47.882	fracture	1617	220	1397	0.36	0.14	49.80	0.0028
892	67.468	-47.886	fracture	1616	220	1396	0.43	0.14	49.80	0.0028
893	67.500	-47.841	fracture	1628	319	1309	0.20	3.83	47.38	0.0014
894	67.499	-47.858	fracture	1627	359	1268	0.21	3.86	47.48	0.0020
895	67.504	-47.919	drained lake; fracture	1603	357	1246	0.43	2.99	49.42	-0.0022
896	67.504	-47.922	drained lake; fracture	1602	351	1251	0.54	3.26	48.10	0.0006
897	67.505	-47.924	drained lake; fracture	1601	343	1258	0.60	3.52	48.10	0.0006
898	67.507	-47.924	drained lake; fracture	1599	321	1278	0.64	5.91	48.10	0.0004
899	67.508	-47.917	drained lake; fracture	1602	338	1264	0.62	6.40	49.24	-0.0015
900	67.508	-47.916	drained lake; fracture	1602	338	1264	0.62	6.40	49.24	-0.0024
901	67.508	-47.919	drained lake; fracture	1601	328	1273	0.56	6.05	49.24	-0.0015
902	67.520	-47.946	fracture	1596	217	1379	0.07	3.38	48.04	0.0005
903	67.520	-47.946	fracture	1596	217	1379	0.07	3.38	48.04	0.0005
904	67.530	-47.989	drained lake; fracture	1590	127	1463	0.10	0.54	46.05	-0.0010
905	67.531	-47.991	drained lake; fracture	1590	127	1463	0.10	0.54	46.05	-0.0010
906	67.522	-48.309	drained lake	1502	390	1112	0.36	1.77	45.99	0.0004
907	67.521	-48.310	drained lake; fracture	1502	390	1112	0.36	1.77	45.99	0.0004
908	67.521	-48.307	drained lake; fracture	1502	387	1115	0.39	1.69	45.07	0.0005
909	67.568	-48.321	fracture	1504	328	1176	0.19	2.44	45.31	0.0024
910	67.560	-47.894	drained lake	1614	138	1476	0.00	4.59	43.49	-0.0012
911	67.566	-47.676		1671	83	1588	0.34	0.28	43.87	-0.0006
912	67.614	-48.003	drained lake	1579	257	1322	0.00	1.42	45.49	0.0018
913	67.585	-48.095	fracture	1561	297	1264	0.27	1.34	47.98	0.0005
914	67.592	-48.089	drained lake; fracture	1561	282	1279	0.14	1.60	46.91	0.0007
915	67.592	-48.081	drained lake; fracture	1562	279	1283	0.21	1.65	46.54	0.0009
916	67.592	-48.080	drained lake; fracture	1562	279	1283	0.21	1.65	46.54	0.0009
917	67.592	-48.082	drained lake; fracture	1562	275	1287	0.19	1.61	46.54	0.0014
918	67.592	-48.082	drained lake; fracture	1562	279	1283	0.21	1.65	46.54	0.0009
919	67.588	-48.099	drained lake; fracture	1560	293	1267	0.24	1.19	45.52	0.0004
920	67.603	-48.274	drained lake; fracture	1501	268	1233	0.21	1.72	46.24	-0.0011
921	67.602	-48.277	drained lake; fracture	1501	270	1231	0.21	1.86	46.24	-0.0011
922	67.600	-48.278	drained lake; fracture	1501	275	1226	0.19	1.10	46.24	-0.0015
923	67.608	-49.296	unknown	1113	498	615	0.53	2.78	68.68	0.0027
924	67.620	-49.157	unknown	1193	334	859	0.45	3.18	58.09	0.0017
925	67.626	-49.208	unknown	1184	463	721	0.10	3.67	64.42	0.0016
926	67.627	-49.208	unknown	1184	463	721	0.10	3.67	64.42	0.0016
927	67.627	-49.208	unknown	1184	463	721	0.10	3.67	64.42	0.0016
928	67.649	-49.222	unknown	1157	340	817	0.21	5.64	63.01	0.0005
929	67.641	-49.260	fracture	1131	386	745	0.43	3.12	60.12	0.0010
930	67.640	-49.260	fracture	1132	390	742	0.36	3.23	60.12	0.0010
931	67.639	-49.261	fracture	1131	398	733	0.24	4.05	60.12	0.0010
932	67.640	-49.273	unknown	1131	398	733	0.49	3.69	62.46	0.0011
933	67.609	-49.354	crevasses	1068	500	568	1.11	1.54	74.47	-0.0010
934	67.609	-49.354	crevasses	1067	496	571	1.00	1.69	74.47	-0.0010
935	67.615	-49.332	crevasses	1087	507	580	0.45	0.98	70.01	0.0022
936	67.637	-49.316	crevasses	1113	439	674	1.29	4.09	70.19	0.0071
937	67.646	-49.296	crevasses	1113	361	752	0.21	1.37	63.39	0.0041
938	67.653	-49.370	crevasses	1062	485	577	0.49	2.27	67.80	-0.0009
939	67.648	-49.416	crevasses	1002	378	624	1.08	1.92	67.91	-0.0038
940	67.641	-49.415	crevasses	1021	375	646	0.30	0.82	66.31	0.0010
941	67.640	-49.420	crevasses	1023	376	647	0.15	0.95	66.31	0.0010
942	67.625	-49.449	crevasses	997	403	594	0.70	3.89	70.73	0.0075
943	67.619	-49.461	crevasses	989	444	545	0.72	3.35	77.11	0.0066
944	67.623	-49.498	crevasses	952	461	491	0.77	2.91	73.95	0.0059

945	67.603	-49.539	crevasses	903	398	505	0.34	1.39	90.16	0.0052
946	67.651	-49.603	crevasses	872	382	490	0.70	2.12	55.93	0.0026
947	67.660	-49.633	crevasses	851	386	465	0.54	3.92	55.88	0.0057
948	67.646	-49.601	crevasses	874	394	480	1.33	5.48	52.64	0.0046
949	67.626	-49.647	crevasses	821	525	296	1.63	3.24	56.26	-0.0013
950	67.636	-49.630	crevasses	829	470	359	2.23	4.77	55.92	-0.0018
951	67.630	-49.729	crevasses	749	471	278	0.97	5.66	48.37	0.0069
952	67.614	-49.707	crevasses	743	523	220	1.06	1.55	51.02	0.0008
953	67.599	-49.740	crevasses	708	469	239	1.84	4.07	50.71	0.0016
954	67.596	-49.725	crevasses	716	447	269	1.11	1.02	52.06	-0.0013
955	67.604	-49.665	crevasses	797	514	283	0.47	4.20	64.05	-0.0043
956	67.589	-49.769	crevasses	659	438	221	2.57	6.99	60.86	0.0000
957	67.617	-49.752	crevasses	702	525	177	1.07	3.94	66.23	0.0150
958	67.553	-49.406	unknown	1035	462	573	0.68	3.66	78.08	0.0047
959	67.553	-49.408	crevasses	1037	470	567	1.01	2.90	78.08	0.0047
960	67.555	-49.401	fracture	1035	458	577	1.09	3.50	78.08	0.0040
961	67.554	-49.406	fracture	1035	462	573	0.68	3.66	78.08	0.0047
962	67.555	-49.409	crevasses	1033	480	553	0.68	2.44	83.62	0.0017
963	67.545	-49.464	crevasses	987	501	486	1.00	3.50	79.26	0.0002
964	67.561	-49.456	crevasses	990	466	524	0.49	1.58	79.50	0.0027
965	67.562	-49.456	crevasses	988	463	525	0.10	1.54	79.50	0.0027
966	67.569	-49.457	crevasses	990	486	504	0.94	3.80	78.22	0.0029
967	67.577	-49.520	crevasses	935	461	474	1.21	1.99	84.27	0.0021
968	67.565	-49.524	crevasses	925	483	442	1.16	4.79	73.10	0.0054
969	67.543	-49.538	crevasses	929	556	373	1.12	4.21	80.38	0.0091
970	67.561	-49.576	crevasses	888	521	367	0.62	2.29	86.80	-0.0004
971	67.560	-49.576	crevasses	888	527	361	0.67	3.46	90.83	0.0011
972	67.571	-49.588	crevasses	869	488	381	1.44	4.92	84.66	0.0076
973	67.575	-49.639	crevasses	810	495	315	0.81	0.95	98.33	0.0057
974	67.563	-49.646	crevasses	804	480	324	1.67	5.92	70.15	0.0122
975	67.551	-49.636	crevasses	803	472	331	1.72	2.60	74.52	-0.0060
976	67.556	-49.703	crevasses	722	543	179	0.94	2.74	81.51	0.0074
977	67.575	-49.686	crevasses	762	499	263	0.77	4.78	123.13	0.0195
978	67.556	-49.747	crevasses	632	462	170	2.23	1.56	106.51	0.0080
979	67.549	-49.794	crevasses	557	308	249	0.62	2.00	95.68	0.0122
980	67.549	-49.794	crevasses	557	308	249	0.62	2.00	93.82	0.0071
981	67.552	-49.795	crevasses	558	329	229	0.43	3.48	93.82	0.0025
982	67.556	-49.807	crevasses	556	335	221	1.52	1.73	85.88	-0.0078
983	67.560	-49.822	crevasses	523	284	239	1.44	1.60	59.46	-0.0208
984	67.546	-49.813	crevasses	544	301	243	1.76	1.31	103.38	0.0075
985	67.531	-49.868	crevasses	462	266	196	1.17	1.46	141.01	-0.0129
986	67.501	-49.973	crevasses	284	115	169	0.95	3.81	56.10	-0.0202
987	67.502	-49.932	crevasses	336	251	85	1.07	3.79	82.58	0.0051
988	67.521	-49.865	crevasses	411	229	182	0.34	4.07	107.59	0.0268
989	67.506	-49.769	crevasses	617	416	201	2.81	27.12	22.43	-0.0091
990	67.532	-49.768	crevasses	600	284	316	1.34	2.18	95.76	0.0070
991	67.531	-49.766	crevasses	604	277	327	0.73	1.55	88.48	0.0053
992	67.529	-49.733	crevasses	640	315	325	1.35	5.64	83.40	-0.0068
993	67.534	-49.754	crevasses	607	296	311	0.24	5.93	75.60	0.0000
994	67.513	-49.720	crevasses	664	257	407	1.24	2.87	64.13	-0.0042
995	67.512	-49.725	crevasses	661	254	407	1.89	3.01	64.13	-0.0032
996	67.525	-49.704	crevasses	677	349	328	3.14	7.60	81.86	-0.0047
997	67.517	-49.646	crevasses	792	539	253	0.97	3.93	85.99	0.0157
998	67.527	-49.637	crevasses	800	588	212	2.45	2.94	89.63	0.0135
999	67.534	-49.624	crevasses	827	607	220	0.34	1.52	85.16	0.0009
1000	67.501	-49.688	crevasses	737	446	291	2.82	6.75	72.50	-0.0146
1001	67.495	-49.609	crevasses	885	509	376	0.67	3.21	73.82	0.0035
1002	67.504	-49.600	crevasses	871	501	370	0.15	2.12	72.60	0.0023
1003	67.510	-49.594	crevasses	885	515	370	1.79	4.11	69.29	0.0074
1004	67.519	-49.564	crevasses	919	526	393	0.73	5.01	64.93	0.0012

1005	67.487	-49.451	crevasses	1009	494	515	0.58	2.23	64.48	0.0006
1006	67.485	-49.412	crevasses	1055	547	508	1.27	4.04	66.33	0.0041
1007	67.463	-49.399	crevasses	1063	515	548	0.24	3.75	51.78	0.0030
1008	67.480	-49.456	crevasses	1001	480	521	2.05	4.47	64.30	-0.0025
1009	67.470	-49.458	crevasses	1005	498	507	1.09	4.05	55.92	0.0008
1010	67.472	-49.457	crevasses	1004	484	520	1.50	2.93	56.44	-0.0009
1011	67.471	-49.458	crevasses	1005	498	507	1.09	4.05	55.92	0.0008
1012	67.461	-49.520	crevasses	952	481	471	1.84	5.27	43.02	-0.0052
1013	67.492	-49.617	crevasses	879	527	352	0.77	2.92	74.46	0.0037
1014	67.481	-49.647	crevasses	821	502	319	1.75	3.82	58.73	-0.0047
1015	67.482	-49.680	crevasses	772	504	268	2.53	0.96	55.87	-0.0129
1016	67.483	-49.678	crevasses	781	511	270	2.95	2.85	55.87	-0.0109
1017	67.451	-49.660	crevasses	789	586	203	0.91	2.73	36.32	-0.0065
1018	67.458	-49.662	crevasses	802	573	229	0.67	3.63	50.84	-0.0023
1019	67.453	-49.680	crevasses	759	553	206	1.99	4.42	36.02	0.0015
1020	67.475	-49.711	crevasses	740	534	206	0.28	2.88	46.86	-0.0021
1021	67.464	-49.728	crevasses	700	544	156	2.69	2.11	41.15	-0.0078
1022	67.455	-49.717	crevasses	727	551	176	2.69	2.43	45.99	-0.0060
1023	67.470	-49.766	crevasses	636	481	155	2.69	2.45	31.25	-0.0111
1024	67.444	-49.692	crevasses	773	650	123	3.02	5.95	36.77	0.0054
1025	67.445	-49.687	crevasses	758	615	143	3.17	6.94	33.37	0.0023
1026	67.409	-49.682	crevasses	796	606	190	1.39	4.74	42.87	0.0011
1027	67.408	-49.663	crevasses	818	572	246	0.95	1.23	42.32	-0.0012
1028	67.427	-49.622	crevasses	865	544	321	1.00	4.73	39.01	-0.0040
1029	67.440	-49.644	crevasses	824	637	187	1.57	4.05	35.31	-0.0045
1030	67.447	-49.587	crevasses	891	599	292	1.37	2.57	36.31	-0.0012
1031	67.435	-49.571	crevasses	901	566	335	2.43	4.89	41.61	-0.0010
1032	67.421	-49.552	crevasses	923	526	397	0.77	1.77	47.29	0.0049
1033	67.414	-49.560	crevasses	915	537	378	1.12	2.01	49.42	0.0013
1034	67.414	-49.569	crevasses	910	547	363	1.88	2.11	50.30	-0.0023
1035	67.408	-49.539	crevasses	922	546	376	0.62	2.12	41.46	-0.0009
1036	67.409	-49.540	crevasses	922	546	376	0.62	2.12	41.46	-0.0009
1037	67.414	-49.641	crevasses	845	548	297	1.06	4.25	37.12	0.0007
1038	67.403	-49.515	crevasses	938	571	367	0.28	0.45	42.03	-0.0057
1039	67.404	-49.516	crevasses	940	572	368	0.34	0.38	42.03	-0.0057
1040	67.440	-49.467	crevasses	993	648	345	0.75	2.29	53.82	-0.0027
1041	67.417	-49.454	crevasses	1007	603	404	1.37	0.89	49.80	-0.0002
1042	67.431	-49.401	crevasses	1065	607	458	0.70	2.93	51.52	0.0031
1043	67.444	-49.410	crevasses	1053	582	471	0.67	0.41	47.84	0.0012
1044	67.450	-49.433	crevasses	1028	573	455	1.49	4.86	47.44	0.0012
1045	67.407	-49.411	crevasses	1056	614	442	0.88	1.29	47.20	0.0017
1046	67.407	-49.413	crevasses	1056	614	442	0.88	1.29	47.20	0.0017
1047	67.414	-49.424	crevasses	1047	629	418	1.87	1.22	47.50	0.0003
1048	67.413	-49.432	crevasses	1036	627	409	2.16	1.24	48.96	-0.0014
1049	67.412	-49.432	crevasses	1039	628	411	2.10	0.79	48.96	-0.0014
1050	67.398	-49.419	crevasses	1057	624	433	0.89	1.22	47.52	0.0034
1051	67.398	-49.420	crevasses	1055	624	431	0.84	1.63	47.52	0.0035
1052	67.387	-49.431	crevasses	1056	606	450	0.57	2.57	50.16	0.0006
1053	67.392	-49.441	crevasses	1038	626	412	0.30	2.31	51.66	-0.0009
1054	67.405	-49.479	crevasses	1000	639	361	0.24	1.49	47.03	0.0025
1055	67.388	-49.488	crevasses	986	598	388	1.40	2.20	48.31	0.0003
1056	67.362	-49.571	crevasses	933	530	403	1.81	1.15	45.71	-0.0023
1057	67.402	-49.573	crevasses	896	573	323	2.28	2.52	47.38	-0.0005
1058	67.394	-49.577	crevasses	902	541	361	0.89	1.39	43.44	-0.0001
1059	67.372	-49.602	crevasses	898	584	314	2.11	2.24	40.16	0.0014
1060	67.397	-49.600	crevasses	873	561	312	0.79	3.86	46.62	0.0054
1061	67.397	-49.600	crevasses	873	561	312	0.79	3.86	46.62	0.0049
1062	67.401	-49.599	crevasses	875	571	304	0.51	2.80	49.66	0.0042
1063	67.399	-49.645	crevasses	826	598	228	2.21	1.15	59.13	0.0070
1064	67.393	-49.645	crevasses	822	562	260	2.33	5.12	51.24	0.0090

1065	67.398	-49.644	crevasses	827	597	230	0.75	2.70	58.16	0.0084
1066	67.378	-49.663	crevasses	810	575	235	1.58	1.93	31.49	-0.0032
1067	67.371	-49.689	crevasses	805	579	226	0.68	2.97	27.05	0.0001
1068	67.367	-49.636	crevasses	865	539	326	2.37	7.01	34.58	-0.0002
1069	67.370	-49.731	crevasses	760	657	103	1.02	5.69	16.72	0.0025
1070	67.368	-49.738	crevasses	762	682	80	1.00	5.14	21.28	0.0033
1071	67.360	-49.740	crevasses	758	648	110	2.95	8.02	20.27	0.0011
1072	67.386	-49.723	crevasses	749	614	135	2.52	2.31	42.85	0.0048
1073	67.385	-49.706	crevasses	756	572	184	0.67	1.93	41.04	-0.0036
1074	67.395	-49.683	crevasses	773	564	209	0.82	1.74	66.73	0.0055
1075	67.398	-49.768	crevasses	639	528	111	1.30	3.42	54.01	-0.0249
1076	67.392	-49.773	crevasses	637	551	86	3.61	3.48	34.22	-0.0206
1077	67.338	-49.805	crevasses	685	509	176	2.60	4.14	29.20	-0.0062
1078	67.310	-49.853	crevasses	615	463	152	2.67	6.97	58.12	0.0025
1079	67.318	-49.844	crevasses	645	551	94	1.28	6.35	56.28	-0.0049
1080	67.312	-49.851	crevasses	623	483	140	1.88	6.01	62.02	-0.0010
1081	67.323	-49.789	crevasses	726	546	180	2.44	3.59	56.49	0.0029
1082	67.320	-49.787	crevasses	721	542	179	1.33	0.21	54.78	0.0049
1083	67.327	-49.759	crevasses	770	545	225	2.30	3.99	58.57	0.0014
1084	67.326	-49.759	crevasses	770	545	225	2.30	3.99	58.57	0.0014
1085	67.349	-49.755	crevasses	741	555	186	0.97	8.02	27.12	-0.0032
1086	67.344	-49.731	crevasses	787	529	258	0.34	2.65	34.14	0.0016
1087	67.328	-49.730	crevasses	803	526	277	1.36	2.52	55.53	-0.0001
1088	67.319	-49.734	crevasses	814	560	254	1.44	0.45	56.77	-0.0008
1089	67.311	-49.730	crevasses	817	564	253	0.58	1.98	56.95	-0.0007
1090	67.357	-49.696	crevasses	814	564	250	2.27	6.33	29.86	0.0003
1091	67.352	-49.665	crevasses	860	507	353	1.64	4.78	40.50	-0.0001
1092	67.335	-49.643	crevasses	888	460	428	1.05	2.29	59.86	-0.0015
1093	67.336	-49.654	crevasses	881	454	427	1.49	1.57	56.85	-0.0007
1094	67.322	-49.673	crevasses	872	540	332	0.36	2.11	57.16	-0.0040
1095	67.323	-49.623	crevasses	929	473	456	0.30	6.52	60.12	0.0049
1096	67.339	-49.582	crevasses	945	455	490	2.03	3.91	63.03	0.0007
1097	67.337	-49.588	crevasses	937	439	498	1.16	3.06	63.04	0.0004
1098	67.336	-49.589	crevasses	936	435	501	0.38	1.12	64.81	0.0003
1099	67.336	-49.589	crevasses	936	435	501	0.38	1.12	64.81	0.0003
1100	67.337	-49.588	crevasses	936	435	501	0.38	1.12	64.81	0.0003
1101	67.337	-49.588	crevasses	936	435	501	0.38	1.12	64.81	0.0003
1102	67.337	-49.588	crevasses	937	439	498	1.16	3.06	64.81	0.0003
1103	67.322	-49.587	crevasses	954	434	520	0.56	0.77	61.88	0.0005
1104	67.322	-49.583	crevasses	954	437	517	0.51	1.45	61.88	0.0005
1105	67.322	-49.585	crevasses	953	434	519	0.14	0.45	61.88	0.0005
1106	67.319	-49.500	crevasses	1025	436	589	0.58	3.43	69.64	0.0020
1107	67.332	-49.457	crevasses	1043	403	640	0.56	3.60	70.74	0.0029
1108	67.310	-49.512	crevasses	1011	445	566	1.02	1.15	66.96	-0.0013
1109	67.310	-49.523	crevasses	998	437	561	2.42	2.07	64.60	-0.0006
1110	67.310	-49.520	crevasses	1004	441	563	2.17	1.85	66.96	-0.0014
1111	67.310	-49.519	crevasses	1004	441	563	2.17	1.85	66.96	-0.0014
1112	67.293	-49.536	crevasses	991	491	500	0.41	3.29	59.57	-0.0016
1113	67.312	-49.566	crevasses	958	416	542	0.75	2.14	56.62	-0.0012
1114	67.285	-49.553	crevasses	970	496	474	0.67	0.97	57.27	-0.0016
1115	67.276	-49.559	crevasses	969	477	492	1.28	6.08	55.91	0.0007
1116	67.314	-49.600	crevasses	951	462	489	1.75	4.34	55.04	0.0022
1117	67.270	-49.679	crevasses	876	365	511	2.03	2.03	48.82	0.0000
1118	67.286	-49.659	crevasses	892	408	484	0.21	2.67	54.40	0.0023
1119	67.312	-49.686	crevasses	853	525	328	1.34	1.03	55.65	-0.0038
1120	67.297	-49.684	crevasses	866	523	343	0.47	6.90	55.30	0.0010
1121	67.275	-49.711	crevasses	838	456	382	0.88	9.39	45.12	-0.0028
1122	67.275	-49.711	crevasses	838	456	382	0.88	9.39	45.12	-0.0028
1123	67.283	-49.736	crevasses	810	405	405	1.53	4.40	60.29	0.0058
1124	67.303	-49.728	crevasses	819	568	251	1.69	1.24	57.74	0.0002

1125	67.306	-49.747	crevasses	783	543	240	2.00	3.92	56.30	0.0028
1126	67.306	-49.747	crevasses	783	543	240	2.00	3.92	56.30	0.0028
1127	67.304	-49.752	crevasses	778	535	243	1.59	3.86	58.44	0.0029
1128	67.303	-49.756	crevasses	772	524	248	1.76	3.42	58.44	0.0029
1129	67.273	-49.796	crevasses	747	415	332	0.30	6.80	54.41	-0.0116
1130	67.282	-49.797	crevasses	725	382	343	2.87	5.93	48.53	-0.0119
1131	67.284	-49.811	crevasses	702	334	368	1.31	3.16	44.92	-0.0057
1132	67.292	-49.779	crevasses	743	454	289	0.15	2.90	55.42	-0.0072
1133	67.305	-49.798	crevasses	721	519	202	2.97	7.68	55.76	-0.0027
1134	67.309	-49.797	crevasses	731	563	168	2.18	2.47	56.71	-0.0022
1135	67.308	-49.813	crevasses	691	512	179	2.23	4.71	57.57	0.0023
1136	67.303	-49.821	crevasses	696	479	217	4.81	9.98	54.73	0.0040
1137	67.299	-49.827	crevasses	689	424	265	1.86	8.53	54.73	0.0008
1138	67.276	-49.826	crevasses	699	271	428	1.35	4.10	37.95	-0.0066
1139	67.266	-49.881	crevasses	621	369	252	0.36	3.78	47.41	0.0025
1140	67.278	-49.869	crevasses	615	239	376	2.30	6.12	38.91	-0.0054
1141	67.285	-49.899	crevasses	555	440	115	6.00	19.40	28.27	0.0000
1142	67.287	-49.862	crevasses	629	251	378	3.11	3.99	46.05	-0.0004
1143	67.239	-49.890	crevasses	715	426	289	2.01	7.62	39.06	0.0029
1144	67.245	-49.842	crevasses	727	563	164	1.22	4.53	30.72	-0.0073
1145	67.257	-49.848	crevasses	722	413	309	1.96	5.20	38.30	0.0036
1146	67.263	-49.810	crevasses	730	299	431	1.30	11.76	39.91	-0.0078
1147	67.255	-49.814	crevasses	748	449	299	0.34	9.89	38.44	-0.0013
1148	67.248	-49.810	crevasses	760	465	295	1.35	4.32	35.65	0.0003
1149	67.246	-49.782	crevasses	787	435	352	1.58	1.47	41.45	-0.0041
1150	67.252	-49.668	crevasses	899	476	423	0.47	2.86	52.18	0.0035
1151	67.257	-49.677	crevasses	886	501	385	0.81	6.42	52.49	0.0015
1152	67.266	-49.612	crevasses	928	420	508	0.48	3.10	47.96	-0.0025
1153	67.263	-49.572	crevasses	962	380	582	1.05	2.30	58.15	0.0026
1154	67.157	-50.006	crevasses	622	436	186	4.52	0.81	15.06	-0.0017
1155	67.146	-49.999	crevasses	617	397	220	2.10	7.31	17.89	-0.0044
1156	67.154	-50.007	crevasses	615	439	176	2.33	0.64	18.62	-0.0020
1157	67.140	-49.944	crevasses	680	430	250	1.22	1.53	27.37	-0.0035
1158	67.150	-49.952	crevasses	670	385	285	1.69	3.53	27.78	-0.0019
1159	67.162	-49.894	crevasses	733	346	387	0.77	14.23	36.58	-0.0023
1160	67.162	-49.895	crevasses	736	354	382	1.83	13.46	36.58	-0.0023
1161	67.164	-49.876	crevasses	757	322	435	0.41	11.84	52.38	-0.0042
1162	67.155	-49.904	crevasses	734	480	254	1.24	6.29	29.33	0.0039
1163	67.133	-49.904	crevasses	751	411	340	1.02	5.20	51.97	0.0006
1164	67.139	-49.845	crevasses	805	383	422	1.43	1.19	55.01	-0.0036
1165	67.092	-49.642	crevasses	868	267	601	0.74	5.96	110.94	-0.0077
1166	67.114	-49.876	crevasses	758	18	740	0.34	5.03	82.38	-0.0004
1167	67.119	-49.887	crevasses	755	126	629	0.19	12.42	76.93	0.0016
1168	67.091	-50.017	crevasses	615	173	442	1.87	7.49	93.35	-0.0001
1169	67.089	-49.758	crevasses	831	32	799	0.86	2.09	106.70	0.0035
1170	67.068	-49.691	crevasses	848	155	693	0.15	4.37	76.36	0.0165
1171	67.047	-49.668	crevasses	866	207	659	0.24	2.84	97.50	0.0037
1172	67.079	-49.669	crevasses	847	115	732	0.67	5.25	49.70	0.0159
1173	67.086	-49.634	crevasses	852	329	523	1.21	8.01	44.45	-0.0097
1174	67.069	-49.629	crevasses	856	143	713	0.89	5.43	40.53	0.0010
1175	67.075	-49.629	crevasses	854	265	589	1.05	13.24	30.26	0.0005
1176	67.063	-49.632	crevasses	869	234	635	0.34	3.98	76.19	0.0024
1177	67.052	-49.557	crevasses	942	299	643	1.35	9.60	75.42	0.0153
1178	67.071	-49.564	crevasses	976	449	527	1.61	3.50	37.91	0.0091
1179	67.047	-49.527	crevasses	954	218	736	1.10	3.20	69.37	0.0086
1180	67.047	-49.425	crevasses	1019	359	660	0.81	5.30	77.53	-0.0039
1181	67.045	-49.423	crevasses	1017	389	628	1.02	11.28	77.53	-0.0067
1182	67.028	-49.447	crevasses	981	363	618	0.97	3.99	67.95	-0.0060
1183	67.018	-49.466	crevasses	963	187	776	0.34	3.37	72.65	0.0050
1184	67.022	-49.463	crevasses	962	222	740	0.51	5.41	66.52	-0.0017

1185	67.026	-49.466	crevasses	960	232	728	0.51	6.83	66.03	0.0016
1186	67.034	-49.497	crevasses	961	198	763	0.58	1.84	67.32	0.0035
1187	67.022	-49.541	crevasses	947	189	758	0.92	3.13	96.79	0.0043
1188	67.040	-49.610	crevasses	911	231	680	0.34	2.31	103.96	0.0037
1189	67.021	-49.650	crevasses	878	252	626	1.18	6.33	69.42	-0.0062
1190	67.015	-49.621	crevasses	890	319	571	1.59	8.98	73.78	-0.0237
1191	67.035	-49.694	crevasses	859	312	547	1.30	9.04	90.76	0.0017
1192	67.039	-49.711	crevasses	856	349	507	0.85	9.11	95.42	-0.0006
1193	66.990	-49.609	crevasses	862	293	569	0.51	17.86	43.98	-0.0052
1194	66.977	-49.623	crevasses	837	559	278	0.54	5.83	68.09	0.0095
1195	66.971	-49.604	crevasses	867	622	245	2.69	5.53	92.72	0.0077
1196	67.001	-49.430	crevasses	988	143	845	0.19	1.30	83.70	-0.0031
1197	67.002	-49.445	crevasses	988	137	851	0.73	2.35	83.14	-0.0011
1198	66.977	-49.376	crevasses	1023	189	834	1.42	3.37	120.03	-0.0037
1199	66.963	-49.563	crevasses	901	539	362	0.14	4.76	100.00	0.0041
1200	67.079	-48.536	unknown	1453	236	1217	0.58	2.60	94.49	0.0021
1201	67.258	-48.682	fracture	1396	196	1200	1.00	2.00	85.44	0.0031
1202	67.258	-48.682	fracture	1396	196	1200	1.00	2.00	85.44	0.0031
1203	67.258	-48.681	fracture	1396	196	1200	1.00	2.00	85.44	0.0031
1204	67.257	-48.680	fracture	1398	191	1207	0.61	2.36	85.44	0.0026
1205	67.259	-48.684	fracture	1392	204	1188	0.79	3.24	86.53	0.0032
1206	67.259	-48.683	fracture	1395	198	1197	0.72	2.72	86.53	0.0032
1207	67.259	-48.691	fracture	1396	206	1190	0.94	3.50	86.53	0.0026
1208	67.258	-48.690	fracture	1396	206	1190	0.94	3.50	86.53	0.0026
1209	67.256	-48.688	fracture	1394	189	1205	0.75	2.01	86.53	0.0030
1210	67.270	-48.623	fracture	1422	196	1226	0.34	1.75	83.27	0.0028
1211	67.233	-48.746	fracture	1373	263	1110	1.42	6.21	94.08	0.0032
1212	67.232	-48.745	fracture	1373	263	1110	1.42	6.21	94.08	0.0032
1213	67.230	-48.743	drained lake; fracture	1372	238	1134	0.82	3.39	96.81	0.0034
1214	67.290	-48.836	unknown	1344	275	1069	0.14	3.10	81.84	0.0029
1215	67.290	-48.838	unknown	1343	262	1081	0.54	3.48	83.09	0.0039
1216	67.150	-48.420	drained lake; fracture	1471	139	1332	0.21	3.72	81.29	0.0034
1217	67.134	-48.686	drained lake; fracture	1351	208	1143	0.49	7.86	93.85	-0.0037
1218	67.137	-48.680	drained lake; fracture	1357	210	1147	0.49	7.71	100.00	-0.0051
1219	67.138	-48.677	drained lake; fracture	1357	215	1142	0.30	6.75	100.00	-0.0037
1220	67.135	-48.694	drained lake	1357	156	1201	0.92	5.17	93.85	-0.0020
1221	67.162	-48.558	drained lake; fracture	1429	165	1264	0.19	3.55	90.23	0.0057
1222	67.162	-48.559	drained lake; fracture	1428	173	1255	0.19	4.12	90.23	0.0057
1223	67.161	-48.568	drained lake; fracture	1429	158	1271	0.21	0.54	92.73	0.0059
1224	67.162	-48.568	drained lake; fracture	1429	158	1271	0.21	0.54	92.73	0.0059
1225	67.165	-48.563	drained lake; fracture	1428	186	1242	0.14	4.31	90.78	0.0055
1226	67.165	-48.573	drained lake	1428	183	1245	0.15	4.85	93.81	0.0062
1227	67.148	-48.814	fracture	1347	246	1101	0.51	9.64	106.97	0.0033
1228	67.131	-48.536	drained lake; fracture	1438	244	1194	0.21	3.87	89.08	0.0024
1229	67.124	-48.099	fracture	1562	326	1236	0.45	0.47	75.79	0.0014
1230	67.123	-48.099	fracture	1562	327	1235	0.38	0.41	75.79	0.0014
1231	67.323	-49.063	fracture	1267	387	880	0.34	3.86	72.85	0.0054
1232	67.324	-49.064	fracture	1268	395	873	0.64	4.32	72.85	0.0054
1233	66.737	-48.864	fracture	1276	418	858	1.35	3.39	75.37	-0.0018
1234	66.765	-49.112	fracture	1128	403	725	1.05	5.37	87.65	0.0001
1235	66.625	-48.383	unknown	1502	514	988	0.53	1.48	45.26	0.0017
1236	66.845	-47.402	drained lake; fracture	1784	227	1557	0.36	0.21	54.47	0.0011

4.11 References

Alley, R. B., Dupont, T. K., Parizek, B. R., and Anandakrishnan, S. (2005). Access of surface meltwater to beds of sub-freezing glaciers: preliminary insights. *Annals of Glaciology*, *40*, 8–14. doi:10.3189/172756405781813483

Andersen, M. L., Nettles, M., Elósegui, P., Larsen, T. B., Hamilton, G. S., and Stearns, L. A. (2011). Quantitative estimates of velocity sensitivity to surface melt variations at a large Greenland outlet glacier. *Journal of Glaciology*, *57*(204), 609–620.

Bamber, J. L., Ekholm, S., and Krabill, W. B. (2001). A new, high-resolution digital elevation model of Greenland fully validated with airborne laser altimeter data. *Journal of Geophysical Research: Solid Earth*, *106*(B4), 6733–6745. doi:10.1029/2000JB900365

Bamber, J. L., Siegert, M. J., Griggs, J. A., Marshall, S. J., and Spada, G. (2013). Paleofluvial mega-canyon beneath the central Greenland ice sheet. *Science*, *341*(6149), 997–9. doi:10.1126/science.1239794

Bartholomew, I. D., Nienow, P., Mair, D., Hubbard, A. L., King, M. A., and Sole, A. (2010). Seasonal evolution of subglacial drainage and acceleration in a Greenland outlet glacier. *Nature Geoscience*, *3*(6), 408–411. doi:10.1038/ngeo863

Bartholomew, I. D., Nienow, P., Sole, A., Mair, D., Cowton, T., and King, M. A. (2012). Short-term variability in Greenland Ice Sheet motion forced by time-varying meltwater drainage: Implications for the relationship between subglacial drainage system behavior and ice velocity. *Journal of Geophysical Research*, *117*(F3), 1–17. doi:10.1029/2011JF002220

Bartholomew, I. D., Nienow, P., Sole, A., Mair, D., Cowton, T., Palmer, S., and Wadham, J. L. (2011). Supraglacial forcing of subglacial drainage in the ablation zone of the Greenland ice sheet. *Geophysical Research Letters*, *38*(8), 1–5. doi:10.1029/2011GL047063

Box, J. E., Cappelen, J., Chen, C., Decker, D., Fettweis, X., Mote, T. L., Tedesco, M., van de Wal, R. S. W., and Wahr, J. (2013). Greenland Ice Sheet. In *Arctic Report Card*. Retrieved from http://www.arctic.noaa.gov/reportcard/greenland_ice_sheet.html

Catania, G. A. and Neumann, T. A. (2010). Persistent englacial drainage features in the Greenland Ice Sheet. *Geophysical Research Letters*, *37*(2), 1–5. doi:10.1029/2009GL041108

Catania, G. A., Neumann, T. A., and Price, S. F. (2008). Characterizing englacial drainage in the ablation zone of the Greenland ice sheet. *Journal of Glaciology*, *54*(187), 567–578. doi:10.3189/002214308786570854

Chandler, D. M., Wadham, J. L., Lis, G. P., Cowton, T., Sole, A., Bartholomew, I. D., Telling, J., Nienow, P., Bagshaw, E. B., Mair, D., Vinen, S., and Hubbard, A. L. (2013). Evolution of the subglacial drainage system beneath the Greenland Ice Sheet revealed by tracers. *Nature Geoscience*, *6*(3), 195–198. doi:10.1038/ngeo1737

Clason, C. C., Mair, D. W. F., Nienow, P. W., Bartholomew, I. D., Sole, A., Palmer, S., and Schwanghart, W. (2014). Modelling the transfer of supraglacial meltwater to the bed of Leverett Glacier, southwest Greenland. *The Cryosphere*, *8*, 4243–4280. doi:10.5194/tcd-8-4243-2014

Cowton, T., Nienow, P., Sole, A., Wadham, J. L., Lis, G. P., Bartholomew, I. D., Mair, D., and Chandler, D. (2013). Evolution of drainage system morphology at a land-terminating Greenlandic outlet glacier. *Journal of Geophysical Research: Earth Surface*, *118*, 1–13. doi:10.1029/2012JF002540

Das, S. B., Joughin, I., Behn, M. D., Howat, I. M., King, M. A., Lizarralde, D., and Bhatia, M. P. (2008). Fracture propagation to the base of the Greenland Ice Sheet during supraglacial lake drainage. *Science*, *320*(5877), 778–81. doi:10.1126/science.1153360

Doyle, S. H., Hubbard, A. L., Dow, C. F., Jones, G. A., Fitzpatrick, A. A. W., Gusmeroli, A., Kulessa, B., Lindback, K., Pettersson, R., and Box, J. E. (2013). Ice tectonic deformation during the rapid in situ drainage of a supraglacial lake on the Greenland Ice Sheet. *The Cryosphere*, *7*(1), 129–140. doi:10.5194/tc-7-129-2013

Fettweis, X., Franco, B., Tedesco, M., van Angelen, J. H., Lenaerts, J. T. M., van den Broeke, M. R., and Gallée, H. (2013). Estimating the Greenland ice sheet surface mass balance contribution to future sea level rise using the regional atmospheric climate model MAR. *The Cryosphere*, *7*(2), 469–489. doi:10.5194/tc-7-469-2013

Fountain, A. G., Schlichting, R. B., Jansson, P., and Jacobel, R. W. (2005). Observations of englacial water passages: a fracture-dominated system. *Annals of Glaciology*, *40*(1), 25–30. doi:10.3189/172756405781813762

Harper, J. T., Humphrey, N. F., and Pfeffer, W. T. (1998). Crevasse patterns and the strain-rate tensor: a high-resolution comparison. *Journal of Glaciology*, *4*(146), 68–76.

Howat, I. M., Negrete, a., and Smith, B. E. (2014). The Greenland Ice Mapping Project (GIMP) land classification and surface elevation data sets. *The Cryosphere*, *8*(4), 1509–1518. doi:10.5194/tc-8-1509-2014

Johansson, A. M., Jansson, P., and Brown, I. A. (2013). Spatial and temporal variations in lakes on the Greenland Ice Sheet. *Journal of Hydrology*, *476*, 314–320. doi:10.1016/j.jhydrol.2012.10.045

Joughin, I., Das, S. B., Flowers, G. E., Behn, M. D., Alley, R. B., King, M. a., Smith, B. E., Bamber, J. L., van den Broeke, M. R., and van Angelen, J. H. (2013). Influence of ice-sheet geometry and supraglacial lakes on seasonal ice-flow variability. *The Cryosphere*, *7*(4), 1185–1192. doi:10.5194/tc-7-1185-2013

Joughin, I., Das, S. B., King, M. A., Smith, B. E., Howat, I. M., and Moon, T. (2008b). Seasonal speedup along the western flank of the Greenland Ice Sheet. *Science, 320*(5877), 781–3. doi:10.1126/science.1153288

Joughin, I., Howat, I. M., Fahnestock, M., Smith, B. E., Krabill, W. B., Alley, R. B., Stern, H., and Truffer, M. (2008a). Continued evolution of Jakobshavn Isbræ following its rapid speedup. *Journal of Geophysical Research*, *113*(F4), 1–14. doi:10.1029/2008JF001023

Joughin, I., Smith, B. E., Howat, I. M., Scambos, T. A., and Moon, T. (2010). Greenland flow variability from ice-sheet-wide velocity mapping. *Journal of Glaciology*, *56*(197), 415–430. doi:10.3189/002214310792447734

Krawczynski, M. J., Behn, M. D., Das, S. B., and Joughin, I. (2009). Constraints on the lake volume required for hydro-fracture through ice sheets. *Geophysical Research Letters*, *36*(10), 1–5. doi:10.1029/2008GL036765

Lampkin, D. J., Amador, N., Parizek, B. R., Farness, K., and Jezek, K. (2013). Drainage from water-filled crevasses along the margins of Jakobshavn Isbrae: A potential catalyst for catchment expansion. *Journal of Geophysical Research: Earth Surface*, *118*, 1–19. doi:10.1002/jgrf.20039

Lampkin, D. J. and VanderBerg, J. (2013). Supraglacial melt channel networks in the Jakobshavn Isbræ region during the 2007 melt season. *Hydrological Processes*. doi:10.1002/hyp.10085

McGrath, D., Colgan, W., Steffen, K., Lauffenburger, P., and Balog, J. (2011). Assessing the summer water budget of a moulin basin in the Sermeq Avannarleq ablation region, Greenland ice sheet. *Journal of Glaciology*, *57*(205), 954–964. doi:10.3189/002214311798043735

Morlighem, M., Rignot, E., Mouginot, J., Seroussi, H., and Larour, E. (2014). Deeply incised submarine glacial valleys beneath the Greenland ice sheet. *Nature Geoscience*, (May), 18–22. doi:10.1038/NGEO2167

Morlighem, M., Rignot, E., Seroussi, H., Larour, E., Ben Dhia, H., and Aubry, D. (2011). A mass conservation approach for mapping glacier ice thickness. *Geophysical Research Letters*, *38*(19), 1–6. doi:10.1029/2011GL048659

Nghiem, S. V., Hall, D. K., Mote, T. L., Tedesco, M., Albert, M. R., Keegan, K., Shuman, C. A., DiGirolamo, N. E., and Neumann, G. (2012). The extreme melt across the Greenland ice sheet in 2012. *Geophysical Research Letters*, *39*(20), 6–11. doi:10.1029/2012GL053611

Palmer, S., Shepherd, A., Nienow, P., and Joughin, I. (2011). Seasonal speedup of the Greenland Ice Sheet linked to routing of surface water. *Earth and Planetary Science Letters*, *302*, 423–428. doi:10.1016/j.epsl.2010.12.037

Phillips, T., Leyk, S., Rajaram, H., Colgan, W., Abdalati, W., McGrath, D., and Steffen, K. (2011). Modeling moulin distribution on Sermeq Avannarleq glacier using ASTER and WorldView imagery and fuzzy set theory. *Remote Sensing of Environment*, *115*(9), 2292–2301. doi:10.1016/j.rse.2011.04.029

Poinar, K., Joughin, I., Das, S. B., Behn, M. D., Lenaerts, J. T. M., and Broeke, M. R. (2015). Limits to future expansion of surface-melt-enhanced ice flow into the interior of western Greenland. *Geophysical Research Letters*, 1–8. doi:10.1002/2015GL063192

Selmes, N., Murray, T., and James, T. D. (2011). Fast draining lakes on the Greenland Ice Sheet. *Geophysical Research Letters*, *38*(15), 1–5. doi:10.1029/2011GL047872

Shepherd, A., Hubbard, A. L., Nienow, P., King, M. A., McMillan, M., and Joughin, I. (2009). Greenland ice sheet motion coupled with daily melting in late summer. *Geophysical Research Letters*, *36*(1), 2–5. doi:10.1029/2008GL035758

Smith, L. C., Chu, V. W., Yang, K., Gleason, C. J., Pitcher, L. H., and Rennermalm, A. K. (2015). Efficient meltwater drainage through supraglacial streams and rivers on the southwest Greenland ice sheet. *Proceedings of the National Academy of Sciences*, *112*(4), 1001–1006. doi:10.1073/pnas.1413024112

Sundal, A. V., Shepherd, A., Nienow, P., Hanna, E., Palmer, S., and Huybrechts, P. (2011). Melt-induced speed-up of Greenland ice sheet offset by efficient subglacial drainage. *Nature*, *469*(7331), 521–4. doi:10.1038/nature09740

Tedesco, M., Fettweis, X., Mote, T. L., Wahr, J., Alexander, P., Box, J. E., and Wouters, B. (2013b). Evidence and analysis of 2012 Greenland records from spaceborne observations, a regional climate model and reanalysis data. *The Cryosphere*, *7*(2), 615–630. doi:10.5194/tc-7-615-2013

Tedesco, M., Willis, I. C., Hoffman, M. J., Banwell, A. F., Alexander, P., and Arnold, N. S. (2013a). Ice dynamic response to two modes of surface lake drainage on the Greenland ice sheet. *Environmental Research Letters*, *8*(3), 034007. doi:10.1088/1748-9326/8/3/034007

Van de Wal, R. S. W., Boot, W., Smeets, C. J. P. P., Snellen, H., van den Broeke, M. R., and Oerlemans, J. (2012). Twenty-one years of mass balance observations along the K-transect, West Greenland. *Earth System Science Data*, *4*(1), 31–35. doi:10.5194/essd-4-31-2012

Van der Veen, C. J. (2007). Fracture propagation as means of rapidly transferring surface meltwater to the base of glaciers. *Geophysical Research Letters*, *34*(1), 1–5. doi:10.1029/2006GL028385

Vizcaíno, M., Lipscomb, W. H., Sacks, W. J., and van den Broeke, M. (2014). Greenland Surface Mass Balance as Simulated by the Community Earth System Model. Part II: Twenty-First-Century Changes. *Journal of Climate*, *27*(1), 215–226. doi:10.1175/JCLI-D-12-00588.1

Yang, K. and Smith, L. C. (2013). Supraglacial streams on the Greenland Ice Sheet delineated from combined spectral – shape information in high-resolution satellite imagery. *IEEE Geoscience and Remote Sensing Letters, 10*(4), 801–805.

Zwally, H. J., Abdalati, W., Herring, T., Larson, K., Saba, J. L., and Steffen, K. (2002). Surface melt-induced acceleration of Greenland ice-sheet flow. *Science, 297*(218), 218–222. doi:10.1126/science.1072708